Using magnetic resonance imaging to investigate early brain injury after aneurysmal subarachnoid haemorrhage



Dr Matthew James Rowland MBBS BSc FRCA

Nuffield Department of Clinical Neurosciences
University of Oxford

This thesis is submitted for the degree of
Doctor of Philosophy

University College Trinity Term 2015

For Annelies and Jacob

Using magnetic resonance imaging to investigate early brain injury after aneurysmal subarachnoid haemorrhage

Dr Matthew James Rowland MBBS BSc FRCA

University College, University of Oxford

Submitted for the degree of D. Phil., Trinity Term 2015

Aneurysmal subarachnoid haemorrhage (SAH) is a devastating disease frequently leading to death or poor functional outcome and the pathophysiological changes that occur acutely post-rupture remain poorly understood. The work presented here describes a series of studies correlating serial magnetic resonance imaging (MRI) scanning and bedside saccadometry with neurocognitive outcomes to investigate early brain injury after SAH. Further experiments investigate the potential of saccadometry as a bedside biomarker of cerebral ischaemia post-rupture and use MRI in a model of cerebral hypoxia to explore the mechanisms underlying the therapeutic effects of nimodipine.

Firstly, results demonstrated significantly increased apparent grey matter volume and restricted diffusion in the first 72 hours post-SAH in patients, suggesting the presence of undiagnosed and significant global cerebral oedema. Furthermore, structural images acquired at this stage enabled us to predict with high accuracy and specificity which patients will develop poor neurocognitive outcomes at three months.

Next we investigated the impact of early brain injury on functional connectivity after SAH. Patients showed significantly increased functional connectivity compared to healthy controls in a number of functional networks associated with complex cognitive or emotional functions at all timepoints post-SAH. Neurocognitive impairment was associated with increased and decreases in functional connectivity and all differences were independent from any effect of altered grey matter volume.

Improving the prediction of which patients are most at risk of developing secondary ischaemia following SAH remains a key area for research focus. We therefore used a portable beside saccadometer to acquire serial measurements of eye movements acutely post-rupture with results demonstrating faster eye movements are correlated with higher cerebral blood flow in the first 72 hours post-SAH.

Finally, we used MRI to quantify the changes in cerebral structure, perfusion and function associated with a healthy volunteer model of acute hypoxia, and the effect of calcium channel blockade with nimodipine on these changes. Results suggest a preferential effect of calcium channel blockade in reversing regional MRI changes under conditions of hypoxia. These changes may help explain the outcome benefit seen in aneurysmal subarachnoid haemorrhage.

This thesis highlights the potential of MRI imaging to offer biomarkers of early brain injury in the acute period post-SAH, to improve prediction of patients most at risk of neurocognitive impairment and to offer new insight into the mechanisms behind the therapeutic benefit seen with nimodipine.

Acknowledgements

Firstly, I would like to thank my supervisors: Dr Kyle Pattinson - thank you for being the inspiration for me starting on my research career and for all your help and encouragement at every single stage of this process. Your attention to detail, dedication, scientific process and vision have been inspirational. I really can't thank you enough for being so supportive and so patient with me - even if my email inbox will likely never recover from this DPhil. Professor Peter Jezzard for all the help and support in getting the MRI sequences used in this study working and for all your support and assistance with my grant, thesis and paper writing. I would also particularly like to thank Dr Jon Westbrook for all the considerable encouragement, support and advice you've given me at every stage of my clinical and research career and Professor Irene Tracey for all the guidance, advice and chats that have always inspired me to keep going as an "academic" anaesthetist and to continually challenge myself.

I would like to say a special thank you to Dr Michael Kelly for helping me so much at the start of my research time with getting the PCASL sequence working and scanning patients. I would also like to thank everyone who has worked with me within our group: Mari Herigstad, Anja Hajen, Liv Faull (especially for your help with running the hypoxia exeperiments), Andrea Dennis, Martyn Ezra, Cat Lamb and a special thanks to my research assistant Payashi Garry. I would also like to acknowledge Julia, Mary and Alison at ONNRU and Richard Wise and his group in Cardiff for all their help and assistance.

This DPhil was dependent on the prompt and accurate MRI scanning of patients. For that I am eternally grateful to everyone at AVIC including Carol Davey, Lukasz Owsiak, Professor Robin Choudhury, the AVIC nurses and especially Mel Jones and Juliet Semple for all the expert button pressing! I would also like to acknowledge and thank Dr Rufus Corkill for kindly reporting all of the MRI scans acquired, Dr Ian Baker for all your help with the neurocognitive testing and analysis, and Dr Chrystalina Antoniades for all the extensive help and guidance with the saccadometry experiments.

There are so many people at FMRIB and in the NDCN who have supported me, from creating the MRI sequences used in this thesis to helping me with approaching the analysis and to working out why my analysis won't run - I really am eternally grateful and apologetic for continually disturbing you! In no particular order: Dave Flitney, Duncan Mortimer, Matt Webster, Jessper Andersson, Dan Bulte, Anderson Winkler, Eugene Duff, Janine Bijsterbosch, Christian Beckmann, Steve Smith, Karla Miller, Nico Filippini, Tom Okell, Jill O'Reilly, Mark Woolrich, Saad Jbabdi, and especially Mark Jenkinson for all the help with registrations that will continue to give me nightmares for years. An extra special thanks must got to Gwen Douaud for the huge amount of support you have given me with the analysis stage of this DPhil - I really can't thank you enough for giving me so much of your time and for setting me straight on so many aspects of MRI research. I would also like to thank Dr Duncan Young for the kind words whenever I have come to you for help or advice regarding anaesthetic and intensive care research.

This research could not have happened without the cooperation of so many patients and relatives. I would like to extend to them my gratitude for all of their time and cooperation without which this DPhil would have been impossible.

This work would also not have been possible without the funding from my sponsors who include the Medical Research Council, UK, the NIHR Oxford Biomedical Research Centre, and the Oxford University Clinical Academic Graduate School. Not only has the funding been comprehensive, enabling me to travel and present my work across Europe, but in addition the OUCAGS academic community in Oxford, with its regular meetings and dinners, have provided ample opportunity for me to discuss my thoughts and findings with other Oxford fellows and investigators, for which I am very grateful.

I would like to thank my parents, my brother and sister-in-law, my extended family and my family-in-law for all their love and support. I am also particularly indebted to both of my grandfathers for providing me with a passion for science and engineering at such an early age and for inspiring me to constantly question everything that people tell you is true.

Finally, I would like to thank my wife Annelies from the bottom of my heart for making this all seem worthwhile and for always supporting me through the highs and the lows of this DPhil - especially the "difficult" last few months of thesis writing. And my son Jacob, for making me so proud to be a father every day.

"If you always do what you've always done, you'll always get what you've always got"

Henry Ford

Table of contents

Declaration **xii**

Manuscripts arising from this thesis **xiii**

List of figures **xv**

List of tables **xviii**

Abbreviations **xx**

1 Overview of thesis **1**

2 Neurocognitive outcomes after aneurysmal subarachnoid haemorrhage - looking beyond "vasospasm" **4**

2.1 Introduction 6

2.2 Vasoconstriction and DCI 8

2.3 Novel theories regarding DCI pathogenesis 9

2.3.1 Early brain injury 9

2.3.2 Cortical spreading depression 13

2.3.3 Microthrombosis 14

2.3.4 Collateral cerebral circulation 17

2.4 How have clinical therapeutic interventions aided the understanding of DCI? 18

2.4.1 Clazosentan 18

2.4.2 Nimodipine 19

2.4.3 Induced hypertension, hypervolaemia and haemodilution (“triple-H" therapy) 20

2.4.4 Magnesium 21

2.4.5 Statins 22

2.4.6 Anti-coagulant/anti-fibrinolytic therapy . . . 23
2.5 Future directions for research . . . 24
2.5.1 Determining the genetic determinants of early brain injury . . . 24
2.5.2 Endothelial nitric oxide synthase . . . 24
2.5.3 Apolipoprotein E . . . 24
2.5.4 What is the interaction between anaesthetic agents and CSD? . . . 25
2.5.5 Can biomarkers for early brain injury and DCI be identified? . . . 26
2.6 Conclusions . . . 27

3 Experimental Methods 29
3.1 Introduction . . . 30
3.1.1 Structural MRI . . . 31
3.1.2 Diffusion-weighted Imaging . . . 32
3.1.3 Resting State Blood Oxygen Level Dependent (BOLD) Imaging . . . 32
3.1.4 Arterial Spin Labeling . . . 34
3.2 Principles of MRI data analysis . . . 36
3.2.1 Data reduction . . . 37
3.2.2 Correction for B0 field inhomogeneities . . . 37
3.2.3 Motion correction . . . 37
3.2.4 Spatial smoothing . . . 39
3.2.5 Temporal filtering . . . 39
3.2.6 Registration . . . 39
3.2.7 Statistical analysis . . . 41
3.3 Neurocognitive Testing . . . 43

4 The relationship between structural, diffusion-weighted and perfusion changes on acute magnetic resonance imaging and neurocognitive outcome after subarachnoid haemorrhage 45
4.1 Introduction . . . 47
4.2 Methods . . . 49
4.2.1 MRI scan acquisition . . . 50
4.2.2 Clinical and Neurocognitive Assessment . . . 51
4.2.3 Post-processing and data analysis . . . 52
4.2.4 Neurocognitive data analysis . . . 55
4.2.5 Control recruitment . . . 55
4.3 Results . . . 55

4.3.1 Clinical Demographics 55
4.4 Physiological data 56
4.5 MRI Results 56
4.5.1 Artifact from coils 56
4.5.2 MRI Results 56
4.5.3 DCI/DCI-related cerebral infarction and relationship to MRI results 71
4.5.4 Neurocognitive outcomes 71
4.6 Discussion 80
4.6.1 Methodological considerations 85
4.7 Conclusions 86
4.8 Supplementary material 86

5 Resting state functional connectivity after Subarachnoid Haemorrhage 88
5.1 Introduction 90
5.2 Methods 92
5.2.1 Pre-processing 92
5.2.2 Amplitude of low frequency fluctuations data analysis 93
5.2.3 Resting state data analysis 93
5.2.4 Anatomical localisation of results 104
5.3 Results 104
5.3.1 Motion 104
5.3.2 ALFF analysis 105
5.3.3 Resting state connectivity analysis 105
5.3.4 Scan 1: <72 hours post-SAH 105
5.3.5 Scan 2: 5-10 days post-SAH 111
5.3.6 Scan 3: 3 months post-SAH 114
5.3.7 Longitudinal changes 119
5.3.8 Relationship with neurocognitive outcomes 119
5.4 Discussion 123
5.4.1 Methodological considerations 130
5.5 Conclusion 132
5.6 Supplementary Data 133

6 Acute impairment of saccadic eye movements is associated with delayed cerebral ischaemia and cerebral infarction after aneurysmal subarachnoid haemorrhage 136

6.1 Introduction . . . 138
6.2 Methods . . . 139
6.2.1 Recording saccadic eye movements . . . 139
6.2.2 MRI scan acquisition . . . 141
6.2.3 Clinical and neurocognitive assessment . . . 141
6.2.4 Statistical analysis . . . 142
6.3 Results . . . 142
6.4 Discussion . . . 145
6.4.1 Methodological considerations . . . 147
6.5 Conclusions . . . 148

7 Investigating the role of calcium channel blockade on early brain injury after acute normobaric hypoxia 149
7.1 Introduction . . . 152
7.2 Methods . . . 154
7.2.1 Experimental Design . . . 154
7.2.2 Experimental Procedure . . . 154
7.2.3 Post-processing of MRI data . . . 157
7.2.4 Statistical Analysis . . . 160
7.3 Results . . . 160
7.3.1 Physiological data . . . 161
7.3.2 Effect of acute poikilocapnic hypoxia . . . 164
7.3.3 Effect of nimodipine under conditions of normoxia . . . 171
7.3.4 Effect of nimodipine under conditions of hypoxia . . . 175
7.4 Discussion . . . 178
7.4.1 Cerebral effects of acute hypoxia . . . 178
7.4.2 Effects of nimodipine on normal cerebral physiology . . . 179
7.4.3 The effect of nimodipine under conditions of cerebral hypoxia . . . 180
7.5 Effect of hypoxia and nimodipine on ALFF . . . 181
7.6 Methodological considerations . . . 181
7.7 Conclusions . . . 182

8 Conclusions 183
8.1 Main findings of the thesis . . . 184
8.1.1 Structural and perfusion changes associated with early brain injury and neurocognitive outcomes after SAH . . . 184

8.1.2 Resting state functional connectivity after SAH 184
8.1.3 The potential for the bedside clinical assessment of SAH patients using saccadometry 185
8.1.4 The role of calcium in early brain injury after SAH 186
8.2 Directions for future research 187
8.2.1 Imaging early brain injury after SAH 187
8.2.2 Therapeutic interventions 188

References **190**

Appendix A: Delayed Cerebral Ischaemia: Looking Beyond Vasospasm **220**

Appendix B: Pseudo-Continuous Arterial Spin Labelling MRI for Non-Invasive, Whole-Brain, Serial Quantification of Cerebral Blood Flow Following Aneurysmal Subarachnoid Haemorrhage **236**

Appendix C: The role of the nitric oxide pathway in brain injury and its treatment - From bench to bedside **246**

Declaration

I certify that this thesis entitled "Using magnetic resonance imaging to investigate early brain injury after aneurysmal subarachnoid haemorrhage" was performed whilst I was a full-time postgraduate student at the University of Oxford. I declare that this thesis is of my own composition, and the research contained herein is my own original work under the supervision of Dr Kyle Pattinson and Professor Peter Jezzard. No portion of this work has been submitted in support of an application for any other degree. This thesis contains fewer than 50,000 words including appendices, bibliography, footnotes, tables and equations and has fewer than 150 figures.

Manuscripts arising from this thesis

Peer reviewed publications

Rowland, MJ, Hadjipavlou, G, Kelly, M, Westbrook, J, Pattinson, KTS. (2012). Delayed cerebral ischaemia after subarachnoid haemorrhage: looking beyond vasospasm. British Journal of Anaesthesia, 109(3), 315–329. Pubmed ID: 22879655

*Kelly, ME, *Rowland, MJ, Okell, TW, Chappell, MA, Corkill, R, Kerr, RS, et al. (2013). Pseudo-continuous arterial spin labelling MRI for non-invasive, whole-brain, serial quantification of cerebral blood flow following aneurysmal subarachnoid haemorrhage. Translational Stroke Research, 4(6), 710–718. Pubmed ID: 24323425

Garry, PS, Ezra, M, Rowland, MJ, Westbrook, J, Pattinson, KTS. (2015). The role of the nitric oxide pathway in brain injury and its treatment - from bench to bedside. Experimental Neurology, 263, 235–243. Pubmed ID: 25447937

Abstracts

Rowland, M.J, Kelly, M.E., Okell, T.W., M. J. Rowland, M. E. Kelly, Jezzard, P., Westbrook, J., Pattinson, K.T.S. (2012) Magnetic resonance imaging measures of cerebral perfusion after subarachnoid haemorrhage. British Journal of Anaesthesia 108 (4): 709–21P

Manuscripts in preparation

Rowland MJ, Garry P, Ezra M, Corkill R, Baker I, Westbrook J, Jezzard P, Douaud G, Pattinson KTS. Acute structural magnetic resonance imaging predicts neurocognitive outcome after aneurysmal subarachnoid haemorrhage

Rowland MJ, Ezra M, Winkler A, Garry P, Okell T, Kelly M, Westbrook J, Douaud G, Pattinson KTS. Calcium channel blockade with nimodipine reverses cerebral effects of acute normobaric hypoxia

List of figures

2.1 Mechanisms of early brain injury after SAH 10
2.2 Mechanisms underlying the formation of cerebral oedema 12
2.3 Cortical spreading depression - normal and pathological responses 15
2.4 Potential mechanisms of microthrombosis formation after SAH 16

3.1 Basis of the BOLD signal 33
3.2 Basis of arterial spin labeling 35
3.3 Basics of boundary based registration 40

4.1 Flowsheet of recruitment into the study 57
4.2 MRI artifact from endovascular coiling 58
4.3 MRI scan 1 v control: SIENAX and VBM data 62
4.4 MRI scan 2 v control: SIENAX and VBM data 64
4.5 MRI scan 3 v control: SIENAX and VBM data 67
4.6 MRI scan 1 v MRI scan 3: SIENAX and VBM changes 69
4.7 SIENAX results for patients at each MRI scan point 70
4.8 Cerebral blood flow in patients with and without DCI/DCI-related cerebral infarction 72
4.9 Complete results from neurocognitive testing at 3 months post-SAH 75
4.10 Relationship between neurocognitive outcome and cerebellum grey matter volume 77
4.11 Neurocognitive outcome and grey matter volume at MRI scan 1 78
4.12 Cerebellum cerebral blood flow at MRI scan 1 79
4.13 Receiver operator characteristic (ROC) curve of the structural data from <72 hours post-SAH 79

5.1 Flowsheet outlining resting state and amplitude of low frequency oscillations data analysis 94

5.2 Template resting state networks from Smith et al. 2009 96
5.3 MRI scan 1 v control: Template spatial maps 98
5.4 MRI scan 2 v control: Template spatial maps 99
5.5 MRI scan 3 v control: Template spatial maps 100
5.6 Longitudinal patient analysis: Template spatial maps 101
5.7 Voxelwise changes in ALFF at each MRI scan point for patients compared to healthy controls 106
5.8 Longitudinal patient voxelwise changes in ALFF 107
5.9 Graphs of mean total spectral power for each MRI scan point in patients and controls 108
5.10 Graphs of mean total spectral power for each MRI scan point in patients and controls with error bars representing standard error of the mean 109
5.11 MRI scan 1 v control: Dual regression results 110
5.12 MRI scan 1 v control: Grey matter correction 112
5.13 MRI scan 1 v control: Between network correlations 113
5.14 MRI scan 2 v control: Dual regression results 115
5.15 MRI scan 2 v control: Grey matter correction 116
5.16 MRI scan 3 v control: Dual regression results 117
5.17 MRI scan 3 v control: Grey matter correction 118
5.18 MRI scan 1 v control: Between network correlations 120
5.19 Longitudinal patient dual regression results: MRI scan 1 v MRI scan 2 121
5.20 Longitudinal patient dual regression results: MRI scan 2 v MRI scan 3 122
5.21 MRI scan 3: Relationship of functional connectivity to neurocognitive outcome 124
5.22 MRI scan 3: Between network correlations and neurocognitive outcomes . . . 125
5.23 MRI scan 1: Relationship of functional connectivity to neurocognitive outcome 126

6.1 Image showing portable saccadometer headpiece used to measure saccadic latency 140
6.2 Longitudinal changes in saccadic latency in patients 144
6.3 Relationship between saccadic latency and DCI/DCI-related infarction 145

7.1 Diagrams showing the study protocol and a schematic of the breathing apparatus used to maintain hypoxic conditions 155
7.2 ETO_2 values from the laboratory and MRI sessions 162
7.3 $ETCO_2$ values from the laboratory and MRI sessions 163

7.4 Apparent diffusion coefficient (ADC) values for whole brain grey matter and thalamus, hippocampus and occipital lobe regions of interest for each of the four experimental conditions. 165
7.5 Apparent diffusion coefficient (ADC) in the hypoxia/placebo condition compared to normoxia/placebo 166
7.6 Grey matter volume values for whole brain grey matter and thalamus, hippocampus and occipital lobe regions of interest for each of the four experimental conditions. 168
7.7 Grey matter cerebral blood flow values for whole brain grey matter and thalamus, hippocampus and occipital lobe regions of interest for each of the four experimental conditions. 169
7.8 Voxelwise changes in cerebral blood flow (CBF) in the hypoxia/placebo condition compared to normoxia/placebo 170
7.9 Spectral power values for whole brain grey matter and thalamus, hippocampus and occipital lobe regions of interest for each of the four experimental conditions. 172
7.10 Whole brain grey matter normalised frequency spectrograms for each of the experimental conditions 173
7.11 Thalamus ROI normalised frequency spectrograms for each of the experimental conditions 174
7.12 Voxelwise changes in apparent diffusion coefficient (ADC) in the hypoxia/nimodipine condition compared to hypoxia/placebo 177

List of tables

2.1 Proposed definitions of DCI and cerebral infarction after SAH for use as an outcome event in clinical trials and observational studies - adapted from [323] . 7

4.1 Overview demographics of successfully recruited patients 59
4.2 Complete demographic and radiological data for successfully recruited patients 60
4.3 Physiological data recorded during each MRI scan session 60
4.4 MRI scan 1: SIENAX, DWI and ASL data for patients <72 hours post-SAH compared to healthy controls. vCSF = ventricular cerebrospinal fluid, ADC = apparent diffusion coefficient, CBF = cerebral blood flow, AAT = arterial arrival time 61
4.5 MRI scan 2 v control: SIENAX, DWI and ASL data 63
4.6 MRI scan 3: SIENAX, DWI and ASL data for patients 3 months post-SAH compared to healthy controls. vCSF = ventricular cerebrospinal fluid, ADC = apparent diffusion coefficient, CBF = cerebral blood flow, AAT = arterial arrival time 66
4.7 Clinical features of patients with and without neurocognitive impairment at three months post-SAH. Mann-Whitney U tests were used to determine significance of group differences. 74
4.8 Mean ACE-R results from patients acquired at each scan point and healthy age/gender paired controls 76
4.9 Scan 1 v Control: Common local peaks (unless specified otherwise) of the significant clusters ($P < 0.05$ FWE-corrected) showing increased GM density in SAH patients compared to controls. Local maximum t values correspond to Fig. 4.3. BA, Brodmann area, GM, grey matter 87

5.1 Motion parameters at each MRI scan point 104

5.2 Scan 1 v Control: Common local peaks (unless specified otherwise) of the significant clusters (P < 0.05 FWE-corrected) showing increased connectivity in patients compared to controls. Local maximum t values correspond to Fig. 5.11. BA, Brodmann area. 133
5.3 Scan 3 v Control: Common local peaks (unless specified otherwise) of the significant clusters (P < 0.05 FWE-corrected) showing increased connectivity in patients compared to controls. Local maximum t values correspond to Fig. 5.11. BA, Brodmann area. GM, grey matter 134
5.4 Scan 3 - Neurocognitively impaired v non-impaired patients: Common local peaks (unless specified otherwise) of the significant clusters (P < 0.05 FWE-corrected) showing increased connectivity in those patients with no neurocognitive impairment compared to those with impairment. Local maximum t values correspond to Fig. 5.21. BA, Brodmann area, GM, grey matter 135

6.1 Overview demographics of successfully recruited patients 143

7.1 Physiological parameters for each experimental condition. Results are presented as mean ± standard deviation (SpO_2=oxygen saturations, HR=heart rate, SBP=systolic blood pressure, DBP=diastolic blood pressure, MAP=mean arterial pressure, ETO_2=end tidal oxygen, $ETCO_2$=end tidal carbon dioxide). 164
7.2 Phase contrast flow values for each carotid and vertebral artery. Results are presented as mean ± standard deviation. (**p=0.00183, *p=0.0328 Friedman test) 170

Abbreviations

ACE-R Addenbrookes Cognitive Examination

ADC Apparent diffusion coefficient

ALFF Low frequency oscillation

AMIPB Adult Memory and Information Processing Battery

ASL Arterial spin labeling

AVIC Oxford Acute Vascular Imaging Centre

BOLD Blood Oxygen Level Dependent

CA Cerebral autoregulation

CBF Cerebral blood flow

CBV Cerebral blood volume

CPP Cerebral perfusion pressure

CSF Cerebrospinal fluid

CTP Computed tomography perfusion

CVLT Digit Symbol Modality Test

DCI Delayed cerebral ischaemia

DWI Diffusion weighted imaging

EBI Early brain injury

EEG Electroencephalogram

eNOS Endothelial nitric oxide synthetase

EPI Echo planar imaging

$ETCO_2$ End-tidal carbon dioxide

ETO_2 End-tidal oxygen

fMRI Functional magnetic resonance imaging

FMRIB Oxford Centre for Functional Magnetic Resonance Imaging of the Brain

FSL FMRIB Software Library

GCS Glasgow Coma Scale

HHH Hypertension

IC Independent component

ICP Intracranial pressure

LFO Low frequency oscillation

MEG Magnetoencephalography

MNI Montreal Neurological Institute

NO Nitric oxide

NRES National Research Ethics Service

PBVC Percentage brain volume change

PCASL Pseudocontinuous arterial spin labeling

PET Positron emission tomography

RCT Randomised controlled trial

RF Radio frequency

ROC Receiver-operator curve

RSN Resting state network

SAH Subarachnoid haemorrhage

TBI Traumatic brain injury

TFCE Threshold-free cluster enhancement

VBM Voxel-based morphometry

WASI Weschler Abbreviated Scale of Intelligence

WFNS World Federation of Neurosurgeons

Chapter 1

Overview of thesis

Overview of thesis

Acquired brain injury remains a leading cause of death of disability worldwide and results in a significant socio-economic and health care burden on society. Of the conditions that contribute towards acquired brain injury, aneurysmal subarachnoid haemorrhage (SAH) is the definition of a devastating disease. Caused by the rupture of a cerebral vessel aneurysm, SAH usually occurs unpredictably in relatively young adults, often previously healthy, in full time employment and with dependents, and frequently leads to significant functional and neurocognitive impairment. Although the initial acute cerebral ischaemia caused by aneurysmal rupture accounts for the majority of the mortality and morbidity from SAH, the pathophysiological changes that occur acutely post-rupture remain poorly understood. Furthermore, the calcium channel blocker nimodipine remain the only therapeutic intervention reliably proven to improve outcomes following aneurysm occlusion. The main aim of this thesis is therefore to use high field strength magnetic resonance imaging (MRI) longitudinally, from the first 72 hours to three months post-SAH, to characterise potential biomarkers of early brain injury after aneurysm rupture and correlate these with neurocognitive outcomes. Further studies investigate the efficacy of measuring saccadic latency of eye movements acutely in patients with SAH as well as using an in-vivo model of cerebral hypoxia to explore the mechanisms underlying the beneficial effect of nimodipine in patients clinically.

Chapter 2 is a review of the current evidence relating to delayed cerebral ischaemia after SAH with particular focus on the the importance of the pathophysiological processes underlying

early brain injury. The therapeutic interventions currently used clinically are reviewed as well as potential directions for future research.

Chapter 3 is an introduction to the relevant structural, perfusion and function MRI sequences and analysis techniques used in this thesis. The rationale behind the testing at three months post-SAH used to assess neurocognitive outcomes is also briefly discussed in the context of other research into this area.

There is a growing awareness of the importance of the acute period post-rupture in the determination of both short term and longer term outcomes after SAH. Advances in MRI physics and analysis now offer a number of objective, reliable and non-invasive tools to measure changes in cerebral structure and perfusion at a tissue level. This approach potentially allows greater insight into the significance of early brain injury on both functional and neurocognitive outcomes and how diagnostic and therapeutic MRI biomarkers might be developed. In Chapter 4, we used structural, diffusion-weighted and perfusion MRI sequences longitudinally in patients from the first 72 hours to three months post-SAH. This data was then correlated with detailed neurocognitive outcomes as well as data from age and sex matched healthy controls for comparison. Despite being "good grade" SAH patients and when compared to healthy controls, there were significant global and regional increases in brain volume in the first 72 hours post-SAH. These changes were associated with restricted diffusion suggesting widespread cytotoxic cerebral oedema that remains undiagnosed using current diagnostic imaging. Results from the study demonstrate the potential for the objective and automated assessment of cerebral structural changes in the period following aneurysm rupture to predict neurocognitive recovery and help risk stratify the need for critical care intervention.

The study of brain activity and connectivity at rest provides a unique opportunity for the investigation of the brain substrates of neurocognitive impairment after SAH. As seen in Chapter 4, even in the less severe SAH patients (WFNS Grade I and II), significant global changes to brain tissue occur in the first hours following aneurysm rupture due to early brain injury which are likely to play a key role in determining neurocognitive outcomes in survivors. However, the process by which early brain injury leads to persistent cognitive impairments in patients and the mechanisms and neural correlates underlying functional recovery after SAH remain unclear. The overall aim of Chapter 5 was therefore to investigate changes in resting state functional connectivity following SAH using a whole brain independent component analysis technique and correlate any changes seen with data from Chapter 4 and subsequent neurocognitive outcomes. Results show that at 3 months post-SAH, patients showed increased

functional connectivity compared to healthy controls in a number of functional networks associated with complex cognitive or emotional functions including the default mode network (DMN) (medial and posterior divisions), cerebellum, basal ganglia/thalamus and executive function networks. These changes persisted despite correction for changes in grey matter density - important to note in the context of the widespread structural changes seen in Chapter 4. Next, these differences were already present in the first 72 hours post-SAH in a number of these networks, suggesting that the pathophysiological effects of early brain injury have a significant effect on functional connectivity. Finally, functional connectivity at 3 months post-SAH correlates with neurocognitive outcomes with those patients with the highest functional connectivity having the least cognitive impairment. This effect is present in the first 72 hours suggesting that damage to network integrity at this stage may underlie subsequent poor neurocognitive outcomes.

Chapter 6 explores the potential for the bedside measurement of the saccadic latency of eye movements patients acutely following SAH. Previous studies have shown that that measurements of the time taken for the eyes to respond to a moving visual stimuli ("saccadic latency") can be used reliably as an objective biomarker of neurocognitive function in more chronic neurological conditions such as Huntington's and Parkinson's diseases. In this chapter, we took serial measurements of saccadic latency acutely and at three months post-SAH to assess the potential of saccadometry as a biomarker of early brain injury. Results show a significant negative correlation between acute saccadic latency within 72 hours of rupture and mean grey matter cerebral blood flow, suggesting that cerebral perfusion changes associated with early brain injury post-SAH are reflected in damage to the pathways of eye movement in the brain.

Finally, Chapter 7 used MRI to quantify the changes in cerebral structure, perfusion and function associated with a healthy volunteer model of acute hypoxia, and the effect of calcium channel blockade with nimodipine on these changes. Results suggest a preferential effect of calcium channel blockade in reversing regional MRI changes under conditions of hypoxia. These changes may underlie the benefit seen in aneurysmal subarachnoid haemorrhage in potentially reducing the impact of the global cytotoxic cerebral oedema seen with early brain injury.

This thesis highlights the potential of MRI imaging to offer biomarkers of early brain injury in the acute period post-SAH, to improve prediction of patients most at risk of neurocognitive impairment and to offer new insight into the mechanisms behind the therapeutic benefit seen with nimodipine.

Chapter 2

Neurocognitive outcomes after aneurysmal subarachnoid haemorrhage - looking beyond "vasospasm"

Chapter Overview

Despite improvements in the clinical management of aneurysmal subarachnoid haemorrhage (SAH), a significant proportion of those patients who survive to discharge experience neurocognitive deficits that affect quality of life. Delayed cerebral ischaemia (DCI) has traditionally been viewed as the single most important cause of morbidity and mortality in those patients that survive the initial bleed. The pathological mechanisms underlying DCI are still unclear and the calcium channel blocker nimodipine remains the only therapeutic intervention to show improved outcomes.

However, recently the focus of investigation has moved away from cerebral artery constriction as the sole cause of DCI towards a more multifactorial aetiology. Potential novel mechanisms have been suggested as contributing towards DCI including damage caused in the first 72 hours after aneurysm rupture ("early brain injury"), cortical spreading depression and microthrombosis. Furthermore, there has been renewed interest in the impact of early brain injury on subsequent neurocognitive outcomes itself. Coupled with the recent failure of a large randomised controlled trial of therapeutic vasodilation using the drug clazosentan to show outcome benefit, a greater understanding of the significance of these pathophysiological mechanisms following aneurym treatment is required for developing new approaches to improve morbidity and mortality following SAH.

The purpose of this chapter is to introduce the studies in this thesis by reviewing current understanding and recent developments in SAH research, relating them to current clinical practice and suggesting potential novel avenues for future research.

2.1 Introduction

Aneurysmal subarachnoid haemorrhage (SAH) is a devastating disease frequently leading to death or poor functional outcome. Although it only accounts for 3-5% of all strokes [300], the economic cost of SAH is disproportionately high as it affects younger patients, who often require long-term care and cannot return to work. Over the last three decades, case-fatality rates for SAH have halved due to improved diagnosis, novel approaches to aneurysm occlusion, and advances in critical care management [216, 190]. Despite this, the physical, emotional and economic toll on survivors and society in general remains significant. Accurately defining these "outcomes" after SAH is problematic as functional independence is not the only factor that contributes to quality of life in survivors. Around a third to a half of SAH patients considered to have good clinical outcomes (as measured by the Glasgow Outcome Scale) are left with significant residual neurocognitive deficits that affect daily life [164, 339]. As a result, 40% of patients are unable to return to previous levels of employments [43] and although cognitive dysfunction improves with time, many "recovered" SAH patients continue to experience cognitive deficits 2-3 years later [141]. Only a third of those patients who survive to discharge resume the same employment as before the event and even those patients with "good" functional outcomes are frequently left with significant residual neurocognitive deficits in areas such as memory, executive functioning and language [1, 278].

Delayed cerebral ischaemia (DCI) is a clinical syndrome of focal neurological and/or cognitive deficits that occurs in approximately 30% of patients unpredictably 3-14 days following the initial haemorrhage [81]. Whilst aneurysmal rebleeding is still a significant complication in the hours following the initial bleed, DCI remains the single most important cause of mortality and morbidity in those patients who survive to definitive aneurysm treatment [151].

Historically, it was widely considered that the primary mechanism underlying delayed neurological deterioration after SAH was narrowing of cerebral blood vessels (due to endothelial hypertrophy and vasoconstriction) leading to tissue ischaemia. This process was thought to be mediated by the presence of extravasated blood in the subarachnoid space. Arterial constriction visualised angiographically, in association with neurological deterioration seen clinically soon led to the use of the term “vasospasm” to describe both the clinical and radiological changes. However, an emerging body of evidence now suggests that DCI is likely to have a multifactorial aetiology beyond pure cerebral arterial constriction. This has

Clinical deterioration caused by DCI
The occurrence of focal neurological impairment (such as hemiparesis, aphasia, apraxia or neglect) or a decrease of at least 2 points on the Glasgow coma scale (either on the total score or on one of the components) This should: (1) Last for at least 1 hour (2) Not be apparent immediately after aneurysm occlusion (3) Not be attributed to other causes by means of clinical assessment, CT or MRI scanning of the brain, and appropriate laboratory studies
Cerebral infarction
The presence of cerebral infarction on either: (1) CT or MRI scan of the brain within 6 weeks after SAH (2) The latest CT or MRI scan made before death within 6 weeks after SAH (3) Proven at autopsy This evidence must not be present on the CT or MRI scan between 24 and 48 hours after early aneurysm occlusion and must not be attributable to other causes such as surgical clipping or endovascular treatment Hypodensities on CT imaging resulting from ventricular catheter or intraparenchymal haematoma should not be regarded as cerebral infarctions from DCI

Table 2.1: Proposed definitions of DCI and cerebral infarction after SAH for use as an outcome event in clinical trials and observational studies - adapted from [323]

significant implications on the identification of patients at risk, diagnosis and therapeutic interventions currently available for prophylaxis and treatment of DCI.

In the past, research into DCI has been complicated by the wide range of terms used to define the condition resulting in confusion regarding the underlying pathophysiology. Furthermore, the differing approaches to treating the ruptured cerebral aneurysm (either surgical clipping or endovascular coil embolisation) has made comparison of trials investigating DCI difficult. In 2010, a consensus statement by a multidisciplinary group proposed new definitions for clinical deterioration caused by DCI and cerebral infarction after SAH (Table 2.1 - adapted from [323].

These new definitions will hopefully simplify study comparisons, standardise clinical endpoints and allow accurate meta-analyses to be conducted in the future. Furthermore, in 2011, the Neurocritical Care Society published consensus guidelines on the critical care management of patients following SAH [75]. These have provided guidance and recommendations for the daily management of patients following SAH with a view to preventing DCI. However,

there remains little focus clinically on the potential damage done immediately following the bleed, with the majority of therapeutic neurocritical care interventions still focused on the period after the aneurysm has been secured.

This chapter therefore aims to concentrate on clarifying the role of "vasospasm" after SAH, highlight novel theories regarding the pathogenesis behind DCI and poor neurocognitive outcomes and to summarise the evidence on current and new therapeutic strategies. Through this we hope to introduce this thesis, highlight some of the unanswered questions and propose directions for future research into improving outcomes after SAH.

2.2 Vasoconstriction and DCI

Acute clinical deterioration during the period after SAH has long been known to occur following aneurysmal rupture. Early case reports showed that some patients with early improvement in neurological state following SAH rapidly and unexpectedly deteriorated and died in the days immediately following the initial SAH [25]. Although the cause of the initial bleed was identified as cerebral aneurysm rupture, the mechanism behind this subsequent deterioration was unclear. In 1949, post-mortem examination of 27 fatal cases of SAH demonstrated infarction remote from the site of the ruptured aneurysm, despite apparently patent cerebral vessels [250]. This was attributed to "temporary spasm of the supplying vessels…even of those vessels remote to the aneurysm" and was the first suggestion that cerebral arterial vasoconstriction was linked to delayed clinical deterioration after SAH.

Radiological evidence of cerebral vasoconstriction in association with SAH in patients was first published in 1951. Through the use of serial carotid arteriograms, Ecker and Riemenschneider described the relationship between cerebral vasoconstriction and ruptured cerebral aneurysms [15]. Vessel narrowing was greatest near the site of the ruptured aneurysm – an area that correlated with the largest amount of extravasated blood products – and it was noted that vasoconstriction was rarely seen in angiograms performed 26 days post-SAH. They hypothesised that following the initial bleed, "vasospasm" of cerebral arteries might lead to impaired circulation in the territory of the brain supplied by the affected vessel. In 1978, a classification for SAH based on the pattern of blood distribution seen on CT in a case series of 47 patients with SAH reported an almost exact correlation between the site of major subarachnoid blood clots and the location of severe angiographic vasoconstriction [100]. Conversely, angiographic vasoconstriction was invariably absent in those patients with minimal subarachnoid blood load. Further angiographic evidence in almost 300 SAH

patients showed that this vasoconstriction began day 3 post-SAH, was maximal at days 6-8 and had disappeared by day 12 [331].

As a result of this work, the concept of extravasated blood from aneurysm rupture leading to a chain reaction of cerebral artery vasoconstriction, tissue infarction and clinical deterioration has been widely held amongst both clinicians and researchers. However, although SAH is undoubtedly associated with cerebral vasoconstriction, and cerebral infarction following SAH is strongly associated with poor clinical outcomes [98, 320], the exact contribution of cerebral vasoconstriction remains unclear for the following reasons:

1. Although the incidence of angiographic vasoconstriction during the second week post-SAH (the period of peak DCI incidence) is around 70% [81], the incidence of DCI as detected clinically is only around 30% [80].

2. Following SAH, patients can develop cerebral infarction in a vascular distribution unaffected by angiographic vasoconstriction [213] and cerebral infarction seems to exert a direct effect on poor outcome independent of angiographic vasospasm [321].

3. The temporal relationship between angiographic evidence of vessel constriction and DCI is poor [205].

4. The calcium channel antagonist nimodipine remains the only pharmacological treatment to improve outcomes from DCI yet this benefit is achieved without angiographic evidence of cerebral vasodilation [97, 237].

5. Treatment of angiographic vasospasm - either pharmacologically or radiologically - does not always lead to improvements in clinical and functional outcomes [192, 243].

Recently a number of new theories have been proposed that may contribute towards understanding the pathophysiology behind both DCI and neurocognitive impairment after SAH.

2.3 Novel theories regarding DCI pathogenesis

2.3.1 Early brain injury

Although the initial acute cerebral ischaemia caused by aneurysmal rupture accounts for the majority of the mortality and morbidity from SAH [41], the pathophysiological changes

that occur at this time remain poorly understood and there are few therapeutic or diagnostic interventions available. "Early brain injury" is a term that refers to the damage that occurs to the brain in the first 72 hours after the initial bleed [166] - see Figure 2.1 . Although this period is before the onset of DCI, it seems probable that the physiological changes occurring at this time may directly influence the likelihood and severity of later ischaemic complications in patients after SAH.

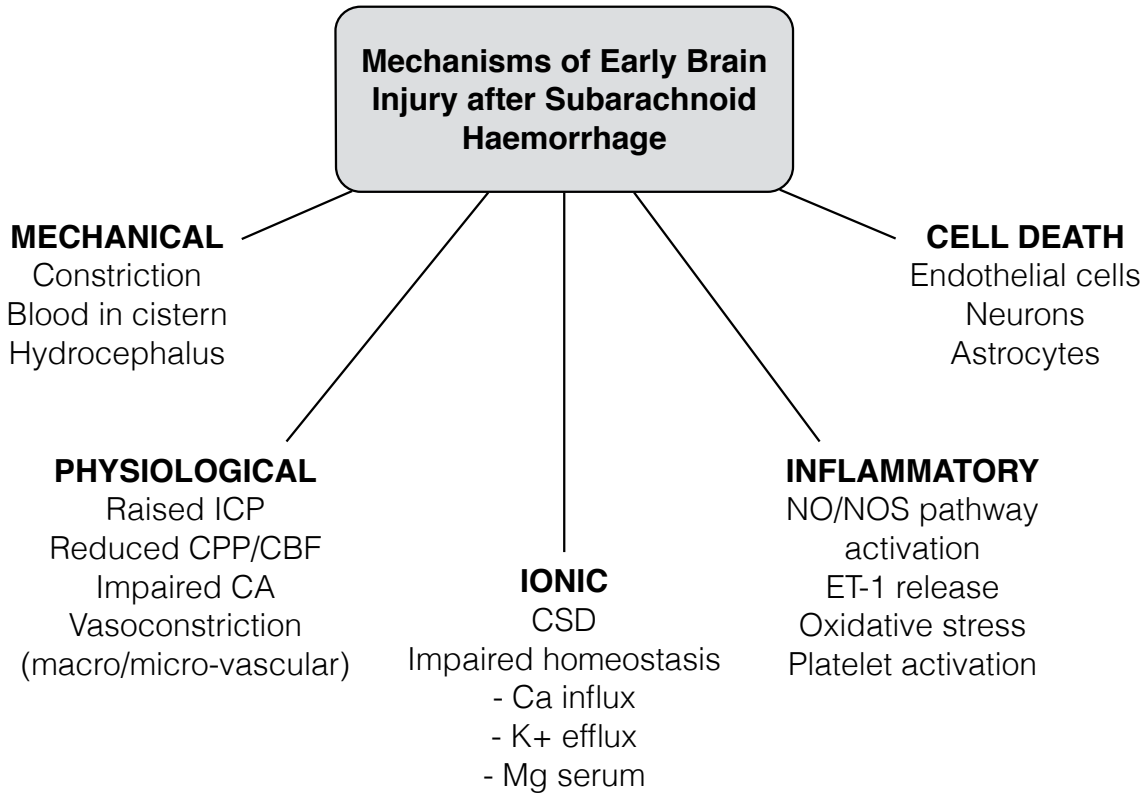


Fig. 2.1: Mechanisms of early brain injury after SAH. Abbreviations: ICP = intracranial pressure, CPP = cerebral perfusion pressure, CBF = cerebral blood flow, CA = cerebral autoregulation, CSD = cortical spreading depression, NO/NOS = nitric oxide/nitric oxide synthetase, ET-1 = endothelin-1. Adapted from reference [280]

The majority of data on the pathophysiological changes that occur at the time of aneurysm rupture derives primarily from animal studies of SAH - mainly in rats. Although results obtained experimentally seem to mirror measurements in patients with aneurysmal re-bleeding and intra-cranial pressure monitoring in situ, the majority of animal models rely on iatrogenic damage to cerebral vessels to simulate aneurysm rupture and induce subarachnoid bleeding. As a result, some authors have questioned the applicability of rat models to the study of SAH

in humans [302] and there is a need for new animal models of SAH with a high incidence of spontaneous cerebral aneurysm rupture [11].

Initial physiological changes

At the time of the SAH, blood extravasates from a rupture in the aneurysm and leaks under high pressure into the subarachnoid space. The size of the rupture defect correlates with the volume of blood clot present [293]. Within minutes of aneurysm rupture, there is an associated rapid rise in intracranial pressure (ICP), with the rate of rise likely to reflect the severity of the initial bleed. This accounts for the "thunderclap" headache seen clinically in patients and is often accompanied by syncope caused by a sudden reduction in cerebral blood flow (CBF) and cerebral perfusion pressure (CPP) [218]. This sharp rise in ICP is likely to be aimed at arresting the initial aneurysmal bleed and preventing subsequent re-bleeding - so called “brain tamponade” [218] - and putative causative mechanisms include increased intracranial volume secondary to the bleed, vasoparalysis (leading to increased cerebral blood volume) and cerebrospinal fluid drainage obstruction due to blood clot [118].

There are two distinct patterns to this rise in ICP. In most patients, ICP rises to a value approximating diastolic blood pressure, then falls to slightly above baseline [28] This is usually accompanied by small volume haemorrhage and the presence of cerebral oedema. The second pattern of ICP rise is less common and is characterised by a sustained rise in ICP due to enlarging haematoma or the development of acute hydrocephalus [219, 16]. Peak ICP values at the time of aneurysmal rupture correspond to both the amount of blood released into the subarachnoid space and the rate of haemorrhage [28, 29, 276]. Marked acute cerebral vasoconstriction at this time has also been described that seems to occur independently of changes in CPP and ICP and is likely to contribute to the cerebral ischaemia from aneurysmal rupture [29].

Cerebral oedema

Cerebral oedema is a common feature after SAH both experimentally and in patients. It is evident on admission CT scans in 6-8% of patients [151, 57] and develops over the first six days in an additional 12% [57] suggesting it develops in the classic biphasic manner commonly described in ischaemic stroke [46]. One of the first complications related to both the pathophysiological aspects of aneurysm rupture and subsequent pathways of early

brain injury is disruption of the blood brain barrier due to apoptosis of endothelial cells and perivascular astrocyte cell death [155, 229, 111, 166] - see Figure 2.2.

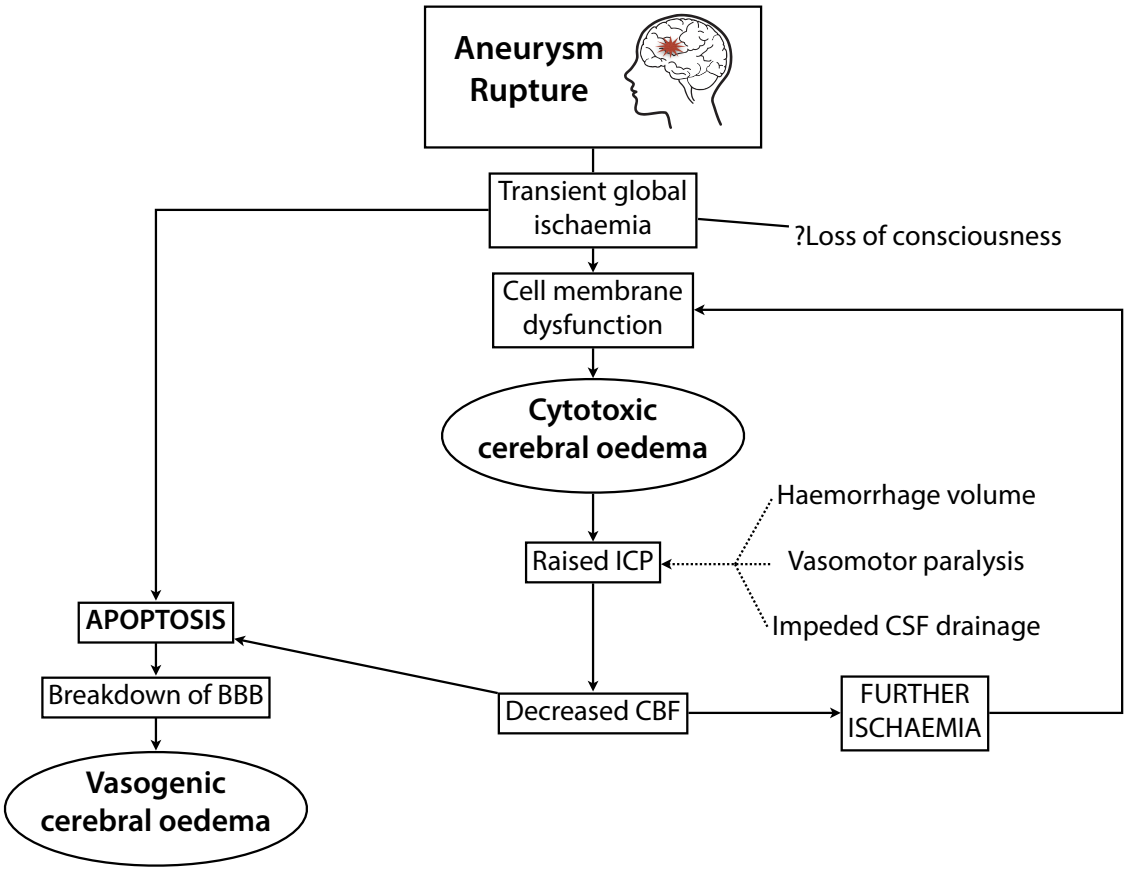


Fig. 2.2: Mechanisms underlying the formation of cerebral oedema after aneurysm rupture in SAH

This results in classic vasogenic oedema which has been documented in animal models of SAH [76]. However, as ICP reaches levels approaching mean arterial pressure, this results in cytotoxic edema as early global ischemic injury causes failure of cell membrane regulatory channels and substantial damage to blood brain barrier integrity.

Cerebral autoregulation

Acute impairment of cerebral autoregulation is seen as a consequence of the initial aneurysmal rupture [246, 172]. Cerebral autoregulation is the inherent ability of blood vessels to keep CBF relatively constant over a wide range of systemic BP levels by means of complex myogenic, neurogenic and metabolic mechanisms [14]. In humans, CBF autoregulation typically operates between mean systemic blood pressures of approximately 60 and 150 mmHg [231]. If these autoregulatory mechanisms are disrupted, CBF becomes dependent on

CPP and blood viscosity and changes in systemic arterial blood pressure and ICP can worsen cerebral oedema and brain tissue ischaemia.

Inflammation and oxidative stress

There is evidence to suggest early activation of inflammatory pathways following aneurysmal rupture and that the extravasated blood is responsible for a cascade of reactions involving the release of pro-inflammatory and vasoactive factors [19]. An early rise in pro-inflammatory cytokines including tumour necrosis factor-alpha, interleukin-6 and interleukin-1 receptor antagonist has been documented in both serum and CSF of patients following SAH, and correlates with acute and delayed cerebral ischaemia and poor outcome [196].

2.3.2 Cortical spreading depression

Over the last few years, cortical spreading depression (CSD) has been identified as a potential novel pathophysiological mechanism contributing to DCI. The term describes a depolarisation wave in cerebral grey matter that propagates across the brain at 2-5 mm/min and results in depression of evoked and spontaneous EEG activity [180]. First demonstrated experimentally in the 1940's in rabbit cortex, the process was originally regarded as experimental artefact with little relevance to neurological disease in humans. Recently however, there has been a resurgence of interest in CSD. Electrocorticographic recordings from invasive subdural recording strips, combined with laser Doppler measurements of regional CBF have allowed accurate quantification of the vascular changes associated with CSD. As a result, it has been implicated in the pathophysiology of a number of neurological diseases including migraine [176], malignant hemispheric stroke [77], traumatic brain injury [299], and DCI following subarachnoid haemorrhage [84].

In order to demonstrate CSD experimentally in healthy brain tissue, either mechanical or electrical stimulation of the cortex is required [179]. Propagation of the CSD wave silences spontaneous and evoked synaptic activity in the brain for 5 to 15 minutes, and is followed by spontaneous return to normal function [177]. Associated with the CSD are characteristic cerebrovascular changes: a brief period of vasoconstriction prior to the CSD, vasodilation accompanying the spreading wave front followed by delayed tissue hypoperfusion after the wave [175] - Figure 2.3.

In contrast to this, in the injured brain, CSDs can occur spontaneously and recovery of normal function can be prolonged, contributing to tissue ischaemia. Along with this, the

classic pattern of a transient, large hyperperfusion accompanying the CSD wave front seems to be different. In SAH, there is good evidence from research in animal models as well as multicentre patient studies, that CSDs occur following the initial bleed [84, 86]. CSDs can occur as isolated events or as clusters and there appear to be three distinct vascular responses to CSD in SAH patients: physiological (i.e. spreading hyperperfusion), absent (i.e. nil change from baseline) and inverse haemodynamic (i.e. spreading ischaemia) [84].

This spreading ischaemia was first described in a rat model of DCI and results from local microvascular dysfunction. It is thought that with each depolarisation, there is an associated profound hypoperfusion of the cortex due to vasoconstriction [284]. With each wave of spreading depression, the hypoperfused segments of cortex do not get the chance to recover and are therefore exposed to recurrent episodes of tissue hypoxia.

The incidence of CSDs measured in patients following SAH also seems to correlate with the time frame for the development of DCI - data from one study demonstrating that 75% of all CSDs recorded occurred between the fifth and seventh day after SAH [37]. CSDs also seem to occur in the absence of angiographic vasoconstriction. Despite placement of nicardipine pellets around the middle cerebral artery (at the time of surgery) to minimise proximal vasoconstriction, spontaneous depolarisations still occurred in 10 out of 13 patients [336], casting further doubt on the exact nature of the contribution of proximal vessel constriction to DCI.

2.3.3 Microthrombosis

A number of studies have shown that the coagulation cascade is activated early following the initial SAH and importantly, preceding the onset of DCI. This is most likely as a result of endothelial damage from aneurysm rupture and subsequent acute cerebral ischaemia and there is serological, clinical and post-mortem evidence that this early activation is an early predictor of both DCI and cerebral infarction.

Serological studies of patients following SAH has demonstrated activation of the coagulation cascade and impairment of the fibrinolytic cascade. Levels of platelet-activating factor (PAF) start to increase within 4 days after SAH suggesting increased platelet activation and adhesion [133]. Furthermore, elevated concentrations of serum von Willebrand Factor (vWF) and CSF tissue factor (the primary initiator of coagulation) in the first few days after SAH have been shown to predict the occurrence of DCI, cerebral infarction and poor outcome [106, 134] Other studies have shown that overactive inhibition of fibrinolysis is associated with DCI

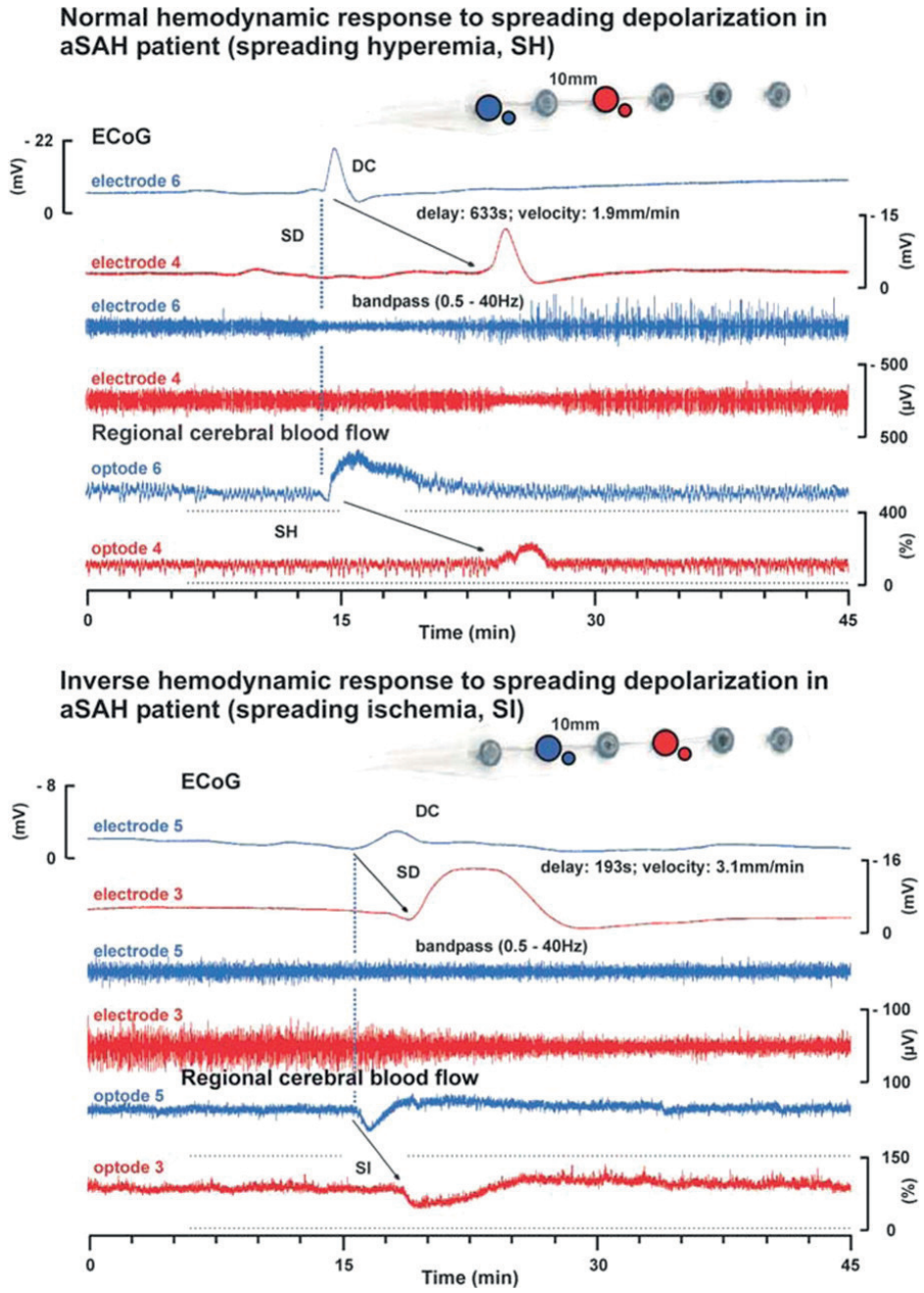


Fig. 2.3: Normal and pathological responses to cortical spreading depression (CSD) in patients with SAH. The upper half of the figure shows the normal hemodynamic response to spreading depolarization (CSD) in the human brain in a patient with SAH. The subdural opto-electrode strip is shown in the upper right corner. The six traces represent simultaneous recordings of a single spreading depolarisation that propagates from opto-electrode 6 (blue) to 4 (red). The calibration bar of trace 4 also applies to trace 3 and that of trace 6 also applies to trace 5. The four upper traces identify the spreading depolarization electrophysiologically. Traces 1 and 2: direct current (DC) electrocorticogram (ECoG) with negative shift of spreading depolarization. Traces 3 and 4: band-pass filtered ECoG (0.5 to 45 Hz) with spreading depression of activity. The spreading depolarization propagates at a rate of about 1.9 mm min21 assuming an ideal linear spread along the recording strip. Traces 5 and 6: Normal spreading hyperaemia in response to spreading depolarization recorded by laser-Doppler flowmetry as reported previously [84]. The lower half of the figure demonstrates the inverse hemodynamic response to spreading depolarization in another patient with aSAH. In this case, the spreading depolarization propagates from opto-electrode 5 (blue) to 3 (red) (propagation rate: 3.1 mm min^{-}1). The high-frequency activity is already suppressed by a preceding CSD at electrode 4 (trace 9), when depression of activity is induced by spreading depolaridation at electrode 5 (trace 10). Traces 11 and 12: typical inverse haemodynamic response to spreading depolarization as characterized by a severe decrease of regional cerebral blood flow (CBF) in response to the depolarization. Such severe decrease of regional CBF in response to CSD is termed spreading ischaemia. The prolonged negative cortical DC shift (compare trace 8) is the defining electrophysiological feature for the inverse haemodynamic response. It indicates that the hypoperfusion is significant enough to produce a mismatch between neuronal energy demand and supply [84, 83].

[142] and that elevated levels of fibrin degradation products and D-dimer in the CSF of patients after SAH are associated with DCI, cerebral infarction and poor outcome [233].

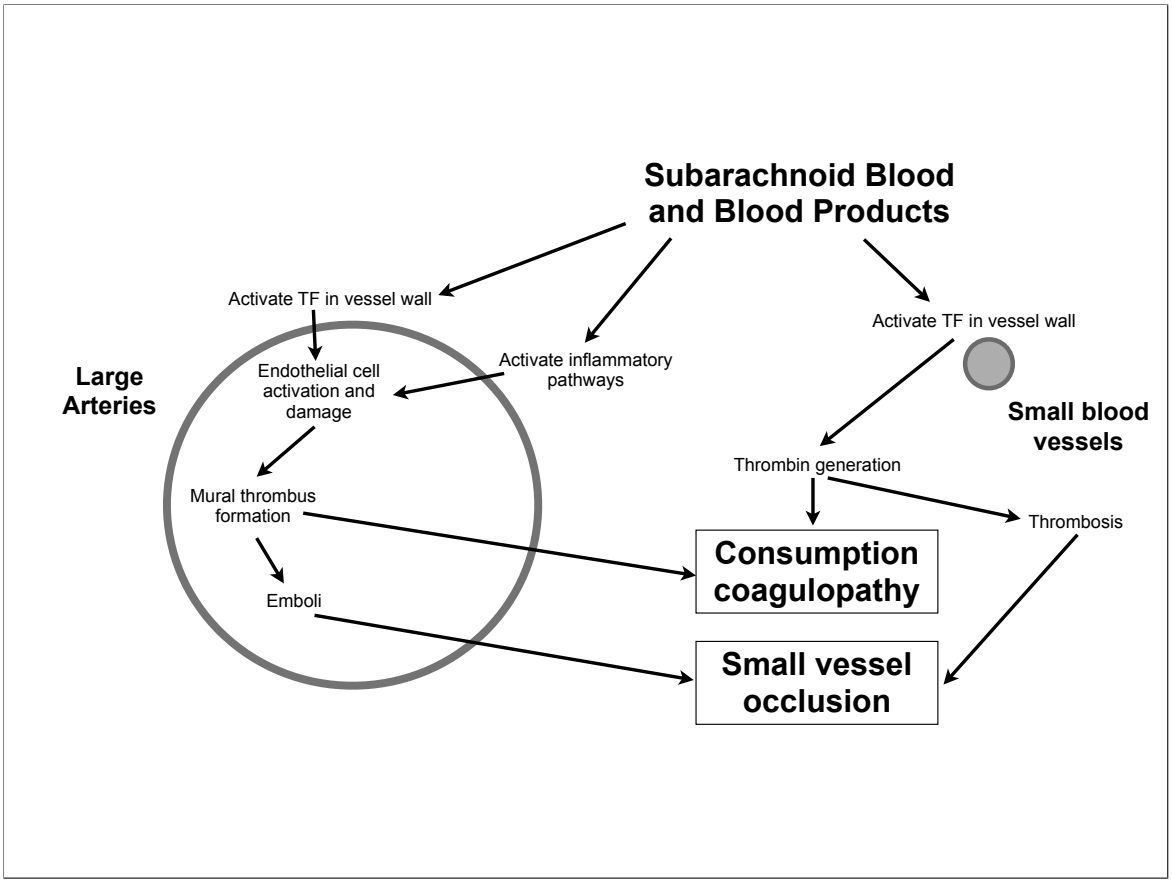


Fig. 2.4: Potential mechanisms of microthrombosis formation after SAH. Abbreviation: TF = Tissue Factor. Adapted from [294].

Further evidence to support the role of microthrombosis in DCI is provided by trans-cranial Doppler (TCD) detection of micro-emboli in SAH patients. A prospective study in which SAH patients were monitored using TCD showed that micro-embolic signals were present in up to 70% of SAH patients, with a non-significant trend towards an increased incidence of micro-emboli in those patients that went on to develop DCI [253].

Pathological studies of SAH patients post-mortem have also demonstrated evidence of micro-thrombi. Patients with DCI have significantly more micro-thrombi in areas showing cerebral infarction than those patients that die from aneurysmal re-bleed or hydrocephalus [301]. Microthrombosis is also correlated with the amount of overlying free subarachnoid blood and clinical and pathological signs of ischaemia [294] Interestingly, a post-mortem study into micro-thrombosis after SAH showed that while cortical ischaemic lesions were present

in 77% of patients, there was no significant association between the presence of these lesions and angiographic vasospasm or aneurysm location [202].

2.3.4 Collateral cerebral circulation

Although the importance of the pathophysiological recruitment of collaterals in the setting of chronic haemodynamic insufficiency (such as carotid artery stenosis) has been well documented [324, 254], the impact of collateral flow in acute cerebral ischaemia such as that seen after SAH is less clear. The cerebral collateral circulation consists of a subsidiary network of vascular channels that stabilise cerebral blood flow when principal conduits fail [184]. Primary collaterals include the anterior and posterior communicating arteries of the circle of Willis, which immediately divert cerebral blood flow to ischaemic regions through existing anastomoses. Secondary collaterals include leptomeningeal vessels and reversal of blood flow in the ophthalmic artery, and are normally only recruited when the primary collateral circulation is inadequate.

Early clinical improvement in ischaemic stroke patients is linked to the presence of cerebral collateral blood supply [309]. MRI studies of patients with ischaemic stroke have also shown that collateral flow in the circle of Willis is associated with a reduction in the prevalence of ischaemic lesions and minimises the degree of residual tissue hypo-perfusion following arterial occlusion [22]. Little attention is generally paid to pre-treatment collateral status in clinical practice in SAH patients. This is despite considerable heterogeneity in the presence of collateral vessels demonstrated in patients with ischaemic stroke [22, 21].

Following SAH, we speculate that it may be that patients with greater capacity for collateral flow suffer less initial ischaemic damage from early brain injury. Furthermore, we speculate that recruitment of collateral vessels may be the mechanism behind the reversal of neurological deficits seen with induced hypertension as part of triple-H therapy. At the moment, clinical assessment of collateral flow is usually limited to CT or MR angiography with the former requiring ionising radiation and both requiring intravenous contrast. Improvements in MRI sequences are allowing the non-invasive assessment of flow in the circle of Willis as well as other cerebral collateral pathways such as the ophthalmic artery. Identifying those patients with poor collateral flow may enable earlier application of treatment strategies such as induced hypertension with the aim of improving cerebral perfusion.

2.4 How have clinical therapeutic interventions aided the understanding of DCI?

At present, the majority of therapeutic strategies targeting DCI are focused on reducing secondary ischaemic brain injury and treating cerebral vasoconstriction. However, as seen above, the exact role of cerebral vasoconstriction remains unclear and as a result, the rationale behind some treatment strategies requires further examination.

2.4.1 Clazosentan

Clazosentan is an endothelin-A antagonist that was heralded as a potential pharmacological treatment for DCI after SAH. As endothelin (ET) is known to play a key role in maintaining vascular tone in blood vessels, it was hypothesised that pharmacological antagonism of ET receptors might be of therapeutic benefit in reducing cerebral vasospasm and DCI in patients. The endothelin receptor antagonist TAK-044 was trialled but showed no beneficial effects on DCI, cerebral infarction or functional outcome at 3 months (as measured by the Glasgow Outcome Score) – a result put down to unselective antagonism of both ET-A and ET-B receptors by the drug [282]. Further studies using clazosentan, a selective ET-A receptor antagonist showed promise with reductions in the frequency and severity of vasospasm after SAH [311] and a reduction of vasospasm-associated impaired cerebral perfusion [24]. Unfortunately, the subsequent multicentre CONSCIOUS-1 randomised control trial showed that despite significant reductions in angiographic cerebral vasoconstriction, clazosentan failed to show significant effect on morbidity and mortality and no obvious effect on functional outcome [192]. The further failure of clazosentan to show significant outcome benefit in a subgroup of SAH patients treated with surgical clipping led to the early termination of the CONSCIOUS-2 trial and the cancellation of the planned CONSCIOUS-3 trial in SAH patients treated with endovascular coiling.

What was behind the failure of clazosentan to improve ischaemic outcomes after SAH despite such early promise? From the above CONSCIOUS trials, it seems that despite questions raised regarding study design, duration of treatment and scoring scales [340] the pathophysiological mechanism behind DCI is likely to extend beyond pure large vessel vasoconstriction. The effect of clazosentan on the cerebral microcirculation is unclear and the drug seems to have little effect on the coagulation disturbances seen after SAH such as microthrombosis [53].

2.4.2 Nimodipine

Despite extensive research into pharmacological treatment of DCI, the L-type dihydropyridine calcium channel antagonist nimodipine remains the only intervention to consistently reduce the incidence of DCI and improve outcomes after SAH. Calcium plays a critical role in cellular communication and regulation and is important for the maintenance of normal cerebral vascular tone [235]. Uncontrolled intracellular shifts in calcium concentration associated with cerebral ischaemia cause irreversible cell destruction and death, especially in the central nervous system [55] and as a result, calcium is likely to play an important role in initiating, mediating and propagating damage to cells following subarachnoid haemorrhage.

Nimodipine was first trialled as a treatment for DCI due to its preferential vasodilation of the cerebral circulation and experimental work showing reduced impairment of post-ischaemic reperfusion [125]. The largest clinical trial investigating the effect of nimodipine on DCI (the British Aneurysm Nimodipine Trial) randomised patients to either oral nimodipine 60mg at 4 hourly intervals or placebo for 21 days following SAH [239]. The trial showed significant reductions in both the incidence of cerebral infarction and poor neurological outcomes at 3 months post-SAH. Further meta-analyses, including a Cochrane review in 2007 [78], have echoed these findings and led to oral nimodipine becoming a standard of care for patients from the time of the initial haemorrhage [78, 97].

The precise mechanism behind the beneficial effects of nimodipine remains unclear and seems independent of any action on large vessel angiographic vasoconstriction [237]. It may be that nimodipine has a neuroprotective effect in SAH by blocking calcium influx following tissue ischaemia at a neuronal level [242]. However, given the fact that nimodipine does not exert a beneficial effect on other diseases that lead to cerebral ischaemia such as ischaemic stroke [135] or traumatic brain injury [173], it seems likely nimodipine is acting on a pathophysiological mechanism specific to SAH. A systematic review of calcium antagonists showed that nimodipine significantly increases endogenous fibrinolytic activity and that this effect does not extend to other classes of calcium antagonists such as phenylalkylamines [322]. This may act to reduce the incidence of microthrombosis after SAH. Finally, there is evidence that nimodipine antagonises cortical spreading ischaemia in rats [85] and this may therefore be of importance given the potential role of CSD in the pathogenesis of DCI.

2.4.3 Induced hypertension, hypervolaemia and haemodilution ("triple-H" therapy)

Haemodynamic strategies to induce hypertension, hypervolaemia and haemodilution remain the mainstay of the neurocritical care management of DCI. However, despite its widespread use, much of the literature supporting triple-H therapy is only of moderate quality with the few randomised controlled trials undertaken only addressing prophylactic use.

The physiological rationale behind triple-H therapy is based on the haemodynamic consequences of cerebral arterial vasoconstriction. As vessel diameter decreases, cerebrovascular resistance shifts from smaller penetrating arterioles to the major branches of the circle of Willis. As a result, brain tissue supplied by these narrowed proximal branches loses its capacity for autoregulation and cerebral blood flow varies directly with systemic blood pressure according to the Hagen-Pouseuille law. Therefore, given that the vessel diameter is fixed, the only variables that can potentially be manipulated to improve cerebral blood flow in patients after SAH are the pressure gradient (i.e. systemic blood pressure) and blood viscosity (i.e. haematocrit).

Early anecdotal evidence showed that hypotension could lead to neurological deficits in patients following "cerebrovascular accidents" [70]. This seemed especially significant in those patients where hypotension was associated with evidence of structural narrowing of major cerebral blood vessels. As a result, induced hypertension was trialled in patients following SAH with an early case series showing reversal of neurological deficits in 6 out of 7 patients through the use of noradrenaline to increase blood pressure and volume expansion with colloid [163]. A larger retrospective review of induced hypertension and volume expansion in 58 patients also demonstrated reversal of neurological deterioration [152]. Of note though were the significant complications that occurred in this study from this approach including aneurysmal re-bleeding (19%), pulmonary oedema (17%), dilutional hyponatraemia (3%) and coagulopathy (3%).

Recent research into the role of triple-H therapy in DCI has attempted to use physiological outcome measures such as brain tissue oxygenation and CBF to assess the individual contribution of each of the components of haemodynamic augmentation i.e. induced systemic hypertension (either through vasopressors or inotropes), volume expansion and haemodilution. A Cochrane review of 3 studies analysing the evidence supporting volume expansion therapy concluded a lack of benefit, and that hypervolaemia could potentially increase compli-

cations after SAH [249]. Furthermore, a recent meta-analysis demonstrated no good evidence from controlled studies for a positive effect of triple-H therapy or any of its components on cerebral blood flow after SAH [67]. Haemodilution did not increase cerebral blood flow and hypervolaemia was only beneficial in one of the seven trials.

The consensus guidelines recently published by the Neurocritical Care Society [75] make a number of recommendations regarding each of the individual components of triple-H therapy. It seems that any benefit that might occur from haemodynamic manipulation of SAH patients is likely to primarily derive from increasing or stabilising systemic blood pressure and avoidance of hypovolaemia. Due to its widespread use, randomised outcome studies of induced hypertension versus untreated control groups are now likely to be difficult to achieve. Further research is needed into the timing and effects of different pharmacological and mechanical strategies for inducing hypertension on outcomes from DCI.

2.4.4 Magnesium

Magnesium is a non-competitive calcium channel antagonist and potent vasodilator with known neuroprotective properties. Hypomagnesaemia occurs in more than half of patients with SAH, is related to severity of bleed and is predictive of DCI [312] As a result, a number of studies have investigated the role of intravenous magnesium therapy in preventing and treating DCI.

In animal models of SAH, magnesium reverses delayed cerebral arterial vasoconstriction and reduces the size of ischaemic lesions [314]. Furthermore, there is evidence to suggest magnesium reduces the rate and frequency of CSD [316]. However, the only phase III randomised controlled trial conducted to date - the Intravenous Magnesium Sulphate for Aneurysmal Subarachnoid Haemorrhage (IMASH) trial – disappointingly showed no difference in the proportion of patients with a favourable outcome at 6 months nor in the incidence of DCI or cerebral infarction [342]. Furthermore, a post-hoc analysis showed an association between high plasma magnesium concentrations and worse clinical outcomes [341].

The results of this trial have considerably dampened enthusiasm for the routine use of magnesium and an updated systematic review and meta-analysis in 2011 further demonstrated no beneficial effect of magnesium in DCI [337]. As a result of this, it has been recommended in the Neurocritical Care Society guidelines that magnesium should not routinely be administered to patients following after SAH (although hypomagnesaemia should be avoided) [75].

2.4.5 Statins

There has been much interest in statins in the management of SAH, for both the prevention and treatment of DCI. Although these drugs are known inhibitors of cholesterol production, there is evidence to suggest that statin therapy has other "pleiotropic" vascular effects that involve restoring or improving vascular function. These include beneficial actions on endothelial inflammation [236], oxidative stress [227] and the inhibition of platelet adhesion and aggregation [303] that may underlie the benefits they exert on atherosclerotic cardiovascular disease. Given statins are relatively safe, cheap and easy to administer, they seem a logical intervention to trial in the prevention of DCI.

Animal studies have demonstrated that statins may ameliorate early brain injury after experimental SAH [54] and improve neurocognitive outcomes [200], providing hope that this beneficial effect in animal models might translate clinically. To date, four prospective, randomised, placebo controlled trials have been published evaluating the efficacy of statins in the prevention of DCI. These investigated a combined total of 190 patients with 3 of the studies trialing simvastatin 80mg for 14-21 days [56, 191, 318] and one study trialing pravastatin 40mg for a maximum of 14 days [310]. Although the first two published studies reported statins to have beneficial effects in reducing episodes of DCI, trans-cranial Doppler vasospasm and mortality, these findings could not be replicated in the more recent publications. There was also significant variation in the proportion of clipped and coiled patients and high-grade patients between the studies making comparison of the results difficult. Additionally, although up to 50% of patients in the pravastatin trial did not complete the course of treatment, results were still analysed on an intention-to-treat basis [310]. A recent meta-analysis of randomised controlled trials into statins included these four studies and reported that statins had no significant effect on any of the relevant outcomes including clinical episodes of DCI, mortality, poor neurological recovery and trans-cranial Doppler vasospasm [319]. These negative results have further been supported by the long awaited publication of the Simvastatin in Aneurysmal Subarachnoid Haemorrhage ("STASH") trial this year which showed no outcome benefit with statins in SAH [159] and a smaller, propensity matched study of statins which showed no effect on cognitive outcomes [343]. Furthermore, any potential benefit of statins does not seem to be dose related [338].

Given the efficacy of statin pre-treatment in animal models [50], the impact of prior statin use in patients presenting with SAH has also been investigated in observational studies. Two studies demonstrated reductions in DCI and improved clinical outcomes in SAH patients

with previous statin use [230, 199]. However, continuity of statin therapy on admission was not clearly discussed in either study and further studies have shown either no benefit or increased risk of DCI in patients pre-treated with statins (although this latter finding was reported as being caused by statin withdrawal on admission) [211, 286].

Although statin therapy seems safe post-SAH in statin-naïve patients, the Neurocritical Care Society Guidelines only recommend that patients on statins prior to presentation with SAH should have their medication continued in the acute phase but only suggest that acute statin therapy "may be considered" in statin-naïve patients [75]. Given the more recent results of studies described above, it now does not seem appropriate to routinely prescribe statins as a therapeutic intervention following SAH.

2.4.6 Anti-coagulant/anti-fibrinolytic therapy

As activation of the coagulation cascade and microthrombi may play a role in the pathogenesis of DCI, attention has focused on drugs targeting these processes. Aspirin was trialled in an attempt to reduce DCI by reducing platelet adhesion and aggregation. A systematic review of 5 trials totalling around 700 patients suggested a reduction in risk of DCI in SAH patients. However, an RCT investigating the effect of 100mg aspirin was stopped early as an interim analysis suggested the probability of a beneficial effect was negligible [313] Furthermore, although a Cochrane review in 2007 suggested a trend towards better outcome in patients treated with anti-platelet agents, this was non-significant and accompanied by the possibility of an increase in the risk of haemorrhagic complications [79].

The role of low molecular weight heparins (LMWH) in DCI has also been investigated. The anti-coagulant activity (via antagonism of antithrombin III) of LMWH may prevent the formation and spread of microthrombi and there is evidence that heparins may have neuro-protective effects. They act on complement and neutrophils to reduce cerebral inflammation in response to ischaemic lesions [112, 183] have anti-oedematous properties [348] and may reduce intra-neuronal calcium release following ischaemic injury [147]. However, two large placebo controlled RCTs studying enoxaparin and DCI demonstrated contradictory results [285, 347] and further, large, multicentre trials are required to clarify whether these drugs have a beneficial effect on reducing DCI.

A Cochrane review of anti-fibrinolytic therapy for the prevention of aneurysmal re-bleeding showed that reductions in mortality from re-bleeding were offset by an increase in poor outcome from DCI [255]. Other studies have investigated the potential of intra-thecal

fibrinolysis and although a systematic review showed a significant risk reduction of DCI and poor outcome, only one of nine included studies was an RCT and the role of intra-thecal fibrinolysis remains unclear [4].

2.5 Future directions for research

2.5.1 Determining the genetic determinants of early brain injury

It seems logical that genotypic variability may define the susceptibility of individual patients to both the initial ischaemic injury caused by aneurysmal rupture and subsequent secondary damage caused by DCI. Furthermore, genetic predisposition to the individual pathophysiological mechanisms that may underlie DCI such as cerebral vasoconstriction, CSD and microthrombosis may vary between individual patients.

2.5.2 Endothelial nitric oxide synthase

As before, much of the research into genetic influences underlying DCI has been focused on reducing cerebral vasoconstriction – in particular through targeting the gene encoding the endothelial isoform of nitric oxide synthase (eNOS). Nitric oxide (NO) inhibits smooth muscle proliferation and inflammation - both pathophysiological features of the cerebral vasoconstriction seen after SAH. There is evidence that certain eNOS polymorphisms are significantly associated with angiographic cerebral arterial narrowing following SAH (as well as cerebral aneurysm rupture itself) [158, 162]. However other research has shown no association between eNOS polymorphisms and cerebral infarction or the incidence of clinical deterioration in patients [162]. This suggests that the influence of eNOS polymorphisms is primarily limited to vascular constriction and further questions the significance of the contribution of vessel narrowing to DCI.

2.5.3 Apolipoprotein E

Further research into the genetics of DCI has investigated the association between apolipoprotein E (ApoE) and neuro-cognitive outcomes after SAH. ApoE is a carrier protein that combines with lipids to form lipoprotein particles which is involved in the metabolism and transport of lipids in the central nervous system. Three common alleles of the ApoE gene are found in humans - ε2, ε3 and ε4. The presence of the ε4 allele is known to be associated

with increased risk of developing Alzheimer's disease [61] as well as poor outcomes after traumatic brain injury [304], and intracerebral haemorrhage [2] - though interestingly this association does not seem to extend to ischaemic stroke [198].

In general, research into the association between ApoE and DCI has been conflicting. Animal models of SAH have shown that mice expressing the 4 protein have greater cerebral vasoconstriction, functional deficit and mortality after SAH than mice with the 3 protein [110]. Further work in SAH patients demonstrated an association between ApoE4 and poor functional outcomes [217] and a meta-analysis of eight observational studies concluded that the expression of the 4 allele is associated with an increased risk of poor outcome and delayed ischemia [174].

However, the most recent prospective study conducted found that neither the 2 or 4 allele were associated with infarction or poor outcome and concluded that ApoE polymorphisms have no prognostic value for outcome after SAH [149]. Furthermore, the largest association study of ApoE and SAH showed no significant difference between the presence of the the ApoE4 genotype and functional outcomes at 3 and 6 months when controlling for age, size of haemorrhage and clinical severity of SAH [208]. However, when severity of cerebral arterial vasospasm was controlled between groups, individuals with the 4 allele had worse functional outcomes at both time points. This suggests that the 4 allele may not directly influence cerebral vasoconstriction and may instead act to modulate the response of brain tissue to ischaemia.

Although a number of theories have been proposed including protection from oxidative injury [208] and suppression of lymphocyte proliferation and glial cytokine secretion [234], further work is required to clarify the specific mechanism by which ApoE is associated with DCI and whether certain alleles can be used to reliably identify patients at risk. Additionally, further investigation of the impact of genetic influences on response to therapeutic interventions such as induced hypertension, statins and nimodipine is required, in addition to further research into those genes that regulate inflammation and fibrinolysis.

2.5.4 What is the interaction between anaesthetic agents and CSD?

Many SAH patients require surgical, endovascular or neurocritical care interventions where significant quantities of anaesthetic sedative agents are required either to facilitate mechanical ventilation or control ICP. Although current evidence indicates that volatile agents, barbiturates and propofol may have neuroprotective actions, the interaction between these sedative

agents and DCI remains unclear. If CSD plays some role in the pathogenesis of DCI (as is likely), then choice of sedative agent may be important. Most of the research investigating the effect of anaesthetic agents on CSD has focused on the effect of volatile inhalational agents on animal models of brain injury, looking for changes in CSD frequency and intensity. Studies in rats have shown that halothane (and to a lesser extent isoflurane and nitrous oxide) protect against the initiation of CSDs in the cortex [240] and that nitrous oxide decreases CSD propagation speed and duration [165]. Furthermore, increasing the concentration of volatile anaesthetic agents results in a dose-dependent reduction in CSD frequency [160] possibly linked to the increase in cerebral blood flow seen with most volatile anaesthetic agents. Although the use of volatile anaesthetic agents in the intensive care or emergency room setting is rare, the AnaConDa device (anaesthetic conserving device) has enabled their use in the treatment of refractory status asthmaticus [306] and may offer a potential solution in SAH patients.

There is currently no data published comparing the effects of inhalational and intravenous agents on CSD. This is especially important in light of the fact intravenous agents such as propofol, fentanyl and remifentanil are extensively used in both neuroanaesthesia and neurocritical care. The effect of propofol on CSD has yet to be formally investigated although evidence that propofol (and thiopental) attenuate gap-junction coupling [332] and that thiopental may reduce the incidence of CSD in-vitro may be relevant [266]. Ketamine, known to increase ICP and therefore rarely used in the management of patients with SAH, may also behave like volatile agents and block CSD [130]. This evidence has been reinforced by case reports showing the inhibition of CSD and restoration of normal electrocorticographic activity with ketamine in intracranial haemorrhage [263]. As a result, more research into the choice of sedative agent and CSD is needed.

2.5.5 Can biomarkers for early brain injury and DCI be identified?

The delay between aneurysmal rupture and the onset of DCI offers a unique opportunity to apply a therapeutic intervention to patients. The recent consensus definitions quoted earlier in this chapter should be commended for providing a clear "threshold" for the clinical diagnosis of DCI in patients. However, given that the majority of patients with poor grade SAH require sedation and mechanical ventilation, diagnosis of DCI by clinical assessment is often impossible. It also seems logical to suggest that DCI is in fact a spectrum of disease with patients exhibiting varying degrees of severity. If this is the case, then the reliance of this clinical definition on a change in Glasgow Coma Scale (which is relatively insensitive

to subtle changes in neuro-cognitive function) may leave some patients with sub-threshold DCI undiagnosed and untreated. Furthermore, there are limited options for diagnosing and objectively quantifying early brain injury after aneurysm rupture - especially in "good grade" WFNS 1 and 2 patients who arguably have the most to gain from prompt therapeutic intervention.

Identifying objective biomarkers for DCI and early brain injury therefore remains a key research priority. Unfortunately, the current uncertainty regarding the pathophysiology occurring after aneurysm rupture has made this process difficult with no specific or sensitive serum or CSF biomarker currently available. Measures of axonal degeneration such as CSF neurofilament heavy chains have shown some early promise in identifying the secondary ischaemic damage after SAH and may be useful in those patients who require CSF diversion on the neurocritical care unit [238]. Other serum markers such as high sensitivity C-reactive protein may identify the cascade inflammatory activation that is likely to contribute towards early brain injury [102].

Currently, the invasive nature of the monitoring currently required negates investigation of the incidence of CSD in those WFNS 1 and 2 patients who do not require neurosurgical intervention. Quantifying the vascular changes associated with CSD – such as via the the suppression of low frequency vascular oscillations [84] - non-invasively using MRI or NIRS may offer a surrogate measure of CSDs in those patients with less severe grade SAH who undergo endovascular aneurysm treatment.

2.6 Conclusions

Despite overall improvements in overall case fatality from SAH [190], neurocognitive impairment remains a significant problem in those patients who survive to hospital discharge. It now seems clear that DCI has a multifactorial aetiology beyond pure cerebral vasoconstriction and that future management strategies are likely to be based on combination therapies targeting vasoconstriction, disturbed neuronal function and disturbed neurovascular coupling relating to early brain injury in the first 72 hours post-SAH. The interval between aneurysmal rupture and the onset of DCI provides a window for the application of preventative pharmacological therapies targeting early brain injury. However, the majority of therapeutic strategies in clinical use remain focused on improving cerebral perfusion in patients after the aneurysm has been secured and the acute and deleterious reductions in both CPP and CBF in the initial period post-bleed early brain injury remains a neglected diagnostic and therapeutic target.

Emerging evidence suggests that CSDs are associated with cerebral ischaemia after poor grade SAH and are likely to contribute towards DCI. However, the absence of non-invasive biomarkers of CSD means the overall frequency of CSDs in patients following SAH remains unknown and the role of inhalational and intravenous anaesthetic agents as well as treatments such as nimodipine and magnesium on CSD requires further investigation. Future studies into DCI will benefit from clear consensus definitions and clinical endpoints and should focus on the following questions that currently remain unanswered:

1. Why does nimodipine remain the only pharmacological treatment to reduce the incidence of DCI and improve ischaemic outcomes and what is the mechanism behind this effect?

2. Can we develop more accurate experimental models of spontaneous aneurysm rupture that might replicate the physiological changes more accurately?

3. Does the initial period post-aneurysmal rupture offer a diagnostic and therapeutic target for interventions aimed at reducing the incidence of DCI and improving outcomes?

4. How important is cortical spreading depression in the aetiology of DCI and what effect do current therapeutic interventions used in SAH have on its incidence and progression?

5. Is it possible to identify objective biochemical, electro cortical or neuroimaging biomarkers of DCI that will allow earlier identification of those at risk (especially in sedated patients) and act as a target for future research into novel treatments?

6. Can we influence DCI at a genetic level both to identify patients at risk and to guide application of therapeutic interventions?

Chapter 3

Experimental Methods

Chapter Overview

The aim of this chapter is to give an overview of the magnetic resonance imaging (MRI) techniques used in this thesis. Firstly, the physical principles underlying MRI will be explained. Then, novel structural, perfusion and functional imaging techniques will be introduced. Next, a brief description of the stages involved in the processing and statistical analysis of the MRI data is outlined. Finally, an overview of the tests used to objectively quantify neurocognitive outcomes is provided.

3.1 Introduction

MRI allows the non-invasive and in-vivo mapping of the structure and function of the brain. Atomic nuclei with an odd number of protons (e.g. hydrogen) possess a net angular momentum or "spin". As human tissue is largely composed of water, it is a rich source of hydrogen nuclei. When a subject is placed in an MRI scanner, the majority of protons in water align with the applied magnetic field which results in a net magnetisation of protons. An alternating radiofrequency (RF) pulse, orientated in a different direction, is then applied to this static field causing the protons to align with the RF field. When the RF pulse is switched off, the protons realign to their original orientation - a process termed "relaxation". This relaxation produces the emission of a small magnetic field that is measured by a receive coil with the rate at which they relax dependent upon the tissue type. By altering the timing between the transmission of the RF pulse and image acquisition, it is possible to modify contrast in the resulting images, so they can be adapted for different imaging applications.

MRI is widely used in research and clinical practice due to its ability to image body structures with good spatial and temporal resolution and without the need for ionising radiation. Although positron emission tomography (PET) is more quantitative, it has poorer spatial resolution and requires the use of radioactive isotopes that have potential harmful effects and restrict its use in longitudinal studies that require repeat investigations. Electroencephalography (EEG) and magnetoencepahlography (MEG) have much greater tempral resolution than MRI but are limited by poor spatial resolution. MRI therefore occupies an important role between PET and EEG/MEG for imaging the brain in clinical and research studies.

Traditionally, MRI has been used to study the structure of the brain but recent increases in magnetic field strength and analysis techniques are allowing MRI to evolve into a key tool for probing changes in neurophysiology and function in both health and disease. Developments such as voxel-based morphometry (VBM) (to investigate regional changes in brain tissue volume), resting state MRI (to map neuronal activity in the brain and estimate connectivity between different brain regions), and arterial spin labelling (ASL) (to obtain quantitative measures of cerebral blood flow) are enabling MRI to become an exciting tool for investigating systems level functional neuroanatomy in both health and disease.

3.1.1 Structural MRI

Conventionally, the use of MRI to evaluate changes in patients after acute neurological injury correlates structural changes in brain anatomy using T1/T2 and diffusion weighted imaging with clinical outcomes. However, interpretation of these images is often qualitative and dependent on the experience of the clinician involved. In recent years, a number of unbiased, objective automated techniques have been developed to quantify both longitudinal and cross sectional changes in whole brain tissue volumes. These techniques have proved especially useful in monitoring changes in chronic neurological conditions such as Alzheimer's disease, multiple sclerosis and Parkinson's disease [69, 105, 204]. Recently, attention has focused on defining the tissue compartments and regions within which any change in brain volume occurs. These regional measures of brain volume changes may help to better define the nature of the pathology underlying acute neurological conditions such as SAH. If relative volume changes across the brain are not homogenous, then regional measures may in principle detect greater local change than measures averaged across the whole brain and thus provide more sensitive indices of change. This could improve correlations with related pathological features in magnetic resonance imaging (MRI) data.

SIENA and SIENAX

SIENA is an automated package for both single-time-point ("cross-sectional") and two-time-point ("longitudinal") analysis of brain change from T1 structural images - in particular, usually for the estimation of atrophy (volumetric loss of brain tissue). SIENA has been used in many clinical studies to estimate percentage brain volume change (PBVC) between two input images, taken of the same subject at different points in time. It registers the baseline and follow-up magnetic resonance image using the skull as scale and skew constraint, and then estimates the displacement of the brain edge for each point of the brain edge between these two scans. The brain edge displacements of all edge points are used to calculate the "overall" PBVC, which is expressed as a single value.

SIENAX estimates total brain tissue volume at a single timepoint, from a single image normalised for skull size. It calls a series of FSL programs to automatically segment brain from nonbrain matter, calculate the brain volume, and apply a normalisation factor to correct for skull size. The normalisation factor is obtained by registering the subject's scan to the Montreal Neurological Institute (MNI) 152 standard image using the skull to normalise spatially. SIENA registers the baseline and follow-up magnetic resonance image using the

skull as scale and skew constraint, and then estimates the displacement of the brain edge for each point of the brain edge between these two scans. The brain edge displacements of all edge points are used to calculate the "overall" PBVC, which is expressed as a single percentage value.

Voxel-based morphometry

Voxel-based morphometry (VBM) is a whole brain technique for characterizing regional volume and tissue concentration differences in structural MRI data [345]. VBM has been designed to be sensitive to small scale structural differences, while discounting positional and other large scale volumetric changes in gross anatomy. The technique compares the brains of different subjects on a voxel-by-voxel basis after deformation fields have been used to spatially normalize the images. When warping a series of images to match a template, it is inevitable that volumetric differences will be introduced into the warped images. For example, if one subject's temporal lobe is half the volume of that of the template, then the volume will be doubled during spatial normalization. This will also result in an artefactual doubling of the voxels labeled grey matter. To remove this confound, the spatially normalized grey matter is adjusted by multiplying by its relative volume before and after warping using the deformation or "Jacobian" field. If warping results in a region doubling its volume, then the correction will halve the intensity of the tissue label.

3.1.2 Diffusion-weighted Imaging

Diffusion-weighted imaging (DWI) remains the mainstay of the clinical radiological evaluation of SAH patients using MRI. The subsequent advent and popularization of diffusion weighted imaging (DWI) and diffusion tensor imaging (DTI) in the early 1990s allowed researchers to characterize ischaemic lesions as hyperintense areas with decreased apparent diffusion coefficient (ADC) values. However, DWI is limited by the fact that it usually only indicates the core of severe ischaemia and that the reporting of DWI lesions in clinical practice is usually qualitative and reliant on the skill of the reporting radiologist to identify subtle changes in DWI signal.

3.1.3 Resting State Blood Oxygen Level Dependent (BOLD) Imaging

In an ideal world, the measurement of neural activity would be directly possible over the whole brain directly. However, this is virtually impossible without invasive surgical

procedures which carry significant risk of morbidity. Functional MRI (fMRI) visualises brain function indirectly by measuring the haemodynamic response to neuronal activation. In traditional fMRI, endogenous contrast is obtained from natural changes in the oxygen saturation of blood in cerebral capillaries and veins that occurs in response to neural activity [222]. This phenomenon is known as the blood oxygen level dependent (BOLD) response.

Neuronal activity involves propagation of action potentials along axons, and synaptic transmission of these action potentials. This increases the energy requirements in active neuronal tissue. To provide adequate glucose and oxygen to meet the increased energy requirements, the blood flow to the neuronally active area increases. In fact, the increase in blood flow exceeds the oxygen requirements resulting in an increase in oxygenated haemoglobin (HbO_2) relative to deoxygenated haemoglobin (Hbr) in metabolically active areas [189]. Hbr and HbO_2 have different magnetic properties: HbO_2 is diamagnetic while Hbr is paramagnetic. Therefore, Hbr perturbs the B0 field more than HbO2 resulting in magnetic field inhomogeneities. The increase in HbO_2 relative to Hbr results in a reduced B0 field inhomogeneity and an increased MR signal. This reduced field inhomogeneity increases the T2* weighted MRI signal in the activated areas relative to the inactive areas generating a contrast between active and inactive neuronal populations. The physiological principle of BOLD contrast is shown schematically in Figure 3.1.

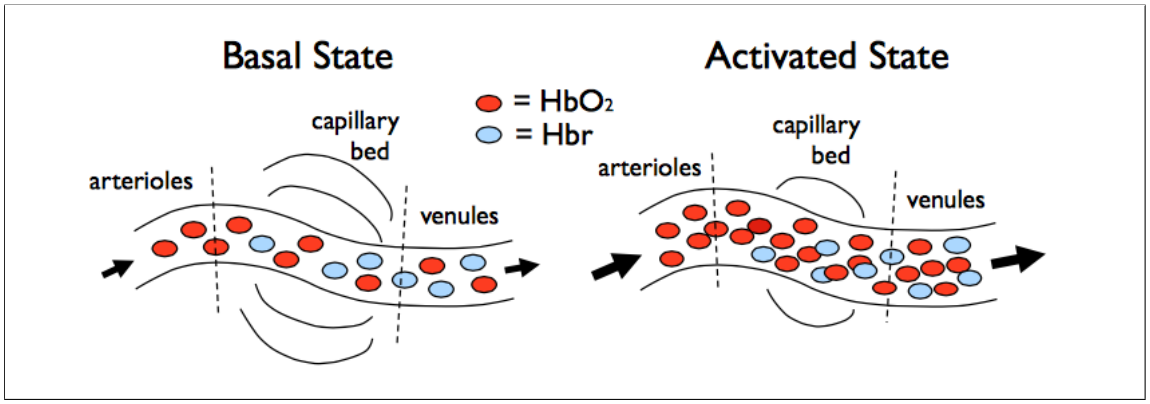


Fig. 3.1: HbO_2 in red depicts the red blood cells with oxygenated haemoglobin and Hbr in blue depicts the red cells with reduced (deoxygenated) haemoglobin. Diagram on the left shows the resting basal state with normal blood flow, basal level of Hbr and basal cerebral blood volume (CBV). Activated state on the right shows the events during neuronal activation. Due to increase metabolic demand there is increased blood flow in excess of the oxygen demand resulting in a decrease in Hbr and an increase in HbO2. As HbO_2 is diamagnetic it reduces the B0 field inhomogeneity (creates a lower field gradient) around the capillaries and the venules. This reduced field inhomogeneity increases the T2* weighted MRI signal in the activated areas relative to the inactivate areas. Adapted from http://fsl.fmrib.ox.ac.uk/fmri_intro/physiology.html

Changes in BOLD contrast can be used for task-based experiments designed to map functional activity onto brain regions. More recently, it has been used to study the intrinsic connectivity of brain networks in task-free settings by mapping temporally synchronous, spatially distributed, and spontaneous low frequency fluctuations in BOLD contrast [104] as described in Chapter 5 after SAH.

3.1.4 Arterial Spin Labeling

Numerous techniques have been developed to attempt to quantify CBF in humans. The development of these techniques has been driven by both scientific research interest as well as the potential clinical benefit of identifying pathological patterns of CBF after acute neurological injury. Despite this, the ultimate goal of a reliable, repeatable and totally noninvasive technique that enables the mapping of CBF with high temporal and spatial resolution over a wide range of blood flows and clinical conditions has still not been achieved.

Arterial spin labelling (ASL) is an MRI method for the quantitative measurement of CBF that utilises magnetically labeled water molecules as an endogenous contrast agent. The water in arterial blood is labelled by applying an RF inversion pulse to the blood before it reaches the area to be imaged in a plane through the neck that includes both carotid and vertebral arteries. After a delay (the transit time) this magnetically labelled blood arrives in the area of brain that is being imaged. The magnetisation of this blood alters the total tissue magnetisation. A tag image is taken during this time. The time between labelling and acquisition of the tag image is called the inversion time. In addition to the tag image, a control image is also taken without labelling. The difference between the tag and the control image is proportional to the CBF (Figure 3.2). To obtain accurate measurements of CBF multiple images can be taken with different inversion times, and a kinetic curve can be calculated that represents the time course of the magnetically labelled blood in the area imaged. CBF can then be calculated from this.

The arterial arrival time (AAT; also described as "arterial transit time" or "bolus arrival time") represents the time it takes for the blood water to move from the tagging plane to the imaging voxel. There is evidence that AAT provides an additional metric in the characterisation of cerebral hypoperfusion due to cerebrovascular disease [35].

The most common ASL techniques used in the past have been continuous ASL (CASL), and pulsed ASL (PASL). CASL uses a long radiofrequency (RF) pulse of several seconds duration to adiabatically invert the spins in arterial blood as the blood flows through a particular slice

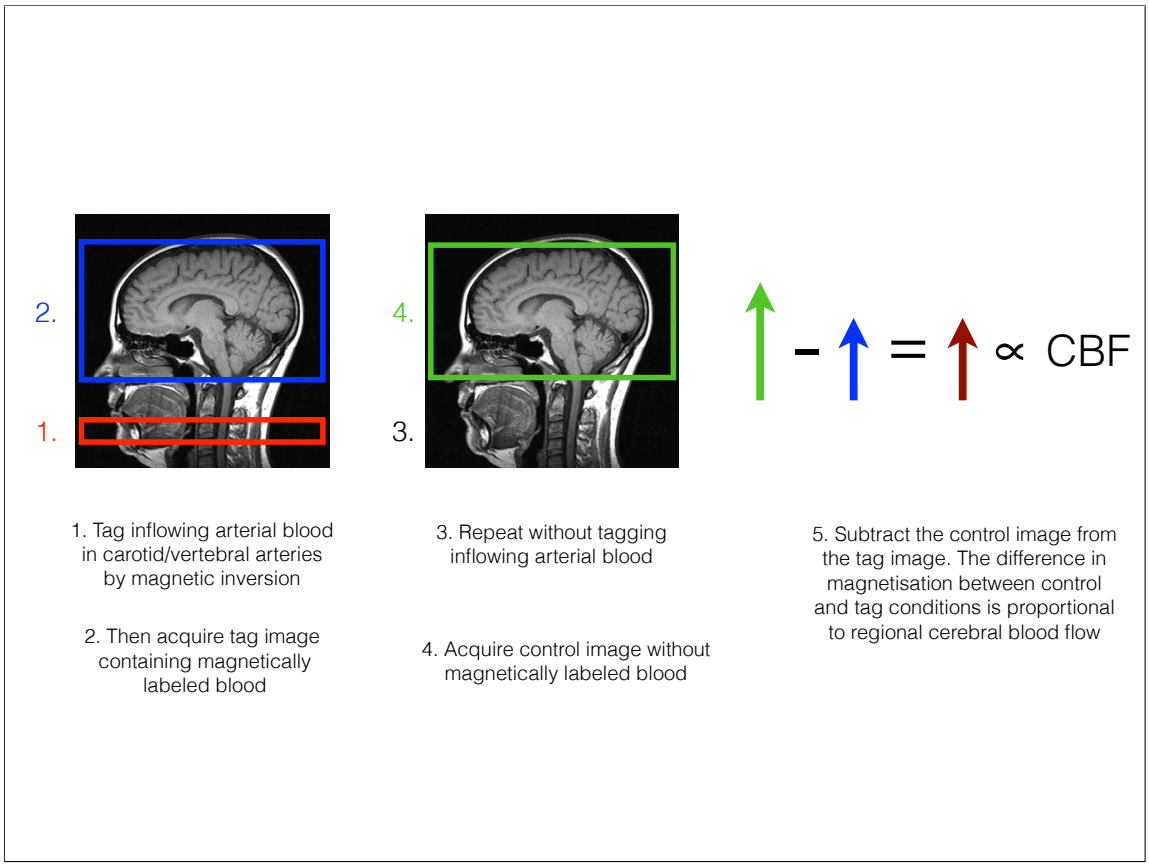


Fig. 3.2: Overview of arterial spin labeling (ASL) MRI

containing a large artery (e.g., internal carotid artery) that feeds the tissue (usually the brain) [334, 73]. PASL employs a short RF pulse of a few milliseconds duration to label a particular plug of arterial blood passing through the labeling slice [168, 90]. Although there are theoretical and exerimental advantages to using CASL, these are offset by a range of technical complications, including the need for a long continuous RF pulse and compensation of MT effects which can restrict applications, especially at high magnetic fields [215]. More recently, a new approach to CASL, termed pseudo-continuous ASL (PCASL)[63] has been introduced that eases the technical restrictions of CASL and provides high labeling efficiency and SNR without the need for custom hardware. PCASL also has good test-retest reliability, with strong consistency across subjects and sessions during rest [203].

Much of the value of ASL is derived from its ability to image tissue at risk for ischemia or infarction and regions that are potentially salvageable with timely intervention. ASL techniques are of interest to both clinical and experimental studies as they offer the ability to investigate long acting cognitive and physiologic states (not possible with BOLD MRI techniques), and to complete multiple repeat scans (e.g., follow-up investigations, longitudinal designs, and pharmacological trials) without cumulative risk to the subject. There is also considerable interest in using ASL for functional mapping of the brain as changes in CBF may be better localised to neural activity than BOLD contrast. ASL is sensitive to arterial-capillary vessels whereas BOLD is more sensitive to venous changes, which are further downstream of the neuronal activity. Furthermore, ASL is a quantitative CBF measure whereas BOLD depends on a complex physiological response to generate contrast. The main disadvantage of ASL is that it suffers poor signal-to-noise ratio (SNR) because the fraction of vessels in the brain is small compared to the amount of brain tissue.

3.2 Principles of MRI data analysis

MRI data analysis involves the use of specialised computer software to measure changes in MRI signal at both an individual and group level and correlate these with measures such as neurocognitive test results. In this thesis, we have used tools from the Oxford Centre for Functional MRI of the Brain (FMRIB) software library (FSL) to analyse the images generated from MRI scanning sessions. Data analysis consists of two main stages. Firstly, several pre-processing steps need to be carried out before any statistical analysis can take place, to correct for motion, noise and signal drifts. This reduces the variability of the data

and helps improve the signal-to-noise ratio (SNR). Next, statistical analysis is applied to identify differences in each sequence that occur at an individual and group level.

3.2.1 Data reduction

This consists of two steps. The four volumes obtained in the first 12 seconds of some of the MRI sequences obtained e.g. the functional and perfusion scans are discarded to ensure that the statistical analysis is performed on scans where T1 recovery has reached a steady state. Secondly, non-brain matter (such as the skull and soft tissue outside the brain) are removed using an automated software algorithm (BET - Brain Extraction Tool) [289].

3.2.2 Correction for B0 field inhomogeneities

MRI images are easily distorted by inhomogeneities in the magnetic field produced by the scanner. These are caused by the difference in magnetic susceptibilities of the tissues that surround the brain - particularly at air, bone and soft tissue interfaces in the brain. As a result, there is loss of signal and geometric distortion of images especially in the brain areas near the frontal and temporal sinuses. This distortion can lead to errors in registration to images in both structural and standard space. By obtaining a measurement of the magnetic field inhomogeneities (field map), it is possible to use FSL tools to minimise these distortions and improve registration.

3.2.3 Motion correction

Image analysis methods examine the behaviour of individual voxels over a period of time. As a result, it is important that each voxel remains in the same place throughout the functional scan. Unfortunately, despite best efforts, inadvertent subject head motion often occurs which can affect the accuracy of results obtained.

Current noise removal methods for motion correction of individual resting fMRI datasets can be divided into two main categories: those that use external physiological recordings and those that are data-driven. In the former category, with techniques like retrospective image correction (RETROICOR [113]), low-order Fourier series are fit to the image data based on the time of each image acquisition relative to the phase of the cardiac and respiratory cycles [117]. However, complete physiological monitoring data are often not available, and often

do not relate to all common forms of head motion artifact. Therefore, other methods have been proposed to estimate and remove the artifacts using only the fMRI data itself.

In this thesis, we have used standard rigid-body head motion correction using the FSL tool MCFLIRT. This tool aligns all of the volumes in a timeseries to a reference volume (usually in the middle), with the volume-to-volume movement of the head described by three translations and three rotations. However, even with perfect geometric correction of head motion, spin history effects can still result in residual motion- related artefacts.

A different option is to use a technique called "scrubbing" to deal with remaining artefacts [244]. With this technique, time points of the MRI data affected by excessive motion are simply excluded from analysis. However, excessive loss of data time points can be associated with an increase in the likelihood of high correlation scores [95].

As a result, to further correct for any potential residual motion effects, an additional FSL tool based on independent component analysis (ICA) called FMRIB Automated XNoisifier (FIX) was applied to the resting state datasets. ICA decomposes the 4D (space versus time) data into multiple components, each described by a single 3D spatial map and an associated time course. Ideally, some components purely reflect BOLD signal, and others purely reflect artefactual processes. If the latter processed can be identified, then they can be subtracted from (or regressed out of) the data. FIX uses an automated approach (once trained) to the cleaning of fMRI data of various types of artefact [264]. The general cleaning procedure in FIX consists of several steps: spatial ICA, component-wise feature extraction, classifier training (using expert-hand-labelled data), classification of components (i.e predicting the likelihood of each components being signal or noise, in new datasets) and denoising (removal of the artefactual components). The first four steps are described in Salimi-Khorshidi et al. [264]. The ICA step is performed using the FSL tool MELODIC [27] which extracts over 180 spatial and temporal features for each ICA component. The training and prediction phases are then performed with a hierarchical fusion of multiple classifiers (K-nearest neighbour, support vector machines and decision trees). The performance of FIX in component classification against manual labelling (the "gold standard" for component classification) has been assessed on various rfMRI datasets and achieved over 99% classification accuracy on the best datasets, and around 95% accuracy on more "standard" acquisitions [117].

3.2.4 Spatial smoothing

Spatial smoothing of the data is necessary for two reasons. Firstly, to increase the signal to noise ratio by reducing the random spatial fluctuation in the signal in each voxel. Secondly, that a minimum smoothness is required to use Gaussian Random Field theory for subsequent statistical analysis of the data. A Gaussian shaped kernel is commonly used. The size of the kernel is largely based on the expected size of activation [344]. A wider kernel will reduce the noise and improve signal to noise ratio. But if the expected area of activation is smaller, then a larger kernel may reduce the signal.

3.2.5 Temporal filtering

High pass temporal filtering is used to remove scanner drifts and some cardio-respiratory effects.

3.2.6 Registration

Accurate image registration is essential for the analysis of multi-subject studies. To register two images means to align them so that common features overlap and differences — for example, changes in resting brain connectivity — are readily apparent. Echo planar imaging (EPI) is a technique often used in perfusion MRI, DWI and fMRI sequences due to the high speed images can be acquired. However, EPI images have a poor resolution and anatomical contrast. Therefore, to identify the location of activation the functional images have to be co-registered with a high-resolution anatomical T1 image of the same subject. For comparison of activity across whole groups of subjects, the image of the brain of each subject is then further transformed using a standard template of the human brain. The standard template of the brain used in this thesis and in the majority of MRI studies is the one created by the Montreal Neurological Institute (MNI). This consists of an average of 152 T1 weighted brain images.

The traditional approach to register EPI to structural images is to use software that uses linear algorithms e.g the FSL tool FLIRT. More recently, the technique of boundary based recognition (BBR) - as used throughout this thesis - has further improved the accuracy of FLIRT. The white-matter boundary of T1 weighted images is mapped to the EPI image and then samples of the EPI intensity are taken at a distance (default of 2mm) either side of points along this boundary (see Figure 3.3).

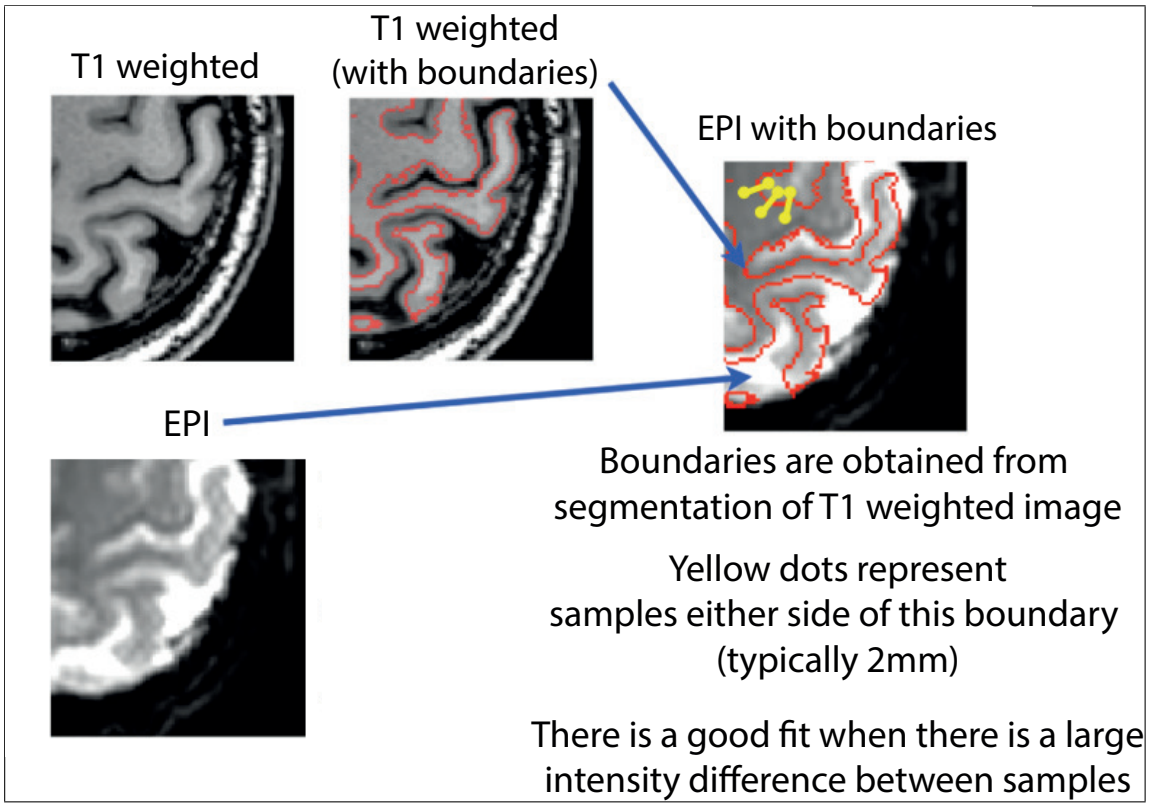


Fig. 3.3: Boundary based registration (BBR) adjusts alignment by maximizing image contrast across tissue boundaries rather than matching intensities between two images or by matching surface shapes (adapted from http://fsl.fmrib.ox.ac.uk/fsl/fslwiki/FLIRT_BBR).

The difference between the intensities in each pair is used to calculate the cost function. To prevent it being unduly influenced by outliers, the difference is run through a sigmoid-like non-linear function to suppress the effect of very large differences. The sign of the difference is also important and it is set-up to expect a higher intensity in the grey-matter in the EPI image.

Non-linear registration software (e.g. FNIRT) is then used to optimise the registration of high resolution structural images to the MNI standard template.

3.2.7 Statistical analysis

Throughout the thesis, data extracted from MRI results as well as other results (e.g. physiological data) were analysed for statistical significance using Prism 6 (GraphPad Software). Shapiro–Wilk tests were applied to mathematically assess distribution normality. Where applicable, results are presented as mean $\pm$ standard deviation and all statistical tests had significance set at $p \leqslant 0.05$.

MRI data

Statistical modelling is used to investigate differences in each MRI modality at both an individual subject and then a group level. Traditionally, parametric analysis techniques have been used in fMRI studies which samples subjects from a population (randomly and independently), assumes a certain distribution for the data and then computes a statistic. All else being equal, an extreme value suggests a difference in the data that is allowed to vary (usually the mean). However, random data sampling is rare in biomedical research and the population model is often violated, along with the assumptions that come with it. Although this approach can be used, assumptions can be invalid in many voxels of the data and different imaging modalities have different properties meaning that a single set of assumptions will be invalid for some modalities.

As a result, non-parametric or "permutation" tests are superior in many ways as there is no underlying theoretical distribution and no stringent assumptions (e.g. normality, independence, homogeneous variances). They allow a wide variety of statistics and are good for smaller datasets as all information needed is in the dataset itself, not on an idealised population. Finally, they are resilient to outliers.

Permutation tests are based on the principle of the general linear model (GLM). This is a statistical linear model that can be summarised as:

$$Y = M\psi + \varepsilon$$

Permute the data (Y) or the rows of the design matrix (M), re-estimate the parameters (ψ) and residuals (ε), compute a new statistic. Repeat this many times, count how often a permuted statistic is greater or equal than the non-permuted, and divide by the number of tests. This produces a statistical p-value for each voxel.

As there are a large number of voxels within the brain, correction for multiple comparisons is required after generating the group specific statistic. If each voxel is treated as an independent unit then application of multiple corrections, such as Bonferroni's, is unrealistic due to falsely assigned large number of 'independent' units. Further, it is inappropriate as the behaviour of the voxels is not functionally independent. Therefore, the number of statistically independent groups of voxels (resolution elements or 'resels') is estimated using Gaussian Random Field (GRF) theory. GRF takes into account the spatial smoothness of the statistic map. Typically, the number of resels is much smaller than the number of voxels so this method is less conservative and more appropriate for MRI datasets.

There is another method of assigning significance to brain activations. First, a voxel-based threshold is applied to the statistical map. Voxels with an activity above an arbitrary Z score (e.g. score > 2.3) are considered for the next step. From all the voxels that are above the predetermined threshold, using GRF theory, significance is assigned to clusters of voxels taking into account the size (spatial extent) of clusters and the initial threshold applied. This "cluster-based correction" is often used in neuroimaging research and makes use of spatial neighbourhood information to boost belief in extended areas of signal. However, a limitation is the need to define the initial cluster-forming threshold which is usually arbitrary. In this thesis, we have therefore used a threshold-free cluster enhancement (TFCE) technique which attempts to keep the sensitivity benefits of cluster-based thresholding while trying to minimise the problems above. The method takes a raw statistic image and produces an output image in which the voxel-wise values represent the amount of cluster-like local spatial support [291].

3.3 Neurocognitive Testing

Neurocognitive assessment comprises a comprehensive evaluation of cognitive status by specific neurologic domains, i.e., memory, attention, language, visuospatial, processing speed and executive function. One of the main difficulties with research into neurocognitive outcomes after all acute brain injury though, is determining what outcomes are most influential and which measures to use to best quantify neurocognitive performance. A number of studies have investigated neurocognitive outcomes after SAH. However, reports on patterns of cognitive deficit related to the site of the aneurysm, are inconsistent [307, 164]. Furthermore, different patterns of cognitive dysfunction may be present in patients with ruptured aneurysms in identical locations [295]. Earlier studies that explored cognitive deficits after subarachnoid hemorrhage from the anterior communicating artery (ACoA) described a special "ACoA syndrome", characterized by personality changes as well as amnesia and confabulation as the main symptoms, where damage to particular anterior cerebral structures was a suspected cause [3, 64, 326]. However, other studies did not find specific deficits in ACoA patients, and a more diffuse pattern of brain damage was thought to be responsible for the deficits [223, 38]. As a result, currently employed neurological outcome measures are often not disease-sensitive enough to detect brain injury in more mild SAH, and this lack of sensitivity may account for the negative results seen in some studies of therapeutic intervention in SAH.

The neuropsychological arm of the International Subarachnoid Aneurysm Trial (N-ISAT) evaluated the cognitive outcome of 573 patients at 12 months after SAH [278]. The N-ISAT battery was developed to evaluate cognitive function including general verbal and nonverbal intellectual skills and memory, language and spatial skills, attention, psychomotor/processing speed, and executive function. A principal components analysis undertaken on this data identified a number of uncorrelated principal components or cognitive "domains". The task of identifying individuals with a cognitive 'complication' (i.e., a classification of 'significant cognitive impairment') involves two key challenges: firstly, determining where to place an appropriate 'cut-off' on individual test scores, (i.e. below which a performance can be said to be 'significantly' impaired). A score may for example be judged relative to that individual's estimated pre-morbid state, a normal control population, or an equivalent clinical population, with each perspective having both advantages and disadvantages. The second challenge is concerned with determining how multiple test scores can be summarised or distilled down into a smaller number of cognitive constructs or 'domains'. Thus for example a particular constellation of impaired tests scores might be said to represent an impairment in language,

spatial memory or executive skills. An individual might be impaired in one or more of these domains (with more or less consistency across tests), and a determination would need to be made about whether that crossed the threshold of functional or clinical significance. In this thesis, we decided to use the N-ISAT battery as the basis for our assessment of neurocognitive outcomes at three months post-SAH. The specific tests used are outlined in Chapter 4.

Chapter 4

The relationship between structural, diffusion-weighted and perfusion changes on acute magnetic resonance imaging and neurocognitive outcome after subarachnoid haemorrhage

Chapter Overview

Damage to the brain in the first 72 hours following aneurysm rupture (so called "early brain injury") is likely to play a key role in determining the likelihood of both short term outcomes such as DCI as well as longer term morbidity and mortality after SAH. However, current methods of quantifying pathophysiological changes associated with early brain injury such as cerebral ischaemia and oedema remain subjective and dependent on clinical assessment/scoring and qualitative interpretation of neuroimaging.

Advances in MRI physics and analysis now offer a number of objective, reliable and non-invasive tools to measure changes in cerebral structure and perfusion at a tissue level. This approach potentially allows greater insight into the significance of early brain injury on functional and neurocognitive outcomes and the development of both diagnostic and therapeutic MRI biomarkers.

To investigate structural and perfusion changes associated with early brain injury, patients with "good" grade SAH (WFNS Grade 1 and 2) were recruited and underwent MRI scanning at three timepoints post-SAH: within the first 72 hours (n=28), in the first 5-10 days (n=27) and at 3 months (n=26). Patients also underwent detailed neurocognitive assessment at 3 months post-SAH to quantify variation in neurocognitive and functional outcomes.

Despite being "good grade" SAH patients and when compared to healthy controls, there were significant global and regional increases in brain volume in the first 72 hours post-SAH. These changes were associated with restricted diffusion suggesting widespread cytotoxic cerebral oedema that remains undiagnosed using current diagnostic imaging. Furthermore, patients with DCI/DCI-related cerebral infarction had a significantly lower global grey matter CBF versus without in the first 72 hours but not between days 5-10 post-SAH - the peak incidence of DCI. Finally, using the VBM data results, it is possible to predict with 84% accuracy and 86% specificity which patients will go on to develop poor neurocognitive outcomes at three months from T1 structural images acquired at baseline, during the acute phase (first 72 hours post-rupture).

This study demonstrates the value of acute MRI scanning to objectively quantify early brain injury in the first 72 hours post-SAH. Scans were well tolerated by patients with no complications and results demonstrate the potential for objective and automated assessment of cerebral structural changes to predict neurocognitive recovery from the start of the disease and help risk stratify the need for critical care intervention.

4.1 Introduction

As described in Chapter 2, over the last three decades, case-fatality rates for SAH have halved due to improved diagnosis, novel approaches to aneurysm occlusion, and advances in critical care management [216, 190]. Despite this, the physical, emotional and economic toll on survivors and society in general remains significant. Accurately defining good outcomes after SAH is also still problematic as functional independence is not the only factor that contributes to quality of life in survivors.

Following successful endovascular or surgical aneurysm occlusion, the acute clinical management of patients with SAH is conventionally focused on the prevention, diagnosis and treatment of secondary brain injury caused by delayed cerebral ischaemia (DCI) and DCI-related cerebral infarction. However, to make decisions about the appropriate level of care and to better inform physicians and relatives, there is still a need for accurate and reliable clinical diagnostic imaging techniques. This would help supplement clinical expertise with the overall goal of accurately predicting neurocognitive outcomes. To have the most clinical relevance, these techniques will need to predict outcome with a high certainty for a given individual patient from the acute phase of the illness i.e. in the first hours following SAH.

Computed tomography (CT) and diffusion weighted magnetic resonance imaging (MRI) evidence of early cerebral ischemia and infarction is common in the acute period after SAH and is associated with worse neurological and physiological admission status as well as poor neurocognitive outcomes [213, 107]. Global cerebral oedema is also a significant feature of early brain injury and is an independent risk factor for mortality and poor outcome after SAH [57, 171]. However, current diagnostic imaging approaches are limited by the qualititative assessment of images by trained clinicians and tend to be "reactive" rather than "proactive" - i.e. waiting for clinical deterioration to trigger clinical imaging rather than proactively scanning patients prior to deterioration. Patients with "good grade" SAH are often managed in a ward environment rather than critical care due to pressures on bed occupancy. Furthermore, current methods to quantify the pathophysiological changes of early brain injury, such as raised intracranial pressure, either depend on invasive monitoring such as the insertion of microdialysis or pressure monitoring probes or the subjective and qualitative assessment of radiological images by a trained clinician.

It therefore seems likely that clinical interventions that target the pathophysiology associated with early brain injury, e.g. reducing cerebral oedema, improving cerebral blood flow and

improving metabolic function, may hold the best promise for preventing neurocognitive dysfunction after SAH. What is needed is a reliable, objective and non-invasive method of quantifying the severity of early brain injury post-rupture.

As described in Chapter 3, a number of new MRI techniques have been developed that allow the non-invasive quantification of changes in cerebral tissue structure and blood flow. Voxel-based morphometry (VBM) allows the investigation of focal differences in grey matter density using statistical parametric mapping. The importance of using a VBM approach is that it is not biased to one particular structure and gives an even-handed and comprehensive assessment of anatomical differences throughout the brain without a priori knowledge of which regions may be affected [17]. For this reason, it is highly suited to the investigation of early brain injury due to the unpredictable nature of the global physiological insult that occurs following aneurysm rupture. Arterial spin labeling (ASL) MRI can be used to quantify regional cerebral perfusion without the use of ionising radiation or contrast agents. The technique uses magnetically labelled arterial blood water as a non-invasive, endogenous tracer for the assessment of cerebral perfusion and can provide whole-brain, quantitative maps of CBF (in units of ml/100g/min) on serial occasions post-SAH [157].

Along with these techniques, novel analysis approaches using machine learning may offer the potential to predict which patients are most likely to have poor outcomes after SAH. Tollard et al. found that diffusion tractography and magnetic resonance spectroscopy measures in patients with traumatic brain injury could separate without overlap patients with unfavorable outcome from those with favorable outcome and healthy controls with up to 86% sensitivity and 97% specificity [308]. This kind of "predictive" approach offers the potential to screen patients according to quantitative and objective MRI data and potentially allow risk stratification to intensive care and therapeutic options such as hypertension-hypervolaemia-haemodilution ("HHH") therapy and extra-ventricular drainage.

To our knowledge, there have been no previous attempts to explore longitudinal whole-brain tissue changes in structure associated with early brain injury on a voxel-by-voxel basis. This is important as a greater understanding of the impact of early brain injury on outcomes in patients with "good grade" SAH (WFNS 1 and 2) remains unclear. The primary aim of this study was therefore to use serial MRI scanning in patients with WFNS grade 1 and 2 SAH at three time-points: in the first 72 hours post-rupture (to characterise MRI biomarkers of early brain injury), in the first 5-10 days (the period of peak incidence for DCI) and 3 months post-SAH (to quantify functional and neurocognitive outcomes). Through this, we aimed to build a greater understanding of the neuroanatomical and neurophysiological

changes that occur following aneurysm rupture and offer potential diagnostic and therapeutic targets for future research. The following hypotheses were specifically tested. Firstly, in the first 72 hours following SAH, early brain injury can be quantified using MRI as identified by abnormal grey matter structure and morphology (as measured with SIENA and VBM), cerebral oedema (as measured by changes in apparent diffusion coefficient and total brain volume) and altered cerebral blood flow. Secondly, that the magnitude of early brain injury in the first 72 hours post-SAH (as characterised above) is predictive of neurocognitive outcomes as measured at three months post-SAH.

4.2 Methods

Participants were recruited as part of a prospective, observational cohort study, run between March 2011 and May 2014 at Oxford University Hospitals NHS Trust - a tertiary referral neurosurgical centre. Approval for the study was granted by the local National Research Ethics Service committee (NRES Committee South Central - Berkshire: 11/SC/0519). Patients were eligible for recruitment to the study according to the following inclusion criteria:

- Male or female, aged between 18-80
- World Federation of Neurosurgeons Grade I and II SAH ("Good Grade")
- Presentation and successful endovascascular aneurysm occlusion within 72 hours of index headache

Contraindications to recruitment into the study were:

- Routine contraindications to MRI scanning e.g. implantable pacemaker/defibrillator, cochlear implant or other implants that are not MRI compatible
- Requirement for surgical clipping of ruptured aneurysm or pre-existing aneurysmal clip - as it may not be possible to validate MR safety especially at these very high field strengths. Clips may also provoke unacceptable levels of image artefact
- Pregnancy

Time of SAH was defined as primary headache associated with medical intervention. Informed written consent was obtained from all participants. Following endovascular aneurysm occlusion, all patients were managed according to a standardised clinical SAH protocol. This

included nimodipine (either 60mg 4 hourly or 20 mg 2 hourly depending on blood pressure) for 21 days following diagnosis of SAH and maintenance of serum magnesium within normal limits.

4.2.1 MRI scan acquisition

MRI scanning for patients was performed on three occasions post-SAH: within 72 hours, between 5-10 days and 3 months. A Siemens MAGNETOM 3T Verio machine (Siemens Healthcare, Erlangen, Germany) with a 12 channel multi-array head coil at the Oxford Acute Vascular Imaging Centre (AVIC) was used for all scans

The complete scanning protocol for the study comprised:

1. **T1-weighted MPRAGE structural:** (whole brain; 1.5 x 1.5 x 1.5mm resolution; TR 1780 ms; TI 900 ms; TE 4.4 ms)

2. **Diffusion-weighted (DWI)/Apparent Diffusion Coefficient (ADC) echo planar, spin echo sequence:** (1 min; TR 5300 ms; TE 91 ms; b values 0 and 1000s/mm^2, voxel size 1.8 x 1.8 x 5mm) in 14 patients

3. **Resting state gradient-echo, echo-planar blood oxygen dependent level (BOLD) imaging sequence:** (6 mins; TR 3000 ms; TE 16ms; flip angle 90°; FOV 240 mm; voxel size 3.0 x 3.0 x 3.0 mm) - data presented in Chapter 5

4. **Time-of-flight MR angiogram:** (1.5 mins; 20 slices; TR 26 ms; TE 3.43 ms;). This was acquired approximately 8 cm below the circle of Willis to visualize the brain's feeding arteries. The labeling plane was aligned perpendicular to the ascending carotid and vertebral arteries. The location of the plane was normalized to a point between the curvatures of the vertebral arteries, where all feeding arteries ran parallel in a transverse plane

5. **Multi-inversion time (TI), pseudo-continuous arterial spin labeling (PCASL) sequence with background suppression:** (0.25, 0.5, 0.75, 1.0, 1.25, 1.5s; labeling duration 1.4s post-labelling delays (0.2s to 1.2s) and a gradient-echo (GE) echo-planar imaging (EPI) readout (TR=3.75s, TE=14ms, 6/8 k-space). The selected range of post-labeling delays (PLD) encompasses those that are commonly used in the literature for both single and multi-PLD ASL approaches, as was recently validated for use in human subjects to adequately model kinetic curves for all voxels across a whole brain

volume [224]. B0 shimming was performed over the imaging region and the labeling plane to minimize off-resonance effects

6. **B0 Fieldmaps:** Corresponding B0 fieldmap images were acquired at each scan point to aid scan registration by correcting for echo-planar imaging distortion artifacts

The structural and DWI-weighted images were reviewed for clinical purposes by a consultant neuroradiologist in the research team and any abnormalities reported back to the clinical team looking after the patient.

Physiological data was also collected during patient and healthy control MRI scanning sessions using an AD instruments (Sydney Australia) Powerlab and gas analyser sampling at 50 Hz. This included non-invasive blood pressure (Invivo Research, Florida, USA), pulse oximetry (MR Systems, USA) and end-tidal carbon dioxide (CO2) and oxygen (O2) levels measured using disposable nasal cannulae - see Table 4.3.

4.2.2 Clinical and Neurocognitive Assessment

While inpatients, recruited subjects underwent daily clinical assessment of neurological status. A rapid neurocognitive screen using the Addenbrookes Cognitive Examination - Final Revised version (ACE-R) was also performed on the same day as each MRI scanning session occcurred. The ACE-R is a brief cognitive test that takes approximately 15 minutes to perform and assesses five cognitive domains: attention/orientation, memory, verbal fluency, language and visuospatial abilities [206]. Total score is 100 with higher scores indicating better cognitive functioning.

Following discharge, patients were invited to return for a follow up appointment at 3 months post-SAH. This involved a set of neurocognitive assessments carried out by trained assistant psychologists, under the supervision of a consultant clinical neuropsychologist involved with the research. As described in Chapter 3, the N-ISAT assessment battery was designed to assess neurocognitive function after SAH [278]. However, the comprehensive nature of the testing protocol may have increased the likelihood of missing datasets. As a result, to keep the time required to complete the battery to a reasonable level and improve compliance, test measures were selected from the overall battery which correlated most highly with five of these domains (verbal memory, general verbal skills, processing speed, nonverbal skills/memory, and executive skills) as per Scott et al [277]. Additionally, we included the Weschler Abbreviated Scale of Intelligence (WASI) subtest of Matrix Reasoning (to provide

overall IQ scores), Stroop and Trail Making Tests (A and B) (to further assess processing speed and executive function) and a repeat ACE-R to compare with data acquired following the acute MRI scan session. Premorbid IQ was estimated using the re-standardised National Adult Reading Test (NART; 2nd Edition) [214].

1. **Verbal Memory:** Adult Memory and Information Processing Battery (AMIPB - mean of immediate and delayed recall), California Verbal Learning Test (CVLT)
2. **General Verbal Skills:** Weschler Abbreviated Scale of Intelligence (WASI) - Vocabulary, Similarities, and Matrix Reasoning
3. **Executive Skills:** Stroop Test, Trails B test, Cantab ID/ED switch
4. **Processing Speed:** Digit Symbol Modality Test (DSMT - mean of oral and written), Phonemic Verbal Fluency, Semantic Verbal Fluency, Trails A test
5. **Non-verbal Skills/Memory:** Rey-Osterrieth Complex Figure (mean of copy and delays), WASI Block Design sub-test

4.2.3 Post-processing and data analysis

All image analysis was performed using FSL tools [144] and MATLAB (The Mathworks Inc.). All other statistical analysis was conducted using Prism 6 (GraphPad Software) and R (http://www.r-project.org/). Data was analysed according to the following structure to address the hypotheses outlined in the introduction:

1. **Cross-sectional analysis:** between patients and controls at each MRI time-point (MRI scan 1: <72 hours post-SAH, MRI scan 2: days 5-10 post-SAH, MRI scan 3: 3 months post-SAH)
2. **Serial longitudinal scans in patients:** between the three time-points above
3. **Post-hoc analysis:** based on neurocognitive outcome and incidence of DCI/DCI-related cerebral infarction

Structural MRI data

As a preliminary analysis, brain tissue volume, normalised for subject head size, was estimated for patients at each time point and control subjects with SIENAX, part of FSL. SIENAX starts by extracting brain and skull images from the single whole-head input data

[289]. The brain image is then affine-registered to Montreal Neurological Institute (MNI) 152 space [145, 143] (using the skull image to determine the registration scaling). This is primarily in order to obtain the volumetric scaling factor, to be used as a normalisation for head size. Next, tissue-type segmentation with partial volume estimation was carried out [353] in order to calculate total volume of brain tissue and separate estimates of grey matter, white matter, and ventricular CSF volume. All tissue segmentations were visually inspected meticulously to ensure consistent segmentation results - especially in patients.

Following this, an optimised voxel-based morphometry (VBM) analysis was undertaken on the structural images acquired to identify regional changes in grey matter volume [82, 114] (FSL- http://fsl.fmrib.ox.ac.uk/fsl/fslwiki/FSLVBM). For each comparison (e.g. MRI scan 1: SAH patients versus healthy controls), to avoid the known bias of using one of the data sets as a reference, the analysis was conducted with equal numbers of subjects in each group and all images were processed following the same protocol. Age was regressed out of all analyses as a nuisance regressor.

First, structural images were brain-extracted and grey matter-segmented before being registered to the (MNI) 152 standard space using non-linear registration. The resulting images were averaged and flipped along the x-axis to create a left-right symmetric, study-specific grey matter template. Second, all native grey matter images were non-linearly registered to this study-specific template and "modulated" to correct for local expansion (or contraction) due to the non-linear component of the spatial transformation. The modulated grey matter images were then smoothed with an isotropic Gaussian kernel with a sigma of 3mm. Finally, voxelwise GLM was applied using permutation-based non-parametric testing (5000 permutations) [335], correcting for multiple comparisons. Results were considered significant at $p<0.05$, FWE-corrected for multiple comparisons across space using Threshold-Free Cluster Enhancement (TFCE) [291].

Diffusion-weighted data

DWI data was acquired in 14 of the recruited patients at each scan point as above and in 14 age ($\pm$ one year) and gender paired healthy controls. ADC maps obtained from the scanner were brain extracted using BET and then co-registered to the corresponding structural using FLIRT with Boundary Based Recognition (BBR). As described in Chapter 3, BBR adjusts the EPI volume registration parameters so as to maximize the intensity contrast across the anatomically-defined surface between the cortical grey and white matter [116]. The

implementation in FSL also incorporates the contrast across other white matter boundaries, particularly near the ventricles, as well as correcting for distortions due to susceptibility-induced magnetic field inhomogeneities (which cause major geometrical distortions in EPI images). The distortion correction is achieved by unwarping the EPI images during the registration process, using information about the magnetic field provided by fieldmap acquisition. Binarised region of interest masks in MNI 152 standard space from the VBM analysis were then transformed back into the image acquisition space of each subject for extraction of grey matter ADC values.

Pseudo-continuous arterial spin labeling data

Raw ASL datasets collected from each subject were stripped of non-brain structures using BET and motion corrected using MCFLIRT. Pairwise subtraction of 'tag' and 'control' images was performed on the data to generate perfusion-weighted images.

All related data processing steps essential for quantification of CBF including tissue segmentation, estimation of equilibrium magnetization of blood (M0b) from the mean CSF (cerebrospinal fluid) magnetization (M0csf) images, and generation of absolute CBF in physiologic units (mL blood/100 g tissue/60 seconds) were completed using FSL tools.

Quantification of absolute blood flow requires estimation of the equilibrium magnetization of arterial blood. To do this, head and body coil images were divided to generate a coil sensitivity map. This map was then used to correct the reference image and the pCASL data before CBF quantification to correct for the uneven sensitivity profile of the 32-channel head coil. Additionally, a pairwise control minus tag subtraction was performed on the pCASL data to generate a perfusion image at each PLD. The resultant voxelwise concentration-time curves were fitted to the general kinetic model[45] to estimate both CBF and AAT. Perfusion parameters were quantified using multicomponent modeling with BASIL—a Bayesian inference tool developed for this purpose (http://fsl. fmrib.ox.ac.uk/fsl/fslwiki/BASIL) [51, 52].

BASIL outputs a voxelwise estimate of absolute CBF, as well as a corresponding voxelwise variance map for each parameter. Importantly, these parameters were estimated for each epoch of data (defined as a full set of PLDs), thus generating a time series of absolute CBF from each acquisition. Ten such epochs were generated from each scan session.

Postquantification processing The timeseries of epochs generated for each scan was averaged using a mixed-effects model, which accounted for the voxelwise variance of the

Bayesian fit. This generated a single CBF image for each scan, with a corresponding variance image. For comparisons, raw echo-planar images were registered first to each subject's structural image using FLIRT with BBR and then non-linearly to MNI 152 standard space. Finally, GM masks generated from the VBM analysis and the MNI Structural Atlas (thresholded at 0.5, binarized). These masks were transformed back into the image acquisition space for extraction of CBF values.

4.2.4 Neurocognitive data analysis

The raw data set from each test was transformed into standardised z-scores (with a mean of 0 and a standard deviation of 1.0) relative to age-matched normal populations, employing standard reference manuals and materials for each test. The only exception to this was the CANTAB Intradimensional/Extradimensional Shift (ID/ED) task, which tests the executive component of set-shifting or cognitive flexibility and was classed as pass or fail. In line with widely accepted clinical practice and as used in the N-ISAT study [278], individuals' test scores that fell at or below the 5th percentile (equivalent to a z-score $\leqslant -1.65$) were then identified and classified as impaired scores or 'deficits'. Failure of the CANTAB ID/ED task was classified as an impaired score. Neurocognitive impairment was defined as presence of at least 2 impaired test scores on $\leqslant 2$ of the 5 cognitive domains described above.

4.2.5 Control recruitment

29 healthy control subjects (mean 55.18, range 31-77), paired by age ($\pm$ 2 years) and gender to study participants and taking no regular medications were recruited. Control subjects underwent one MRI scanning session using the same sequences as described above and on the same 3T scanner as the patient study. Control subjects also completed an ACE-R examination to assess global neurocognitive status.

4.3 Results

4.3.1 Clinical Demographics

Between March 2011 and March 2014, 63 patients were screened for eligibility into the study. Of these, 29 matched inclusion criteria and were recruited into the study. One patient was subsequently excluded due to aneurysmal re-bleed prior to MRI scan 1 and one patient was

excluded due to significant image artifact observed during MRI scan 1 from dental braces. One patient declined the MRI scan 2 due to severe headache. As regards follow-up, only one of the recruited patients declined to attend for follow-up at 3 months post-SAH. Additionally, one patient attended for follow-up MRI scanning and ACE-R but declined to complete the rest of the formal neurocognitive assessment.

Mean time from SAH to MRI scan 1 was 52 hours post-SAH (range 29-65 hours), to MRI scan 2 was 6 days post-SAH (range 5-10) and to MRI scan 3/neurocognitive testing was 84 days post-SAH (range 74-108). Figure 4.1 is a flowsheet outlining recruitment into the study. Table 4.1 shows a summary of the demographics of recruited patients who completed the study and Table 4.2 shows demographic and radiological data for each recruited patient.

4.4 Physiological data

Physiological data from each scan session is presented in Table 4.3

4.5 MRI Results

4.5.1 Artifact from coils

Figure 4.2 shows a selection of structural and EPI images from one patient demonstrating the image artifact and dropout resulting from the platinum endovascular coils used to occlude the ruptured aneurysm post-SAH.

The coils result in a prominent metal streak artefact in computed tomography (CT) images used clinically often making them difficult to interpret. In the structural and echo-planar imaging MRI images, only the region immediately surrounding the endovascular coil suffers from signal dropout (B) and (C). Therefore, the signal dropout artifact has a minimal effect when investigating global changes following SAH.

4.5.2 MRI Results

Scan 1: <72 hours post-SAH

Table 4.4 shows the complete SIENAX, DWI and CBF results. SIENAX analysis demonstrated a significant apparent increase in total brain volume in patients compared to healthy

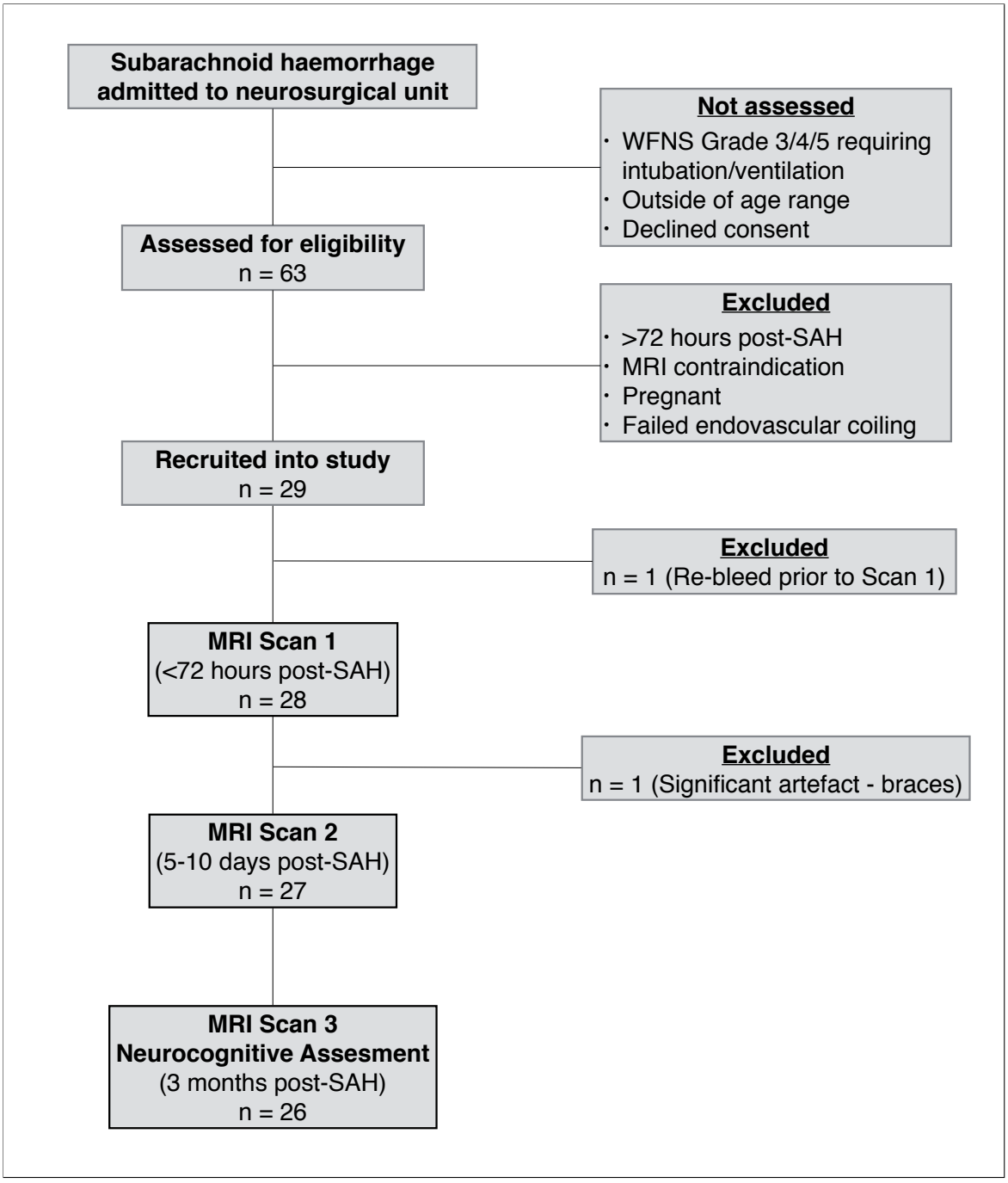


Fig. 4.1: Flowsheet of recruitment into the study

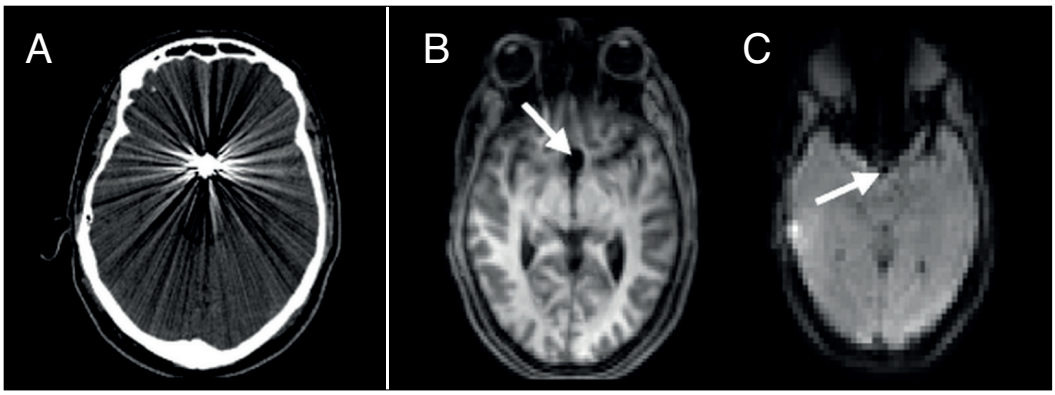


Fig. 4.2: Artifact from endovascular coiling on computed tomography (A), structural (B) and echo-planar (C) magnetic resonance images. White arrows show artifact/dropout resulting from platinum endovascular coils used to secure the ruptured aneurysm

controls (1521 $\pm$ 66mm^3 v 1461 $\pm$ 90mm^3, p=0.0114 unpaired Students t-test) in the first 72 hours post-SAH. Whole brain grey matter volume was also significantly higher in patients compared to controls (790 $\pm$ 44 mm^3 v 746 $\pm$ 50mm^3, p=0.0011 unpaired Students t-test - Figure 4.3: A). Further analysis using VBM to look for regional effects confirmed this difference in grey matter volume included areas bilaterally such as the frontal poles, paracingulate gyri, basal ganglia, thalamus, precuneus and cerebellum (Figure 4.3: B). White matter volume was also significantly higher in patients compared to controls (731 $\pm$ 28ml v 706 $\pm$ 54 ml, p=0.0324 Mann-Whitney U test) and although mean ventricular CSF (vCSF) volumes were higher in patients than controls, this was not statistically significant (45 $\pm$ 18ml v 37 $\pm$ 8ml, p=0.0563 Mann-Whitney U test).

The increased apparent mean grey matter volume in the first 72 hours post-SAH was also associated with a significant decrease in mean grey matter ADC values for patients compared to controls (1023 $\pm$ 17 x 10^{-6}mm^2/s v 1105 $\pm$ 12 x 10^{-6}mm^2/s (unpaired Students t-test, p<0.001) in the DWI data but no overall significant difference in mean grey matter CBF using PCASL (53.83 $\pm$ 2.08ml/100g/min v 57.25 $\pm$ 1.35m/100g/min, p=0.1737 unpaired Students t-test). However, mean grey matter arterial arrival time was prolonged in patients compared to controls (1.52 $\pm$ 0.51s v 1.36 $\pm$ 0.17s, p=0.005 unpaired Students t-test).

Table 4.1: Demographics of recruited patients

Overall Demographics	
n	27
Age (mean/range)	54.66 (31-77)
Gender (M:F)	11:18
WFNS Grade	
1	18
2	19
Modified Fisher Grade	
1	0
2	0
3	6
4	21
Aneurysm Location (%)	
Anterior circulation	12 (44%)
Middle cerebral Artery	6 (22%)
Internal carotid artery	8 (30%)
Posterior circulation	1 (4%)
Left side	12 (44%)
Right side	13 (48%)
Midline	2 (8%)
Complications	
Hydrocephalus	13 (44%)
Extraventricular drain	2 (8%)
DCI/DCI-related cerebral infarction	8 (30%)
Aneurysmal rebleed	0 (0%)
Angiographic vasoconstriction	1 (3%)

Table 4.2: Complete demographic and radiological data for successfully recruited patients

Patient	Age	Sex	Location	Side	WFNS	Fisher	Hydrocephalus	DCI/cerebral infarction
1	77	F	Distal ACA	Left	1	4	Mild/moderate	No
2	30	M	A1/A2 Junction	Left	1	4	None	No
3	55	M	MCA bifurcation	Left	1	4	None	No
4	47	F	Distal ACA	Right	2	4	None	Yes
6	41	F	MCA bifurcation	Left	1	4	None	No
7	62	F	MCA bifurcation	Left	2	4	Mild/moderate	No
8	37	F	PCommA	Left	1	4	None	No
9	44	F	PICA	Right	1	4	Mild/moderate	No
10	62	M	PCommA	Right	1	4	None	No
11	58	F	PCommA	Right	1	4	None	No
12	48	F	ACommA	Midline	2	4	Severe	Yes
13	70	F	PCommA	Right	2	4	Severe	No
14	45	M	ICA	Left	1	4	None	No
15	66	F	MCA bifurcation	Right	1	3	None	Yes
16	44	F	A1/A2 junction	Left	1	3	None	No
17	43	M	Para-opthalmic	Left	1	4	Mild/moderate	No
18	60	M	A1/A2 junction	Right	2	3	Mild/moderate	No
19	69	F	MCA	Left	1	3	None	Yes
20	66	F	A1/A2 junction	Left	1	4	Mild/moderate	No
21	69	F	PCommA	Right	2	4	Mild/moderate	No
22	51	M	A1/A2 junction	Right	1	4	Mild/moderate	Yes
23	59	F	PCommA	Left	2	3	None	Yes
24	39	F	A1/A2 junction	Right	2	4	Mild/moderate	Yes
25	67	M	MCA bifurcation	Right	1	4	None	No
26	49	M	A1/A2 junction	Right	1	3	None	No
27	68	F	A1/A2 junction	Right	1	3	Mild/moderate	No
29	51	F	ACommA	Midline	1	4	Mild/moderate	Yes

Table 4.3: Physiological data recorded during each MRI scan session

	Scan 1		**Scan 2**		**Scan 3**	
	Mean	SD	Mean	SD	Mean	SD
HR (bpm)	73	19	66	13	71	16
MAP (mmHg)	88	9	91	11	86	7
SpO_2 (%)	98.4	2	99.1	1	99.3	2

Table 4.4: MRI scan 1: SIENAX, DWI and ASL data for patients <72 hours post-SAH compared to healthy controls. vCSF = ventricular cerebrospinal fluid, ADC = apparent diffusion coefficient, CBF = cerebral blood flow, AAT = arterial arrival time

	Patients Mean (SD)	**Controls** Mean (SD)	**p value**
SIENAX			
Total brain volume (mm^3)	1521 (66)	1461 (90)	**0.0114**
Grey matter volume (mm^3)	790 (44)	746 (50)	**0.0011**
White matter volume (mm^3)	731 (28)	706 (54)	**0.0324**
vCSF volume (ml^3)	45 (20)	37 (8)	0.0563
DWI			
Mean grey matter ADC (x $10^{-6}mm^2/s$)	1023 (17)	1105 (12)	**<0.001**
PCASL			
Mean grey matter CBF (ml/100g/min)	53.83 (9.73)	57.25 (6.31)	0.1737
Mean grey matter AAT (s)	1.52 (0.51)	1.36 (0.17)	**0.005**

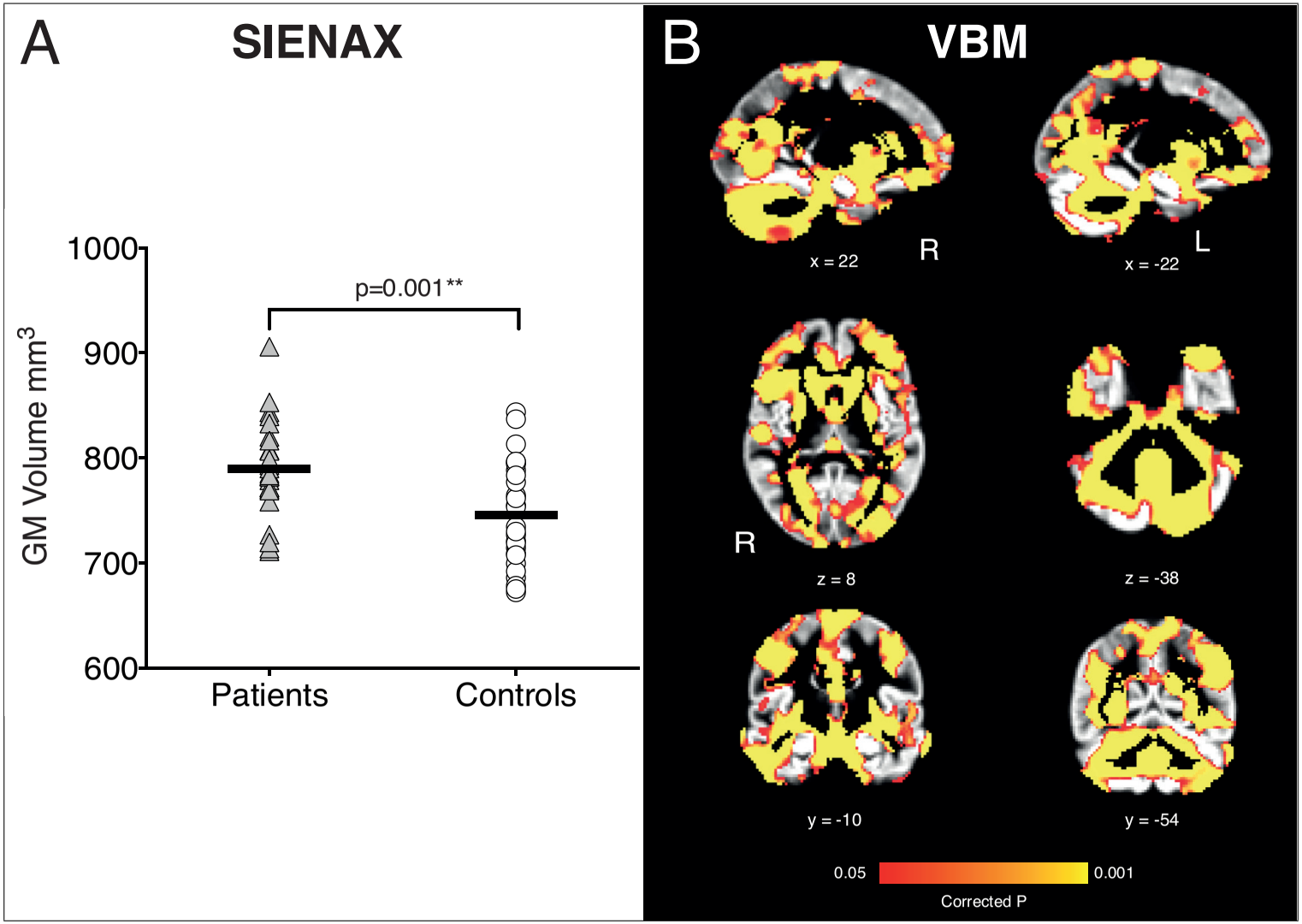


Fig. 4.3: Changes in grey matter volume 72 hours post-SAH compared to healthy controls. **A**: Results from the SIENAX analysis showing a significantly increased apparent whole brain grey matter volume in patients compared to healthy controls - solid bars indicate mean values (**p=0.0011).**B**: Results from the VBM analysis. Regional areas of increased apparent grey matter volume in patients compared to healthy controls (In yellow, p<0.001 FWE-corrected for multiple comparisons, overlaid onto the average of all 54 grey matter volume images)

Table 4.5: MRI scan 2: SIENAX, DWI and ASL data for patients <72 hours post-SAH compared to healthy controls. vCSF = ventricular cerebrospinal fluid, ADC = apparent diffusion coefficient, CBF = cerebral blood flow, AAT = arterial arrival time

	Patients Mean (SD)	**Controls** Mean (SD)	**p value**
SIENAX			
Total brain volume (mm^3)	1502(68)	1455 (99)	0.0708
Grey matter volume (mm^3)	773 (54)	748 (48)	0.0527
White matter volume (mm^3)	729 (29)	707 (54)	0.0901
vCSF volume (ml^3)	46 (20)	37 (8)	**0.037**
DWI			
Mean grey matter ADC (x $10^{-6}mm^2/s$)	991 (48)	1120 (42)	**0.0001**
PCASL			
Mean grey matter CBF (ml/100g/min)	46.95 (6.11)	59.13 (6.28)	**<0.0001**
Mean grey matter AAT (s)	1.64 (0.13)	1.28 (0.58)	**0.0001**

Scan 2: 5-10 days post-SAH

Table 4.5 shows the complete SIENAX, DWI and CBF results. By scan 2, there was no significant difference in total brain volume or white matter volume compared to healthy controls. Although grey matter volumes were higher in patients compared to controls, this was no longer significant. However, ventricular CSF volume was significantly higher in patients (46 $\pm$ 20ml v 37 $\pm$ 8ml, p=0.037 unpaired Students t-test) compared to controls. Again though, more detailed analysis with VBM showed significant differences in regional grey matter volume in patients compared to controls, especially still in the regions of the basal ganglia (caudate and putamen bilaterally), occipital cortex, precuneus and cerebellum.

In the patients, there was a significant reduction in mean grey matter ADC (991 $\pm$ 48 x $10^{-6}mm^2/s$ v 1120 $\pm$42 x $10^{-6}mm^2/s$, p=<0.0001 Mann-Whitney U test) and mean grey matter CBF (46.95 $\pm$ 6.108ml/100g/min v 59.13 $\pm$ 6.28ml/100g/min, p=<0.0001 Mann-Whitney test) compared to healthy controls. AAT was further prolonged in patients compared to controls (1.64 $\pm$ 0.13s v 1.28 $\pm$ 0.58, p=<0.0001 Mann-Whitney U test).

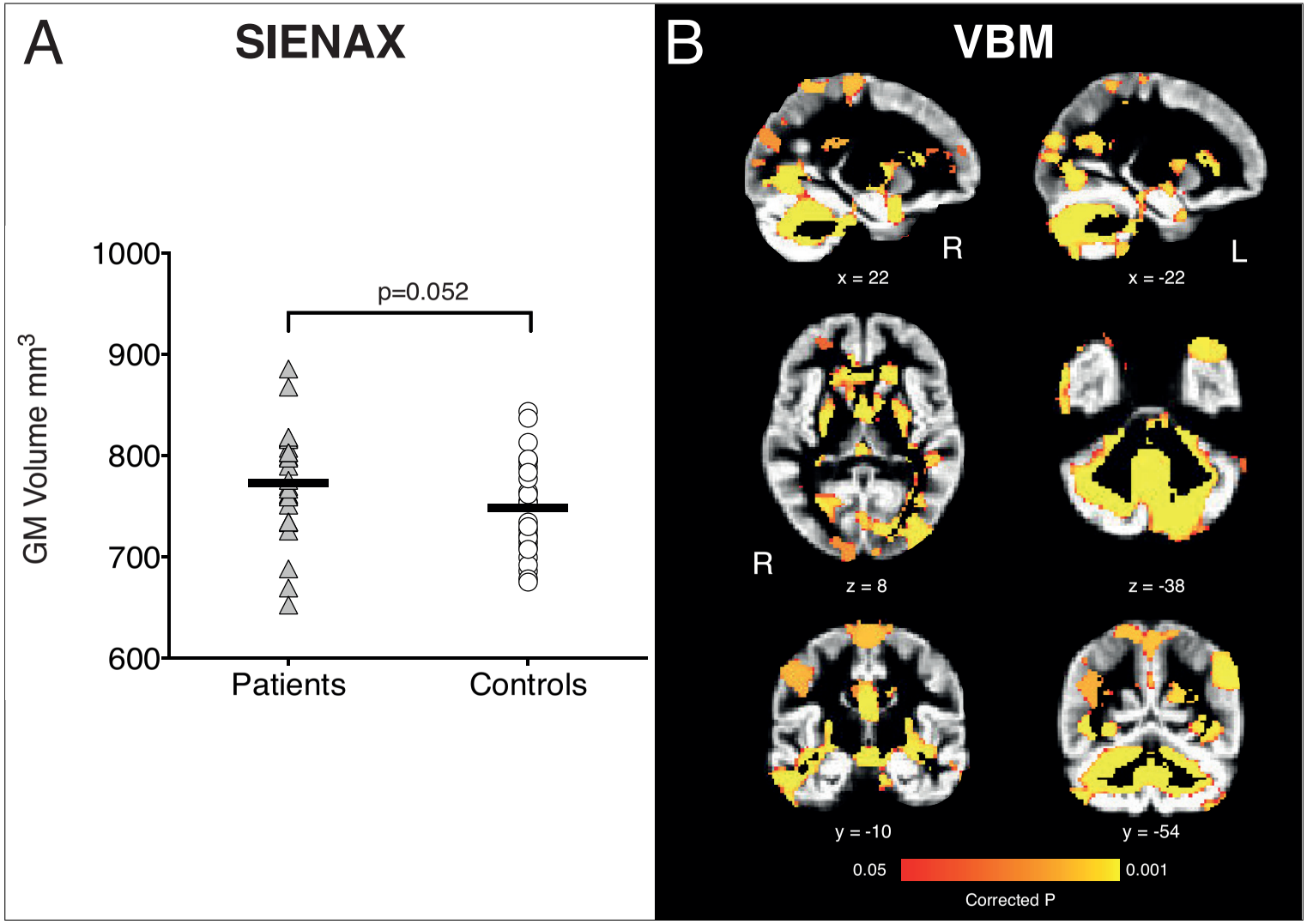


Fig. 4.4: Changes in grey matter volume 5-10 days post-SAH compared to healthy controls. **A**: Results from the SIENAX analysis showing no significant difference in whole brain grey matter volume in patients compared to healthy controls - solid bars indicate mean values (p=0.052).**B**: Results from the VBM analysis. Regional areas of increased apparent grey matter volume in patients compared to healthy controls (In yellow, p<0.001 FWE-corrected for multiple comparisons, overlaid onto the average of all 52 grey matter volume images)

Scan 3: 3 months post-SAH

Table 4.6 shows the complete SIENAX, DWI and CBF results. At 3 months post-SAH, the SIENAX analysis showed no significant difference in total brain volume ($1480 \pm 61mm^3$ v $1461 \pm 90.05mm^3$, p=0.3885 unpaired Students t-test), grey matter volume ($765 \pm 45mm^3$ v $748 \pm 50mm^3$, p=0.2126 unpaired Students t-test), or white matter volume $718 \pm 23mm^3$ v $708 \pm 55mm^3$, p=0.4325 unpaired Students t-test) between patients and controls. However, there remained a significant increase in ventricular CSF volume in patients when compared to controls (55 ± 26ml v 37 ± 8ml, p=0.0021, unpaired Students t-test). There was no significant difference in whole brain grey matter ADC (1140 ± 65 x $10^{-6}mm^2/s$ v 1096 ± 13 x $10^{-6}mm^2/s$, p=0.0998 Mann-Whitney U test), CBF (53.44 $/pm$ 8.73 ml/100g/min v 56.11 $/pm$ 6.23 ml/100g/min, p=0.2843 unpaired Students t-test) nor AAT (1.28 $/pm$ 0.42 v 1.34 $/pm$ 0.28, p=0.1033 Mann-Whitney U test)

However, the VBM analysis highlighted a persistent and significantly increased apparent grey matter volume in patients compared to controls in the cerebellum (Crus I, Crus II and VIIb regions bilaterally – Figure 4.5-B). Using this area as an ROI, neither grey matter ADC (910 ± 54 x $10^{-6}mm^2/s$ v 874 ± 39 x $10^{-6}mm^2/s$, unpaired Students t-test p=0.0711) nor CBF (51.98 ± 13.40ml/100g/min v 55.03 ± 15.62ml/100g/min, p=0.362 unpaired Students t-test) were significantly different between patients and controls.

Table 4.6: MRI scan 3: SIENAX, DWI and ASL data for patients 3 months post-SAH compared to healthy controls. vCSF = ventricular cerebrospinal fluid, ADC = apparent diffusion coefficient, CBF = cerebral blood flow, AAT = arterial arrival time

	Patients Mean (SD)	**Controls** Mean (SD)	**p value**
SIENAX			
Total brain volume (mm^3)	1480 (61)	1461 (90)	0.3885
Grey matter volume (mm^3)	765 (45)	748 (50)	0.2126
White matter volume (mm^3)	718 (23)	708 (55)	0.4325
vCSF volume (mm^3)	55 (26)	37 (8)	**0.0021**
DWI			
Mean grey matter ADC (x $10^{-6}mm^2/s$)	1140 (65)	1096 (13)	**<0.00998**
PCASL			
Mean grey matter CBF (ml/100g/min)	53.44 (8.73)	56.11 (6.23)	0.2843
Mean grey matter AAT (s)	1.28 (0.42)	1.34 (0.28)	0.1033

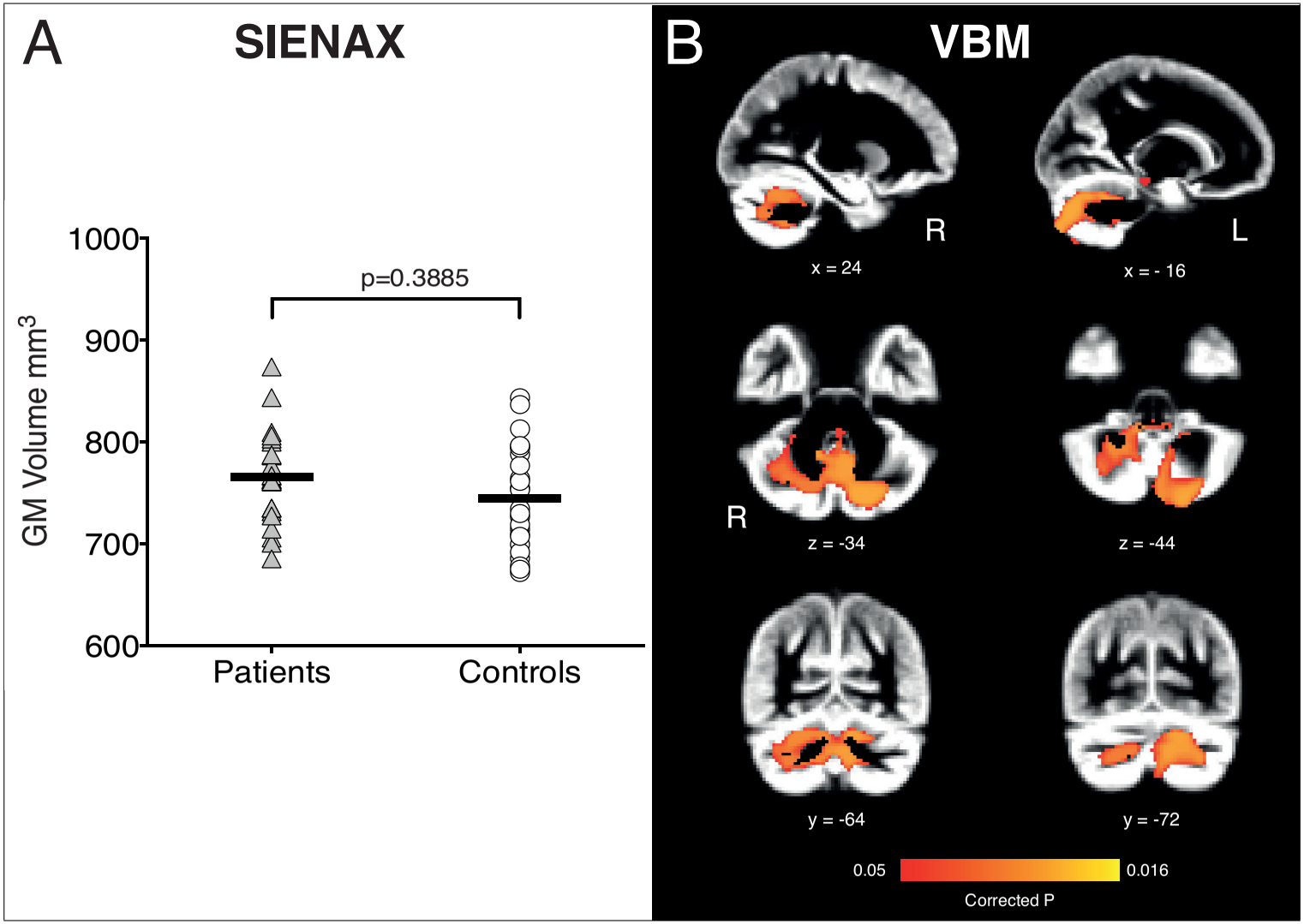


Fig. 4.5: Changes in grey matter volume 3 months post-SAH compared to healthy controls. **A**: Results from the SIENAX analysis show no significant difference for whole brain grey matter volume in patients compared to healthy controls - solid bars indicate mean values. **B**: Results from the VBM analysis highlight a regional increased apparent grey matter volume in the cerebellum bilaterally in patients compared to healthy controls (In yellow, $p<0.016$ FWE-corrected for multiple comparisons, overlaid onto the average of all 50 grey matter volume images).

Longitudinal changes: Scan 1 (<72 hours), scan 2 (5-10 days) and scan 3 (3 months) post-SAH

Figure 4.7 shows the longitudinal changes in the SIENAX data for each time point. There was no significant difference between scan 1 and scan 2 for total brain, grey matter, white matter or ventricular CSF volumes. Between the first 72 hours and 3 months post-SAH, analysis with SIENA showed a -0.42 percentage reduction in total brain volume. Over the same period, there was a significant reduction in total brain volume (1521 $\pm$ 66ml v 1461 $\pm$ 90ml, p=0.0038 repeated measures (RM) ANOVA), grey matter volume (792 $\pm$ 46ml v 748 $\pm$ 50ml, p=0.0141 RM ANOVA) and white matter volume (733 $\pm$ 28ml v 708 $\pm$ 55ml, p=0.0185 RM ANOVA) in patients compared to controls. Associated with these decreased brain volumes was an increase in ventricular CSF volume in patients (45 $\pm$ 18ml v 54.93 $\pm$ 26ml, p=0.0293 RM ANOVA). Figure 4.6-A and 4.6-B shows the changes in grey matter in the SIENAX and VBM analyses.

DWI imaging showed no significant difference between scan 1 and 2 (1023 $\pm$ 60 x 10^{-6}mm^2/s v 990.8 $\pm$ 48 x 10^{-6}mm^2/s, p = 0.142 RM ANOVA) and in parallel with the structural changes, a statistically significant increase in whole brain grey matter ADC values in patients was seen (1023 $\pm$ 17 x 10^{-6}mm^2/s v 1140 $\pm$ 19 x 10^{-6}mm^2/s, p<0.001 RM ANOVA) between scan 1 and scan 3. Mean grey matter CBF was significantly decreased between scan 1 and scan 2 (53.83 $\pm$ 9.71ml/100g/min v 46.95 $\pm$ 6.10ml/100g/min, p=0.0150 RM ANOVA) and mean grey matter arterial arrival time was significantly prolonged (1.52 $\pm$ 0.51s v 1.64 $\pm$ 0.13s, p=0.0010 RM ANOVA).

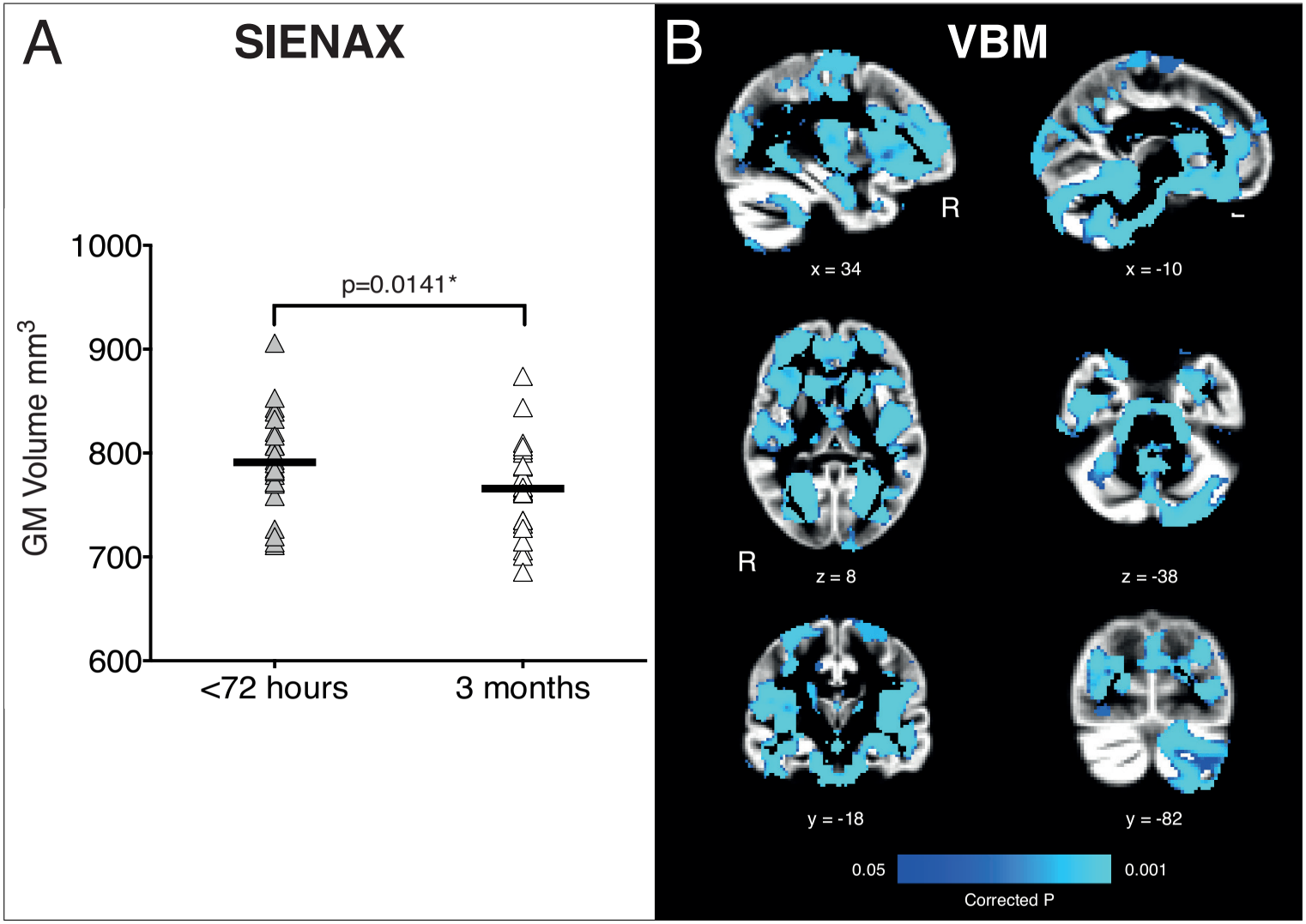


Fig. 4.6: Grey matter volume at <72 hours and 3 months post-SAH. **A**: Results from the SIENAX analysis show a significant decrease in whole brain grey matter volume in patients compared to healthy controls - solid bars indicate mean values (**p=0.0047).
B: Results from the VBM analysis show widespread decreased grey matter volume at 3 months compared to <72 hours post-SAH (In blue, p<0.001 FWE-corrected for multiple comparisons, overlaid onto the average of all 50 grey matter volume images).

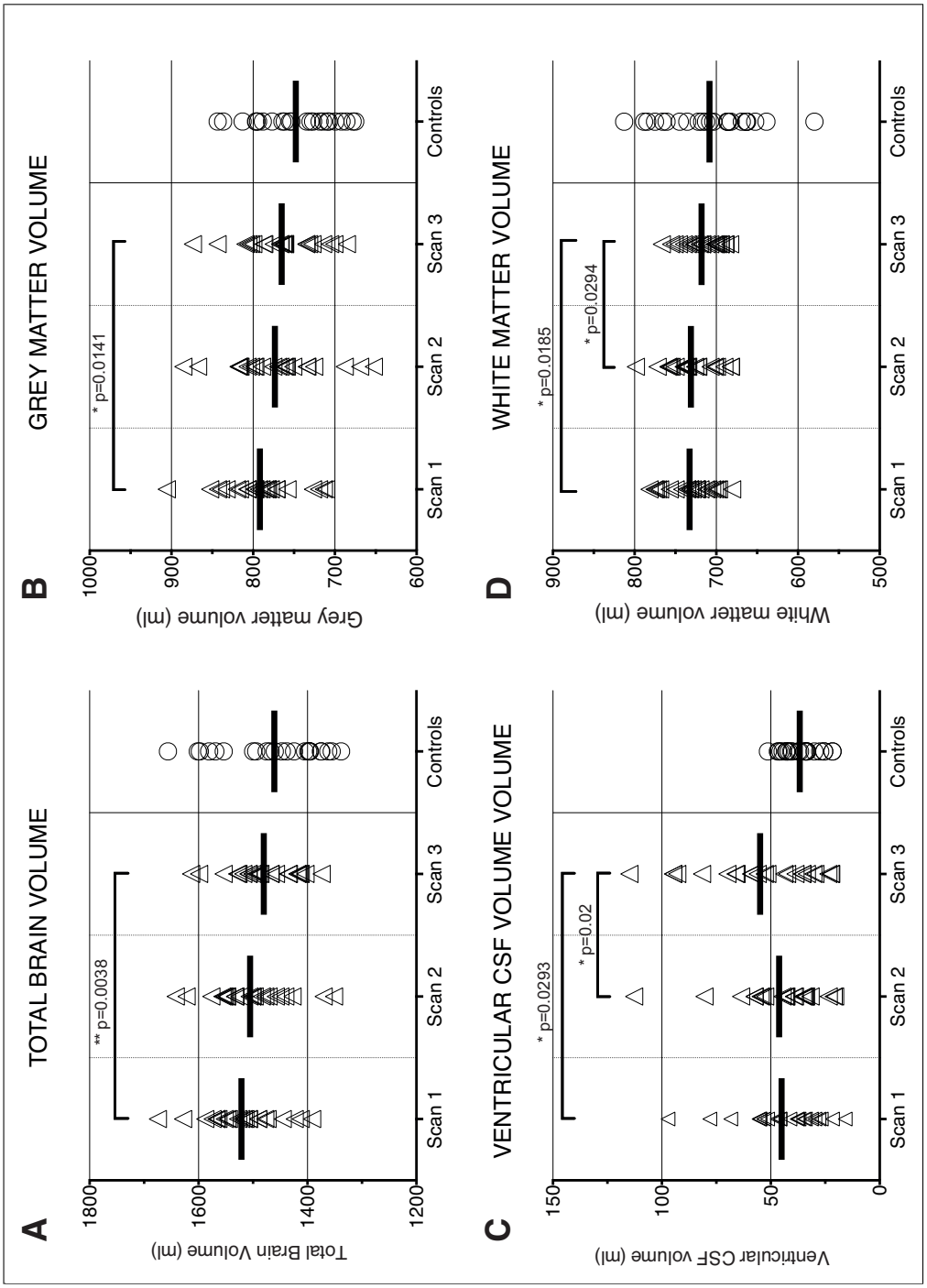


Fig. 4.7: SIENAX results for patients at each MRI scan point: <72 hours, 5-10 days and 3 months post-SAH. **A**: Total brain volume, **B**: Grey matter volume, **C**: Ventricular CSF volume, **D**: White matter volume. Solid bars indicates mean values. Healthy control data is included for comparison

4.5.3 DCI/DCI-related cerebral infarction and relationship to MRI results

A total of twelve patients (44.4%) were diagnosed with radiological evidence of new cerebral infarction on early DWI sequences and/or follow-up MRI imaging at 3 months. Of these, 5 were diagnosed with DCI during their acute admission as per the consensus guidelines. However, on further examination by a consultant neuroradiologist, infarcts seen in four of the patients were confirmed within 24 hours of treatment on DWI MRI sequences and by new transient neurological deficits when waking up after treatment and were therefore excluded as being likely to be caused by peri-procedural embolisation. This left a total of eight patients (29.6%). New clinical neurological deficits developed between day 3 and 15 in all patients diagnosed with DCI, and the location of cerebral infarction corresponded to the arterial territory distal to the maximum collection of blood on admission CT imaging in six out of these eight patients (75%).

There was no significant structural differences in grey matter volume seen with either the SIENAX or VBM analyses in the first 72 hours post-SAH and incidence of DCI or DCI-related infarction. Numbers of patients who underwent DWI imaging was too low to interpret differences in ADC values. However, those patients with DCI/DCI-related infarction had significantly lower grey matter CBF values in the first 72 hours than those without (49.36 ± 6.88ml/100g/min v 37.00 ± 10.48ml/100g/min, p=0.0020 unpaired Students t-test). There were no further significant differences between the groups in grey matter CBF at either scan 2 or scan 3 (Figure 4.8).

4.5.4 Neurocognitive outcomes

Neurocognitive outcome testing

Complete normalised data from the formal neurocognitive testing at 3 months is presented in Figure 4.9 on page 75. At 3 months post SAH, 11 patients (44%) had cognitive deficits in the domain of executive function, 4 patients (16%) had deficits in verbal memory, 4 (16%) patients had defects in non-verbal skills/memory, 4 (16%) patients had deficits in general verbal skills and 7 patients (28%) had deficits in processing speed.

Of the 25 patients who attended and completed formal neurocognitive testing, 11 patients were diagnosed as being neurocognitively impaired as per the criteria described in section

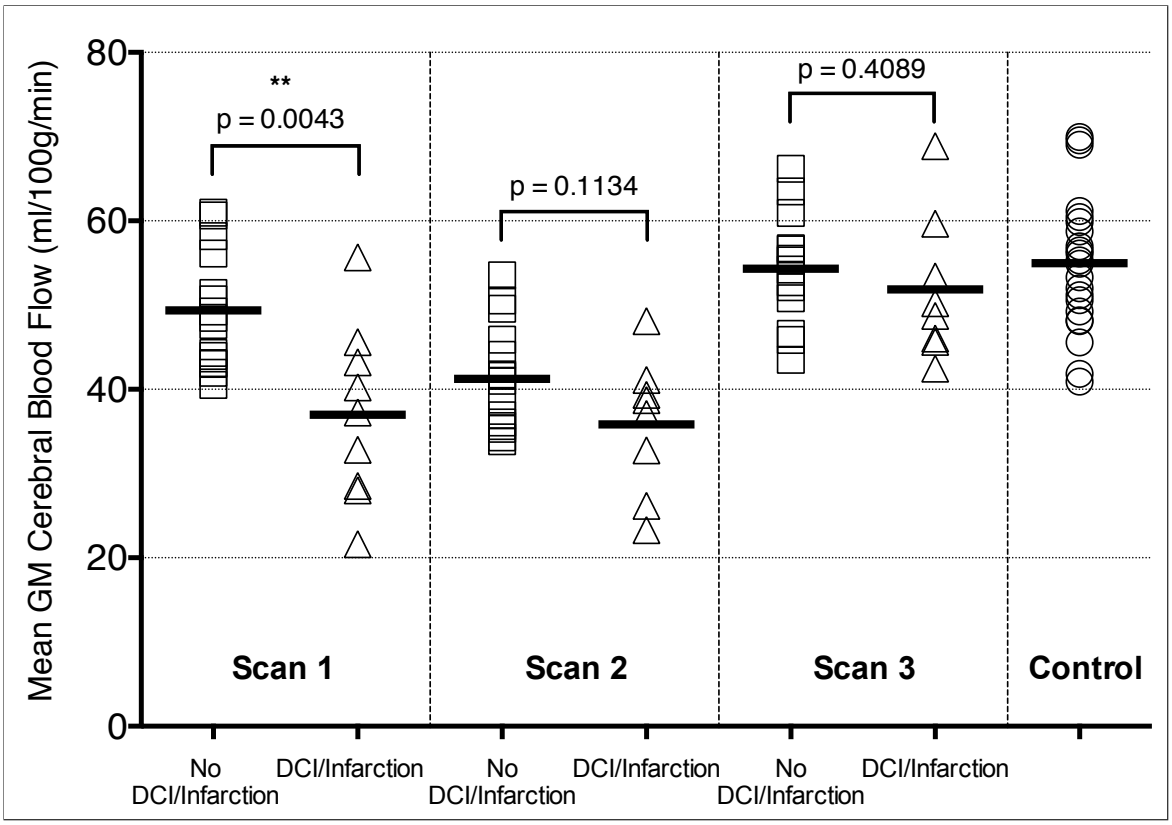


Fig. 4.8: Differences in mean grey matter cerebral blood flow for patients with and without DCI/DCI-related cerebral infarction at each MRI scan point. Those patients with DCI had significantly lower mean grey matter CBF in the first 72 hours than those without. Control data is included for comparison.

4.2.4 on page 55. There were no differences in baseline neurocognitive function between patients with impairment and those without as measured by the NART (99.09 $\pm$ 2.09 v 105.9 $\pm$ 3.11, p = 0.1133 unpaired Students t-test). There was however a significant difference in post-SAH IQ (as measured by the WASI - a test not included in defining neurocognitive impairment) between those patients diagnosed with neurocognitive impairment and those without (91.73 $\pm$ 13.03 v 107.4 $\pm$ 12.64, p=0.0062 unpaired Students t-test).

At three months post-SAH, patients with neurocognitive impairment were significantly worse in the cognitive domains of executive skills, processing speed and non-verbal skills as well as having significantly lower ACE-R scores (93.44 $\pm$ 4.871 vs 88.78 $\pm$ 5.286, p=0.0292 Mann Whitney U test) than those patients with no impairment.

There was no significant difference between the impaired and non-impaired groups in terms of age (p=0.8401), gender (p=>0.99), Fisher score (p=0.8527). Interestingly, patients with no neurocognitive impairment had a higher mean WFNS score than those with impairment (p=0.0421) and more patients with DCI/cerebral infarction.

Table 4.7: Clinical features of patients with and without neurocognitive impairment at three months post-SAH. Mann-Whitney U tests were used to determine significance of group differences.

	Impaired	**Non-impaired**	**p-value**
n	11	14	
Age (mean years, range)	52.73 (37-72)	54.57 (31-70)	0.8401
Gender (male : female)	4 : 7	5 : 9	0.99
Premorbid IQ (Mean NART, SD)	99.09 (2.09)	105.9 (3.11)	0.1133
WFNS Grade			
Mean	1.1	1.5	0.0421*
1	10	7	
2	1	7	
Fisher Grade			
Mean	3.7	3.6	0.8527
1	0	0	
2	0	1	
3	3	4	
4	8	10	
Ruptured Aneurysm Location			
Anterior	5 (45%)	6 (43%)	
ICA	0 (0%)	2 (14%)	
MCA	3 (27.5%)	2 (14%)	
Posterior	3 (27.5%)	4 (29%)	
Left side	4	7	
Right side	6	6	
Midline	1	1	
Other			
Hydrocephalus	4	8	0.4283
Angiographic vasospasm	0	1	>0.99
DCI	3	5	>0.99

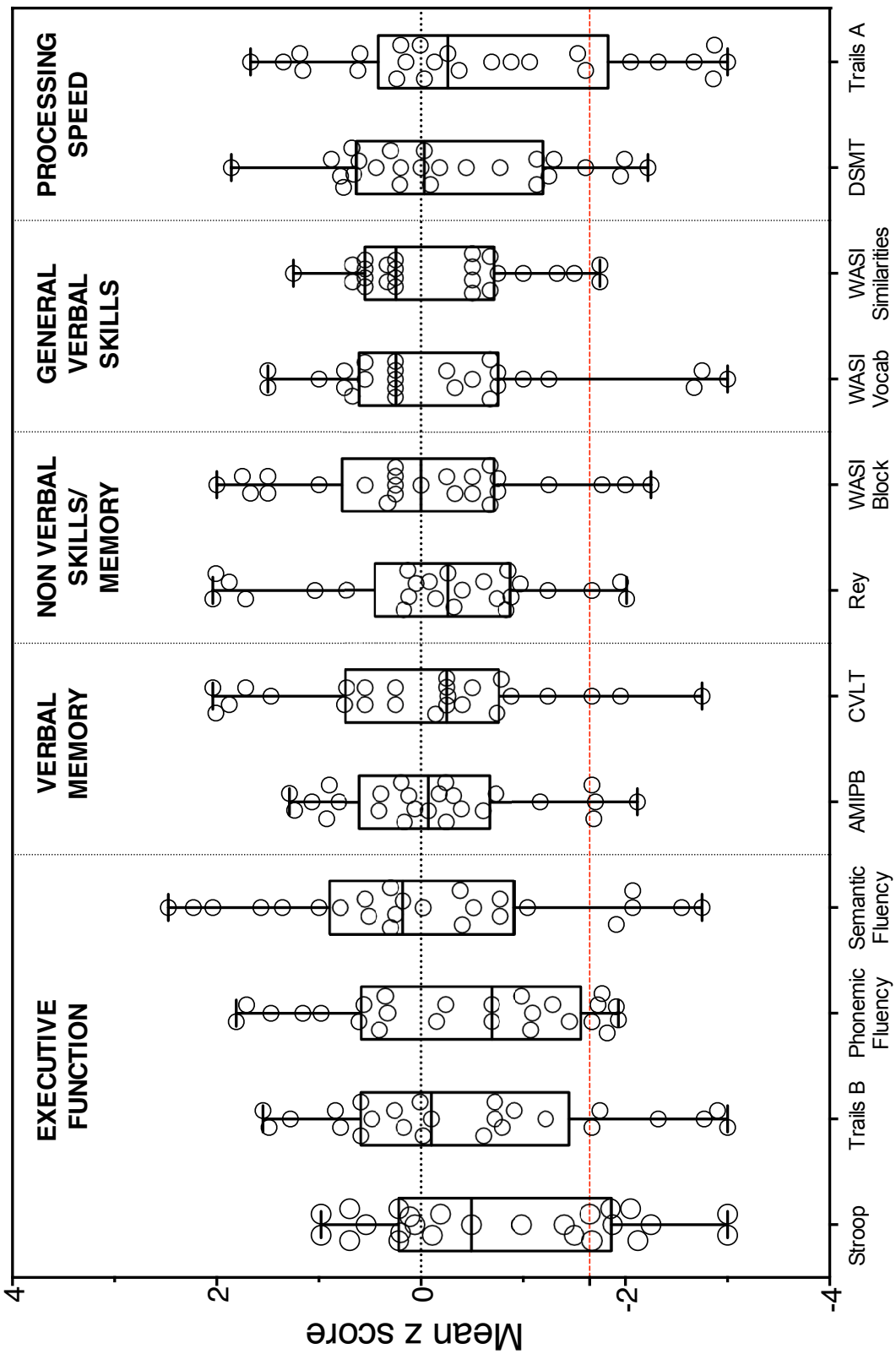


Fig. 4.9: Box and whisker plots showing data from each neurocognitive test at 3 months post-SAH. Individual data points for each patient are plotted on top of each index box-and-whisker plot with tests grouped by the cognitive domain assessed. The line in the box plot indicates the median value, the width of the box shows the interquartile range and the whiskers show the minimum and maximum values. The hatched line on the *y*-axis represents a *z*-score of -1.67 corresponding to the 5th centile.

Table 4.8: Mean ACE-R results from patients acquired at each scan point and healthy age/gender paired controls

ACER	**Scan 1**		**Scan 2**		**Scan 3**		**Control**	
Component	**Mean**	*SD*	**Mean**	*SD*	**Mean**	*SD*	**Mean**	*SD*
Attention	15.7	*2.4*	16.2	*2.0*	16.8	*1.4*	17.3	*0.6*
Memory	18.3	*4.8*	20.8	*4.0*	23.2	*2.8*	24.7	*1.7*
Fluency	8.1	*2.8*	8.4	*2.7*	11.3	*1.9*	12.1	*1.7*
Language	22.3	*3.5*	22.9	*3.8*	24.5	*1.9*	25.6	*0.6*
Visuospatial	12.8	*3.5*	13.2	*3.2*	15.1	*1.1*	15.6	*0.6*
Total	77.4	*12.7*	81.5	*11.5*	91.1	*6.4*	95.4	*3.2*

Relationship between early brain injury and neurocognitive outcomes

We next sought to investigate the relationship between MRI data from the first 72 hours and neurocognitive outcomes. There was a significant negative correlation between grey matter volume for the cerebellum and performance on the ACE-R test (r = 0.389, p=0.006 - Pearson's correlation) - i.e. the greater the cerebellum grey matter ROI volume, the worse the performance on the ACE-R at 3 months. Furthermore, those patients diagnosed with neurocognitive impairment at 3 months post-SAH had higher grey matter volumes for the cerebellum ROI than those with no neurocognitive impairment (Figure 4.10-A). Cohen's d is an effect size calculator used to indicate the standardised difference between two means with $d \geq 0.2$ considered a 'small' effect size, $d \geq 0.5$ a 'medium' effect size and $d \geq 0.8$ a 'large' effect size [58]. Cohen's d calculated between patients with impairment and those without for grey matter volumes in the cerebellum ROI is 0.72 - suggesting a medium to large effect size difference between the two groups.

Figure 4.10-B shows that compared to those patients with no neurocognitive impairment, patients with neurocognitive impairment also demonstrated increased apparent grey matter volume in the same cerebellum ROI with similarly large differences in effect size between the two groups in scan 1 (Cohen's d = 2.03) and scan 2 (Cohen's d = 1.03).

Looking at the first 72 hours post-rupture, analysis of the VBM data showed that patients who develop neurocognitive impairment post-SAH already demonstrate significantly higher grey matter values compared to those patients with no impairment in a similar cerebellum ROI to that in Scan 3, involving executive areas such as Crus I, Crus II and VIIb - figure 4.11. Although there was no difference in overall mean grey matter CBF between impaired and non-impaired patients at Scan 1, this VBM ROI was associated with reduced grey

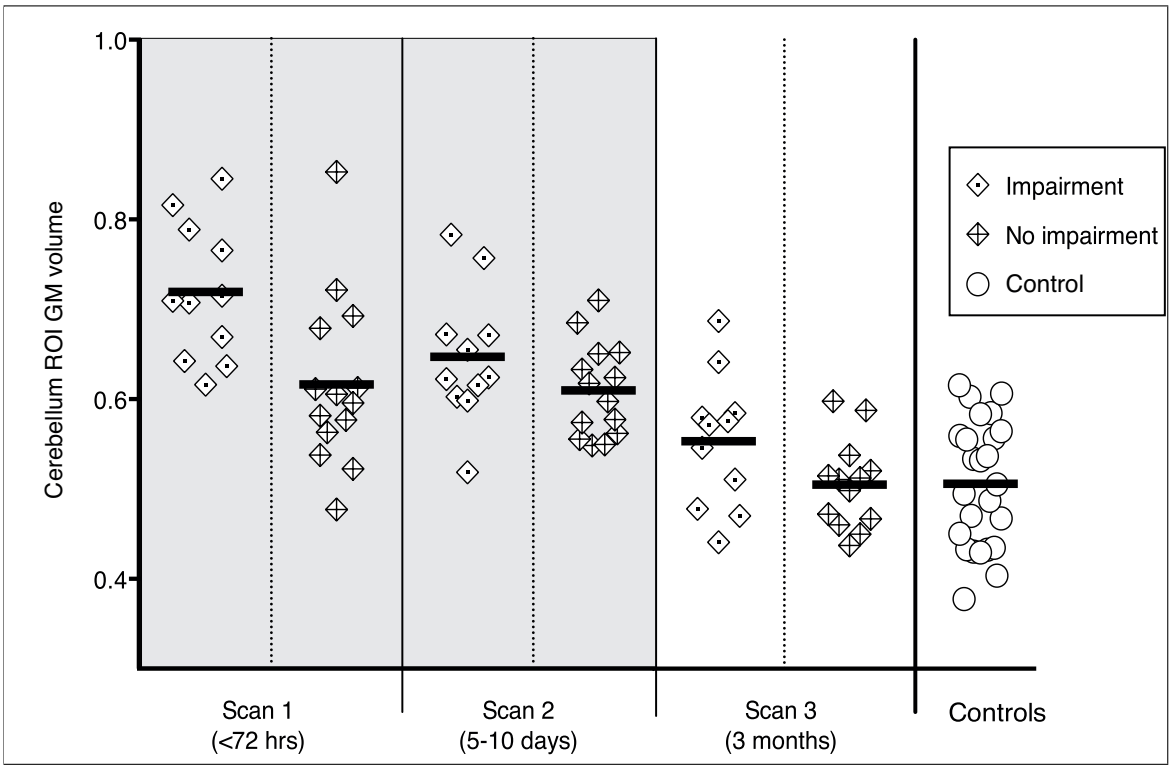


Fig. 4.10: **A**: Grey matter volume data for the area of significance between patients and controls at 3 months post-SAH versus neurocognitive outcome. At scan 3, there is a small effect size difference between values for grey matter volume in the cerebellum ROI in all patients compared to controls. However, splitting the patients by neurocognitive outcome, there is a relatively large effect size difference between those patients with neurocognitive impairment and those without. This suggests that group structural changes seen at 3 months post-SAH are being driven by those patients with worse neurocognitive outcomes. This difference in grey matter volume for the cerebellum ROI between patients with neurocognitive impairment and those without is also present at the two earlier acute MRI scan points (highlighted in the grey background).

matter cerebral blood flow in those patients with neurocognitive impairment compared to those without (51.19 $\pm$ 13.64ml/100g/min v 32.53 $\pm$ 11.71ml/100g/min, p=0.0013 unpaired Students t-test - figure 4.12).

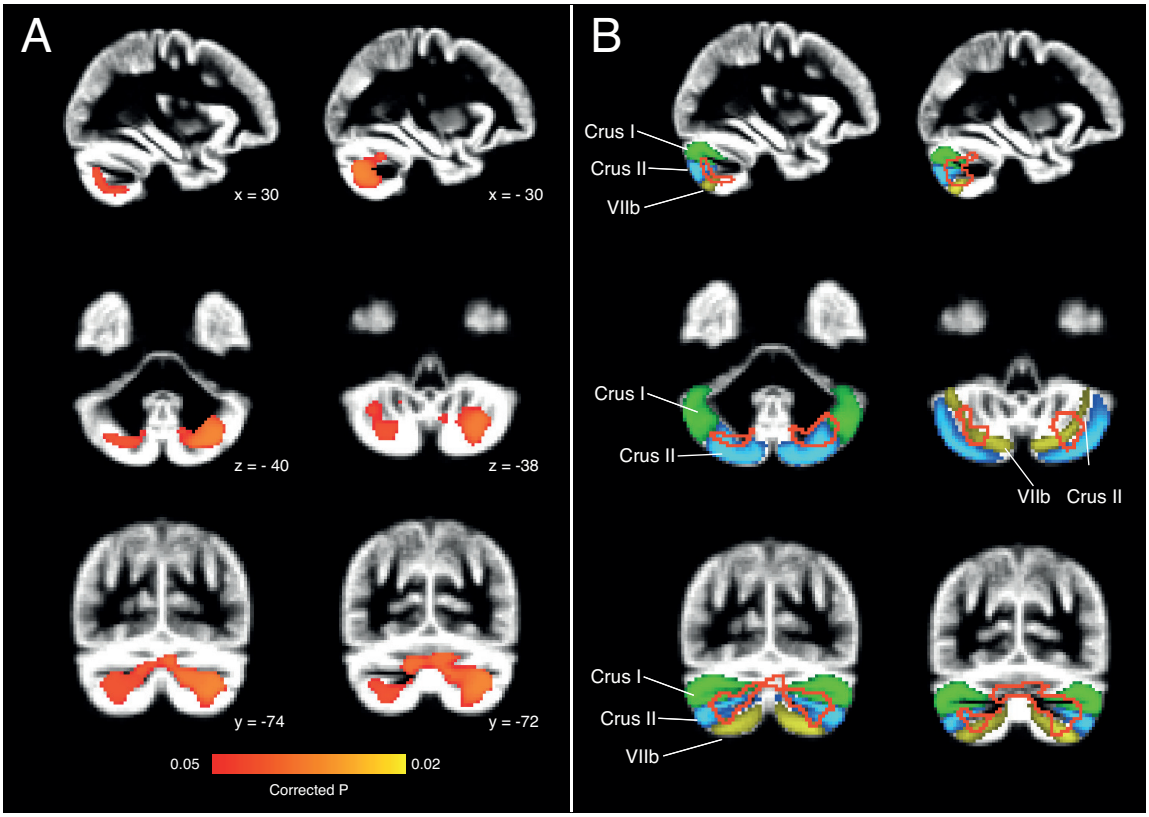


Fig. 4.11: Results from VBM analysis showing regional changes in grey matter volume in patients <72 hours post-SAH. Patients who go on to develop neurocognitive impairment demonstrate higher grey matter volumes in a cerebellum ROI including crus I, crus II and VIIb bilaterally. (In yellow, p<0.02 FWE-corrected for multiple comparisons, overlaid onto the average of all 25 grey matter volume images).

Finally, a receiver operating characteristic (ROC) curve demonstrated that neurocognitive impairment could be accurately predicted from structural images acquired from the first 72 hours post-SAH. Weighted average grey matter volume values were obtained from the T1-weighted scans of the 28 patients only at baseline (<72 hours post-rupture), using a region of interest in the cerebellum. This was defined as the only region showing significant difference when comparing the entire group of patients at 3 months post-SAH with the healthy controls (out-of-sample data).

Based on these GM volume values, 84% accuracy could be achieved for patients with subsequent neurocognitive impairment with a grey matter volume threshold of 0.1792, for

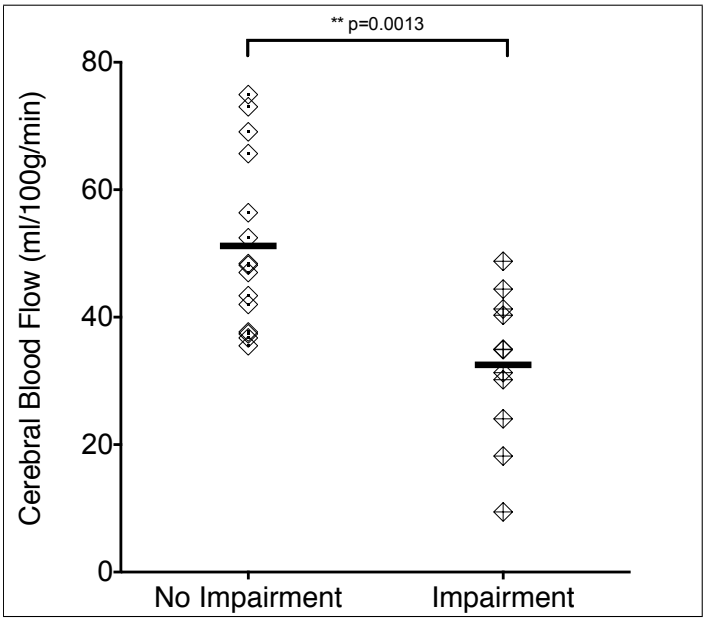


Fig. 4.12: Mean cerebral blood flow in the cerebellum VBM ROI <72 hours post-SAH is lower in patients with neurocognitive impairment compared to those with no impairment.

which the sensitivity is 81.8% and the specificity 85.7%. The receiving operator characteristic (ROC) curve is shown in figure 4.13.

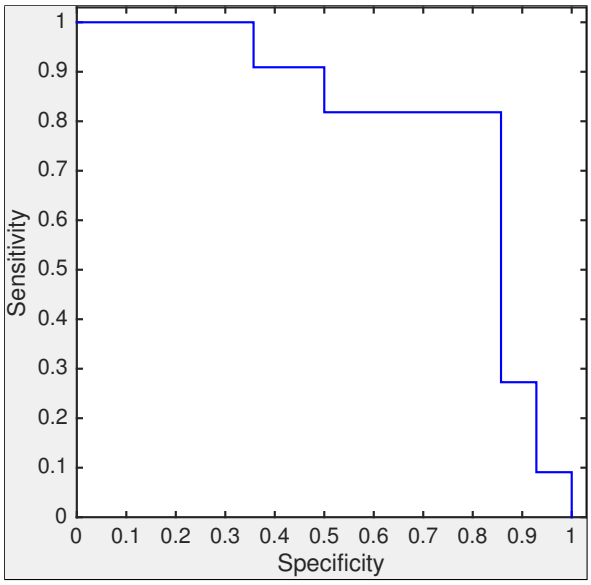


Fig. 4.13: Receiver operator characteristic (ROC) curve of the structural data from <72 hours post-SAH

In the control group, there were no significant correlations across whole brain grey matter volume and neurocognitive function as measured by ACE-R scores.

4.6 Discussion

The aim of this study was to use longitudinal MRI imaging in the acute phase and at three months post-SAH in good grade SAH patients undergoing embolisation to characterise the global and regional changes in brain structure and perfusion that occur as a result of early brain injury and to investigate the impact of these changes on short term neurocognitive outcomes. We have demonstrated that MRI is well tolerated by patients, even acutely post-rupture, and can be used to objectively quantify pathophysiological changes in grey matter volume, ADC and CBF. A number of significant findings have emerged from these results which are discussed below.

Global and regional changes in brain structure and perfusion due to early brain injury can be objectively quantified using MRI in the acute period post-SAH

Firstly, using an unbiased SIENAX and whole-brain voxelwise VBM approach, results from the structural analysis demonstrate that despite being "good grade" SAH (WFNS 1 and 2), apparent grey matter volume was increased significantly throughout the brain in the first 72 hours post-SAH compared to gender and age paired controls, in areas including the prefrontal regions, precuneus, cerebellum and the basal ganglia - areas known to be especially vulnerable to hypoxic-ischaemic injury. Associated with this rise in grey matter volume was a significant decrease in grey matter ADC values compared to controls, suggesting restricted diffusion and that changes in grey matter volume seen in the VBM analysis are likely to be the result of cytotoxic cerebral oedema. This is in concordance with other studies in both animals [44] and patients [267, 60]. Interestingly, though other studies using DWI imaging acutely post-rupture have shown conflicting results with increased grey matter ADC values compared to healthy controls - although the timings of scan sessions post-SAH was later than in our study (mean 9 days post-SAH) and specific multiple regions of interest were used [187]. It may be that this represents a transition from cytotoxic oedema initially post-SAH to more vasogenic oedema in the subsequent days.

Global cerebral oedema is a well recognised feature of early brain injury in both experimental and clinical SAH, the incidence in “good grade” subarachnoid patients remains unknown and may play a key role in both short and long term outcomes. It is evident on admission CT scans in 6 – 8% of patients [57, 151] and develops over the first 6 days in an additional 12% but is

difficult to objectively quantify with routine clinical neuroimaging [57, 280]. The incidence of global cerebral oedema in "good grade" SAH patients (WFNS I and II) is unknown and the results of more recent studies suggest that the incidence in all SAH patients may be much higher than previously quoted and in the region of 57-81% of patients [350, 268]. Given that global cerebral oedema is associated with worse initial clinical condition [350] and early brain metabolic distress [129] as well as poor clinical and neurocognitive outcomes [164], it remains an important therapeutic and diagnostic target in the acute period post-rupture.

The ASL results demonstrate a wide variation in cerebral blood flow response in the first 72 hours post-SAH when compared to healthy controls. Although mean grey matter CBF was not significantly different between patients and controls, there was a significant increase in mean grey matter AAT that might be due to microvascular cerebral vasoconstriction given that the incidence of angiographic vasospasm was so low in our study. There was no significant difference in mean grey matter CBF between patients and controls but looking more closely at the data, this is probably due to the heterogeneous grey matter CBF response in patients post-rupture ranging from reduced flow, to normal flow, to hyperaemia. Although early brain injury is associated with global cerebral ischaemia in experimental models of SAH, similar varying CBF results acutely post-rupture in patients have been reported in other studies of SAH patients using PET, CT perfusion and single TI PCASL [205, 138, 12]. These results call into question current neurocritical care strategies targeted towards maintaining an arbitrary cerebral perfusion pressure and suggest that whilst CBF is important, other measures of cerebral injury such as global cerebral oedema and metabolic markers may be of more value.

"Good grade" SAH is still associated with high levels of subtle neurocognitive deficits and impairment

Despite being "good grade" SAH, results from the neurocognitive testing show the incidence of cognitive symptoms at 3 months post-SAH remains high. 11 out of 25 patients studied (44%) were defined as being neurocognitively impaired with significant deficits (z-score of $\leqslant -1.645$) in the cognitive domains of executive functioning, processing speed and memory most commonly seen in our study. This is in agreement with other studies which have suggested that the incidence of neurocognitive deficits after SAH ranges from 7 to 62% of patients [140].

As described in the introduction, accurately defining outcomes after SAH is difficult. In the majority of large studies, outcome is normally assessed using either the Glasgow Outcome Scale (GOS) [146] or the modified Rankin scale [96]. Although these scales enable predictions to be made regarding the effects of treatment in patients with a range of acute brain injuries, there are doubts as to whether a simple scale from 0-6 or 1-5 can accurately capture the exact and full range of neurocognitive deficits seen post-SAH. As a result, subtle neurocognitive deficits that exert a disproportionately significant impact on quality of life can go undiagnosed. Interestingly, few studies have specifically focused on outcomes in patients with good clinical grade SAH (i.e. WFNS 1 and 2). This seems strange given this group potentially has the most to benefit from the accurate diagnosis and management of subtle neurocognitive deficits and impairment that may be missed by more simple outcome scales.

Although the large variability in the prevalence of cognitive deficits can partly be attributed to the heterogeneous nature of SAH e.g. aneurysm location, blood load and incidence of hydrocephalus and DCI etc., some of this variability may also be due to the absence of standardised criteria for diagnosing patients with neurocognitive impairment. Just as both research and clinical practice have benefited from consensus guidelines for the definition of DCI and DCI-related cerebral infarction, the accuracy of assessing outcomes post-SAH would benefit from a clear definition for deficits in cognitive domains and overall neurocognitive impairment. As there is no validated threshold for impairment, the majority of studies define impairment using arbitrary cutoffs. We specifically used the same criteria to define neurocognitive impairment as that used in two large prospective trials to assess neurocognitive impairment post-SAH - the N-ISAT trial [279, 278] and Wong et al. [339].

DCI and DCI-related infarction are associated with lower mean grey matter CBF <72 hours post-SAH but not neurocognitive outcomes

Five patients were diagnosed with DCI during hospital admission. All progressed to develop DCI-related cerebral infarction as seen on 3 month MRI scanning. However, a further three patients had evidence of DCI-related cerebral infarction but did not meet the criteria for DCI whilst in hospital suggesting that they may have had clinical symptoms of DCI that were "sub-threshold" for diagnosis and again highlights that it might be more appropriate to consider DCI as a "spectrum" of disease rather that a binary phenomenon acutely post-SAH [261]. This is further supported by the group reduction in mean grey matter CBF and prolonged arterial arrival time (AAT) between the first 72 hours post-SAH and days 5-10 - potentially due to cerebral vascoconstriction causing a reduction in arterial flow velocity.

In our study, there was a significant difference in mean grey matter CBF in the first 72 hours post-SAH in patients diagnosed with DCI or DCI-related cerebral infarction that was not seen subsequently at either days 5-10 (peak incidence for DCI) or 3 months post-SAH. This is in agreement with other studies quantifying admission CBF in the first 72 hours post-SAH [317, 248, 170]. A recent systematic review and meta-analysis of CT perfusion (CTP) and DCI showed that admission CTP cannot be reliably used to predict DCI but could predict DCI at the time of clinical deterioration [62]. However, this discrepancy can be potentially explained by the multitude of different definitions for DCI and techniques for measuring perfusion used in the studies included in the systematic review and further large studies using standardised imaging modalities and protocols are needed to investigate this further.

Finally, we found no relationship between mean grey matter CBF assessed within 72 hours post-SAH and cognitive outcomes at three months. This is in agreement with a recent study using CT perfusion [138] and provides further evidence that the pathophysiology behind neurocognitive impairment post-SAH extends beyond reductions in CBF and may involve other pathways underlying early brain injury.

Changes in cerebellum grey matter volume <72 hours post-rupture can predict neurocognitive outcomes at 3 months post-SAH

The origin of the long-term cognitive symptoms after SAH and the role played by acute pathophysiological and clinical changes post-rupture remains poorly understood. Although ADC and cerebral blood flow appear to resolve back to control levels by 3 months post-SAH, the VBM analysis highlighted a persisting increased apparent grey matter volume in patients in the cerebellum - mainly localized to an ROI including the Crus I, II and VIIb regions bilaterally. This difference appears to be driven by those patients who have developed neurocognitive impairment post-SAH (Cohen's d = 0.72) and grey matter volumes for this ROI negatively correlate with ACE-R performance. Furthermore, from the first 72 hours post-rupture, patients who go on to develop neurocognitive impairment have already significantly increased apparent grey matter volumes in an ROI including the crus I, II and VIIb regions compared to those patients who go on to good neurocognitive recovery. There was no significant difference between clinical features such as Fisher score, age, gender, hydrocephalus and angiographic vasospasm and patients with and without impairment and interestingly, the mean WFNS score was higher for those patients with no impairment. Finally, we have showed that based on the remaining structural VBM abnormalities seen at scan 3 across all patients vs controls, in the first 72 hours post-rupture it is possible to predict

with 84% accuracy and 86% specificity which patients will go on to poor neurocognitive outcomes.

During a mild-to-moderate reduction in perfusion, the brain's autoregulatory mechanisms preserve blood flow to "older" regions such as the brain stem, cerebellum, and basal ganglia. As the cerebellum is mainly composed of grey matter, it has a higher risk of injury due to its high metabolic requirement for oxygen and glucose to supply the large number of synapses. Therefore, if cerebral perfusion is markedly reduced, all of the brain is affected but those areas with higher metabolism such as the cerebellar cortex suffer the most [137]. It is therefore highly likely that damage to the cerebellum sustained as a result of early brain injury may influence the degree of neurocognitive impairment exhibited by patients at 3 months post-SAH.

There is increasing convergent and multi-modal evidence from both basic science and clinical studies that the cerebellum has an expanded role beyond motor control and coordination into perceptual processes and higher cognitive functions. A dichotomy between sensorimotor and cognitive areas of the cerebellum has been suggested [270, 271] with the cerebellar anterior lobe primarily focused on motor control, the cerebellar vermis involved in affective processing, and the posterior cerebellum contributing to more complex cognitive operations [296]. More recently, studies have used resting-state functional magnetic resonance imaging (fMRI) to probe the topography of cerebral–cortical connectivity in the cerebellar cortex [226]. This has provided further support for a cerebellar role in both motor and cognitive tasks, and better established the existence of functional cerebellar subregions and their connections to other cortical networks [119, 297]. The areas of the cerebellum showing increased apparent grey matter volume in scan 1 and scan 3 mainly incorporate Crus I, Crus II and VIIb regions. In humans, functional imaging studies have highlighted the role of Crus I in executive functions, such as abstract reasoning [210], working memory [71], information updating [59], and response selection [72]. Impairment in verbal fluency has also been reported with lesions of the right Crus II [247].

To our knowledge, there have been no other studies reporting structural, DWI or perfusion changes to the cerebellum after SAH. There is evidence of abnormal cerebral volumes in patients at 6 months post-SAH but differences for grey matter parenchyma were not significant.[68] Volume loss at one year post-SAH in the hippocampus and amygdala has also been reported in SAH patients with good or moderate outcomes.[30] Of particular interest to our study is the pathophysiology behind the raised cerebellar volumes seen in patients compared to controls at 3 months post-SAH. One plausible hypothesis for the increased

apparent grey matter volume is that this represents residual cerebral oedema. The exact time course of oedema resolution after SAH remains unknown. Studies in animals suggest that cerebral oedema following traumatic brain injury resorbs over a period of a week.[23] Although there was not a significant difference in ADC between patients and controls in the cerebellum, it is entirely possible that patients may still experience some degree of grey matter oedema at 3 months post-SAH and that this may also reflect the increased ability of VBM to detect differences in grey matter volumes at a voxelwise level.

Another hypothesis is that this increased apparent grey matter volume at a fairly early stage in recovery post-SAH may represent a sequelae of Wallerian degeneration - a process of neuronal degeneration that occurs following axonal injury in the brain. Following Wallerian degeneration of the axons distal to the region of injury, macrophages remove the debris during the first 2-4 weeks and there is the formation of a dense astrocytic scar [42]. Wallerian degeneration can be seen on MRI imaging between 4-12 weeks after ischaemic stroke [305] and may underlie the increased regional grey matter volumes detected in patients post-SAH in the cerebellum – although it would be more likely that this would result in reduced rather than increased volume.

Finally, the study population of "good grade" SAH patients included a large number with high blood load (Modified Fisher grade 4 and 5). It is therefore entirely plausible that the recumbent nature of many patients during the acute admission post-SAH has led to the cerebellum sustaining an increased injury due to gravity resulting in a higher blood load and the subsequent haemotoxicity.

4.6.1 Methodological considerations

Although we have studied a cohort of patients representative of the standard clinical population of patients with "good grade" SAH, there are some potential limitations that need to be considered. Although the number of participants in the study is relatively small, the VBM MRI data was analysed on a whole brain basis using a non-parametric technique and correcting for multiple comparisons over all voxels. Other data analysis was conducted using non-parametric techniques when data was non-normally distributed. Secondly, the VBM, SIENA/SIENAX analysis ADC and CBF values obtained may be affected by residual blood in the subarachnoid space and ventricles post-SAH. As the number of patients with high blood load (Fisher grade 3 and 4) was high in our study, this may potentially act as a confound on the reliability of the tissue segmentations achieved using the FMRIB tool

FAST (used in the structural analysis pipeline) and the calculation of ADC values. Although VBM differences around the ventricular system should be interpreted with caution due to the likelihood of large amounts of blood, the majority of difference seen were in areas separated from the ventricles e.g. basal ganglia, cerebellum and precuneus are therefore likely to be correct. Furthermore, the VBM results from Scan 3 suggest significant differences between patients and controls at a time when any extravasated blood should have been broken down and metabolised. Controls were also not available for test-retest assessment of the imaging variables used in this study. Finally, as the control group consisted of healthy volunteers, we were unable to control for the impact of the aneurysm on pre-morbid cerebral morphology, physiology and neurocognitive status that might have confounded the neurocognitive testing at 3 months post-SAH. The group was however tightly matched for age/gender to the recruited patients and although we cannot exclude that recruited patients had pre-existing cognitive deficits, the NART test undertaken as part of the neurocognitive assessment is a measure of pre-existing cognitive status and was not significantly different between those patients with neurocognitive impairment and those without.

4.7 Conclusions

Results from this study demonstrate the potentially under-recognised and key role of cerebellar injury in modulating neurocognitive outcomes after SAH and that VBM represents an objective and accurate method of quantifying global cerebral oedema in patients acutely following SAH. The study shows that a simple T1 structural MRI scan in the first 72 hours post-SAH can objectively predict short term neurocognitive outcome with 80% success. The high sensitivity of VBM to global and regional changes in grey matter volume also demonstrates that significant global cerebral oedema occurs acutely "good grade" SAH as a result of early brain injury. Damage to the cerebellum acutely is likely to result in neurocognitive impairment and along with, may act as a therapeutic and diagnostic marker of early brain injury.

4.8 Supplementary material

Table 4.9: Scan 1 v Control: Common local peaks (unless specified otherwise) of the significant clusters (P < 0.05 FWE-corrected) showing increased GM density in SAH patients compared to controls. Local maximum t values correspond to Fig. 4.3. BA, Brodmann area, GM, grey matter

			MNI (mm)			
	Cortical region	**Side**	**x**	**y**	**z**	**Local maximum t**
Scan 1 v Control	Cerebellum (I-IV)	Lt	0	-46	-22	7.2
	Cerebellum (Crus II)	Rt	50	-64	-46	3.82
		Lt	-50	-58	-50	3.44
	Cerebellum (VIIb)	Rt	34	-76	-54	
	Frontal pole	Lt	42	40	2	3.28
	Premotor cortex (BA 6)	Rt	26	-26	68	3.81
	Primary motor cortex (BA4a)	Rt	6	-28	74	3.46
	Cingulate gyrus	Lt	-10	34	16	4.47
		Rt	14	34	16	4.39
	Paracingulate gyrus	Lt	-2	48	28	3.34
	Superior parietal lobule	Rt	-18	-38	40	3.66
	Inferior parietal lobule	Lt	-42	-84	30	3.31
	Broca's area (BA44)	Rt	50	10	14	4.18
	Visual cortex V1 (BA17)	Rt	22	-62	2	4.85
	Visual cortex V4	Lt	-20	-76	-4	3.49
	Primary auditory cortex	Rt	56	-18	8	3.54
	Lateral occipital cortex	Lt	-58	-58	38	4.89
	Temporal fusiform cortex	Rt	32	-56	-4	5.49
	Precuneus cortex	Rt	-20	-56	18	3.03
	Insular cortex	Lt	-36	-22	-2	5.42
	Putamen	Lt	-26	-6	12	3.34
		Rt	26	-6	10	3.09
	Caudate	Lt	-10	8	16	4.47
		Rt	16	6	24	4.64
	Hippocampus	Lt	-18	-26	-16	4.63

Chapter 5

Resting state functional connectivity after Subarachnoid Haemorrhage

Chapter Overview

The study of brain activity and connectivity at rest provides a unique opportunity for the investigation of the brain substrates of neurocognitive impairment after SAH. This knowledge may contribute to improve clinical management during the acute phase post-rupture and help target appropriate rehabilitation programs. Typically, functional magnetic resonance imaging (fMRI) studies investigate regional changes in neuronal activity compared to a baseline level while completing a task or in response to a stimulus. However, this approach is not practical when dealing with acutely unwell patients post-SAH. Resting-state functional connectivity studies provide information about brain activity and connectivity in the absence of task performance, allowing researchers to investigate patient populations with more significant brain injury as no specific cognitive ability is demanded. The overall aim of this study therefore was to investigate changes in resting state functional connectivity following SAH using a whole brain independent component analysis technique and correlate any changes seen with data from Chapter 4 as well as neurocognitive outcomes.

Results demonstrate that at 3 months post-SAH, patients showed increased functional connectivity compared to healthy controls in a number of functional networks associated with complex cognitive or emotional functions including the DMN (medial and posterior divisions), cerebellum, basal ganglia/thalamus and executive function networks. These changes persisted despite correction for changes in grey matter density - important to note in the context of the widespread structural changes seen in Chapter 4. These differences were already present in the first 72 hours post-SAH in a number of these networks, suggesting that the pathophysiological effects of early brain injury have a significant effect on functional connectivity. Finally, functional connectivity and ALFF at 3 months post-SAH has a positive correlation with neurocognitive outcomes. This effect is present in the first 72 hours suggesting that damage to network integrity at this stage may underlie subsequent poor neurocognitive outcomes.

Finally, results are discussed in the context of other studies and we hypothesise that altered functional connectivity in the cerebellum and basal ganglia plays a key role in modulating neurocognitive outcomes after SAH.

5.1 Introduction

SAH is a disease associated with a particularly high rate of neurocognitive impairment in those patients who survive to hospital discharge, particularly in the domains of attention, working memory and executive function [283, 339, 120, 140]. As seen in Chapter 4, even in the less severe SAH patients (WFNS Grade I and II), significant global changes to brain tissue occur in the first hours following aneurysm rupture due to early brain injury which are likely to play a key role in determining neurocognitive and functional outcomes in survivors. However, the process by which early brain injury leads to persistent cognitive impairments in patients and the mechanisms and neural correlates underlying functional recovery after SAH remain unclear.

Cognitive functions rely on the integrated operation of large-scale distributed brain networks [201]. The interaction between regions within a network (i.e. the functional connectivity), and the interactions between networks are both important for efficient cognitive function [156, 181]. Recent methodological advances in fMRI analysis allow both structural and functional connectivity to be studied in vivo in both healthy volunteers and clinical populations. These approaches hold the promise of dramatically improving the understanding of the impact of both acute and chronic brain injury on neurocognitive outcomes, and the compensatory mechanisms that such injuries trigger [351]. This is likely to be particularly important in understanding the cognitive effects of SAH, due to the global nature of the initial pathophysiological damage caused by aneurysm rupture.

Typically, functional magnetic resonance imaging (fMRI) studies investigate regional changes in neuronal activity compared to a baseline level while completing a task or in response to a stimulus. However, this approach is not practical when dealing with acutely unwell patients post-SAH. Resting-state functional connectivity studies provide information about brain activity and connectivity in the absence of task performance, allowing researchers to investigate patient populations with more significant brain injury as no specific cognitive ability is demanded. Functional connectivity can be defined as the temporal correlation between spatially remote neurophysiological events, expressed as deviation from statistical independence across these events in distributed neuronal groups and areas [34]. When individuals are at rest and not engaged in task-related activity ("resting state"), blood oxygen dependent level (BOLD) MRI can be used to study the intrinsic connectivity of brain networks in task-free settings by mapping temporally synchronous, spatially distributed, spontaneous low frequency signals [104]. Resting-state fMRI (rfMRI) experiments are less prone to

multi-site variability, allow a wider range of patients to be scanned and make it possible to study multiple cortical systems from one dataset [103].

A number of group studies have reported changes in RSNs in clinical populations. Changes in the functional connectivity of the default mode network (DMN) have been hypothesised to underlie the behavioural symptoms seen in chronic neuro-psychiatric illnesses such as schizophrenia [333, 186], depression, chronic pain and autism. However, there is a growing awareness that altered patterns of functional connectivity may also play a role in cognitive recovery from more acute illness such as traumatic brain injury [228] and ischaemic stroke [329] as well as SAH.

Recently, an index named amplitude of low-frequency fluctuation (ALFF) of the resting-state fMRI signal has been suggested to reflect the intensity of regional spontaneous brain activity. Few studies have considered the ALFF in patients at rest and its implications in terms of cognitive dysfunction. ALFF has been found to be decreased in patients with mild cognitive impairment and Alzheimer disease and increased and positively correlated with neurocognitive outcomes in patients at four years post traumatic brain injury [228]. This makes it an interesting target for research in patients with SAH - both as a potential biomarker of early brain injury as well as in helping to interpret potential changes in resting state connectivity.

The only studies to investigate resting state connectivity changes after SAH have used a seed-based, "a priori" approach rather than looking at changes over the whole brain. The overall aim of this study therefore was to investigate changes in resting state functional connectivity following SAH using a whole brain independent component analysis technique and correlate any changes seen with neurocognitive outcomes. The following hypotheses were specifically tested. Firstly, in the first 72 hours following SAH, early brain injury is associated with altered functional connectivity in resting state brain networks that support high-level cognitive function and that changes are sustained at three months post-SAH. Secondly, that abnormal resting state connectivity is related to structural changes in grey matter that occur due to early brain injury in the first 72 hours post-SAH (as seen in Chapter 4) which will be tested by correlating functional changes with grey matter structural results obtained from the VBM analysis. Finally, that changes in functional connectivity seen in patients correlate with impairments in neurocognitive function.

Taken together with Chapter 4, we aim to link acute abnormalities in structural and functional brain connectivity with subsequent recovery in the months following SAH, and demonstrate how sustained changes in network function relate to neurocognitive impairment.

5.2 Methods

Patients were recruited and clinical, MRI and neurocognitive data acquired as described in Chapter 4.

5.2.1 Pre-processing

Analysis of ALFF and resting state MRI data was conducted using tools from the FMRIB Software library (www.fmrib.ox.ac.uk/fsl) and customised MATLAB scripts (The MathWorks Inc.). Individual data sets were pre-processed by first removing the first 6 seconds from each time series to ensure magnetization equilibrium, brain extraction with the FSL tool BET, motion correction using MCFLIRT, high-pass filtering with a frequency cut-off at 100 s (to remove slow drifts e.g. associated with the MRI scanner) and spatial smoothing at 6mm full-width half-maximum. Each dataset was then affine linearly registered to the respective structural T1 image acquired and then non-linearly registered to the MNI 152 standard template.

Data de-noising

As described in Chapter 3, we decided to implement ICA data de-noising using FIX given the high potential for movement artefact in acutely unwell SAH patients and the necessity for additional respiratory bellows equipment in the RETROICOR approach that might increase scanning time and reduce patient tolerance.

Whilst FIX can be automated for larger datasets, we decided to individually review each dataset to ensure maximum accuracy. First level ICA data for each subject and healthy control was reviewed using the FSL tool MELVIEW. Each component was labelled as signal or noise according to predetermined templates (See [264]). Any component that did not fit discretely into either group was left in the dataset and not removed. Following this, FIX was used as follows:

1. To regress the full space of the motion confounds obtained from MCFLIRT from both the data and from all the ICA component timeseries

2. To estimate the contribution of both “signal” and “noise” components in order to identify the noise specific variance

3. Remove the unique contribution of the components identified as "noise" from the data

5.2.2 Amplitude of low frequency fluctuations data analysis

Calculation of ALFF was performed with customised MATLAB (Mathworks Inc.) scripts. The power of the low frequency fluctuations in the frequency range 0.01-0.1Hz was measured using a multi-taper spectral estimation using discrete prolate spheroidal (Slepian) sequences with five tapers, and fast Fourier transform algorithm for the resting-state time series for each voxel. Finally, voxelwise GLM was applied using permutation-based non-parametric testing with the FSL tool Randomise using 5000 permutations and correcting for multiple comparisons across space. This analysis was constrained to grey matter using the relevant grey matter group mask obtained from the VBM analysis described in Chapter 4.

5.2.3 Resting state data analysis

Figure 5.1 shows the overall analysis pipeline used for the analysis of the resting state data.

For each separate group analysis, resting state MRI data were analysed in three parts:

Estimation of independent spatial components

First, resting state networks common to all patients at each MRI scan time point and age/gender paired healthy controls were identified using probabilistic independent component analysis implemented in MELODIC [26]. This group ICA approach offers much more robust delineation of identifiable networks [290, 161].

For this analysis, the resting scans for all subjects were combined into a single 4D data set for each group analysis (Scan 1 v Control, Scan 2 v Control, Scan 3 v Control, Longitudinal Patients). This was then decomposed into spatio-temporal components that represent large-scale patterns of co-activating voxels accounting for statistically independent sources of variation in the measured functional MRI signal[26]).

Automatic model-order estimation identified the following independent spatial components:

- Scan 1 v Control: 26 independent spatial component networks

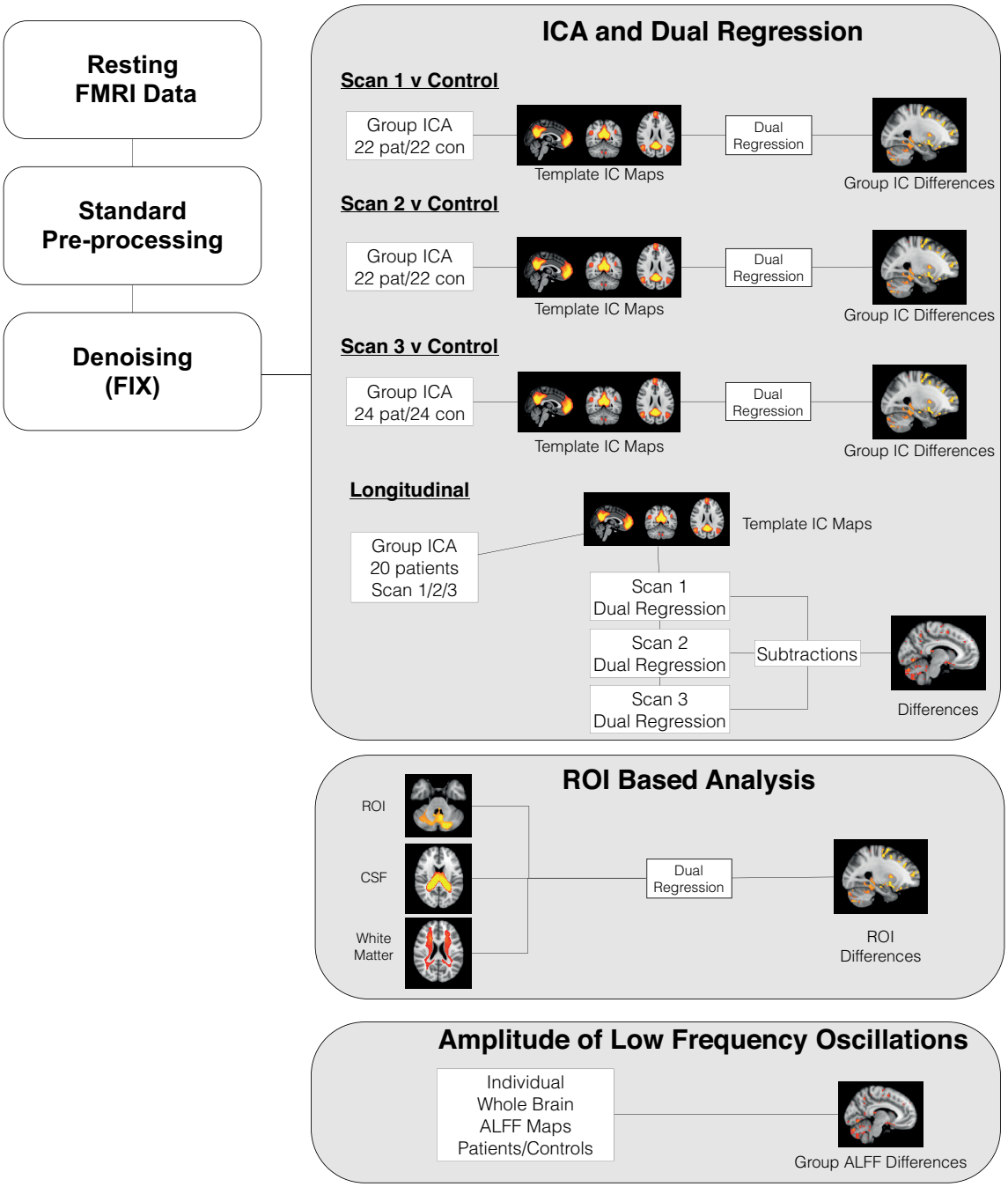


Fig. 5.1: Flowsheet outlining the analysis of resting state functional connectivity and amplitude of low frequency oscillations data

- Scan 2 v Control: 23 independent spatial component networks
- Scan 3 v Control: 28 independent spatial component networks

Of these, for each comparison, we selected those components for further analysis based on visual neuroanatomical correspondence and cross-correlation ($p<0.05$) with consistently identified resting state networks described in the literature (e.g. Smith et al, 2009 [290] - see Figure 5.2). For each comparison, 13 networks were identified as being potentially functionally relevant. The remaining components were classified as noise demonstrating either head motion, cerebrospinal fluid signal, and B0 artifact amongst others as discussed previously [66, 290]. Figures 5.3, 5.4, 5.5 and 5.6 show these functionally significant networks for each comparison.

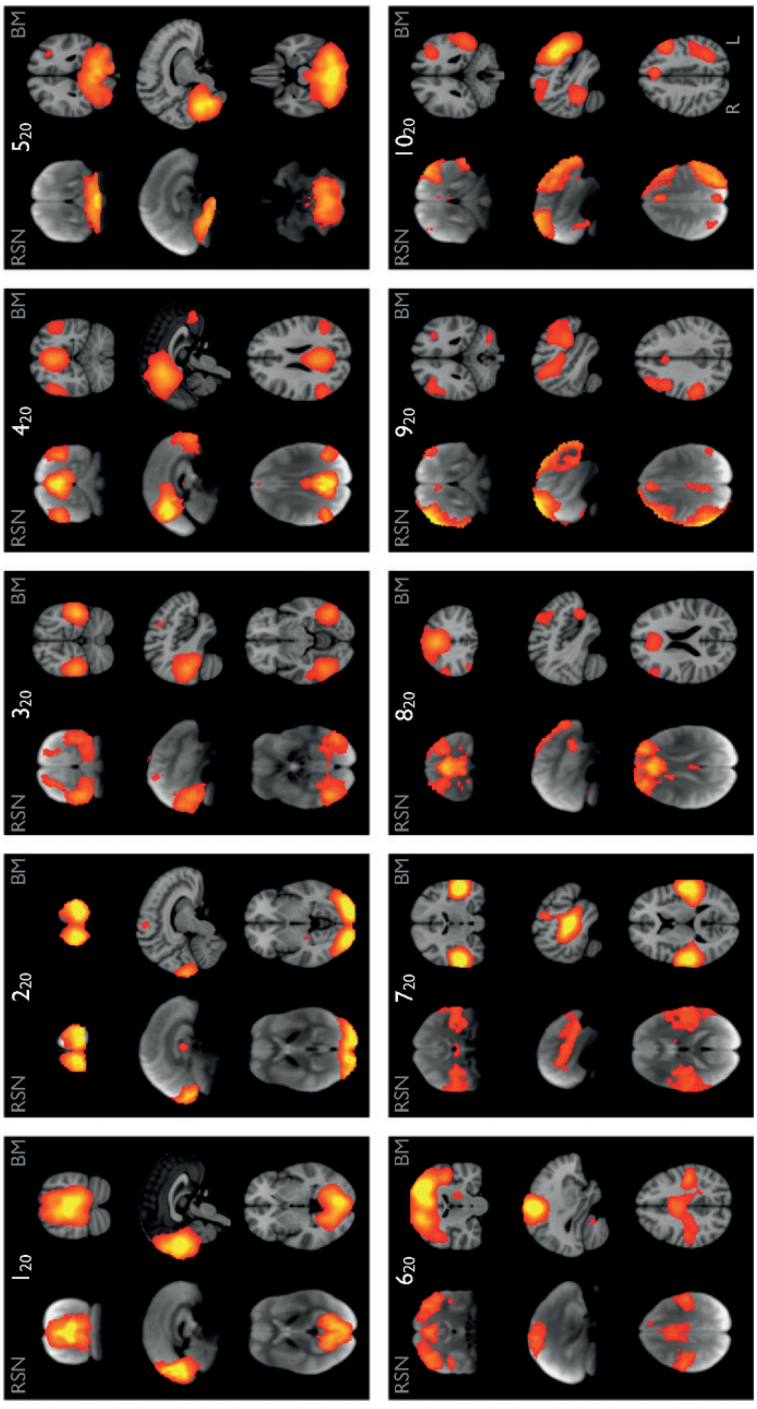


Fig. 5.2: Ten well matched pairs of template networks from analysis of the BrainMap activation database (right hand column) and a separate analysis of 36 subject resting fMRI dataset (left hand column) [290]. The figure shows the 3 most informative orthogonal slices for each pair. Networks 1,2 and 3: medial, occipital pole and lateral visual areas. Network 4: default mode network. Network 5: Cerebellum. Network 6: Sensorimotor. Network 7: Auditory. Network 8: Executive control. Network 9: Right frontoparietal. Network 10: Left frontoparietal

These maps show spatial patterns consisting of regions previously known to be involved in visual processing (IC 01, IC 02 and IC 03), the DMN (IC 04, IC 05, and IC 06), somatosensory/motor function (IC 08), executive functioning (IC 09), fronto-parietal function (IC 11 and IC 12) and auditory perception (IC 13). There are interesting differences though. Firstly, in each group analysis the DMN appears to be split into 3 components: IC 04 consists of the "classic" medial components of the DMN (medial prefrontal cortex, posterior cingulate also extending to the precuneus, and the left and right inferior parietal cortex). IC 05 contains mainly the anterior components of the DMN anterior part of the DMN, encompassing the superior and middle frontal gyrus, posterior cingulate, bilateral middle temporal gyri, and bilateral superior parietal regions. Finally, IC 06 contains only the posterior areas of the DMN: the posterior cingulate and bilateral superior parietal regions. The second difference is the addition of a separate component encompassing the basal ganglia and in MRI scan 3, the thalami bilaterally. Although under-reported, other resting-state fMRI studies have detected a basal ganglia network during rest, which subsumes the striatum, the thalamus and sometimes the amygdala and is reproducible [251].

Analysis of individual resting-state functional connectivity

Next, we obtained for every subject (i.e. controls and patients) the spatial map corresponding to each of these group-level networks using a two-step dual regression approach [99]. First, for each subject, the group-average set of spatial maps is regressed (as spatial regressors in a multiple regression) into the subject's 4D space-time dataset. This results in a set of subject-specific timeseries, one per group-level spatial map. Next, those timeseries are regressed (as temporal regressors, again in a multiple regression) into the same 4D dataset, resulting in a set of subject-specific spatial maps, one per group-level spatial map. This results in a set of subject-specific timeseries (one per group-level spatial map) which can then be compared between groups using permutation based testing.

In order to account for the repeated measures nature of the longitudinal patient analysis, dual regression analyses were carried out separately at each MRI time point using the 30 group RSN maps obtained from the group longitudinal ICA. The second stage outputs from each MRI scan were then subtracted from each other (in both directions) using FSL tools to investigate the impact of early brain injury on recovery and a single sample t-test applied to look for significant changes in each direction (i.e. areas where MRI scan 1 > MRI scan 2 and vice versa).

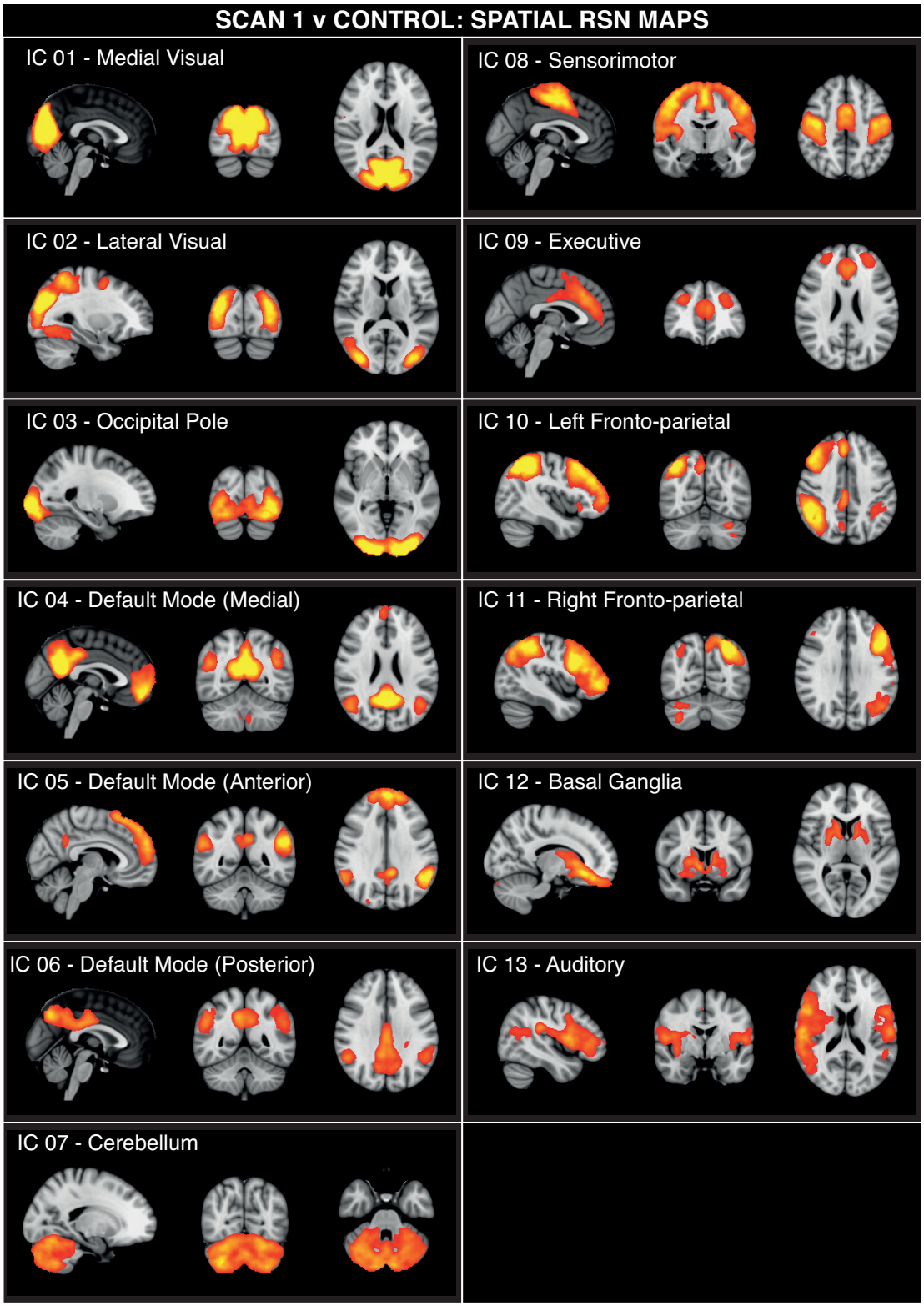


Fig. 5.3: MRI scan 1 v control: Template spatial maps. All spatial maps are shown thresholded at z = 3 and superimposed onto the MNI152 standard space template. IC = Independent Component. RSN = Resting State Network

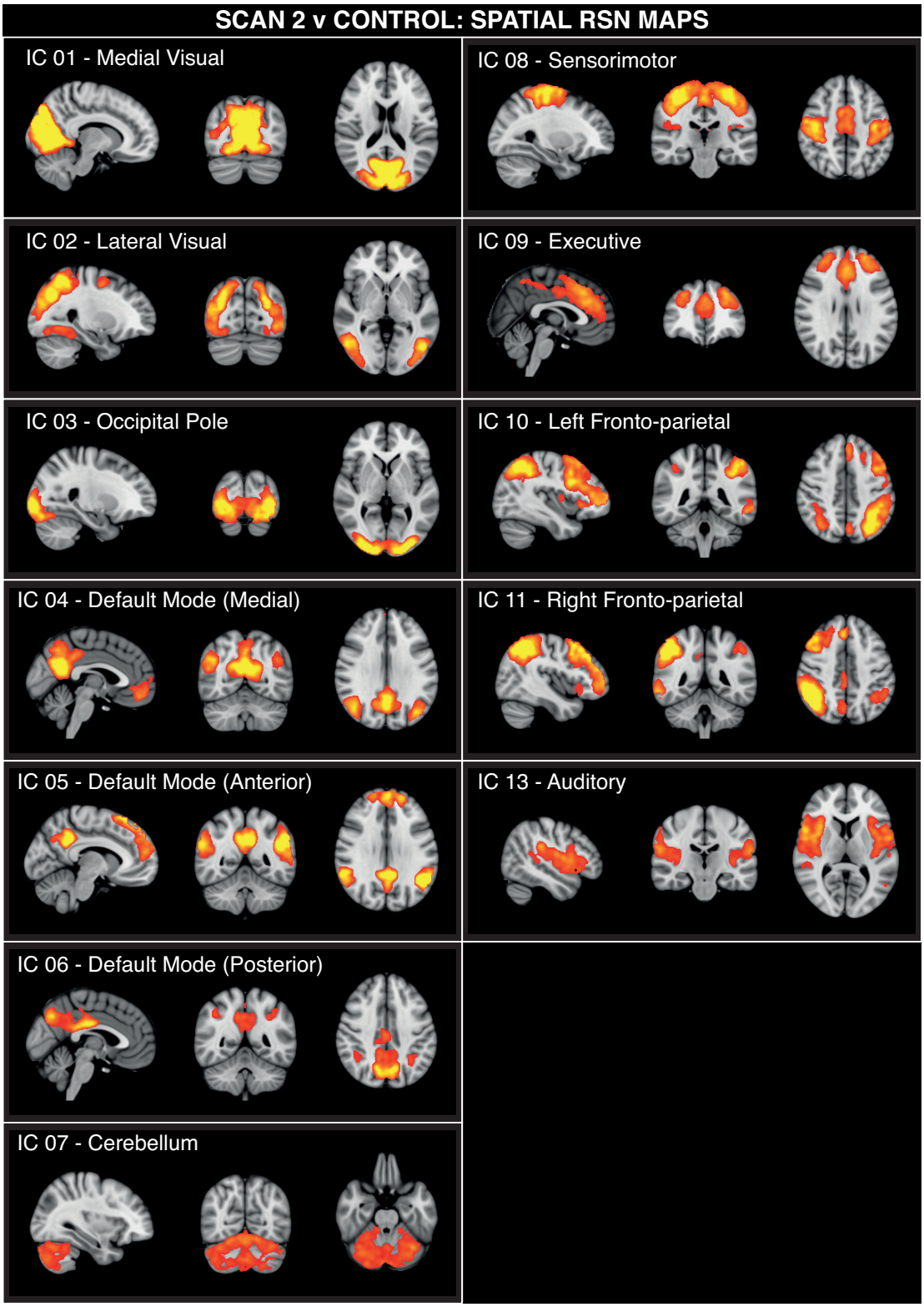


Fig. 5.4: MRI scan 2 v control: Template spatial maps. All spatial maps are shown thresholded at z = 3 and superimposed onto the MNI152 standard space template. IC = Independent Component. RSN = Resting State Network

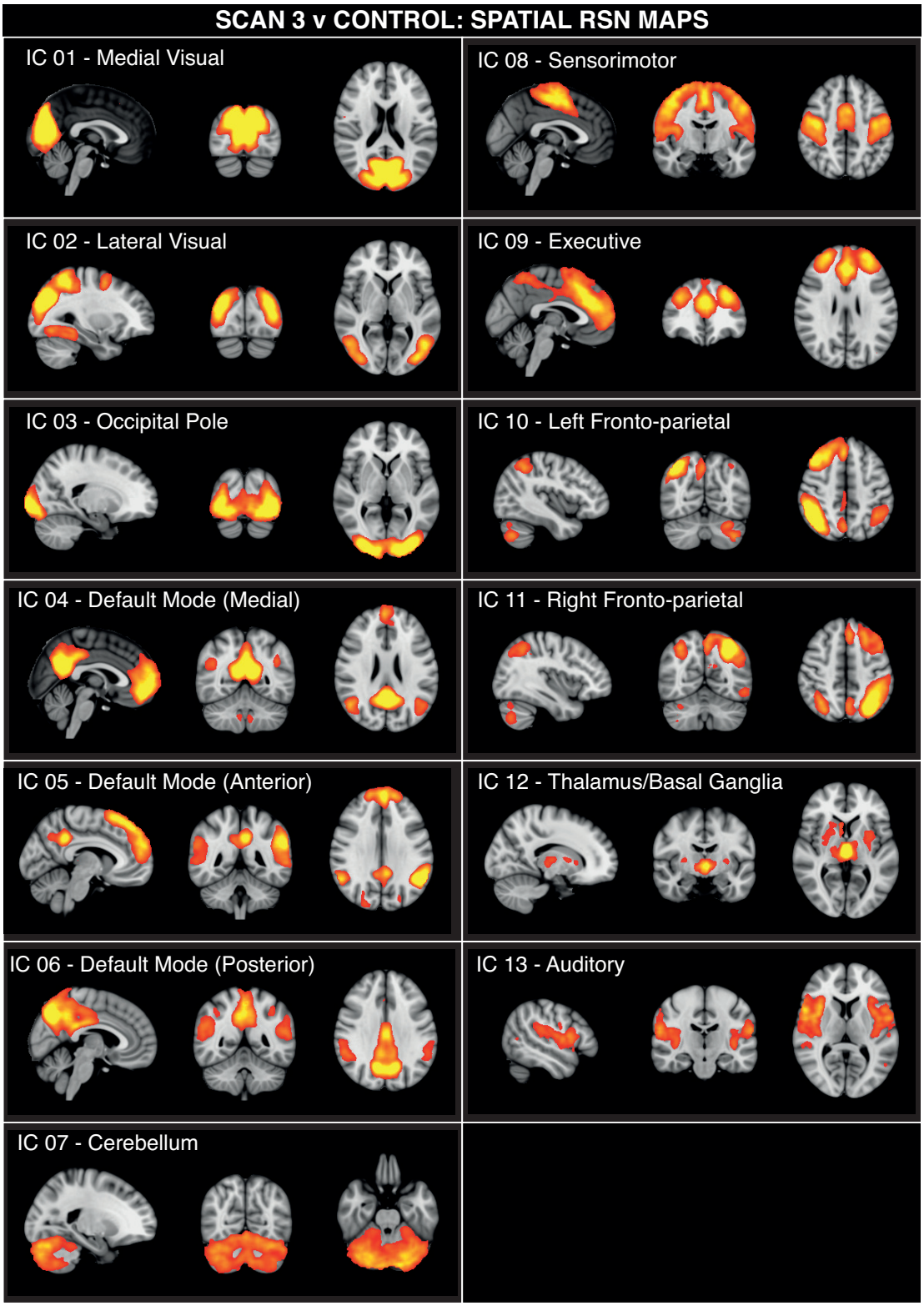


Fig. 5.5: MRI scan 3 v control: Template spatial maps. All spatial maps are shown thresholded at z = 3 and superimposed onto the MNI152 standard space template. IC = Independent Component. RSN = Resting State Network

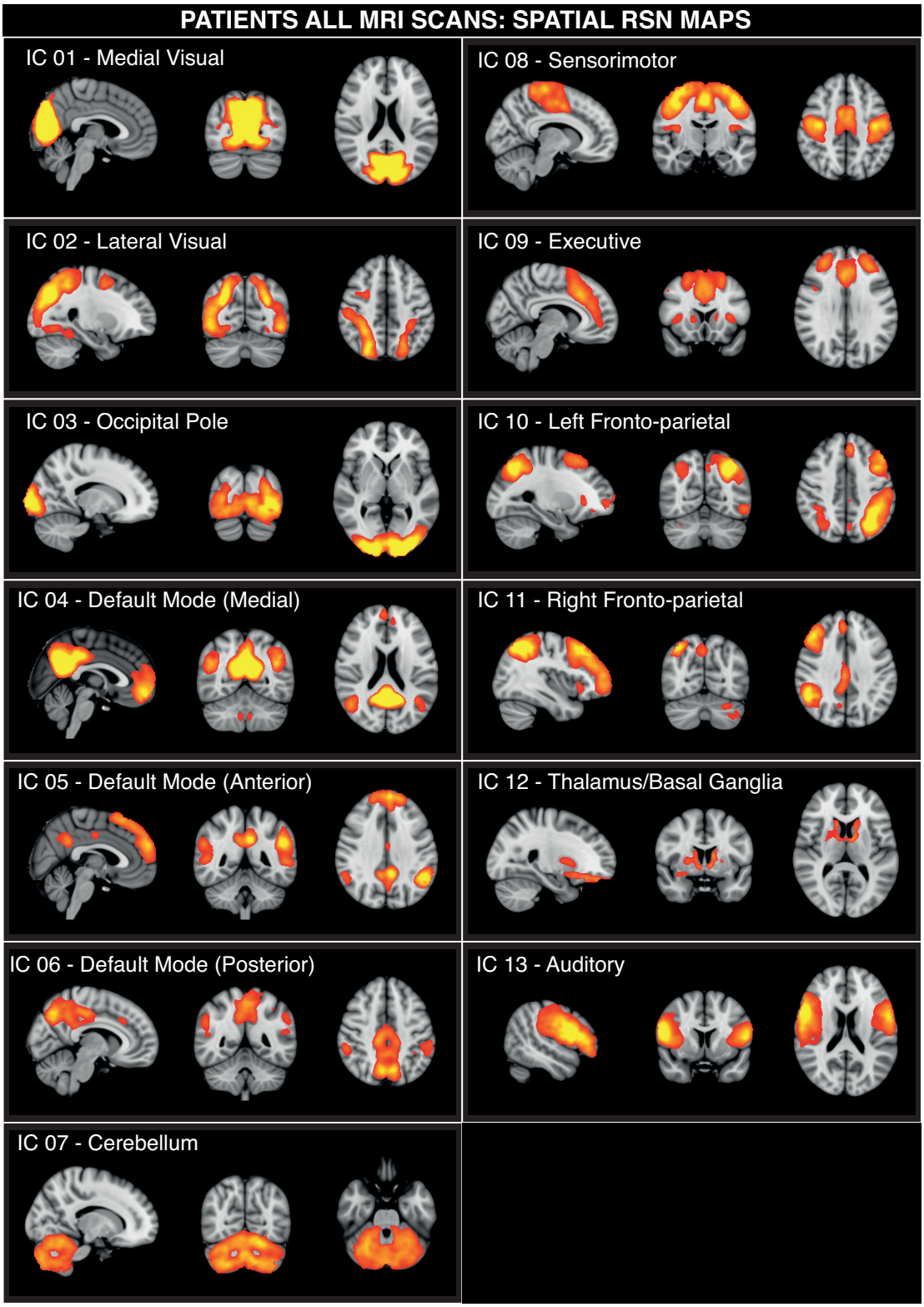


Fig. 5.6: Longitudinal patient analysis: Template spatial maps. All spatial maps are shown thresholded at z = 3 and superimposed onto the MNI152 standard space template. IC = Independent Component. RSN = Resting State Network

Statistical tests for voxelwise group differences in functional connectivity were then conducted within a general linear model framework using the FMRIB Software Library's Randomise using 5000 permutations. Results were considered significant at $p<0.05$, FWE-corrected for multiple comparisons across space using Threshold-Free Cluster Enhancement (TFCE). The group mean grey matter mask obtained from each VBM analysis from Chapter 4 was used to constrain group analyses to cortical grey matter for each analysis. We chose this approach, rather than constraining analyses to a given network, to improve sensitivity to changes occurring outside the boundaries defining the spatial map of each component.

Analysis of between-network resting-state functional connectivity

In order to investigate potential changes in the temporal correlations *between* individual RSNs in patients and controls, which might suggest alterations of long range functional connections following SAH, we used customised scripts from the FSLNets package (http://fsl.fmrib.ox.ac.uk/fsl/fslwiki/FSLNets) implemented in Matlab (The MathWorks Inc.). Correlations between pairs of ICs were computed using both partial and full correlations. To obtain information on connectivity between RSNs,the FSLNets package was used (http://fsl.fmrib.ox.ac.uk/fsl/fslwiki/FSLNets) implemented in Matlab (The MathWorks Inc.). In a preliminary step, the FSLNets tool performed an unsupervised grouping (clustering) of these networks to assess potential similarities and implicitly broad functional roles. Subsequently, we tested inter-network connection strength differences between groups (e.g. patients versus controls) using the non-parametric analysis tool Randomise. For each scan v control contrast, the FSLNets input data were the subject specific versions of the spatial components obtained by running dual regression on the MELODIC group-ICA average spatial maps:

- Scan 1 v Control: 44 subject-specific versions of the 26 independent spatial component networks
- Scan 2 v Control: 44 subject-specific versions of the 23 independent spatial component networks
- Scan 3 v Control: 48 subject-specific versions of the 28 independent spatial component networks

The group-ICA time courses related to spatial maps were then normalised to the overall standard deviation of all data points for each subject. Only the previously selected "good"

resting state networks networks were submitted to further long-range analysis. Then, subject-wise correlation matrices of both full correlation and regularized partial correlation of each of the RSNs time courses were created. The resulting correlation coefficients were Fisher z-transformed and corrected for temporal autocorrelation. After averaging all individual correlation matrices and doing one-group t test across them, the resulting nodes were clustered hierarchically by using the information about temporal similarity of the full correlation matrices. The network matrices were then tested across subjects for a two-group difference. For group comparison, we used a General Linear Model on the partial correlation values as these reflect direct network connections better than the full correlation values. Results were corrected for multiple testing by applying a family-wise error correction, thresholded at p=0.05. GM was not included as a covariate in the between network analyses.

Effect of grey matter structural change

One of the major challenges in interpreting changes in functional connectivity are associated changes in structural neuroanatomy in patients. As seen in Chapter 4, even "good grade" i.e. WFNS Grade I and II SAH is associated with significant changes in grey matter morphology, across the whole brain. To test whether functional connectivity differences might be explained by regional changes in grey matter density, GM structural volumes from the VBM analysis in Chapter 4 were included as a voxel-dependent covariate in the statistical model [65]. By including structural information, the results of both the ALFF and functional connectivity analyses are corrected for differences in gray matter density and the effects of possible misregistrations are accounted for [220].

Motion

Despite motion correction of individual data sets with MCFLIRT and FIX data de-noising, differences in head motion can have a profound effect on the activation signal from fMRI studies [122, 244]. The relative root mean square (rRMS) is the square root of the sum of the square of all 6 motion parameters - three translations (x,y and z planes) and three rotations (x,y and z planes) - relative to the time point before. The rRMS was averaged for each individual scan session and then group averages calculated for each scan point as well as for control subjects as a summary measure of scan head motion at each scan point. Additionally, demeaned average rRMS was included as a covariate of no interest in all group analyses to account for the potential effect of motion on group differences obtained.

5.2.4 Anatomical localisation of results

The Cerebellum atlas in MNI 152 space (after normalisation with FNIRT), the Juelich histological atlas [91] and the Harvard-Oxford cortical and subcortical atlases (Harvard Center for Morphometric Analysis) provided with FSL software were used to identify the anatomical characteristics of both template RSNs and group analyses.

5.3 Results

Study design, demographics of recruited patients, MRI protocols, clinical data and results of neurocognitive assessment at three months post-SAH are as previously reported in chapter 4. Complete resting state BOLD datasets were acquired in 22 patients at MRI scan 1, 22 patients at MRI scan 2 and 24 patients at MRI scan 3. Healthy volunteer subjects were recruited and scanned as previously described.

5.3.1 Motion

Data from head motion (mean relative RMS) for each scan point and control subjects is shown in Table 5.1. In both acute MRI scans, patients had significantly higher head motion than controls (Scan 1 - p=0.0005, Mann-Whitney U test, Scan 2: p = 0.002, Mann Whitney U test). However, by three months post-SAH, there was no significant difference between the two groups (p = 0.0960, Mann-Whitney U test).

Table 5.1: Motion: Mean Relative RMS Values for patients and controls from each group comparison

Timepoint	Patients	Controls	P values
Scan 1	0.2025 ($\pm$ 0.161)	0.094($\pm$ 0.044)	p = **0.0005**
Scan 2	0.1709 ($\pm$ 0.132)	0.091 ($\pm$ 0.046)	p = **0.0020**
Scan 3	0.130 ($\pm$ 0.078)	0.094 ($\pm$ 0.046)	p = 0.0960

There was no significant difference in relative RMS values between patients with neurocognitive impairment and those without at either Scan 1 (median 0.157 v 0.192, p=0.3155 Mann-Whitney test), Scan 2 (median 0.111 v 0.155, p=0.7136 Mann-Whitney test) or Scan 3 (median 0.112 v 0.09, p=0.3698 Mann-Whitney test).

5.3.2 ALFF analysis

Figure 5.9 is a graph of mean total power spectrum for each patient MRI scan and healthy controls. At all time points, the total power in the low frequency spectrum is higher in patients compared to controls (Figure 5.10 shows the same mean total power spectrum with the standard error of the mean included). Interestingly, there is a large increase in total spectral power between MRI scan 1 and scan 2 which then returns towards but not exactly back to baseline control levels.

Looking at voxelwise changes, at all three scan points post-SAH, this increase in ALFF was present globally throughout the grey matter (corrected $p < 0.05$) compared to healthy controls (Figure 5.7-A, B and C). Longitudinal analysis highlighted that between MRI scan 1 and MRI scan 2, there is a significant increase in ALFF in certain regions including the cerebellum (Crus I and II), basal ganglia (bilaterally) and prefrontal areas (bilaterally) (Figure 5.8-B). By MRI scan 3 at three months post-SAH, there is a decrease in ALFF in most of the grey matter compared to the MRI scan 2 but ALFF in the right caudate and cerebellum remains sustained (Figure 5.8-C).

5.3.3 Resting state connectivity analysis

5.3.4 Scan 1: <72 hours post-SAH

Individual network functional connectivity

Compared with healthy controls, SAH patients showed significant increased functional connectivity in the cerebellum network (IC 07), sensorimotor network (IC 08), left frontoparietal network (IC 10) and the basal ganglia network (IC 12) - see Figure 5.11 and Supplementary Table 5.2.

Connectivity within the cerebellum network (IC 07) was significantly increased in patients, especially between the crus I (right), crus II (bilaterally) and IX (right) regions. Given that the analysis method used a whole brain approach which does not constrain the within network analysis to the boundaries of that network, it is possible that clusters are detected outside the network boundaries that show between group differences with that same network.[325] As a result, increase connectivity was also seen outside the boundaries of the network to the left parahippocampal gyrus.

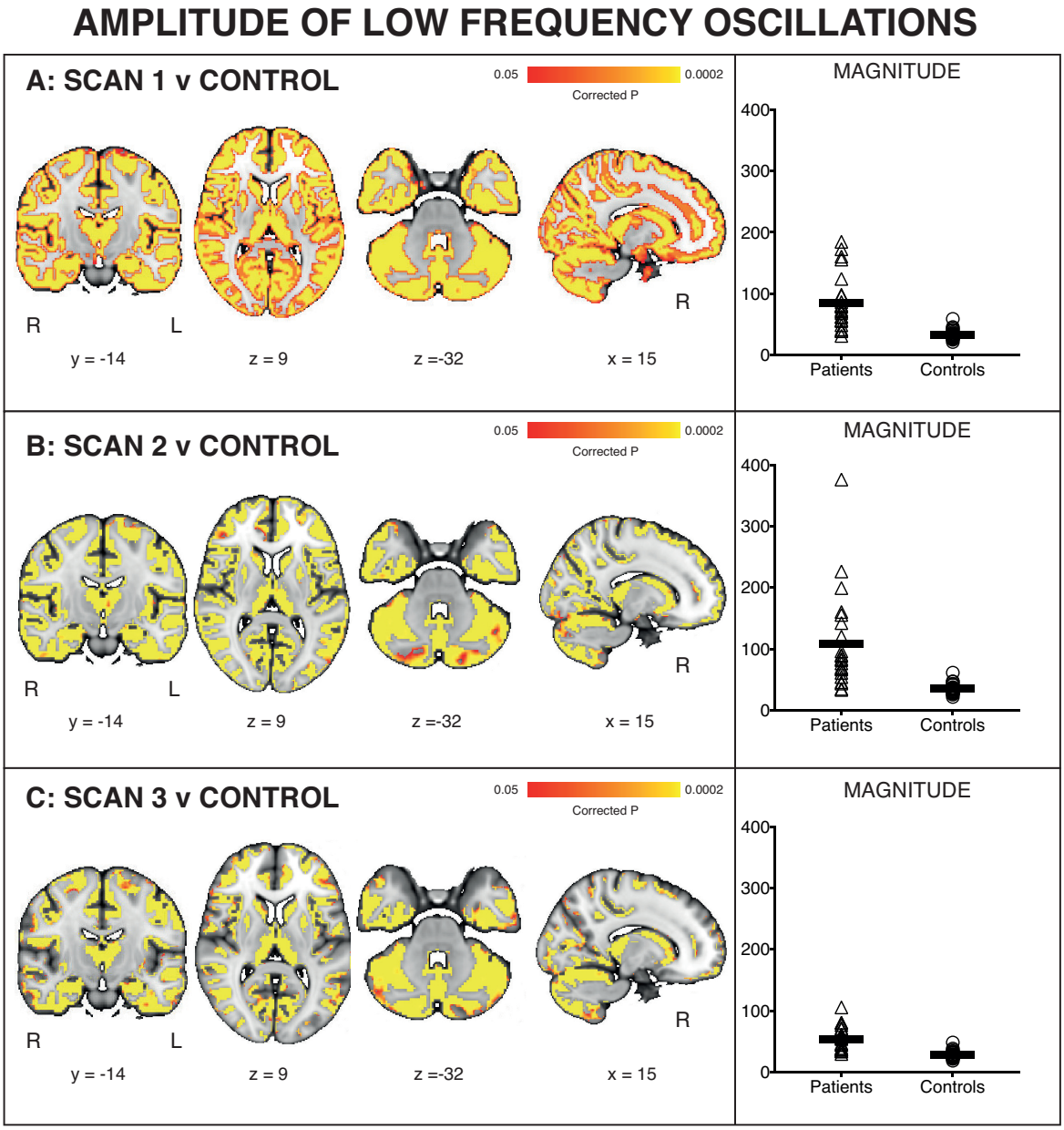


Fig. 5.7: Voxelwise changes in ALFF in the resting state at each MRI scan point in patients with SAH compared to healthy controls. Clusters showing significantly increased (red/yellow) ALFF in patients are overlaid onto an MNI152 standard space template. Plots of the ALFF effect magnitude extracted from significant clusters are shown. L = left; R = right

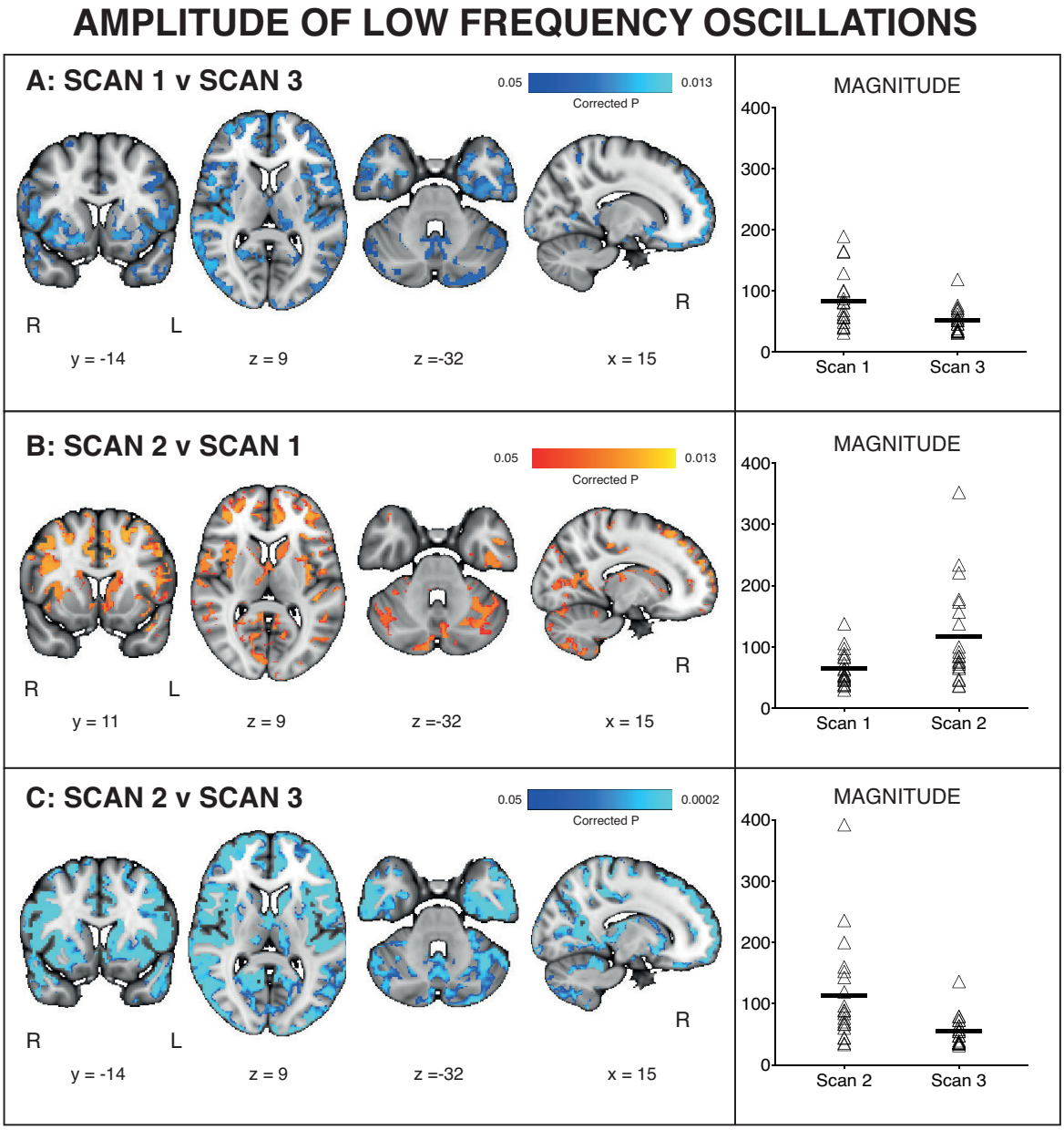


Fig. 5.8: Longitudinal patient voxelwise changes in ALFF in the resting state at each MRI scan point in patients with SAH compared. Clusters showing significantly increased (red/yellow) or decreased (blue/light blue) ALFF in patients are overlaid onto an MNI152 standard space template. Plots of the ALFF effect magnitude extracted from significant clusters are shown. L = left; R = right

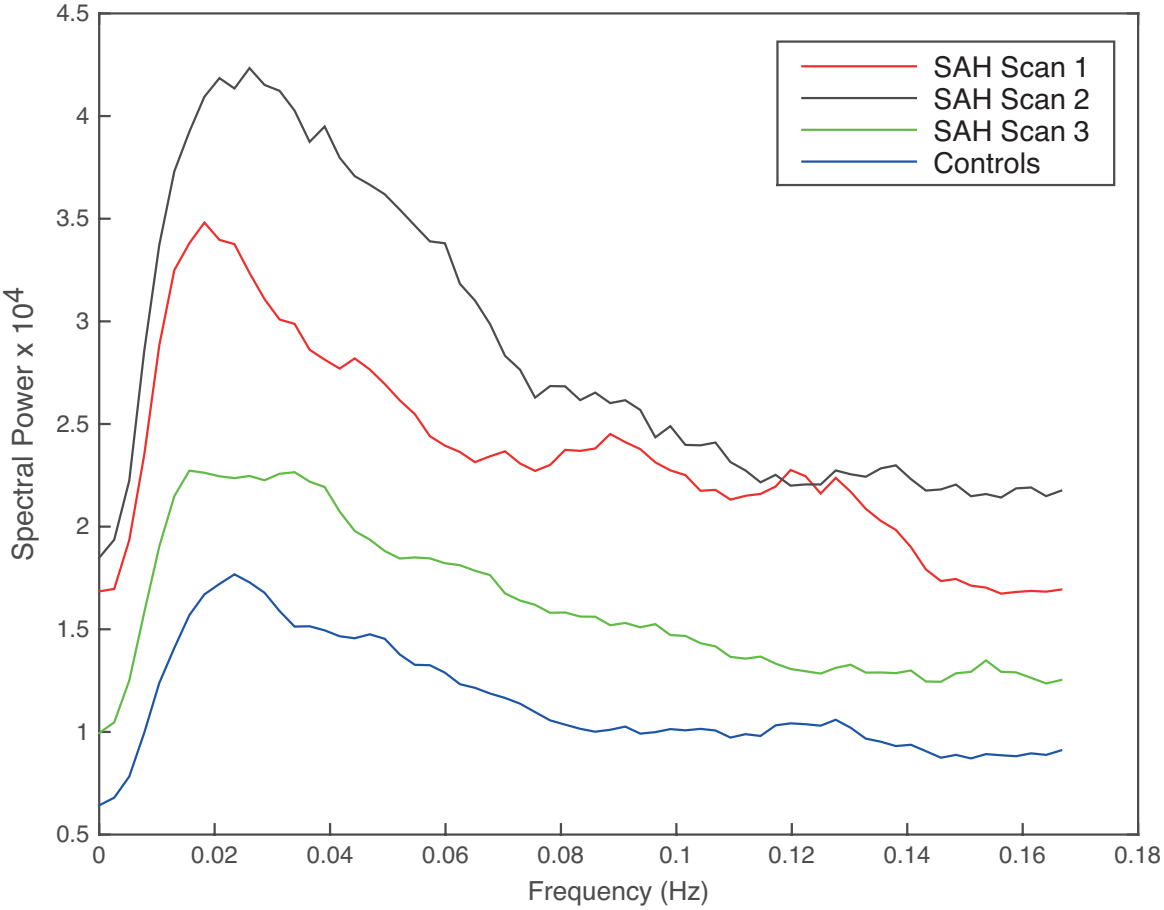


Fig. 5.9: Graphs of mean total spectral power for each MRI scan point in patients and controls

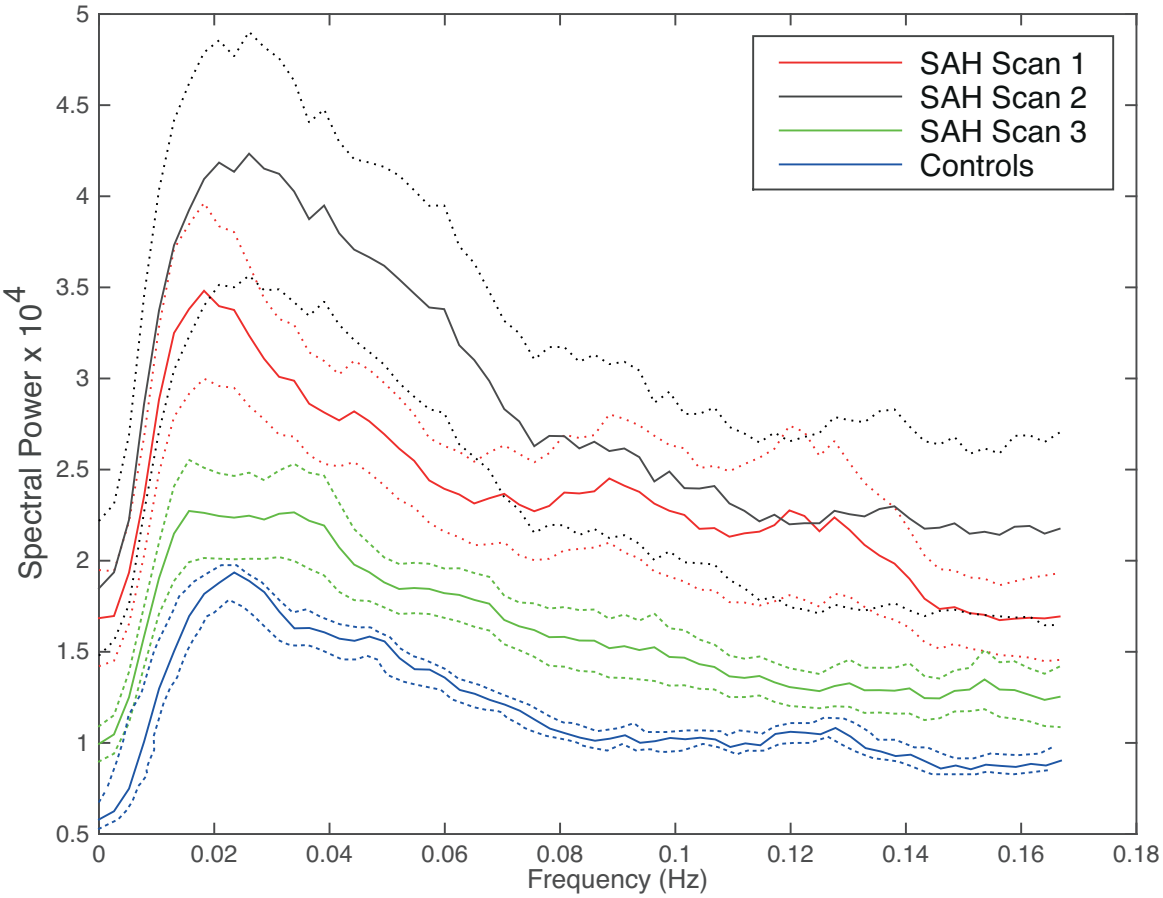


Fig. 5.10: Graphs of mean total spectral power for each MRI scan point in patients and controls with error bars representing standard error of the mean

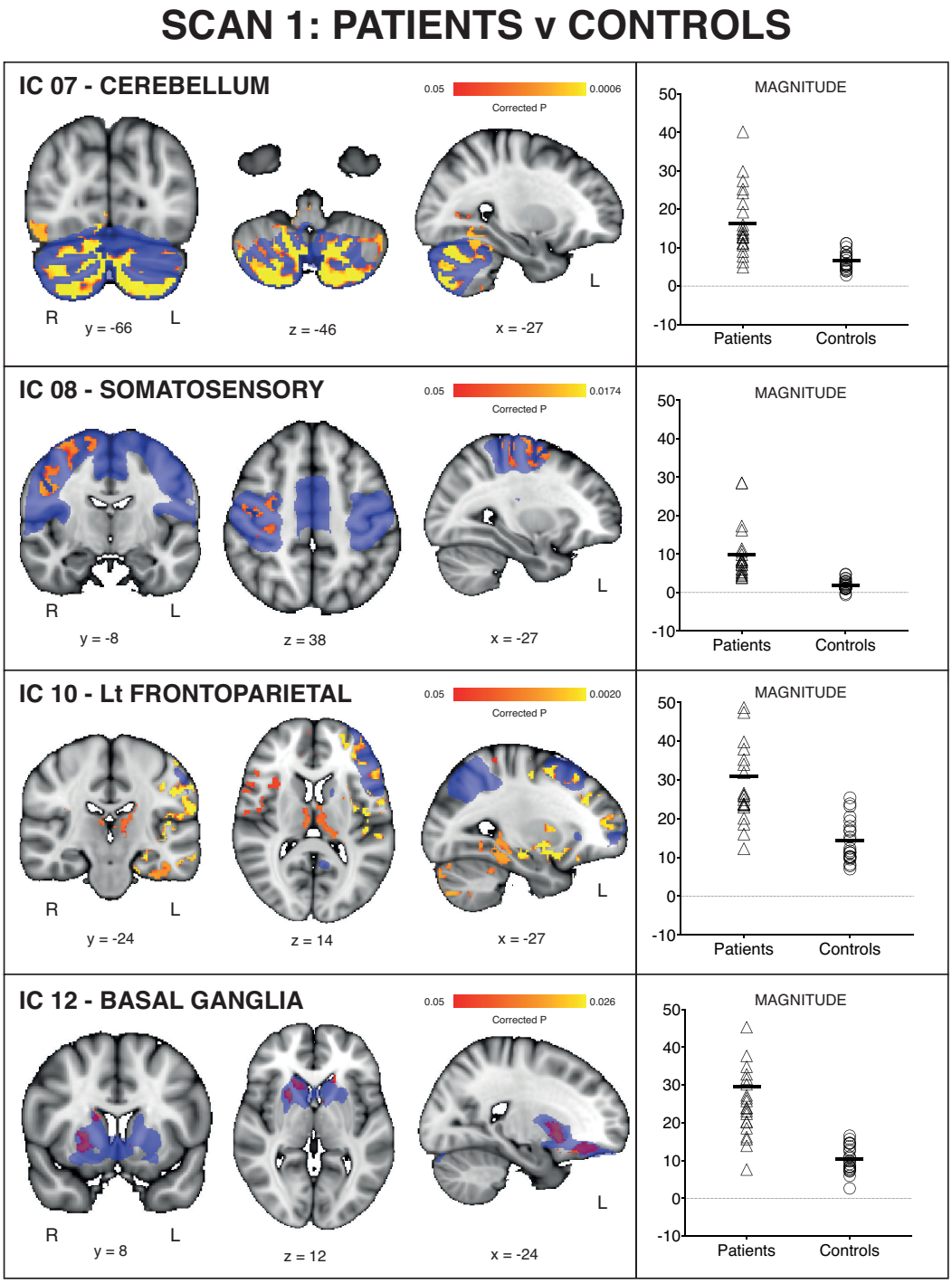


Fig. 5.11: MRI scan 1 v control: Whole-brain group-wise results of permutation tests (TFCE-corrected to P<0.05) conducted within each of the 10 resting state networks in patients and controls. ICs showing significant increase in patients versus controls are shown. Clusters showing significantly increased (red/yellow) functional connectivity in patients are overlaid over the template resting state network (transparent purple). All images are shown overlaid onto an MNI152 standard space template. Plots of the connectivity effect magnitude extracted from significant clusters are shown. IC = independent component; L = left; R = right

Cortically, patients exhibited an significant increase in resting state connectivity within the somatosensory network (IC 08), mainly within the primary somatosensory cortex (Brodmann area (BA) 3b). There was also increased connectivity within the left frontoparietal network (IC 10) in the frontal pole, precentral gyrus and the left superior frontal gyrus (BA9) as well as outside the network to clusters in the thalamus, insula cortex and cerebellum (left Crus II and right I-IV). Finally, the basal ganglia network (IC 12) showed increased connectivity within the right putamen and the caudate bilaterally as well as outside the boundaries of the network to the right amygdala, right insula cortex and the left fronto-medial and fronto-orbital cortices.

The significant differences seen in all four networks persisted despite correction for changes in grey matter density between patients and controls (Figure 5.12). However, some effects were reduced and a few regions were no longer significantly different. In other words, in these regions it was not possible to distinguish functional connectivity differences from gray matter density effects or registration error.

There were no networks in which patients exhibited reduced functional connectivity compared to controls.

Between network functional connectivity

The strength of connectivity between the cerebellum and basal ganglia networks was significantly increased in controls relative to patients (p=0.019, FWE-corrected - Figure 5.13-A) - controls having a positive correlation between the two networks and patients having a negative correlation. Patients also demonstrated higher connectivity between the posterior DMN and the right frontoparietal networks (p=0.024, FWE-corrected - Figure 5.13-B).

5.3.5 Scan 2: 5-10 days post-SAH

Individual network functional connectivity

At 5-10 days post-SAH, SAH patients continued to show significant increased functional connectivity within the cerebellum network (IC 07). Interestingly, this now included multiple areas outside the boundaries of the network - specifically the thalamus (left and right), hippocamus (left and right) and the cingulate gyrus. As at MRI Scan 1, there was also persisting increased within network connectivity in the sensorimotor network (IC 08) and left frontoparietal network (IC 10) - see Figure 5.14. Additionally though, at this time point,

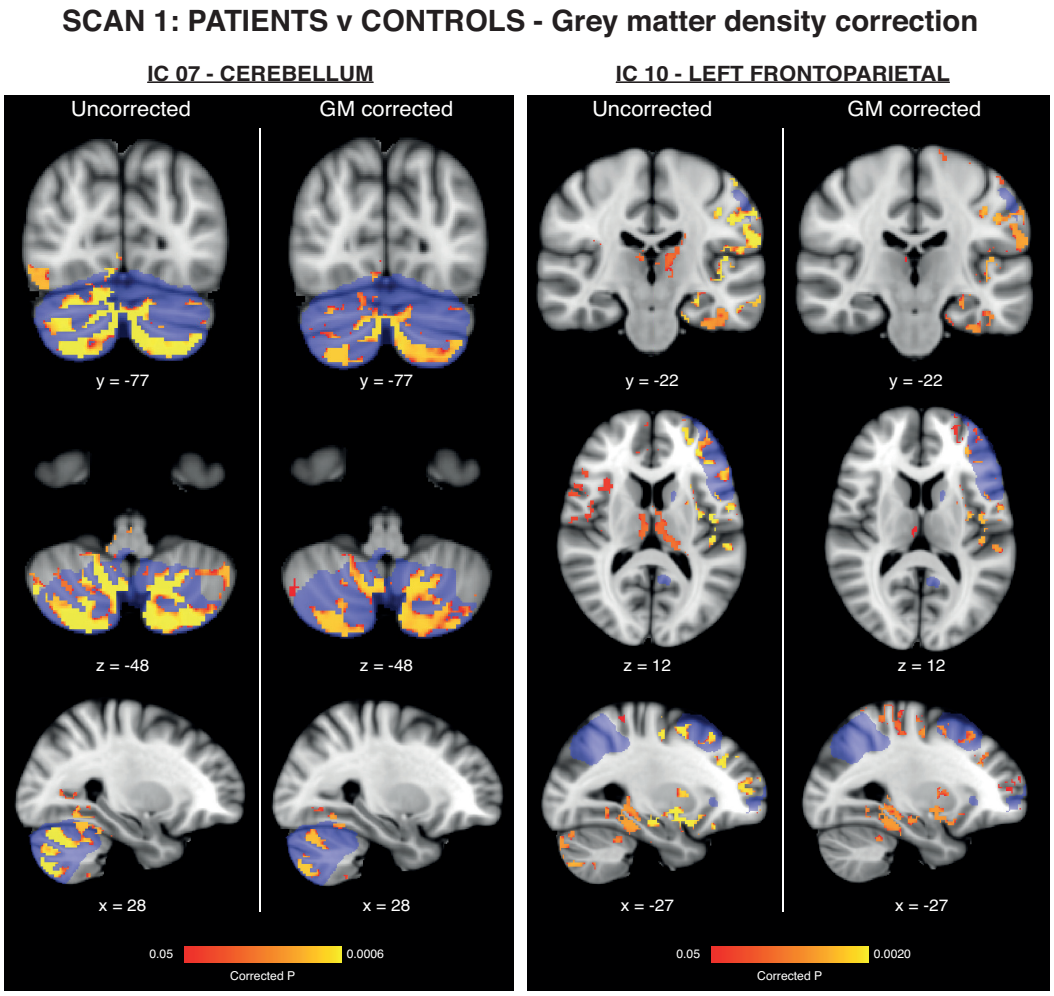


Fig. 5.12: MRI scan 1 v control: Effect of correction for changes in grey matter density. Clusters showing significantly increased (red/yellow) functional connectivity from figure 5.11 are shown in the left hand column of each group. Clusters showing significantly increased (red/yellow) functional connectivity in patients following GM correction are shown on the right-hand column of each group. All images are shown overlaid onto the MNI152 standard space template. Again, in purple are the original template RSNs. IC = independent component; L = left; R = right.

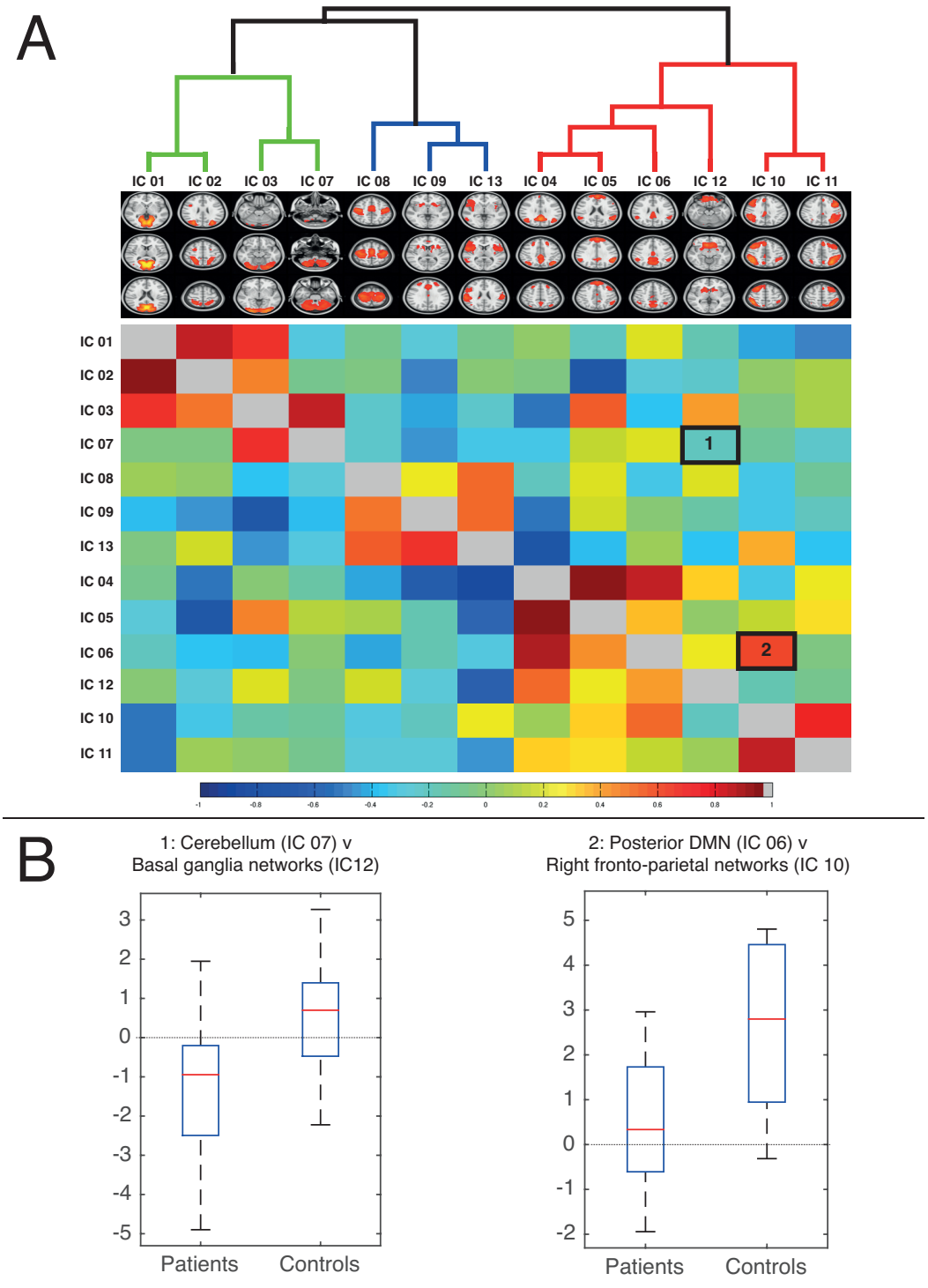


Fig. 5.13: FSL Nets between network correlations: MRI scan 1 v control: Full correlations are shown below the diagonal line with partial correlations shown above the diagonal line. Numbers on each axis indicate specific components from Figure 5.3. Number 1 represents a significant difference in partial correlations between the cerebellum and basal ganglia networks (Controls greater than Patients). Number 2 represents a significant difference in partial correlations between the posterior DMN and right frontoparietal networks (controls greater than patients). Groupings on top of each matrix represents hierarchical clustering of component timeseries.

there was also increased connectivity within the medial default mode network (IC 04) and the executive function network (IC 08).

Again, these results persisted following correction for changes in grey matter density.

Between network functional connectivity

At this point, there were no significant differences between patients and controls in between network connectivity.

5.3.6 Scan 3: 3 months post-SAH

Individual network functional connectivity

Finally, at 3 months post-SAH, patients continued to show significant increased functional connectivity within the cerebellum network (IC 07). There was also again significant increased connectivity to multiple regions outside of the network including the thalamus (bilaterally), and precuneus.

In addition to this, increased connectivity in patients was also seen in the DMN (medial and posterior networks), sensorimotor, executive function and basal ganglia/thalamus networks - see Figure 5.16 and Supplementary Table 5.3. Both the medial and posterior DMN showed significant connectivity to similar regions outside of the boundary of the network including the thalamus (bilaterally) and the cerebellum. Other regions showing increased connectivity to the DMN include the insular cortex, basal ganglia (caudate and putamen), the hippocampus and the amygdala.

Following correction for changes in grey matter density, the significantly increased functional connectivity in the medial DMN, cerebellum, executive control and basal ganglia/thalamus networks in patients persisted. However, changes previously seen in the posterior DMN became non-significant

Between network functional connectivity

By 3 months post-SAH, the strength of connectivity between the executive function and posterior DMN networks was significantly increased in controls relative to patients (partial correlation - p=0.013, FWE-corrected - Figure 5.18-A) - again with controls having a positive correlation between the two networks and overall, patients having a negative correlation.

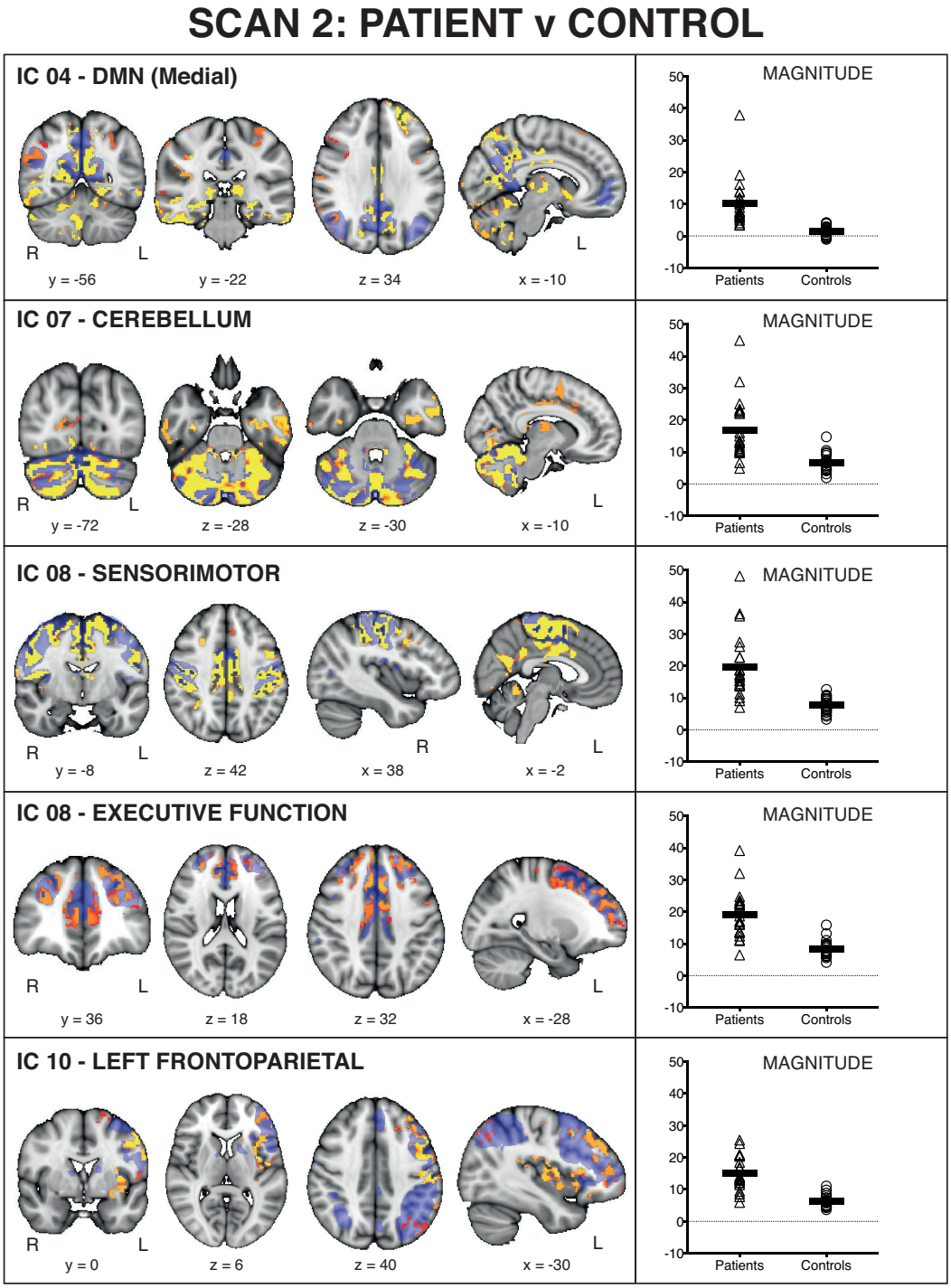


Fig. 5.14: MRI scan 2 v control: Whole-brain group-wise results of permutation tests (TFCE-corrected to P<0.05) conducted within each of the 10 resting state networks in patients and controls. ICs showing significant increase in patients versus controls are shown overlaid onto the MNI152 standard space template. Clusters showing significantly increased (red/yellow) functional connectivity in patients are overlaid over the template resting state network (transparent purple). Plots of the connectivity effect magnitude extracted from significant clusters are shown. IC = independent component; L = left; R = right.

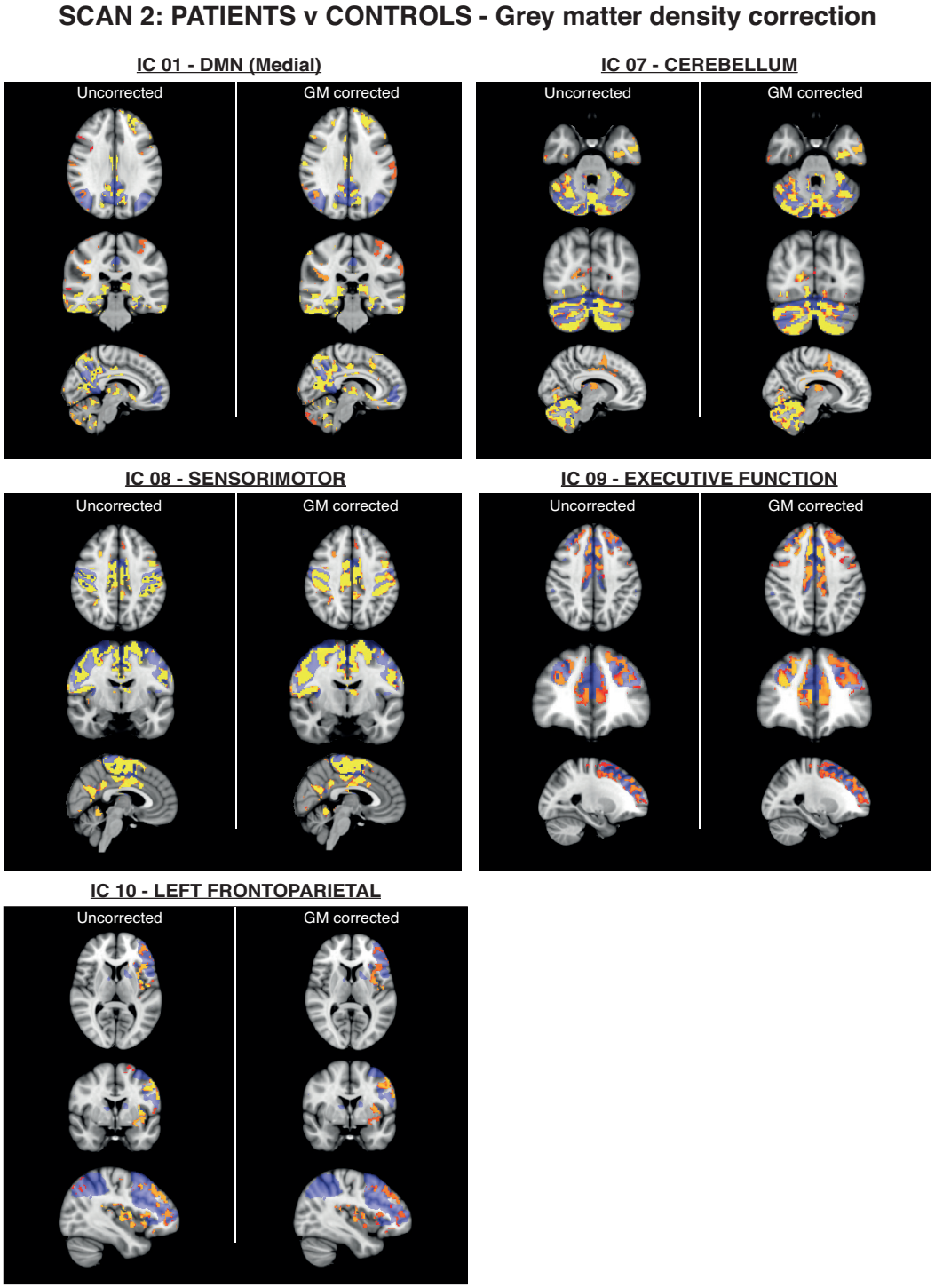


Fig. 5.15: MRI scan 2 v Control: Effect of correction for changes in grey matter density. Clusters showing significantly increased (red/yellow) functional connectivity from figure 5.14 are shown in the left hand column of each group. Clusters showing significantly increased (red/yellow) functional connectivity in patients following GM correction are shown on the right-hand column of each group. All images are shown overlaid onto an MNI152 standard space template. Again, in purple are the original template RSNs. IC = independent component; L = left; R = right.

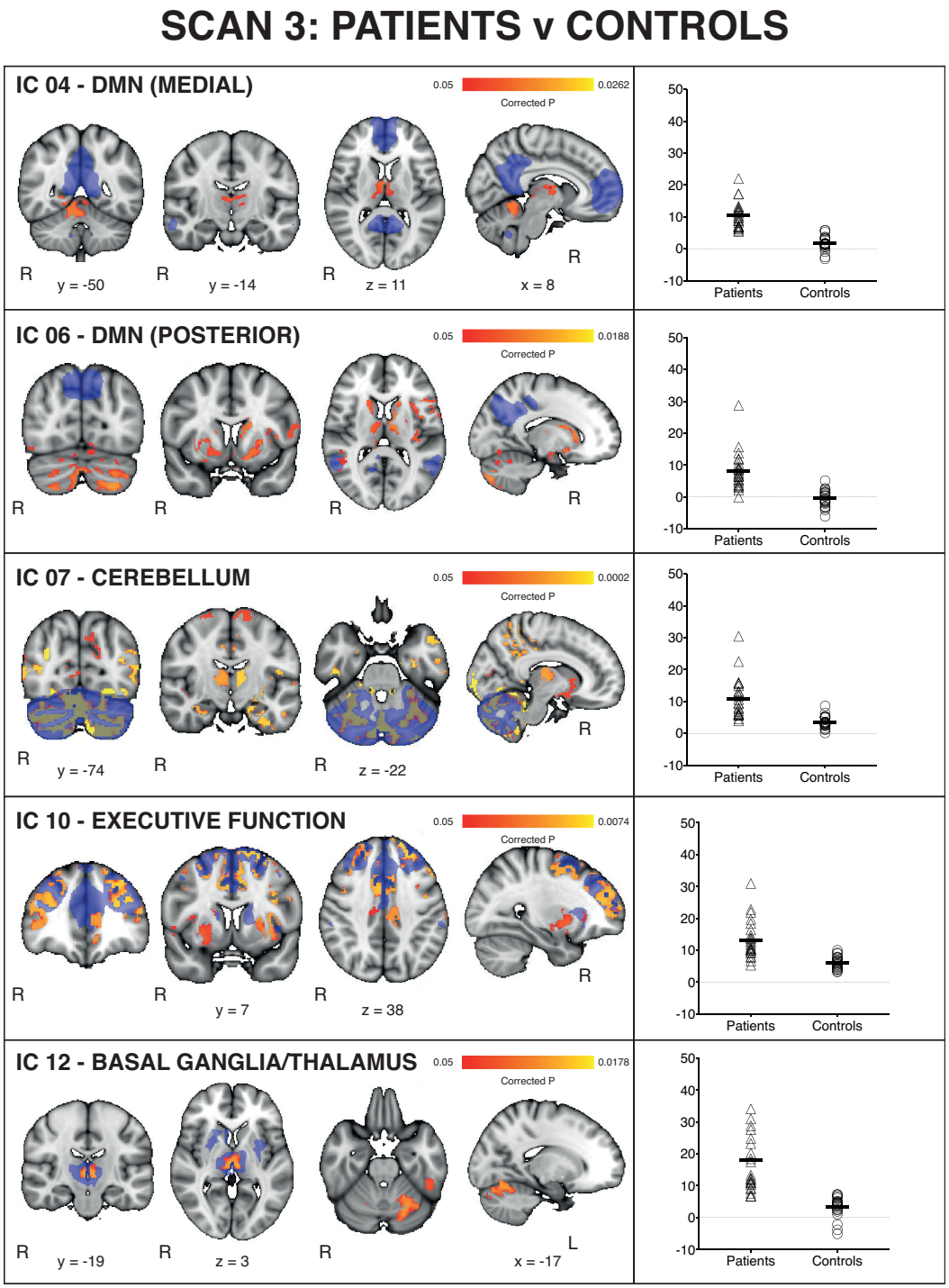


Fig. 5.16: MRI scan 3: Whole-brain group-wise results of permutation tests (TFCE-corrected to P<0.05) conducted within each of the 10 resting state networks in patients and controls. ICs showing significant increase in patients versus controls are shown. Clusters showing significantly increased (red/yellow) functional connectivity in patients are overlaid over the template resting state network (transparent purple). Plots of the connectivity effect magnitude extracted from significant clusters are shown. IC = independent component; L = left; R = right.

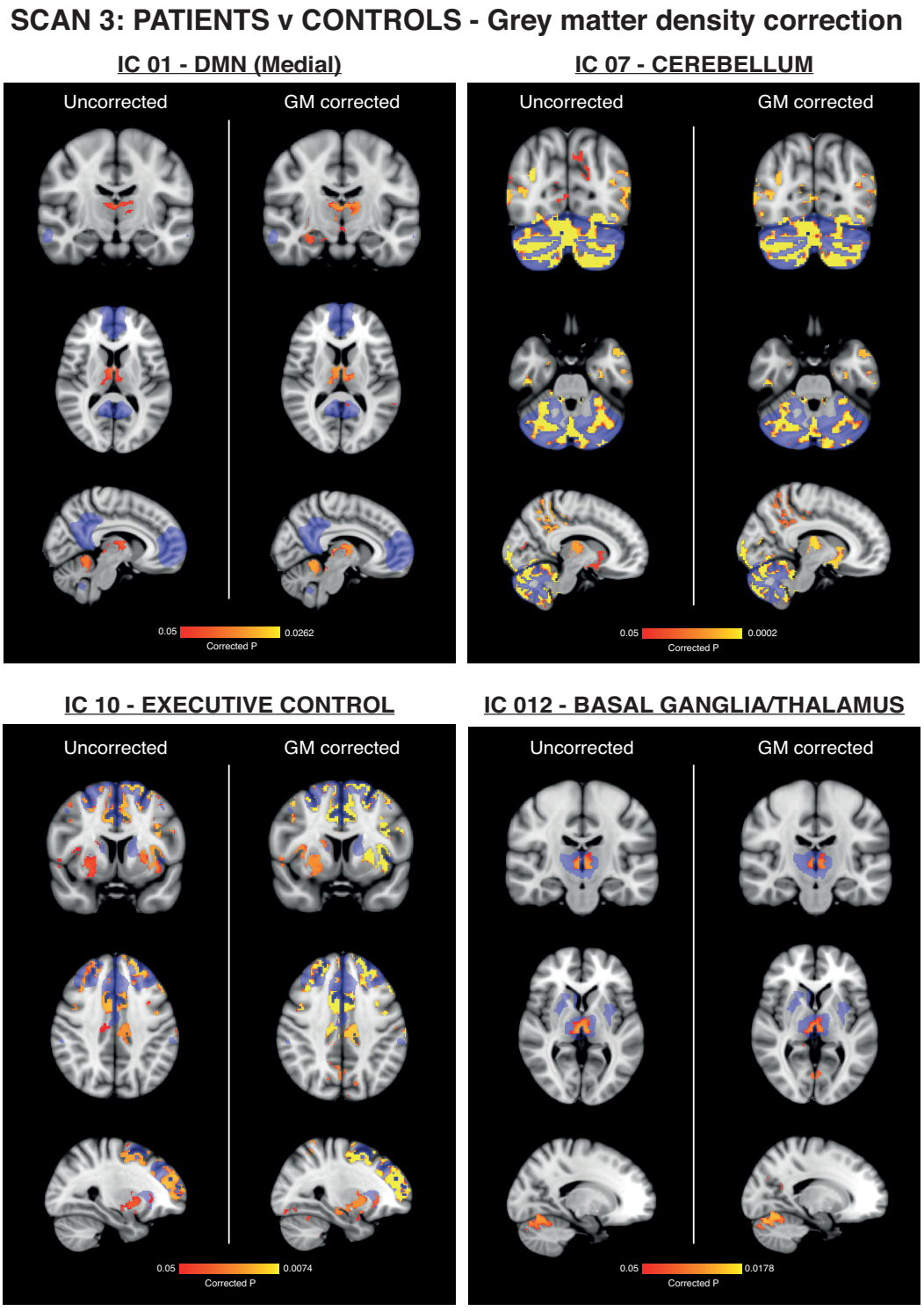


Fig. 5.17: MRI scan 3 v control: Effect of correction for changes in grey matter density. Clusters showing significantly increased (red/yellow) functional connectivity from figure 5.16 are shown in the left hand column of each group. Clusters showing significantly increased (red/yellow) functional connectivity in patients following GM correction are shown on the right-hand column of each group. All images are shown overlaid onto the MNI152 standard space template. Again, in purple are the original template RSNs. IC = independent component; L = left; R = right.

Patients also demonstrated higher connectivity between the posterior DMN and the right frontoparietal networks (partial correlation p=0.024, FWE-corrected - Figure 5.13-B)

5.3.7 Longitudinal changes

MRI scan 1 v MRI scan 2

By MRI scan 2, there was significantly increased connectivity within the basal ganglia (IC 012) and cerebellum networks (IC 07) when compared to MRI scan 1 5.19. Functional connectivity to the basal ganglia network was also significantly increased outside of the boundaries of the network including the thalamus bilaterally and the insula cortex on the right. There were no networks where connectivity was increased in MRI scan 1 compared to MRI scan 2.

MRI scan 2 v MRI scan 3

Following on from the above, there was a significant decrease in functional connectivity between MRI scan 2 and MRI scan 3 in a number of networks: sensorimotor (IC 08), left frontoparietal (IC 10), right frontoparietal (IC 11), cerebellum (IC 07) and basal ganglia (IC 12). Again, no networks were increased in MRI scan 3 compared to MRI scan 2.

MRI scan 1 v MRI scan 3

Finally, looking at changes between the first 72 hours post-rupture and 3 months, interestingly, there were no significant differences in functional connectivity in any of the networks in either direction.

5.3.8 Relationship with neurocognitive outcomes

At 3 months post-SAH, in patients, ALFF was positively correlated with cognitive performance (Spearman r = 0.587; P = 0.003). Patients with neurocognitive impairment also showed significantly increased connectivity within and to areas outside the basal ganglia network and the executive function network (IC 12 and IC 09 - Figure 5.21-A. Those patients with no neurocognitive impairment showed the opposite with significantly higher within network connectivity in the posterior DMN (IC 06) and the left frontoparietal network (Figure 5.21-B). This also included a large number of areas outside of the boundaries of the networks

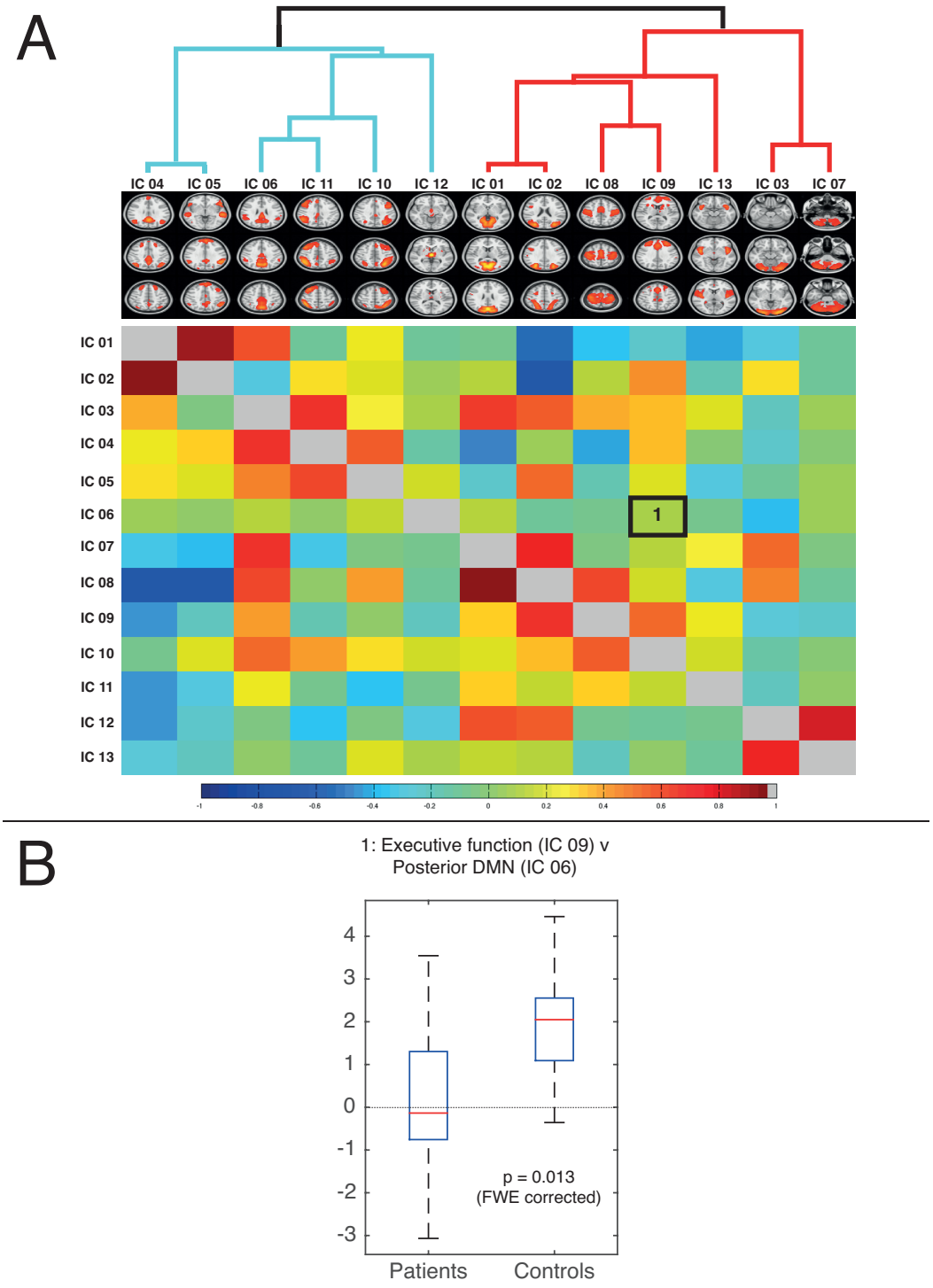


Fig. 5.18: FSL Nets between network correlations Scan 3 v Control: Full correlations are shown below the diagonal line with partial correlations shown above the diagonal line. Numbers on each axis indicate specific components from Figure 5.3. Number 1 represents a significant difference in partial correlations between the executive function and posterior DMN networks (Controls greater than SAH patients). Groupings on top of each matrix represents hierarchical clustering of component timeseries

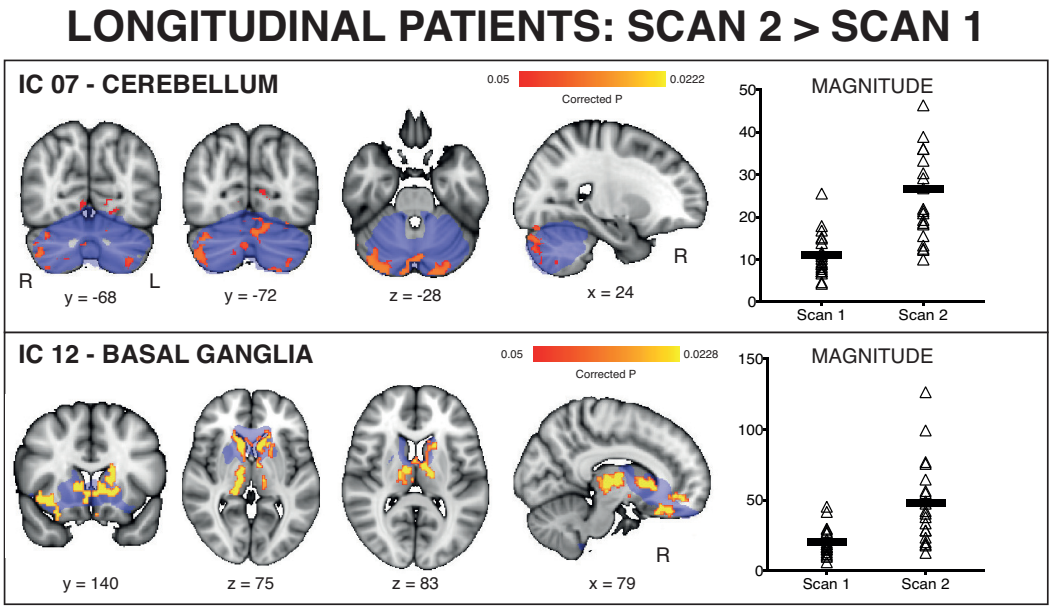


Fig. 5.19: Longitudinal Patient MRI scans - MRI scan 1 v MRI scan 2: Whole-brain group-wise results of permutation tests (TFCE-corrected to p<0.05) conducted within each of the 10 resting state networks in patients. ICs showing significantly increased connectivity in MRI scan 2 versus MRI scan 1 are shown. Clusters showing significantly increased (red/yellow) functional connectivity in MRI scan 2 compared to MRI scan 1 are overlaid over the template resting state network (transparent purple). Images are shown overlaid onto the MNI152 standard space template. Plots of the connectivity effect magnitude extracted from significant clusters are shown. IC = independent component; L = left; R = right.

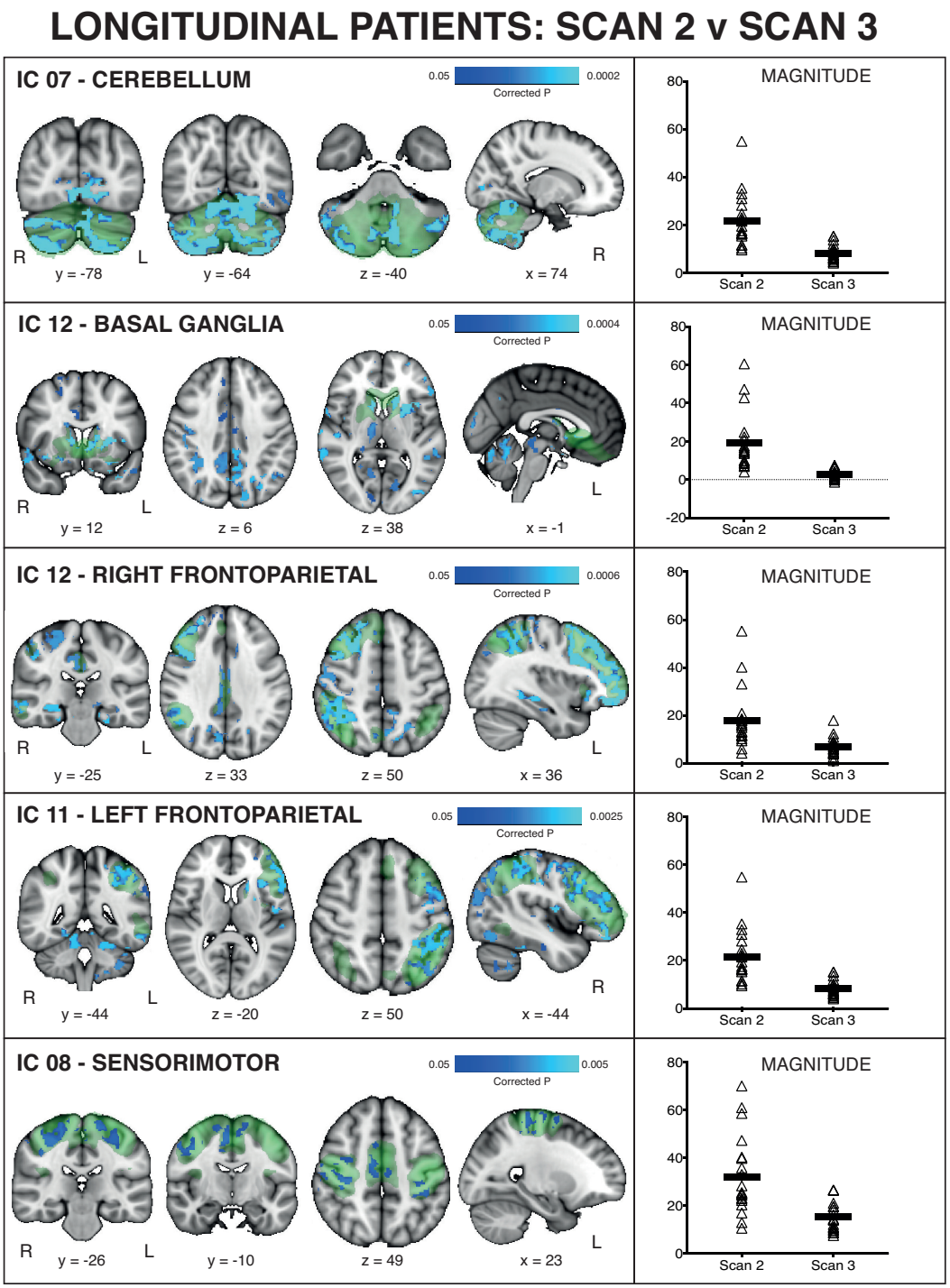


Fig. 5.20: Longitudinal Patient MRI scans - Scan 2 v Scan 3: Whole-brain group-wise results of permutation tests (TFCE-corrected to $p<0.05$) conducted within each of the 10 resting state networks in patients. ICs showing significantly decreased connectivity in MRI scan 3 versus MRI scan 2 are shown. Clusters showing significantly decreased (blue/light blue) functional connectivity in patients are overlaid over the template resting state network (transparent green this time for clarity against the blue/light blue). Images are shown overlaid onto the MNI152 standard space template. Plots of the connectivity effect magnitude extracted from significant clusters are shown. IC = independent component; L = left; R = right.

including the thalami, right amygdala and insula, hippocampi, left caudate and cerebellum (left Crus II, V and VI). There was also a significant positive correlation between functional connectivity in the area of significant difference in the posterior DMN network and ACER-R values i.e. the higher the connectivity, the better the overall neurocognitive performance (Spearman r = 0.476, p = 0.019). This was the opposite for the areas of significant difference in the executive function network with a negative correlation between functional connectivity and ACE-R (Spearman r = -0.461, p=0.023).

Between network connectivity at 3 months post-SAH was also significantly influenced by neurocognitive outcomes. There was a significant difference in connectivity between the cerebellum network (IC 07) and the posterior DMN (IC 06 - p=0.013 FWE-corrected) - with those patients with no neurocognitive impairment having a negative correlation between the two networks and patients with impairment exhibiting a positive correlation (Figure 5.22.

Looking back to the first 72 hours post-SAH, those patients with no neurocognitive impairment at 3 months post-SAH had significantly increased within network connectivity in the medial DMN (IC 04), the sensorimotor network (IC 08), and the basal ganglia network (IC 12) (Figure 5.23).

However, there was no relationship between neurocognitive outcome and differences in between network connectivity at this point.

5.4 Discussion

Few studies have investigated the integrity of functional connectivity after SAH - either acutely or in the months following rupture. Many of the previous studies in both SAH and other acute conditions such as TBI have used a seed-based analysis approach and pre-defined regions of interest. In this chapter, we have used an unbiased, data-driven approach based on ICA that can highlight broader changes in functional connectivity not restricted to a set of predefined seeds. This is especially important in a disease like SAH where both focal and global ischaemic and metabolic injury can coexist and where abnormal functional connectivity may extend beyond a given network and involve multiple brain regions.

There are several notable findings from this chapter. At 3 months post-SAH, patients showed increased functional connectivity compared to healthy controls in a number of functional networks associated with complex cognitive or emotional functions including the DMN (medial and posterior divisions), cerebellum, basal ganglia/thalamus and executive function

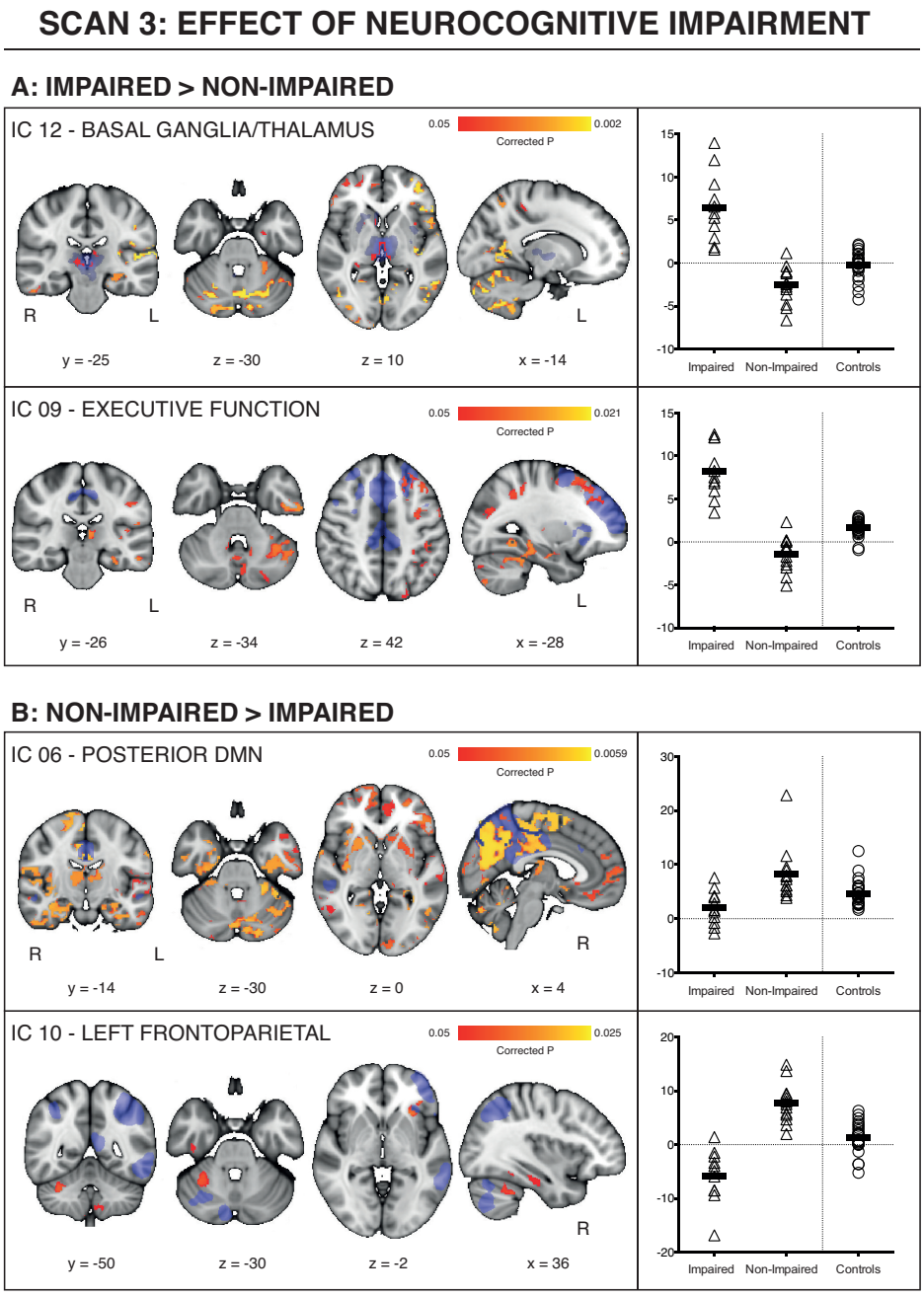


Fig. 5.21: MRI scan 3: Whole-brain group-wise results of permutation tests (TFCE-corrected to p<0.05) conducted within each of the 10 resting state networks between those patients with neurocognitive impairment and those without. A: ICs with clusters showing significantly increased (red/yellow) functional connectivity in neurocognitively impaired patients B: ICs with clusters showing significantly increased (red/yellow) functional connectivity in patients with no neurocognitive impairment. Images are shown overlaid onto the MNI152 standard space template. IC = independent component; L = left; R = right.

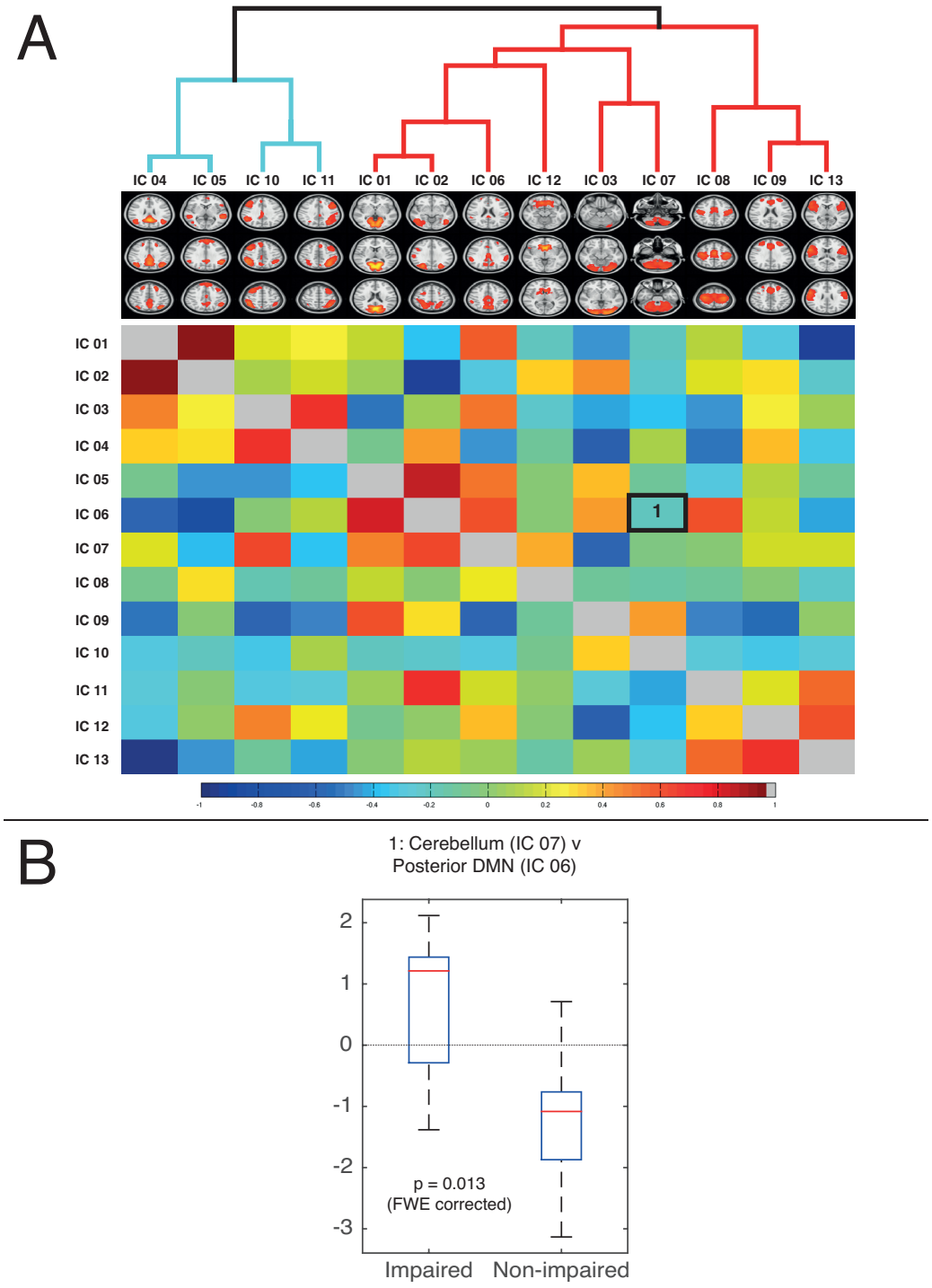


Fig. 5.22: FSL Nets between network correlations: MRI Scan 3 - Neurocognitively impaired v non-impaired patients: Full correlations are shown below the diagonal line with partial correlations shown above the diagonal line. Numbers on each axis indicate specific components from Figure 5.3. Number 1 represents a significant difference in partial correlations between the cerebellum and posterior DMN networks (Controls greater than Patients). Groupings on top of each matrix represents hierarchical clustering of component timeseries.

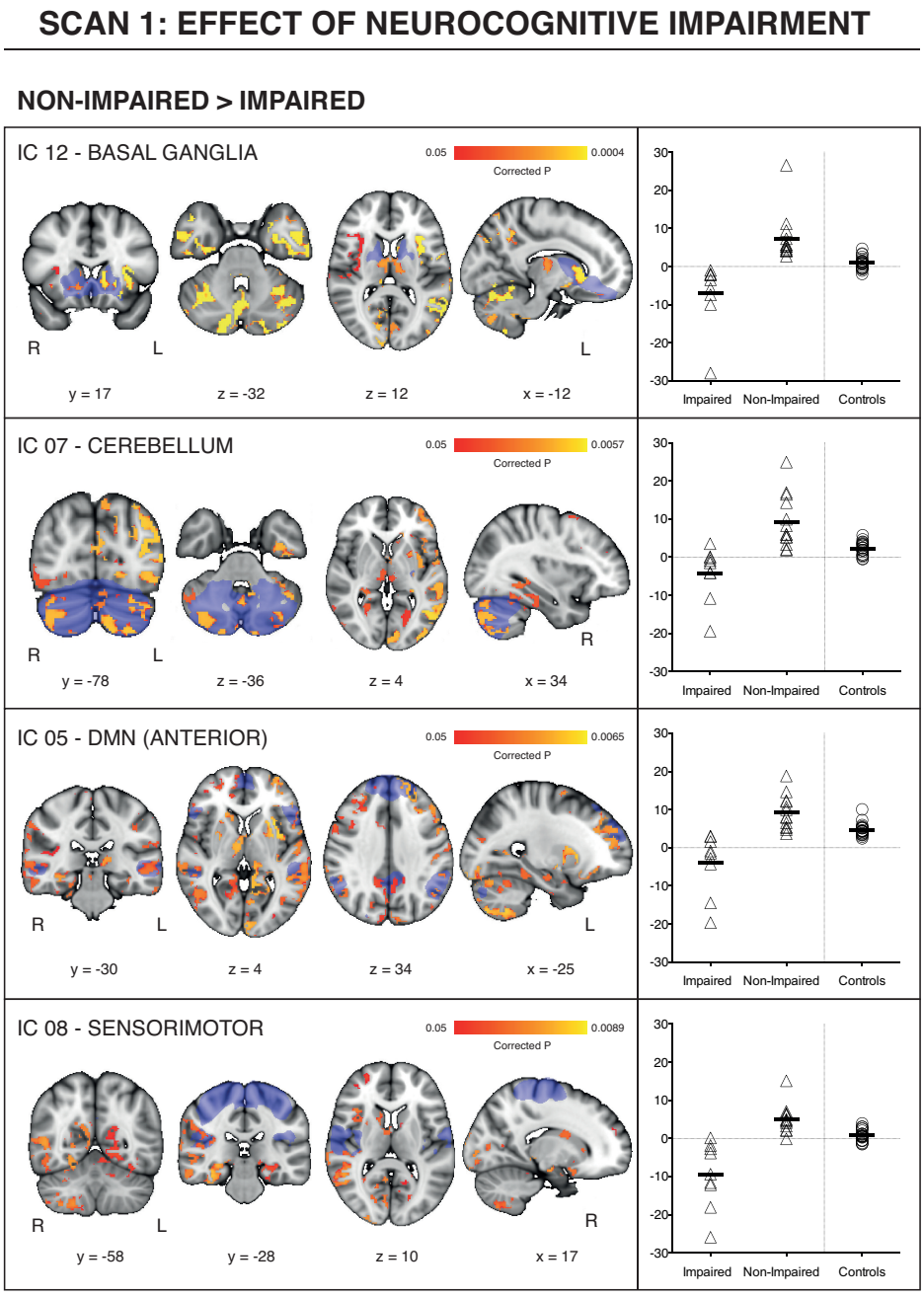


Fig. 5.23: Scan 1: Whole-brain group-wise results of permutation tests (TFCE-corrected to P<0.05) conducted within each of the 10 resting state networks between those patients with neurocognitive impairment and those without. A: ICs with clusters showing significantly increased (red/yellow) functional connectivity in neurocognitively impaired patients B: ICs with clusters showing significantly increased (red/yellow) functional connectivity in patients with no neurocognitive impairment compared to those with neurocognitive impairment. IC = independent component; L = left; R = right.

networks. These changes persisted despite correction for changes in grey matter density - important to note in the context of the widespread structural changes seen in Chapter 4. Secondly, these differences were already present in MRI scan 1 in a number of these networks, suggesting that the pathophysiological effects of early brain injury have a significant effect on functional connectivity from as early as the first 72 hours post-SAH. Finally, functional connectivity at 3 months post-SAH correlates with neurocognitive outcomes with those patients with the highest functional connectivity having the least cognitive impairment. This effect is also present in the first 72 hours suggesting that the severity of damage to network integrity at this stage may correlate with subsequent poor neurocognitive outcomes.

The key question underlying these findings is why functional connectivity is increased in patients relative to healthy controls and what relevance (if any) this has clinically. Results from this study show that from as early as the first 72 hours post-rupture, patients with SAH demonstrate consistently increased functional connectivity within a number of networks involved with higher cognitive functioning such as the cerebellum, left fronto-parietal and basal ganglia/thalamus networks and that this effect persists at 3 months post-SAH. The presence of significant differences in between network connectivity in a number of these networks also suggests that the global nature of early brain injury post-rupture may also affect longer distance connections between networks and affect subsequent neurocognitive outcomes. The consistent increased in connectivity between multiple networks and the cerebellum and thalamus at all three time points post-SAH lends further support to the hypothesis presented in Chapter 2 that the cerebellum is particularly susceptible to damage from early brain injury acutely post-rupture and, along with the thalamuus, may play a key role in mediating neurocognitive outcomes after SAH.

Few studies have investigated changes in resting state connectivity at such an acute stage following significant brain injury. Our results are in keeping with other studies investigating functional connectivity in SAH patients that reported similar increased functional connectivity at 3 months post-SAH - specifically in fronto-parietal regions and the precuneus [194]. However, these results do not seem to be consistently reproduced in other conditions resulting in acute brain injury. Studies of resting connectivity in traumatic brain injury (TBI) utilising resting state fMRI have found alterations that reflect both increases [228, 281, 36] and decreases in functional connectivity [195, 13]. Furthermore, the contradictory findings of structural disconnection and increased functional connectivity have also been shown to coexist in patients recovering from TBI [281]. Other studies in patients recovering from ischaemic stroke have demonstrated that some networks (e.g DMN) show increased

connectivity compared to controls, whereas other networks (e.g. fronto-parietal) show reduced connectivity [329].

What does this mean at a clinical level to patients with SAH? Intuitively, neurocognitive impairment following acute brain injury would seem likely to occur as a result of reduced network connectivity. As a result, increased functional connectivity in patients recovering from brain injury has often been interpreted as a compensatory or adaptive mechanism due to the frequent positive correlation with cognitive outcomes [281, 197, 36]. At three months post-SAH, those patients with good neurocognitive outcomes showed significantly higher within network functional connectivity in the posterior DMN and left fronto-parietal networks - including to other areas such as the thalamus, cerebellum and basal ganglia outside of the boundaries of these networks. On the other hand, patients with neurocognitive impairment demonstrated significantly increased functional connectivity in both the basal ganglia and executive function networks - with both networks showing increased connectivity outside the network boundaries to the cerebellum. Looking at between network connectivity, there was a significant difference in connectivity between the posterior DMN and cerebellum networks dependent on neurocognitive outcome - patients with neurocognitive impairment showed a positive connection between the two networks compared to a negative correlation in those with no impairment.

This is partially in agreement with other studies in patients with TBI which demonstrated that patients with the highest functional connectivity had the least cognitive impairment [281, 197, 36]. Interestingly, the only other study of functional connectivity in SAH patients, demonstrated the opposite with increased frontoparietal connectivity in patients with neurocognitive impairment - although this study was limited by the constraints of a seed based approach [194].

This increased thalamic and cerebellum functional connectivity seen in patients with SAH compared to controls might be considered a physiological and "compensatory" response to SAH-related loss of structural network integrity as evidenced by the finding that those patients with the best neurocognitive outcomes had higher functional connectivity. Varying the functional connectivity within resting state networks might therefore ‘tune’ the responsiveness of a network, and influence the efficiency of the behaviour supported by that network [281]. Furthermore, the increased functional connectivity within the posterior default mode network is positively correlated with overall neurocognitive performance as measured using the ACE-R - a relationship observed across both patients and controls. These results suggest that dynamic changes in default mode network function may be made more efficient by greater

functional connectivity at 'rest' [156], in which case an increase in default mode network functional connectivity could promote the appropriate and sustained deactivation necessary for focused goal-directed and cognitively demanding behaviour. Secondly, a variable degree of structural disconnection caused by SAH that modulates functional connectivity within and between networks - with particular focus on the role of the basal ganglia and cerebellum. It may be that the interaction between these factors means that patients with more significant early brain injury post-rupture would be unable to maintain increased functional connectivity, either because of damage to the internal connections within networks or in connections with other networks.

Another hypothesis is that the increase in connectivity seen in patients actually represents a loss of neuronal "dynamic repertoire". Populations of neurons are dynamic systems capable of displaying oscillatory behavior. When neural populations are connected in a network, then the network connectivity will shape the dynamic repertoire of the entire network. If there is damage to the system caused by acute brain injury, then the increased functional connectivity seen in patients may represent a loss of overall neuronal variability due to the loss of the normal cortical dynamic repertoire.

One of the difficulties in interpreting altered functional connectivity in patients is establishing the neuroanatomical and structural correlates underlying these changes. Despite the extensive gray matter differences seen in Chapter 4, analysis using gray matter density as a voxel-dependent covariate revealed persistent and significant functional connectivity differences remaining in many of the networks that initially showed group differences across all three scan points. Although we did not include GM as a voxel-dependent covariate for the between-network analyses, these results suggest that the increases in functional connectivity seen in patients, both within and between networks, are likely to reflect functional changes in cortical tissue - either neuronal or cerebrovascular - rather than changes in grey matter density or regional cortical atrophy.

In contrast to the functional connectivity methods that measure temporal synchronization between brain regions, the ALFF approach performed here allows us to localise voxelwise functional alterations in the brain. This provides additional information to understand the disturbances of neural networks demonstrated in the resting state data. Results from the patient versus control comparisons show that there is a significant increase in ALFF across the whole brain in the acute period post-SAH in patients when compared to healthy controls. The graphs of total power spectrum show that at all time points, the total power in the low frequency spectrum is higher in patients compared to controls. Although this could be

explained by the significant difference in motion between patients and controls at both MRI scan 1 and MRI scan 3, there was no difference at MRI scan 3. Interestingly, there was an increase in mean total spectral power between MRI scan 1 and scan 2 with voxelwise analysis demonstrating regional increased in the basal ganglia and cerebellum by MRI scan 2 compared to MRI scan 1 - this may reflect ongoing damage as a result of early brain injury or potentially, adaptive changes in cerebellum-basal ganglia connectivity. Other studies have demonstrated that the network strength as measured by ICA is selectively correlated with ALFFs within the corresponding network [32] The network strength measured by ICA reflects the extent that a particular voxel correlates with the whole independent component. As a result, correlations between ALFFs and network strengths implies that the within network connectivity is correlated with the local ALFF. Interestingly, ALFF has been found to be decreased in patients with more chronic neurological diseases such as mild cognitive impairment and Alzheimer disease [330]. In neurodegenerative diseases, these decreases in amplitude probably reflect a loss of neurons that consecutively provokes connectivity deficits and disorganisation or breakdown of brain networks. In our study, when comparing whole-brain ALFF in the resting state between patients and controls, patients with SAH showed increased amplitudes throughout the whole brain grey matter. Moreover, higher ALFF at 3 months post-SAH was correlated with a better general cognitive outcome (as measured by the ACE-R) - in keeping with studies in patients with TBI [228]. This suggests that functional and efficient brain reorganization occurred to compensate for acute brain damage and improve cognitive performance. This finding, together with changes in resting state connectivity, may constitute an objective measure of long-term cognitive outcome after SAH.

5.4.1 Methodological considerations

There are a few potential limitations to our study. Firstly, as mentioned in Chapter 4, the study population is relatively small and may not reflect the heterogeneity of demographics in SAH patients as a group. However, we have obtained highly significant results using non-parametric, whole brain statistics. Furthermore, using a voxel-wise dual regression approach enables us to quantify the degree to which individual voxels contribute to each resting-state network and compare different groups through permutation testing. This is done without an a priori hypothesis or model of brain activity. By taking account of multiple simultaneous voxel-wise relationships, this approach is able to detect interacting networks of regions, rather than the single region-dominant (pre-defined by region of interest) networks

produced by seed-based correlation. On the other hand, the network selection is based on visual inspection of independent spatial components following ICA. We have addressed this limitation by performing a cross correlation with template resting state networks (from [290]) and selecting only those networks from each temporal concatenation that were strongly correlated with this template set of networks. Finally, it is also important to note that controls were carefully matched by age to patients ($\pm$ 1 year) as increasing age has been shown to affect functional connectivity in a number of different RSNs [346, 94, 49].

Motion has been identified as a potential significant confound in studies of resting state connectivity and ALFF in patients, with group differences often at least partially explained by motion artifact [244, 269]. Furthermore, it is also plausible that ALFF are more likely to be affected by physiological noise. Even though ALFF is considered to be a measure of amplitude of neural activity, recent studies have shown that ALFF correlates highly with the neurovascular responses associated with a breath holding task [33, 74]. Although the field of denoising, especially with respect to motion, is rapidly evolving, there is still currently little consensus about which methods are most successful at removing motion artifact, or even how to measure success in removing motion artifact. We have used motion correction at two different points. Firstly in the immediate pre-processing of the raw fMRI data using the FSL tool MCFLIRT - an intra-modal motion correction tool designed for use on fMRI time series and based on optimization and registration techniques used in the FSL tool FLIRT, a fully automated robust and accurate tool for linear (affine) intra- and inter-modal brain image registration. Secondly, we have used FIX to identify components of the ICA that are most likely to represent motion artifact and remove them from the data. Finally, given that there was a significant difference in head motion between the patients and controls at MRI scan 1 and 2, we used the rMS values from MCFLIRT as a covariate of no interest to exclude any potential effect this might have on the results.

SAH is associated with changes in cerebral blood flow (CBF) which may be of significant importance given the underlying reliance of BOLD fMRI on the haemodynamic response of the brain. Results from previous studies in healthy volunteers have suggested that while variations in blood flow might contribute to functional connectivity maps, BOLD signals play a dominant role in the mechanism that gives rise to functional connectivity in the resting human brain [34]. However, this could still represent a confound in interpreting the results from our study.

We were also unable to control for the timings (and dosing regimes) of drugs such as nimodipine and analgesia during the acute period nor the cessation of the drug before MRI

Scan 3. This along with changes in haemoglobin and blood oxygen levels (caused by pulmonary consolidation) may potentially have affected the interpretation of the longitudinal contrasts in the study. However, all patients received 2L/min of oxygen via nasal speculae during each scan session as standard (to account for potential differences between the acute and follow up scans) and there were no significant differences in Sp_2, ETO_2 or $ETCO_2$ between each scan point.

Lastly, although strict correction for multiple comparisons was used for each voxelwise individual and group comparison, we did not correct for the use of multiple RSNs in each group analysis. Again, following extensive research of the literature and discussion with experts in the field, there appears to be no clear consensus on the best approach to use to correct for multiple comparisons of RSN maps in resting state data analysis. For full consideration of multiple RSN comparisons, more stringent correction should probably be applied. If Bonferroni correction were adopted here, then an appropriate threshold should be p (already corrected over space and two-tailed testing) $p<0.0025$ (0.05/20) for the 10 components used in each analysis. However, this means significantly increasing the likelihood of a type 2 error - i.e. incorrectly rejecting potentially significant results. In the future, we hope to use a new FSL tool PALM to analyse data like this to help account for this multiple comparisons issue.

5.5 Conclusion

In summary, results from this study provide evidence for cognitively important changes in both individual network and between network connectivity following SAH. There is evidence for increased functional connectivity and ALFF within the cerebellum and basal ganglia networks from as early as the first 72 hours post-SAH and that this change may be adaptive, perhaps through an influence on the responsiveness of networks engaged during focused neurocognitive activity. Increased ALFF at 3 months positively correlated with measures of cognitive function suggesting that functional and efficient brain reorganization occurs post-SAH to compensate for acute brain damage and improve cognitive performance. Results suggest that axonal damage as a result of early brain injury disrupts functional connectivity following SAH and may play a key role in determining subsequent neurocognitive impairment.

5.6 Supplementary Data

Table 5.2: Scan 1 v Control: Common local peaks (unless specified otherwise) of the significant clusters (P < 0.05 FWE-corrected) showing increased connectivity in patients compared to controls. Local maximum t values correspond to Fig. 5.11. BA, Brodmann area.

			MNI (mm)			
Network	**Cortical region**	**Side**	**x**	**y**	**z**	**Local maximum t**
IC 07: Cerebellum	Crus I	R	26	-74	-28	5.1
	Crus II	R	8	-78	-36	4.98
	Crus II	L	-6	-80	-34	4.47
	IX	R	6	-60	-52	4.53
	Parahippocampal Gyrus	L	-30	-28	-24	4.31
IC 08: Somatosensory	Primary somatosensory cortex (BA3b)	R	30	-34	66	4.89
IC 10: Left frontoparietal	Inferior parietal lobule (supramarginal gyrus)	L	-60	-24	26	4.23
	Superior frontal gyrus (BA9)	L	-26	-2	64	4.17
	Subcallosal cortex	R	6	10	-10	4.03
	Frontal pole	R	18	42	-20	4.11
	Thalamus	R	4	-18	12	4.61
	Precentral gyrus (BA44)	R	-54	8	28	3.75
	Cerebellum I-IV	R	6	-44	-18	3.94
	Cerebellum Crus II	L	-28	-88	-32	3.88
	Premotor cortex (BA6)	L	-22	-16	56	3.94
	Insula cortex	L	-34	10	2	3.54
IC 12: Basal ganglia	Putamen	R	18	14	-4	4.5
	Frontal medial cortex	L	-2	50	-24	3.98
	Frontal orbital cortex	L	22	32	-16	3.81
	Caudate	L	-8	6	-2	3.5
	Caudate	R	12	2	18	3.56
	Amygdala	R	28	2	-12	3.15
	Insular cortex	R	38	4	-14	2.6

Table 5.3: Scan 3 v Control: Common local peaks (unless specified otherwise) of the significant clusters (P < 0.05 FWE-corrected) showing increased connectivity in patients compared to controls. Local maximum t values correspond to Fig. 5.11. BA, Brodmann area. GM, grey matter

			MNI (mm)			
Network	**Cortical region**	**Side**	**x**	**y**	**z**	**Local maximum t**
IC 04: DMN (Medial)	Cerebellum I-IV	Rt	10	-50	-20	4.51
	Cerebellum I-IV	Lt	-18	-34	-22	3.8
	Cerebellum V	Lt	-12	-48	-16	2.8
	Cerebellum VI	Rt	20	-56	-28	3.21
	Thalamus	Rt	2	-10	10	5.17
	Thalamus	Lt	-14	-14	14	2.63
	Hippocampus	Rt	30	-36	2	4.25
	Parahippocampal gyrus	Lt	-18	-34	-8	4.08
	Visual Cortex V4	Rt	32	-76	-12	3.05
IC 06: DMN (Posterior)	Cerebellum (Crus II)	Lt	-28	-76	-48	4.56
		Rt	24	-80	-50	4.12
	Cerebellum (VIIb)	Rt	8	-70	-46	3.27
	Cerebellum (IX)	Rt	8	-60	-48	3.18
		Lt	-8	-56	-42	3.31
	Thalamus	Rt	16	-10	12	4.39
		Lt	-12	-10	12	4.92
	Insular cortex	Rt	36	12	-6	3.87
	Caudate	Lt	-18	18	4	3.93
		Rt	18	20	8	3.39
	Putamen	Rt	20	10	4	3.14
		Lt	-26	-8	10	3.25
	Inferior temporal gyrus	Rt	48	-58	-10	3.64
	Middle temporal gyrus	Rt	49	-42	8	3.62
	Frontal operculum cortex	Lt	-40	24	2	3.62
	Thalamus	Lt	16	-10	12	4.39
	Amygdala	Lt	-16	-8	-14	3.04
IC 07: Cerebellum	VIIIa	Rt	16	-66	-48	6.83
	V	Rt	10	-60	-12	4.88
	Crus II	Lt	-8	-78	-42	4.7
	Superior temporal gyrus	Rt	52	-34	0	5.56
	Vermis Crus II	Lt	0	-78	-42	4.98
	VI	Lt	-26	-58	-18	4.89
	Crus II	Rt	16	-86	-42	4.56
IC 09: Executive function	GM Premotor cortex BA6	Lt	-24	6	66	5.47
	Cingulate gyrus	Rt	8	8	38	3.95
		Lt	-2	18	28	3.77
	Putamen	Lt	-26	14	-2	4.79
	Frontal pole	Lt	-28	40	20	4.03
		Rt	32	40	20	4.5
	Superior frontal gyrus	Lt	12	34	56	3.82
	Central Opercular Cortex	Lt	-36	4	10	3.92
	GM Visual cortex V1 BA17	Lt	-2	-72	14	3.71
IC 11: Basal ganglia/thalamus	Thalamus	Lt	-6	-22	2	4.57
	Cerebellum (VI)	Lt	-26	-64	-30	4.0
		Rt	20	-60	-22	2.33
	Cerebellum (V)	Rt	8	-60	-8	2.52
		Lt	-8	-60	-10	2.46
	Temporal occipital fusiform cortex	Lt	-38	-62	-18	3.82
	Inferior temporal gyrus	Lt	-48	-42	-24	3.23
	Lateral occipital cortex	Lt	-36	-72	-6	2.75

Table 5.4: Scan 3 - Neurocognitively impaired v non-impaired patients: Common local peaks (unless specified otherwise) of the significant clusters (P < 0.05 FWE-corrected) showing increased connectivity in those patients with no neurocognitive impairment compared to those with impairment. Local maximum t values correspond to Fig. 5.21. BA, Brodmann area, GM, grey matter

			MNI (mm)			
Network	**Cortical region**	**Side**	**x**	**y**	**z**	**Local maximum t**
IC 05: Posterior DMN	Cerebellum (V)	Lt	-24	-26	-24	5.23
	GM Premotor cortex (BA 6)	Rt	4	-2	62	4.45
	GM visual cortex V4	Rt	40	-78	-18	3.98
	GM Broca's area BA44	Lt	-52	14	10	4.73
	Precuneus cortex (superior parietal lobule)	Rt	4	-72	40	3.97
	Frontal pole	Rt	14	60	-18	4.23
	Central opercular cortex	Rt	56	-14	20	4.29
	Inferior frontal gyrus	Rt	50	16	20	3.98
	Hippocampus	Rt	36	-10	-38	4.31
		Lt	-28	-12	-18	3.83
	Primary motor cortex (BA4a)	Rt	6	-28	52	3.77
	Amygdala	Rt	14	-6	-18	4.24
	Inferior parietal lobule	Rt	56	-36	12	4.00
	Insula cortex	Rt	36	16	-12	4.06
	Cerebellum (VI)	Lt	-6	-76	-20	4.28
	Caudate	Lt	-14	0	18	3.67
	Superior frontal gyrus	Lt	8	52	22	3.64
	Cerebellum (Crus II)	Lt	-38	-52	-44	4.21
	Frontal orbital cortex	Lt	-44	32	-6	4.1
	Inferior temporal gyrus	Lt	50	-12	-36	3.87
	Paracingulate gyrus	Rt	-6	46	-4	3.66
	Putamen	Rt	32	-12	-8	3.53
	Thalamus	Lt	-10	-18	14	4.32
		Rt	10	-12	12	4.12

Chapter 6

Acute impairment of saccadic eye movements is associated with delayed cerebral ischaemia and cerebral infarction after aneurysmal subarachnoid haemorrhage

Chapter Overview

Improving the prediction of which patients are most at risk of developing significant neurocognitive impairment following SAH remains a key area for research focus. Measurement of eye movements has previously been shown to predict outcomes in a range of chronic neurological disorders such as Parkinson's and Huntington's diseases as well as correlating with outcomes after more acute injury such as trauma. In this chapter, we used saccadometry following SAH to quantify longitudinal impairment of eye movements compared to healthy controls. We also sought to correlate these changes with DCI/cerebral infarction and neurocognitive impairment at 3 months post-SAH. The results of this study show that speed of eye movement (measured as median saccadic latency) is significantly impaired in the first 72 hours post-SAH compared to a group of age matched controls. This improves significantly and back to control level by recovery at 3 months post-SAH. Results from this study suggest saccadometry potentially offers an objective, reliable and rapid biomarker to diagnose secondary brain injury early in patients following a range of neurological insults and facilitate prompt transfer to a critical care unit to prevent irreversible cerebral damage.

6.1 Introduction

The acute management of patients with SAH as well as brain injury from other insults such as trauma, ischaemic stroke and cardiac arrest suffers greatly from the absence of an objective and non-invasive bedside marker of ischaemic tissue damage. Unlike other specialities, e.g. cardiology, where patients with chest pain can be rapidly triaged into high and low risk of myocardial infarction with high specificity and sensitivity based on an electrocardiogram (ECG) and blood test, quantifying the severity of brain injury in patients still remains dependent on mechanism of injury, subjective clinical assessment and qualitative neuroimaging. What is needed is a similar clinical test for the brain that would allow clinicians to rapidly triage patients with acute head injuries by severity, guide therapeutic outcomes and as a result, prioritise intensive care admissions.

As discussed in Chapter 2, there has been a recent increased focus on the importance of early brain injury in the first hours following aneurysm rupture in patients with SAH. Unfortunately, it remains difficult to quantify the severity of early brain injury non-invasively. The sensitivity and specificity of commonly used neurological scoring tools such as the Glasgow Coma Scale (GCS - developed for the assessment of patients with traumatic brain injury) and the National Institute of Health Stroke Scale (NIHSS - designed to assess patients with ischaemic/haemorrhagic stroke) remains unknown and depends on relatively large clinical deteriorations to trigger intervention.

Traditionally used imaging markers of cerebral ischaemia such as trans-cranial Doppler and angiographic vasoconstriction used to monitor SAH patients correlate poorly with each other and with functional outcomes [108]. Non-contrast CT scanning is often requested to exclude re-bleeding or hydrocephalus but has poor sensitivity to the detection of early cerebral ischaemia and infarction [47].

Previous studies have shown that that measurements of the time taken for the eyes to respond to a moving visual stimuli ("saccadic latency") can be used reliably as an objective biomarker of neurocognitive function in more chronic conditions such as Huntington's and Parkinson's diseases [10, 9]. Recently, prolonged saccadic latencies have also been reported in patients recovering from acute traumatic head injury [128, 127, 232]. The reaction time measured through saccadometry reflects the function of global brain circuitry involving the brainstem, cerebellum, basal ganglia and the cortex [182, 212]. Lesion studies [327, 298] and imaging evidence [275] indicate that the cerebellum is predominantly responsible for the adaptation

of visually-guided (reflexive) saccades. The adaptation of other types of saccades, however, may be mainly mediated by the frontal eye field (scanning saccades) or the dorsolateral pre-frontal cortex (memory-guided saccades) [35]. In addition, there are suggestions that structures which are functionally further 'downstream' in the initiation of saccades, such as the basal ganglia, are also important for these adaptation processes [132]. Assessing the integrity of these structures and pathways through saccadometry is therefore likely to be of considerable interest in patients with other types of global brain injury such as that seen in SAH, especially during the acute phase.

In this study, we aimed to investigate the efficacy of using a portable saccadometer acutely in patients with SAH to measure eye movements. Given the likely poor clinical status of patients in the first hours post-rupture, we focused on visually-guided "reflexive" saccades to improve accuracy of results patient compliance. We hypothesised that these eye movements might provide a sensitive and objective functional marker of early brain injury in SAH and specifically that saccadic latency would be increased acutely following aneurysm rupture and would correlate with the incidence of delayed cerebral ischaemia/cerebral infarction and neurocognitive impairment.

6.2 Methods

Ethics approval was granted as previously discussed in Chapter 4. The same inclusion and exclusion criteria for recruitment were used with the addition that patients with cranial nerve palsies affecting visual function/movement were excluded. As no population normal values exist for saccadometry, data from ten healthy volunteers taken from a different study performed by members of our research group was included, matched as a group by age to the patients recruited in the study (mean age 53.92, range 29-67). These control subjects were in good health with no significant medical history, no previous stroke or cerebral haemorrhage and taking no regular medications.

6.2.1 Recording saccadic eye movements

Visually evoked horizontal saccades were recorded acutely within the first 72 hours post-aneurysmal rupture and between day 5-10 - timed to coincide with MRI scan sessions. A repeat set of saccadometry data was also acquired at the neurocognitive and MRI follow up visit at 3 months post-SAH. Control subjects underwent one session of saccadometry recording only.

A miniaturised infra-red 1 kHz saccadometer, was used to measure saccadic latency (see Figure 6.1).

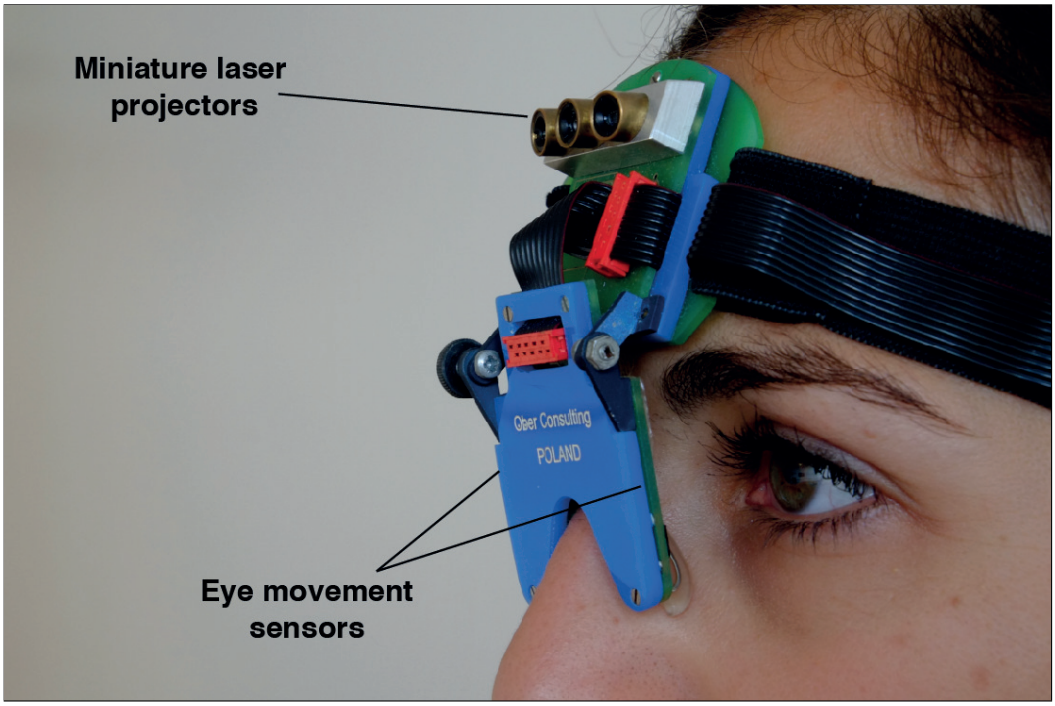


Fig. 6.1: Portable saccadometer headpiece (oculometer) used to measure saccadic latency. The device is worn across the bridge of the nose and against the forehead. The headpiece contains 3 lasers to project either a central fixation point or a visual target to the left or right of the central fixation, to which the participants were instructed to follow with their eyes

The device was worn on the head, secured by an elastic strap and resting on the bridge of the nose; three built-in low-power lasers projected red spots subtending some 0.1 degrees in a horizontal line in the midline at $\pm$ 10 degrees [221, 5]. Patients were invited to lie down and the spots were projected onto the ceiling (a white background). Because the stimuli move exactly with the head, no head restraint was necessary and sessions were well tolerated throughout the study with no patients declining testing. Experimental set-up was as described by Antoniades et al. [7]. In each trial, the central fixation target was displayed for a random fore period of 1.0–2.0s. It then moved to one of two peripheral positions on the left and right, chosen at random, and remained illuminated until 200ms after the end of the saccade [6]. The patient was instructed to keep their head still and follow the target with their eyes as it moved. If required (due to headache), patients were able to perform this task lying recumbent with the target projected onto the ceiling. A single experimental run consisted of twelve calibration trials followed by 80 experimental trials, and lasted approximately three minutes; aberrant records contaminated by excessive head movement and blinks were automatically

removed by proprietary software. This software also determined the saccadic latency using a saccade-detection algorithm based on velocity and acceleration.

6.2.2 MRI scan acquisition

As described in Chapter 4, recruited subjects underwent MRI scanning at three time points post-SAH - within 72 hours, between 5-10 days and 3 months. Scans were performed on a Siemens MAGNETOM 3T Verio machine (Siemens Healthcare, Erlangen, Germany using sequences described previously in chapter 4. Structural T1 and T2 weighted and diffusion weighted images from these scans were reviewed by a consultant neuroradiologist blinded to neurocognitive outcomes and saccades data. Scans were assessed for evidence of cerebral infarction which was defined as the appearance of new restricted diffusion lesions (high signal on the B1000 DWI image and low signal on the ADC map), T2 hyperintensity or T1 hypointensity in an ischaemic pattern on follow up imaging. Arterial spin labeling data was analysed as described previously to provide measurements of mean grey matter cerebral blood flow.

As all participants underwent CT angiography (CTA) prior to endovascular intervention and also underwent MRI scanning 24 hours post-embolisation, this enabled identification and exclusion of those patients with infarcts present on the admission CTA or on this first MRI scan (primarily embolic and procedurally related) in order to improve the accuracy of the diagnosis of cerebral infarction as per consensus guidelines [321].

Control subjects underwent one MRI scan as described in Chapter 4.

6.2.3 Clinical and neurocognitive assessment

A member of the research team reviewed study participants daily. Changes in clinical condition were noted as well as any new neurosurgical interventions e.g. cerebrospinal fluid drainage. DCI was diagnosed clinically as per the recent consensus guidelines above.

Neurocognitive assessment was conducted at three months post-SAH as described previously in Chapter 4 on page 51.

6.2.4 Statistical analysis

Data were analysed using Prism 6 (GraphPad Software). A Shapiro–Wilk test was first applied to the saccadic eye movement data to mathematically assess distribution normality. As the data was non-parametrically distributed, paired differences were compared using a Wilcoxon-matched pairs signed test and unpaired differences were compared using a Mann-Whitney U test. Differences between infarct and no infarct groups at each time point were compared using a Mann-Whitney U test. Non-parametric Spearman's rank correlation coefficient was used to measure the strength of association between variables. Where applicable, results are presented as mean $\pm$ standard deviation and all statistical tests had significance set at $p \leqslant 0.05$.

6.3 Results

24 patients of those recruited as per chapter 4 met the inclusion criteria for this part of the study and underwent measurement of saccadic latency acutely (i.e. within 72 hours of rupture and between days 5-10). Two patients were subsequently excluded from this study due to cranial nerve palsy affecting eye movements and preventing measurement of saccades. Of those 22 patients who underwent successful acute saccadometry, 20 returned for neurocognitive and MRI follow-up at 3 months post-SAH and had saccadometry data collected. Two patients declined follow-up at 3 months but underwent MRI scanning at 6 months post-SAH as part of standard clinical protocol so were included. In total, eight patients were diagnosed with either DCI or DCI-related cerebral infarction on outcome imaging. Four of these patients were diagnosed with clinical deterioration due to DCI and also went on to develop cerebral infarction. A further four patients were not diagnosed as having clinical symptoms of DCI as per consensus guidelines but had evidence of DCI-related cerebral infarction on follow-up MRI. Demographics for all 24 patients studied are shown in Table 6.1.

Table 6.1: Demographics of recruited patients

Overall Demographics	
n	22
Age (mean/range)	54.66 (31-70)
Gender (M:F)	8:14
WFNS Grade	
1	15
2	7
Modified Fisher Grade	
1	0
2	1
3	5
4	16
Aneurysm Location (%)	
Anterior circulation	7 (32%)
Middle cerebral Artery	6 (27%)
Internal carotid artery	8 (36%)
Posterior circulation	1 (5%)
Left side	11 (50%)
Right side	10 (45%)
Midline	1 (5%)

Figure 6.2 shows the main saccadometry results from the study. Saccadic latency was significantly prolonged in patients in the first 72 hours post-rupture when compared to healthy age matched controls (224.9 $\pm$ 24.7ms v 181.4 $\pm$ 26.5ms, p=0.0013 Mann-Whitney U test). There was an overall significant decrease in median saccadic latency between the first 72 hours post-SAH and at 3 months (224.9 $\pm$ 24.7ms v 191.8 $\pm$ 34.56ms, p=0.0001 Wilcoxon-matched pairs signed test). Patients at 3 months had no significant difference in median saccadic latency to age matched controls (191.8 $\pm$ 34.56ms v 181.4 $\pm$ 26.5ms, p=0.6422 Mann-Whitney U test.

Taking a cut off for median saccadic latency of 215 milliseconds, for our study population this gives a sensitivity of 87.5% and a specificity of 64.7% for detecting DCI and cerebral infarction post-SAH.

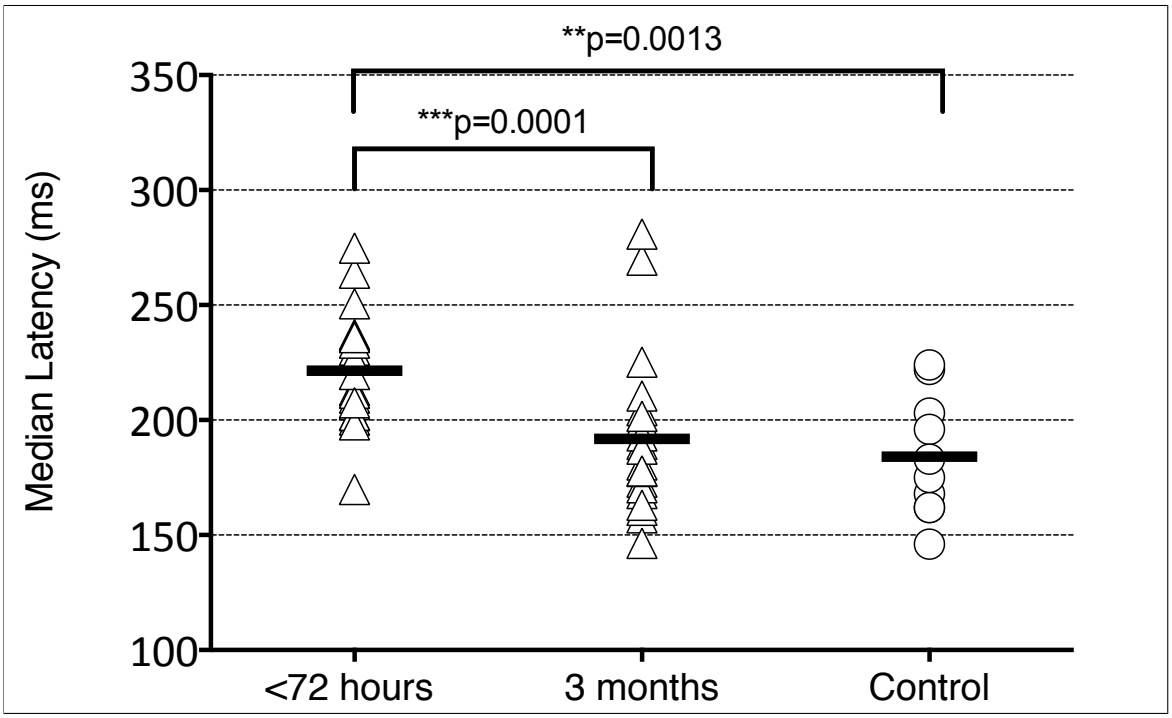


Fig. 6.2: Longitudinal differences in median saccadic latency for patients in the first 72 hours post-SAH and 3 months post-SAH and healthy control subjects. Solid bars represent median values.

Saccadic latency in the first 72 hours was negatively correlated with mean grey matter cerebral blood flow (r=-0.57, p=0.009, Spearman's correlation). Furthermore, those patients diagnosed with DCI or evidence of DCI-related cerebral infarction had a significantly higher median saccadic latency in the first 72 hours than those patients without infarction (214.8 $\pm$ 23.7ms v 243.0 $\pm$ 27.9ms, p=0.0258) with a Cohen's d calculated ROI is 1.09 - suggesting a large effect size difference between the two groups. This difference was even more significant during the second scan at days 5-10 post-SAH during the peak incidence for DCI (210.0 $\pm$ 36.8ms v 322.7 $\pm$ 76.4ms, p=0.0003 Mann-Whitney U test) with a Cohen's d of 1.8.

There was no significant difference in saccadic latency at either 72 hours or 3 months post-SAH between patients diagnosed with neurocognitive impairment and those with no neurocognitive impairment. There was also no significant correlation between median saccadic latency and ACE-R within the first 72 hours post-SAH (r=0.11) nor at 3 months post-SAH (r=0.26).

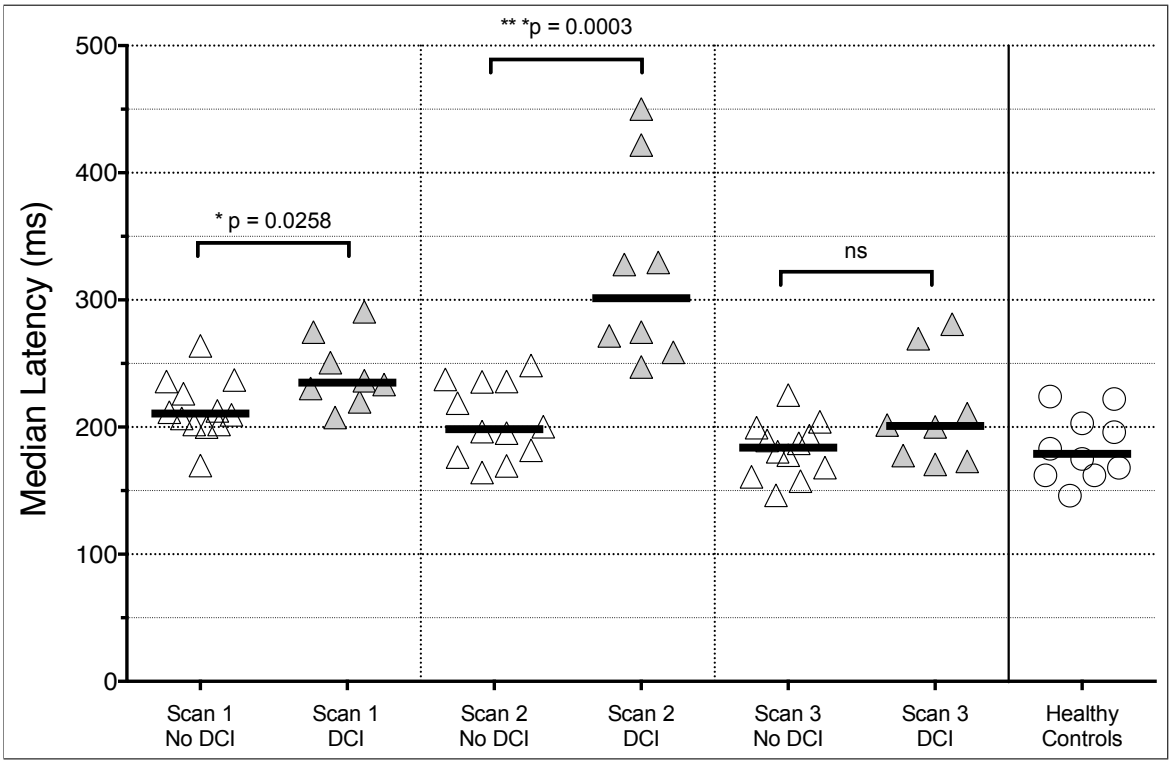


Fig. 6.3: Differences in median saccadic latency for patients with and without DCI/DCI-related cerebral infarction at each MRI scan point. Those patients with DCI had significantly higher mean saccadic latency in the first 72 hours and between days 5-10 than those without. By three months, there was no significant difference between the two groups. Control data are included for comparison. Solid bars represent median values.

There were no significant differences in age (p=0.3734), gender (p=0.6494) or WFNS grade (p>0.99) between those patients with evidence of cerebral infarction on follow up MRI scan and those without. Interestingly, modified Fisher grade (often used as a risk factor for DCI) on admitting CT was significantly higher in those patients without cerebral infarction at 6 months (p=0.0091). Only one patient required insertion of a ventriculoperitoneal shunt and this was in the non-infarction group.

6.4 Discussion

This is the first study to prospectively investigate the utility of acutely measuring eye movements in critically unwell SAH patients and to correlate these changes with short term outcomes after SAH. There are a number of notable results. Firstly, our results demonstrate saccadic eye movement is adversely affected in patients in the first 72 hours post-rupture when compared to healthy control subjects. Furthermore, saccadic latency in the first 72

hours was negatively correlated with mean grey matter cerebral blood flow - the higher the CBF, the faster the saccadic latency. Those patients that progressed to developing DCI and/or DCI-related cerebral infarction had significantly slower saccades in the first 72 hours and between days 5-10 (the peak incidence for DCI) than those patients with no DCI/infarction. There was no significant difference in saccadic latency at either 72 hours or 3 months post-SAH between those patients diagnosed with neurocognitive impairment and those with no neurocognitive impairment.

Results from Chapter 4 demonstrate that patients exhibit a wide range of CBF values in the first 72 hours post-SAH and that acute impairment of cerebral autoregulation is often seen as a consequence of the initial aneurysmal rupture [246, 172]. It is probable that the prolonged latencies seen in patients in the first 72 hours post-SAH are as a result of acute neuronal damage caused by early brain injury. This is supported by the significant negative correlation between median saccadic latency and mean grey matter cerebral blood flow in the first 72 hours post-SAH. The control of eye movements is complex and involves a number of different brain areas such as the brainstem, cerebellum, basal ganglia, and cerebral cortex.[8] Early brain injury occurs in the first 72 hours post-SAH and includes raised intracranial pressure, cerebral oedema, microthrombosis and inflammation [280], resulting in a global neurological insult. The non-focal character of these pathophysiology changes coupled with the heterogenous functional structure of the oculomotor system makes it difficult to assign the slower saccadic latency to distinct or specific cerebral regions. However, deficits in eye movements are to be expected if the functional integrity of corresponding neural pathways is compromised as may be the case acutely following SAH.

There is evidence that factors relating to the initial aneurysm rupture such as clinical grades of severity e.g. WFNS and Hunt and Hess, and the thickness of subarachnoid blood (as measured by Fisher score) commonly used in clinical practice to risk stratify patients, do not correlate well with either DCI or functional and neurocognitive outcomes [185, 171]. It is therefore likely that ischaemic and metabolic damage occurring in the first hours post-rupture due to early brain injury may play a much more important role in predicting subsequent recovery post-SAH. As a result, there has been increasing interest in the use of multimodal monitoring post-SAH to optimise diagnosis and individualise therapeutic interventions aimed at preventing secondary neuronal injury [265]. However, the majority of techniques currently in use in neurointensive care such as tissue oxygen monitoring and microdialysis remain unsuitable for monitoring those patients with good grade SAH who do not require sedation and mechanical ventilation.

We have proven that saccadometry is well tolerated by patients and that those patients who go on to develop DCI or cerebral infarction have significantly higher median saccadic latency in the first 72 hours and at days 5-10 than those without. In contrast, age, admission GCS, Fisher grade and WFNS score showed no significant differences between those patients with DCI and those without. The prolonged saccadic latencies in those patients with DCI and cerebral infarction may therefore represent an objective and non-invasive biomarker of the severity of global tissue damage due to early brain injury. This might allow earlier and more accurate risk stratification and resource allocation of intensive care interventions such as invasive pressure monitoring and "triple H therapy" (induced hypertension, hypervolaemia and haemodilution) to those patients who might benefit the most. Although the specificity of the test is comparatively low, this would not necessarily be a barrier to introducing saccadometry into routine clinical use. Although a small number of patients would undergo unnecessary intensive care admission, this would be offset by the high sensitivity of the test (87.5%) to identifying those patients at risk of DCI/cerebral infarction who would benefit from such interventions. Given this is a non-invasive test that takes minutes to perform, saccadometry could play a key role in providing objective bedside measurements to support other clinical data such as GCS and imaging in predicting and diagnosing patients with DCI at risk of cerebral infarction.

6.4.1 Methodological considerations

We have studied a cohort that is representative of the standard clinical population of patients with SAH. There are however some potential limitations to the study. The number of subjects recruited is relatively small and assessment of saccadometry test-retest reliability in patients was not performed due to issues with test tolerance and concerns about increasing the study drop out rate. However, group comparisons were performed using non-parametric statistics and saccadometry has been shown to have high test-retest reliability over time in healthy volunteers as well as excellent within-test internal consistency [93]. Furthermore, the Cohen's d of > 1.0 for the difference seen in median saccadic latency between those patients with DCI and those with no DCI at both 72 hours and 5-10 days post-SAH suggests a large effect size difference between the two groups. We were unable to accurately address the question of whether the location of ruptured aneurysm has an impact on saccadic latency due to subject numbers but hope to investigate this in a future larger study. Finally, although all patients were clinically good grade (WFNS I or II) and therefore required no sedative drugs, patients did receive opioid analgesia and other medications e.g. anti-hypertensives during the study

period that were difficult to standardise across recruited participants. Studies have shown that administration of opioid analgesia can acutely affect measurements of eye movements [260] and this may have acted as a potential confound in our study. As regards other potential confounds e.g. lack of sleep, sleep deprivation has not been shown to have an effect on reflexive saccades [356].

6.5 Conclusions

To our knowledge, this is the first study to use saccadometry in patients acutely post-SAH. Results demonstrate that measurement of saccadic latency in the first 72 hours post-SAH is significantly associated with incidence of DCI and DCI-related cerebral infarction and negatively correlated with cerebral blood flow. This highlights the potential role of the measurement of saccadic eye movements in helping to understand the pathophysiology underlying secondary brain injury after SAH. Future larger studies are needed to explore the potential of saccadometry to offer an objective, reliable and rapid biomarker to diagnose secondary brain injury following a range of neurological insults and facilitate prompt transfer to a critical care unit to prevent irreversible cerebral damage.

Chapter 7

Investigating the role of calcium channel blockade on early brain injury after acute normobaric hypoxia

Chapter Overview

Calcium plays a key role in neuronal cellular communication and the maintenance of cerebral vascular tone. Following acute cerebral ischaemia, there are rapid shifts in calcium concentration that are likely to cause cellular damage and death across the brain. However, there is considerable evidence to suggest variability in the tolerance of different regions of the brain to hypoxic-ischaemic damage. As a result, calcium regulation is likely to play a key role in mediating damage to cells after cellular hypoxia. The drug nimodipine is an L-type calcium channel blocker with cerebral selectivity that, as described in Chapter 2, has been consistently shown to exert an outcome benefit after SAH. However, the mechanism behind this benefit remains unknown and the drug has failed to show outcome benefit in other neurological insults such as traumatic brain injury, ischaemic stroke and cardiac arrest. The objective of this study was to quantify the effect of acute poikilopcapnic normobaric hypoxia on apparent diffusion coefficient (ADC), low frequency blood oxygen level dependent (BOLD) oscillations, cerebral blood flow and tissue volume in the thalamus and hippocampus and to compare these with changes in whole brain grey matter and the occipital lobe. Then to investigate the impact of nimodipine at standard clinical doses on any changes seen due to cerebral hypoxia.

We conducted a prospective, double blinded, randomised cohort study of 18 right handed, non-smoking participants (11 male and 9 female, mean age 28.28 $\pm$ 7.77 years) with no pre-existing medical disease and no recent exposure to altitude or depth. Subjects underwent four experimental sessions in which they were exposed to either acute normobaric poikilocapnic hypoxia (end-tidal O_2 7.3KPa) or normoxia and either nimodipine 30mg or placebo. The main outcomes measurements were apparent diffusion coefficient (ADC), cerebral blood flow (CBF), grey matter volume and low frequency signal amplitude of blood oxygen level dependent (BOLD) oscillations (ALFF) in the thalamus, hippocampus, occipital lobe and whole brain grey matter

Acute hypoxia resulted in a significant decrease in ADC values and an increase in grey matter volume in the thalamus and hippocampus regions of interest when compared to the normoxia condition. There was also a significant decrease in ALFF in the hypoxia condition versus normoxia across all regions. Administration of nimodipine significantly increased ADC values in the subcortical structures of the thalamus and hippocampus back towards baseline normoxia levels and caused a reduction of ALFF in the thalamus. There was no significant difference in CBF between conditions in either the subcortical or cortical structures.

Results from this study provide evidence for a preferential effect of calcium channel blockade with nimodipine under conditions of acute poikilocapnic normobaric hypoxia in reversing regional changes in ADC and ALFF. These changes to ADC and ALFF may underlie the benefit seen in aneurysmal subarachnoid haemorrhage in reducing the impact of global cytotoxic cerebral oedema seen with early brain injury. Further research is needed into the importance of changes in ALFF with hypoxia and whether this represents a biomarker of cerebral tissue hypoxia in acute neurological conditions such as SAH.

7.1 Introduction

Many important cellular processes are mediated by changes in the concentration of cytosolic free calcium and as a result, the movements and storage of calcium are normally subject to tight regulatory control, primarily through the action of voltage-gated calcium channels [31]. Cerebral ischaemia rapidly causes an imbalance of ions inside and outside neurons and glia and uncontrolled intracellular shifts in calcium concentration can lead to irreversible cell destruction and death [55, 207, 124]. As a result, elevated levels of intracellular calcium may constitute the final common pathway of cell injury from ischaemia [55] and L-type calcium channels are likely to play an key role in mediating or propagating hypoxic neuronal cellular damage [241].

As described in Chapter 2, Nimodipine is a dihydropyridine L-type calcium channel blocker characterised by a highly selective action on cerebral blood vessels and a high affinity to receptors in the cerebral cortex. This preferential cerebral action of the drug has been explained by high transfer across the blood brain barrier compared to other calcium channel blockers [315]. In experimental models of focal and global ischaemia, nimodipine has been shown to have a neuroprotective effect, attenuating cognitive dysfunction in experimental hypoxia and increasing the hypoxic tolerance of brain tissue [121, 115].

In both focal and global ischaemic studies, there is substantial evidence to suggest variability in the tolerance of different regions of the brain to hypoxic-ischaemic damage. What is particularly interesting is why this differential sensitivity of brain structures to hypoxic-ischaemic injury exists and whether this is to some degree an evolutionary adaptation, protecting those brain regions most susceptible to damage. Furthermore, the distribution of these voltage-gated calcium channels varies within the areas of the brain and their subtype in neurons is not homogeneous [92]. The thalamus is a central relay and processing station for a wide variety of neural signals. Incoming sensory information, as well as descending cortical input, drives excitation of thalamocortical (TC) cells which then project to the cortex and other regions [139]. Animal models of global ischaemia have suggested a selective vulnerability of sub-cortical structures such as the thalamus and thalamic nuclei, the hippocampus and the basal ganglia (caudate and putamen) to hypoxic-ischaemic injury [48, 153, 39]. Thalamic structures like the ventral posterior lateral nuclei also seem to have a greater tolerance to regional blood flow reduction when compared to cortical regions [40, 169]. Poor neurological recovery has also been linked to damage in the thalamus in animal studies [287] as well as following cardiac arrest and traumatic brain injury in patients [256, 257]. Furthermore,

voltage gated calcium channels expressed in thalamic neurons seem to play a key role in determining the activity of the thalamo-cortical network in different states of consciousness [188].

These findings therefore suggest that the thalamus and hippocampus could be particularly interesting brain structures to focus investigation into the role of nimodipine in cerebral hypoxia. This is due to their selective vulnerability to hypoxic-ischemic insults, the role they appear to play in cognitive dysfunction following neuronal injury and the importance of thalamic and hippocampal L-type calcium channels to higher level cortical functions.

As described in Chapter 5, there has been recent interest in the significance of the amplitude of low frequency oscillations (ALFF) (0.01 to 0.1Hz) in the blood oxygen dependent level (BOLD) signal both in health and in disease. Despite the increased appreciation of spontaneous LFO in BOLD fMRI resting state data, the properties and regional characteristics of spontaneous LFO are rarely examined directly. Instead, most resting state fMRI studies focus on mapping the spatial distribution of temporal correlations amongst these spontaneous fluctuations. Studies have shown increases in ALFF following traumatic brain injury[228] and in Parkinson's disease [352, 167]. However, there is still no quantitative understanding of the relative contribution of spontaneous neuronal/glial oscillations and oscillations that reflect hemodynamic coupling to the resting-state BOLD signal. A recent study demonstrated that low frequency oscillations in calcium (a marker of cellular oscillations) show frequencies similar to those of deoxyhemoglobin (main contributor to the BOLD signal) and precede them by 5–6 seconds [87]. Changes in ALFF might therefore represent a sensitive biomarker of resting cellular function and reflect early pathophysiological changes seen during periods of acute cerebral hypoxia.

The first objective of this study was to develop a model of acute normobaric hypoxia in healthy volunteers and use MRI scanning to quantify changes in apparent diffusion coefficient (ADC), amplitude of low frequency oscillations, grey matter volume and cerebral blood flow that occur. We then aimed to investigate the impact of calcium channel blockade with nimodipine at a standard clinical dose on these changes. We hypothesised that acute normobaric poikilocapnic hypoxia would have a heterogeneous effect on the brain with selective focus on the difference between the cortex (occipital lobe) and subcortical structures (thalamus and hippocampus). Through this, we hoped to develop an in vivo model to improve our understanding of the mechanisms by which nimodipine seems to exert a differential outcome benefit following different types of clinical neurological injury.

7.2 Methods

Approval for the study was granted by the local UK National Research Ethics Service committee (NRES Committee South Central - Berkshire: 11/SC/0519) and informed written consent was obtained from all participants. 20 right handed, healthy volunteers (11 male and 9 female, mean age 28.28 $\pm$ 7.77 years) with no significant disease or regular medication were recruited and studied over a one year period. Specific exclusion criteria included routine contraindication to MRI scanning, history of smoking and air travel or exposure to high altitude in the last 3 months.

7.2.1 Experimental Design

Participants attended for four separate experimental sessions (minimum one week apart), each lasting approximately five hours with the order of each session randomised. The experimental conditions were:

1. Poikilocapnic normoxia ("Normoxia")/Placebo
2. Poikilocapnic normoxia ("Normoxia")/Nimodipine
3. Poikilocapnic hypoxia ("Hypoxia")/Placebo
4. Poikilocapnic hypoxia ("Hypoxia")/Nimodipine

All sessions were conducted in a normobaric environment. Drug/placebo conditions were doubled blinded for each session with doses prepared by a colleague independent of the research group. Hypoxia/normoxia conditions were blinded only to participants and not the researchers running the session. First level MRI analysis was undertaken blinded to both normoxia/hypoxia and drug/placebo conditions and un-blinding was only performed once all first level analysis had been performed.

7.2.2 Experimental Procedure

The study protocol consisted of a continuous four hour session in a physiology laboratory breathing either breathed room air, with the normal fraction of inspired oxygen (FiO_2) of 21%, or a hypoxic gas mixture with end-tidal oxygen (ETO_2) maintained at 7.3 kP, followed by an MRI scan with ETO_2 maintained as above (See Figure 7.1-A). Participants received

either nimodipine 30mg or placebo at one hour and three hours into the protocol depending on the experimental condition.

Hypoxia

Modulation of oxygen content in the air during the laboratory and MRI sessions was achieved using a custom built breathing apparatus (Figure 7.1-B).

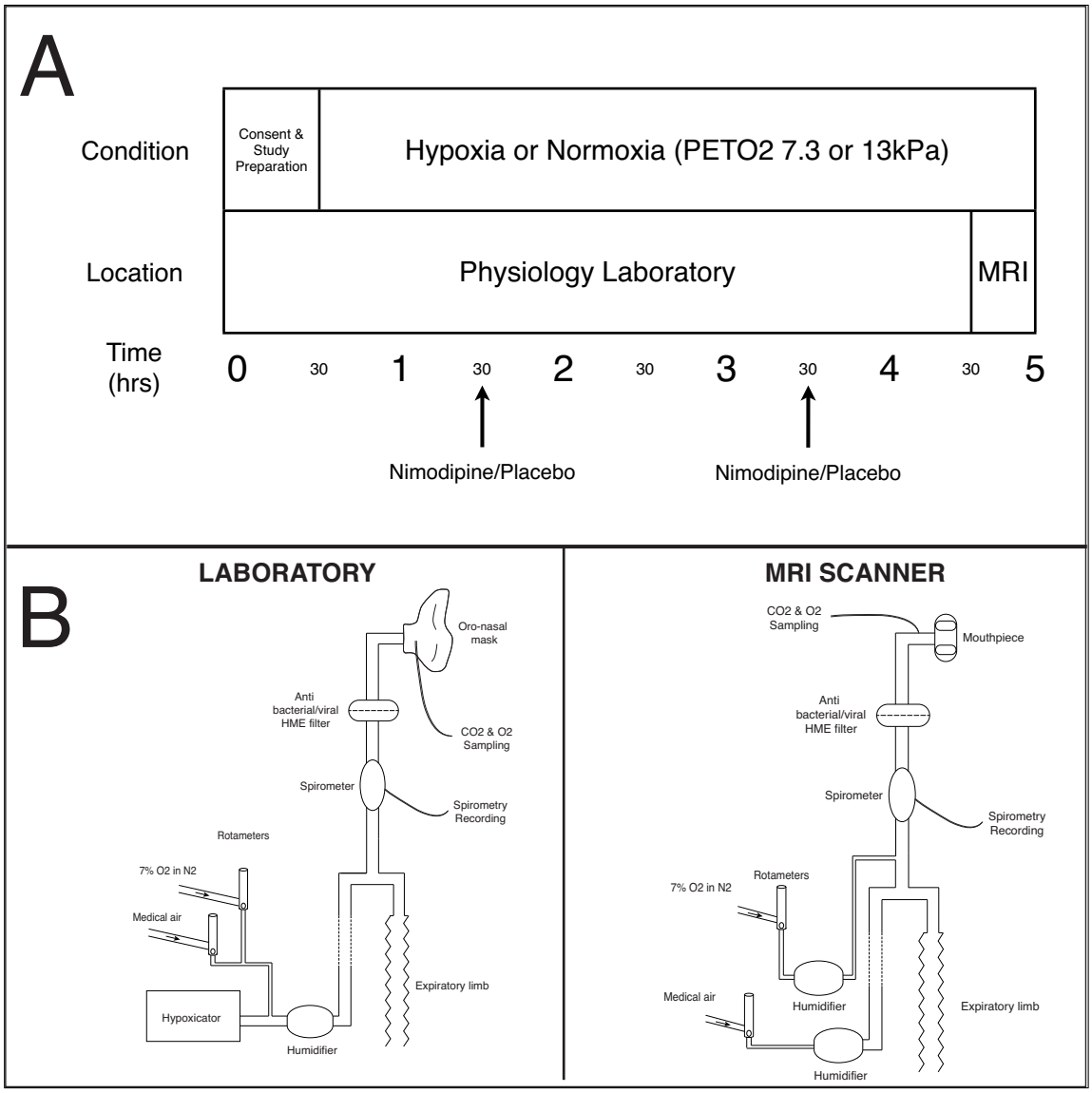


Fig. 7.1: A: Study protocol. B: Schematic diagram of the breathing apparatus used to maintain hypoxic conditions in both the laboratory and MRI sessions.

During the laboratory hypoxia condition, subjects inhaled gas from a hypoxicator unit (HYP-123 Hypoxicator generator, Hypoxico Inc) via a tight fitting silicone facemask (Hans Rudolph, 7540 series V2, Kansas City, MO, USA). Additional 7% oxygen in nitrogen from a cylinder was added to the system to maintain an ETO_2 of 7.3KPa. During the normoxia condition, subjects received medical air through the same system. End-tidal carbon dioxide ($ETCO_2$) was not explicitly controlled throughout the laboratory and MRI sessions to replicate normal cerebral physiological responses to hypoxia. Continuous physiologic recordings were obtained for $ETCO_2$ and ETO_2 (Gas Analyzer, AD Instruments, UK). Oxygen saturations (SpO_2), heart rate and non-invasive blood pressure (NIBP) were measured every five minutes (Dinamap Procare 300, GE Healthcare). For each subject, the hypoxicator was turned on during all four sessions to ensure the background noise was the same and that subjects remained blinded to the gas mixture condition.

During the MRI session, participants used a similar breathing apparatus and a diving mouthpiece (Scubapro Ltd, UK) to maintain the same ETO_2 as used in the laboratory session for the whole scan duration.

Nimodipine

Nimodipine and placebo doses were produced by Ipswich NHS Pharmacy Manufacturing Unit and matched in colour, size and shape to ensure participants and investigators remained blinded to the experimental condition. Participants received a dose of either nimodipine 30mg or placebo at 1 hour and 3 hours into the laboratory session. The dosing and route were chosen to replicate standard clinical practice and timed to aim for maximum cerebral concentrations of the drug at the start of the MRI scanning session (as per Hernandez-Hernandez et al.

MRI Scanning

A Siemens MAGNETOM 3T Verio scanner (Siemens Healthcare, Erlangen, Germany) with a 32-channel head coil and situated immediately adjacent to the physiology laboratory was used for all scanning sessions. At the end of the four hour laboratory session, participants were moved immediately to the scanner room and placed directly onto the breathing system while keeping the disconnection time to an absolute minimum. Heart rate, SpO_2 and NIBP were continuously monitored during MRI studies using an MRI-compatible physiological monitoring system (3150/3155 MRI patient monitor, In Vivo Research). ETO_2 and $ETCO_2$ were monitored using a gas analyser (Gas Analyzer, AD Instruments, UK).

The scanning protocol included:

1. **T1-weighted MPRAGE structural** (2 mins 22 s, whole brain; 1.5 x 1.5 x 1.5mm resolution; TR 1780 ms; TI 900 ms; TE 4.4 ms; FOV 228mm, 192 slices)
2. **Resting state gradient-echo, echo-planar blood oxygen dependent level (BOLD) imaging sequence** (6 mins; 24 slices, TR 3000 ms; TE 16 ms; flip angle 90°; FOV 240 mm; voxel size 3.0 x 3.0 x 3.0 mm)
3. **Diffusion-weighted (DWI)/Apparent Diffusion Coefficient (ADC) echo planar, spin echo sequence** (1 min; TR 5300 ms; TE 91 ms; b values 0 and 1000s/mm2, voxel size 1.8 x 1.8 x 5mm)
4. **Time-of-flight MR angiogram** (1.5 mins; 20 slices; TR 26 ms; TE 3.43 ms;)
5. **Multi-inversion time (TI), vessel-encoded pseudo-continuous arterial spin labelling (VEPCASL) perfusion-weighted imaging** (5 mins 55 s, 3.4 x 3.4 x 4.5 mm, field of view 220m; TR 4080 ms; TE 14 ms, echo planar imaging, 24 slices) with multiple post-labelling delays (six delays: 0.25 s, 0.5 s, 0.75 s, 1 s, 1.25 s, 1.5 s) (Okell et al., 2013 [224]) to measure cerebral blood flow
6. **Phase contrast scan** 1 min 27 s, 1.9 x 1.9 x 5mm, TR 58.75 ms, TE 6.06, flip angle 15 degrees

Corresponding B0 fieldmap images were acquired at each scan to aid scan registration by correcting for echo-planar imaging distortion artifacts. In order to quantify any potential change in velocity through the carotid and vertebral as a result of either hypoxia or nimodipine, phase contrast images were acquired. This technique utilises the phase of an image to encode the velocity of flowing spins and has been validated for angiogram and quantitative flow measurements [225].

7.2.3 Post-processing of MRI data

All image analysis was performed using FSL[144] and MATLAB (The Mathworks Inc.).

Volumetric structural data analysis

An optimised voxel-based morphometry (VBM) analysis was undertaken on the structural images acquired to identify regional changes in the thalamus and whole brain grey matter

volume [82, 114] (FSL- http://fsl.fmrib.ox.ac.uk/fsl/fslwiki/FSLVBM). For each comparison, to avoid the known bias of using one of the data sets as a reference, all images were processed following the same protocol. First, structural images from all four experimental conditions were brain-extracted and grey matter-segmented before being registered to the MNI152 standard space using non-linear registration. The resulting images were averaged and flipped along the x-axis to create a left-right symmetric, study-specific grey matter template. Second, all native grey matter images were non-linearly registered to this study-specific template and "modulated" to correct for local expansion (or contraction) due to the non-linear component of the spatial transformation. The modulated grey matter images were then smoothed with an isotropic Gaussian kernel with a sigma of 3mm. The group mean grey matter mask obtained from the VBM analysis was used to obtain values for cortical grey matter. A probabilistic mask of the thalamus, hippocampus and occipital lobe in MNI152 standard space and thresholded at 35% was used to obtain values for grey matter volume between each of the four experimental conditions. In addition, to investigate changes over the whole brain, voxelwise GLM was applied using permutation-based non-parametric testing (Randomise with 5000 permutations)[335]. Results were considered significant at $p<0.05$, FWE-corrected for multiple comparisons across space using Threshold-Free Cluster Enhancement (TFCE) [291].

DWI analysis

ADC maps obtained from the scanner were brain extracted using the FSL tool BET [289] before being registered to MNI 152 standard space using non-linear registration. A probabilistic mask of the thalamus, hippocampus and occipital lobe in MNI152 standard space and thresholded at 35% was then used to obtain values for ADC between each of the four experimental conditions Finally, voxelwise GLM was applied using permutation-based non-parametric testing (5000 permutations), correcting for multiple comparisons across space to look for global changes in grey matter ADC between conditions of interest.

Amplitude of low frequency fluctuations analysis

Pre-processing of individual resting state BOLD data sets was undertaken using FSL tools as described in Chapter 5. Head motion was corrected using multi-resolution rigid body co-registration of volumes, as implemented by MCFLIRT [143]. Brain extraction was carried out for motion corrected BOLD volumes with optimization of the deforming smooth surface model, as implemented in BET [292]. This procedure was verified with visual inspection

of the extraction result. Data denoising was performed with FIX as discussed in Chapter 3 and Chapter 5. Multi-resolution affine co-registration as implemented in FLIRT was used to co-register fMRI volumes to T1 structural volumes of corresponding subjects and FNIRT was used to non-linearly register the structural volumes to MNI152 standard space. The images were smoothed with 6mm full width at half maximum (FWHM) smoothing. Calculation of ALFF was then performed with customised MATLAB (Mathworks Inc.) scripts. The power of the low frequency fluctuations in the frequency range 0.01-0.1Hz was measured using a multi-taper spectral estimation using discrete prolate spheroidal (Slepian) sequences with five tapers, and fast Fourier transform algorithm for the resting-state time series for each voxel. The power between the 0.01-0.1Hz was divided by the total power of the whole frequency spectrum to calculate normalised spectral power for that low frequency band. This was performed to normalise to look specifically at changes within this low power band.

A probabilistic mask of the thalamus, hippocampus and occipital lobe in standard MNI152 space and thresholded at 35% was then applied to obtain average values for ALFF in the thalamus region. Finally, for whole brain analysis, voxelwise GLM was applied using permutation-based non-parametric testing (5000 permutations), correcting for multiple comparisons across space.

ASL data analysis

All related data processing steps essential for quantification of CBF including tissue segmentation, estimation of equilibrium magnetization of blood (M0b) from the mean cerebrospinal fluid CSF magnetization (M0csf) images, and generation of absolute CBF in physiologic units (ml blood/100g tissue/minute) were completed using FSL tools.

Multi-TI pseudocontinuous arterial spin labeling (PCASL) was processed using a non-linear fit to the general kinetic model for all voxels within a brain mask to quantify CBF [52, 224]. Multi-resolution affine co-registration as implemented in FLIRT was used to co-register total perfusion maps to T1 structural volumes and FNIRT was used to non-linearly register the structural volumes to MNI152 standard space. Once again, the same probabilistic masks for the regions of interest described above were used papersfor each subject to obtain regional values for CBF.

Phase contrast (PC) MRI was used to assess the blood velocity in the carotid and vertebral arteries at the location of the PCASL labelling plane [20]. The PC MRI acquisition was cardiac-gated using a pulse oximeter. Vessel ROIs were manually created and applied to

the cardiac gated velocity maps to provide plots of blood velocity over the cardiac cycle. Average velocity was then computed and compared to a simulated plot of inversion efficiency versus velocity. Average vessel velocities in the range of 15 cm/s to 45 cm/s result in an inversion efficiency of approximately 0.9 [18], and were in this range for all subjects. As a result, the effects of blood velocity at the labelling plane on inversion efficiency were likely to be consistent across all subjects.

7.2.4 Statistical Analysis

The contrasts of interest between conditions were:

1. Normoxia/Placebo v Hypoxia/Placebo (Effect of hypoxia on brain)
2. Normoxia/Placebo v Normoxia/Nimodipine (Effect of nimodipine in normoxia)
3. Hypoxia/Placebo v Hypoxia/Nimodipine (Effect of nimodipine in hypoxia).

A Shapiro–Wilk test was first applied to each dependent variable in the analysis to mathematically assess distribution normality. A one way, repeated measures analysis of variance (RM ANOVA) correcting for the three comparisons as above was then used to investigate differences between normally distributed physiological and MRI data. A Friedman test (non-parametric alternative to a RM ANOVA) correcting for the three comparisons above was used for non-parametric data analysis. Significance for all two-tailed tests was established at an alpha level of $p<0.05$ and data are expressed as a mean $\pm$ standard deviation. For the voxelwise analysis, results were considered significant at $p<0.05$, FWE-corrected for multiple comparisons across space using Threshold-Free Cluster Enhancement. All other statistical analysis was conducted using Prism 6 (GraphPad Software).

7.3 Results

Complete laboratory and MRI datasets were obtained in 18 subjects. Two subjects withdrew from the study due to scheduling and time commitment issues. The remaining subjects that completed all four sessions were able to complete each protocol without discomfort. During pre-processing and prior to unblinding, significant motion artifact was discovered in the ASL sequence for one subject dataset which had to be excluded.

7.3.1 Physiological data

Figures 7.2 and 7.3 show changes in mean end tidal oxygen (ETO_2) and end tidal carbon dioxide ($ETCO_2$) levels throughout the laboratory and MRI sessions for all participants.

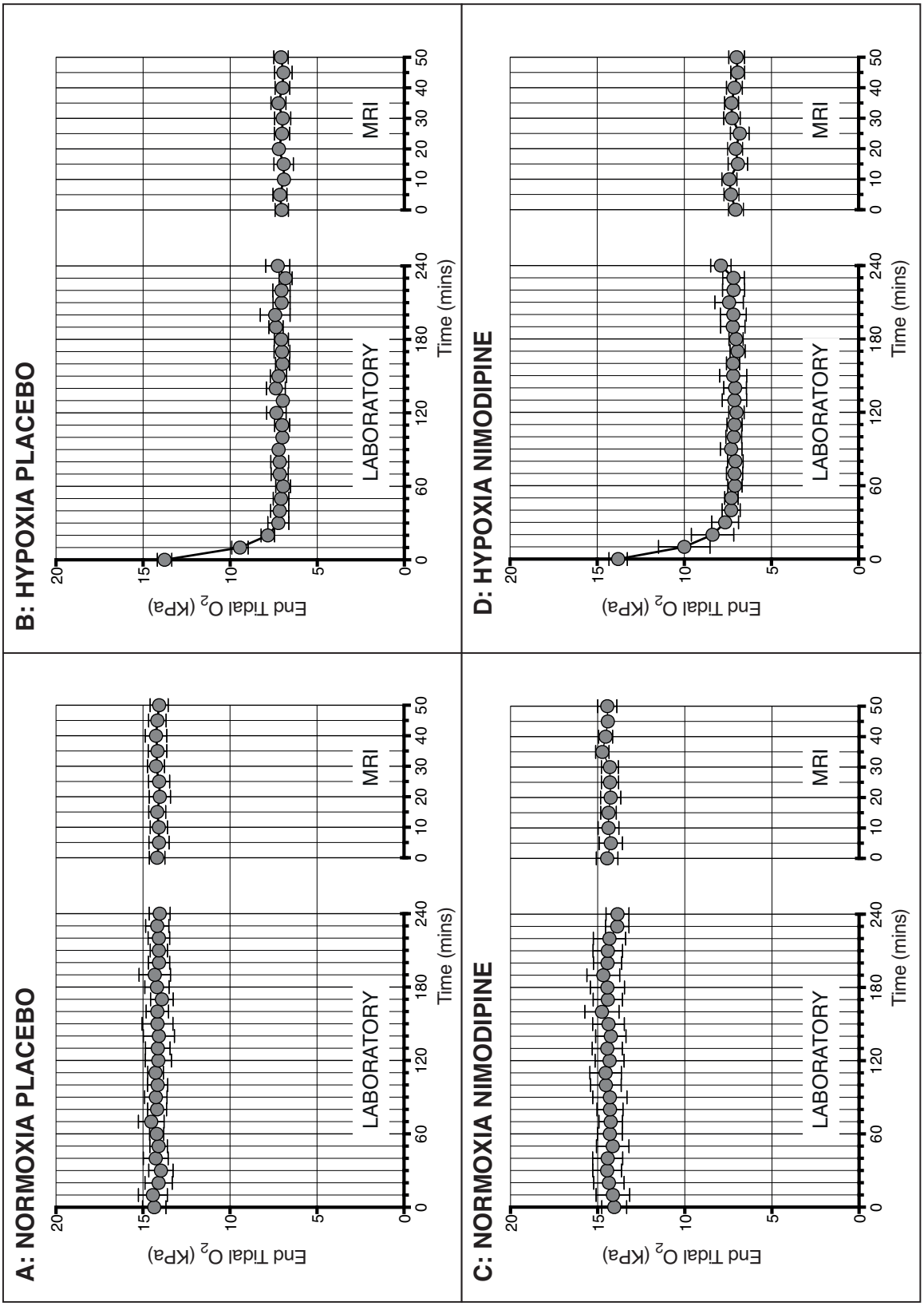


Fig. 7.2: ETO_2 values from the laboratory and MRI sessions

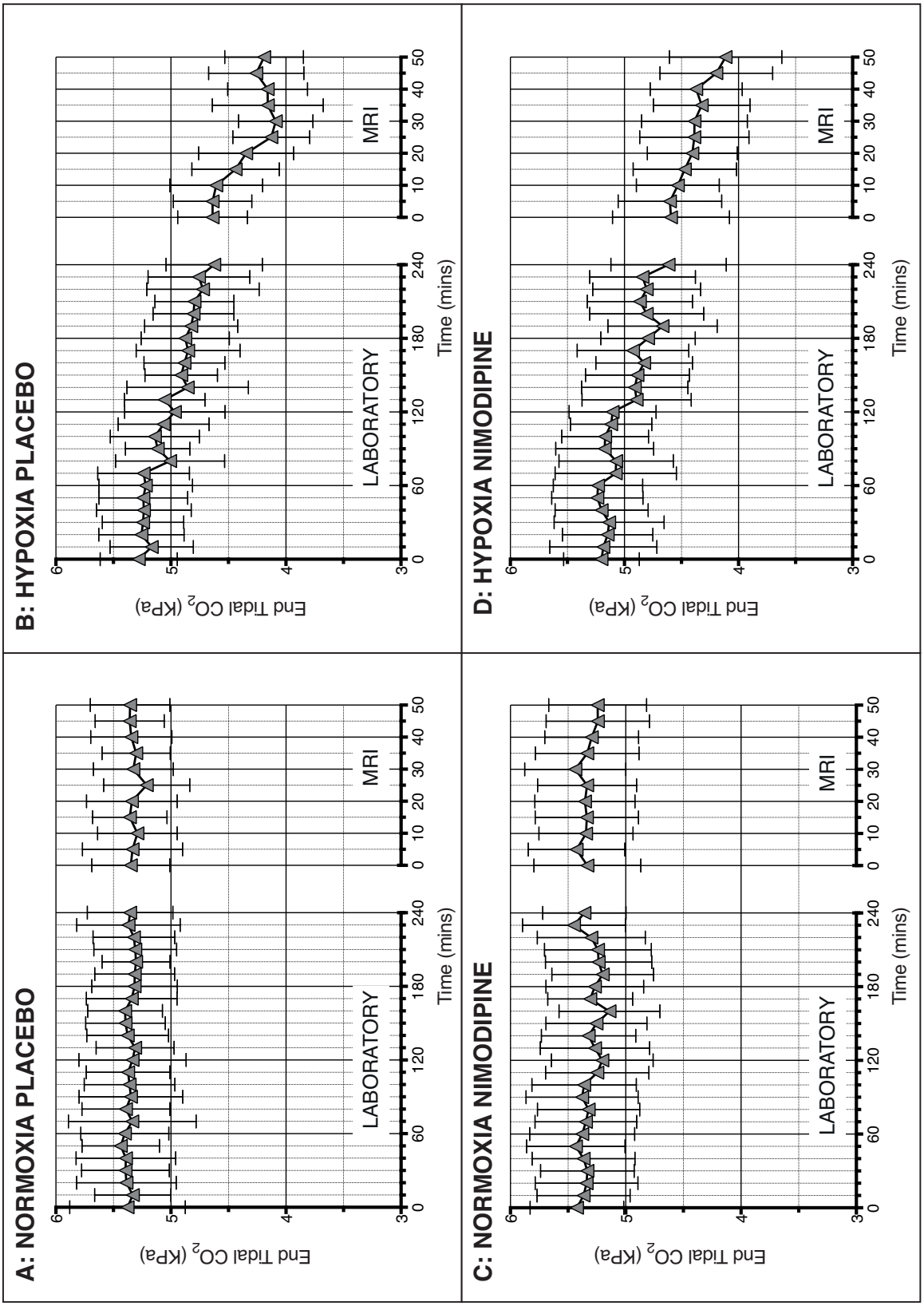


Fig. 7.3: $ETCO_2$ values from the laboratory and MRI sessions

Table 7.1: Physiological parameters for each experimental condition. Results are presented as mean ± standard deviation (SpO_2=oxygen saturations, HR=heart rate, SBP=systolic blood pressure, DBP=diastolic blood pressure, MAP=mean arterial pressure, ETO_2=end tidal oxygen, $ETCO_2$=end tidal carbon dioxide).

	Normoxia Placebo	**Normoxia Nimodipine**	**Hypoxia Placebo**	**Hypoxia Nimodipine**
SpO2 (%)	98 ± 1	98 ± 1	85 ± 6	84 ± 7
HR (bpm)	67 ± 2	68 ± 2	77 ± 3	79 ± 3
SBP (mmHg)	115 ± 15	114 ± 12	119 ± 12	116 ± 16
DBP (mmHg)	64 ± 6	62 ± 7	64 ± 6	64 ± 6
MAP (mmHg)	80 ± 7	79 ± 9	82 ± 9	82 ± 8
ETO_2 (KPa)	14.17 ± 0.12	14.36 ± 0.19	7.38 ± 1.18	7.48 ± 1.21
$ETCO_2$ (KPa)	5.35 ± 0.04	5.32 ± 0.08	4.80 ± 0.37	4.83 ± 0.29

The changes in $ETCO_2$, ETO_2, oxygen saturations, heart rate and non-invasive blood pressure during each condition are summarised in Table 7.1.

As expected, the hypoxia condition significantly reduced the ETO_2 in both the placebo (14.17 ± 0.12 v 7.38 ± 1.18 KPa, p=0.0001 RM ANOVA) and nimodipine (14.36 ± 0.19 v 7.48 ± 1.21 KPa, p=0.0001 RM ANOVA) conditions compared to normoxia. Likewise, there was a significant compensatory drop in $ETCO_2$ values for both the placebo (5.35 ± 0.04 v 4.80 ± 0.37 KPa) and nimodipine conditions (5.32 ± 0.08 v 4.83 ± 0.29 KPa) p=0.0001 RM ANOVA) as the laboratory and MRI sessions progressed. There were no significant differences in ETO_2 or $ETCO_2$ with nimodipine in either the normoxia or hypoxia conditions.

Hypoxia resulted in a significant drop in oxygen saturations in both placebo (98 ± 1 v 85 ± 6%, RM ANOVA p=0.0023) and nimodipine (98 ± 1 v 84 ± 7%, RM ANOVA, p=0.0013) conditions. There was no significant difference in mean arterial pressure between normoxia and hypoxia and with nimodipine. Finally, hypoxia resulted in a significant increase in heart rate in both placebo (67 ± 2 v 78 ± 3 bpm, p=<0.0001 RM ANOVA) and nimodipine (68 ± 2 v 79 ± 3 bpm, p=<0.0001 RM ANOVA).

7.3.2 Effect of acute poikilocapnic hypoxia

Diffusion-Weighted Imaging

Figure 7.4 shows the results from the DWI data.

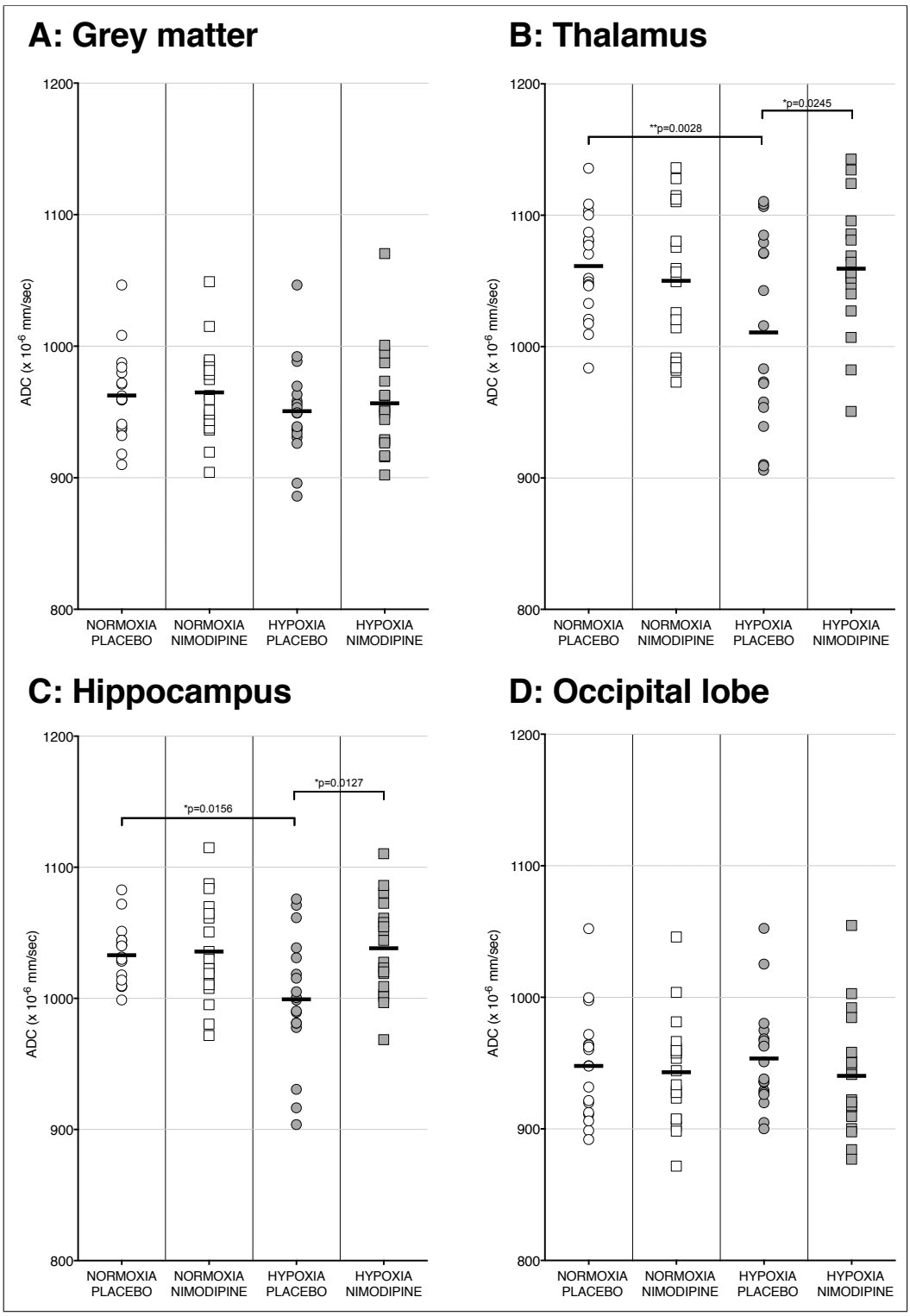


Fig. 7.4: Apparent diffusion coefficient (ADC) values for whole brain grey matter and thalamus, hippocampus and occipital lobe regions of interest for each of the four experimental conditions.

Looking at mean grey matter ADC values in both placebo studies, there was no significant change in the mean grey matter ADC values in the hypoxia condition compared to the normoxia condition (963 $\pm$ 33 v 951 $\pm$ 36 x 10^{-6}mm^2/s, p=0.157 RM ANOVA) for the placebo studies. There was however a significant decrease in ADC values in the thalamus ROI for the hypoxia condition compared to the normoxia condition (1061 $\pm$ 40 v 1011 $\pm$ 75 x 10^{-6}mm^2/s, p=0.0028 RM ANOVA - Figure 7.4-B). This was also the case for the hippocampus ROI (1033 $\pm$ 22 v 999 $\pm$ 49 x 10^{-6}mm^2/s, p=0.0156 RM ANOVA - Figure 7.4-C). However, when looking at the occipital lobe, there was no significant difference between the normoxia and hypoxia conditions (948 $\pm$ 41 v 954 $\pm$ 40 x 10^{-6}mm^2/s, p=0.5931 RM-ANOVA - Figure 7.4-D). Finally, whole brain grey matter voxelwise analysis confirmed this regional variation in grey matter ADC decreases with the hypoxia condition with especially noticeable decreases in the subcortical structures (thalamus, basal ganglia, hippocampus) as well as the cerebellum (Crus I and II regions) - Figure 7.5.

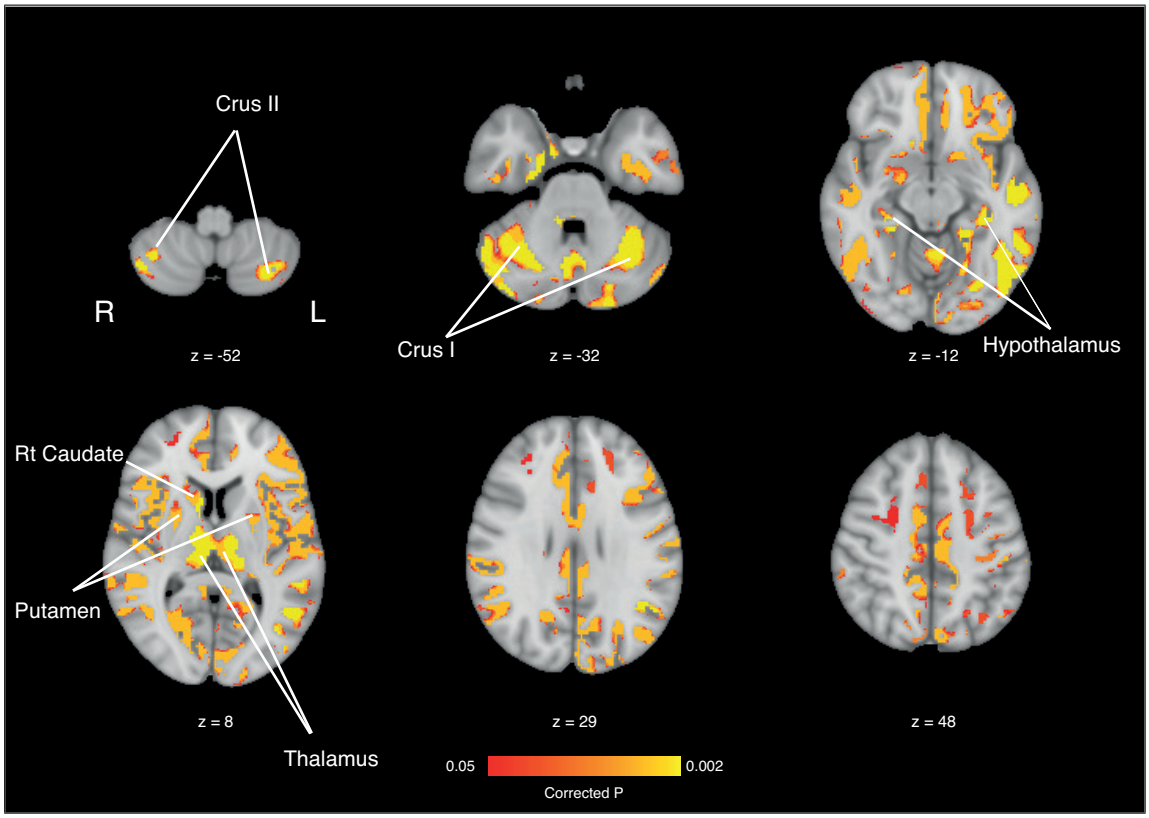


Fig. 7.5: Regional areas of decreased grey matter apparent diffusion coefficient (ADC) in the hypoxia/placebo condition compared to normoxia/placebo. (In yellow, p<0.002 FWE-corrected for multiple comparisons, overlaid onto an MNI152 standard template

Structural imaging

Figure 7.6 shows the results from the structural data analysis.

Looking at the VBM analysis, there was no significant difference in whole brain grey matter volume with hypoxia compared to normoxia (0.489 $\pm$ 0.018 v 0.490 $\pm$ 0.019, p=0.9050 RM ANOVA - Figure 7.6: A) and no significant difference at a voxelwise level. Again though, there were subtle but marked regional differences. Hypoxia resulted in a significant apparent increase in grey matter volume in the thalamus ROI when compared to normoxia (0.370 $\pm$ 0.037 v 0.3924 $\pm$ 0.028, p=0.0055 RM ANOVA - Figure 7.6: B) as well as in the hippocampus (0.667 $\pm$ 0.044 v 0.707 $\pm$ 0.085, p=0.0275 RM ANOVA - Figure 7.6: C). This was not accompanied by any significant change in grey matter volume in the occipital lobe (0.441 $\pm$ 0.027 v 0.4427 $\pm$ 0.030, p=0.9818 RM ANOVA - Figure 7.6: D).

Perfusion-weighted ASL imaging

Figure 7.7 shows the results from the ASL perfusion-weighted imaging data for each experimental condition.

There was no difference in mean grey matter CBF between the normoxia and hypoxia conditions (45.03 $\pm$ 10.58 v 42.18 , 9.70 ml/100g/min, p=0.8163 RM ANOVA). This was the same for the occipital lobe ROI (46.59 $\pm$ 11.31 v 43.26 $\pm$ 12.69 ml/100g/min, p=0.7906 RM ANOVA - Figure7.7-D). Although there was a small increase in CBF in the thalamus ROI for the hypoxia condition, this did not reach statistical significance (59.15 $\pm$ 10.00 v 50.34 v 6.68 ml/100g/min, p=0.0678 RM ANOVA - Figure 7.7-B). This was also the same for the hippocampus ROI (55.03 v 7.822 v 50.92 $\pm$ 5.419 ml/100g/min, p=0.0575 RM ANOVA - Figure 7.7-C).

Looking at the voxelwise analysis, there were no areas of significant change in grey matter CBF between normoxia and hypoxia when correcting for multiple comparisons. However, the uncorrected voxelwise statistics demonstrate significant regional increases in CBF bilaterally in the hippocampus and thalamus (Figure 7.8).

Table 7.2 shows the results for the phase contrast imaging for each experimental condition. Flow through both carotid arteries was significantly higher in the hypoxia condition when compared to normoxia. This was not the case for the vertebral arteries where there was no significant difference in flow.

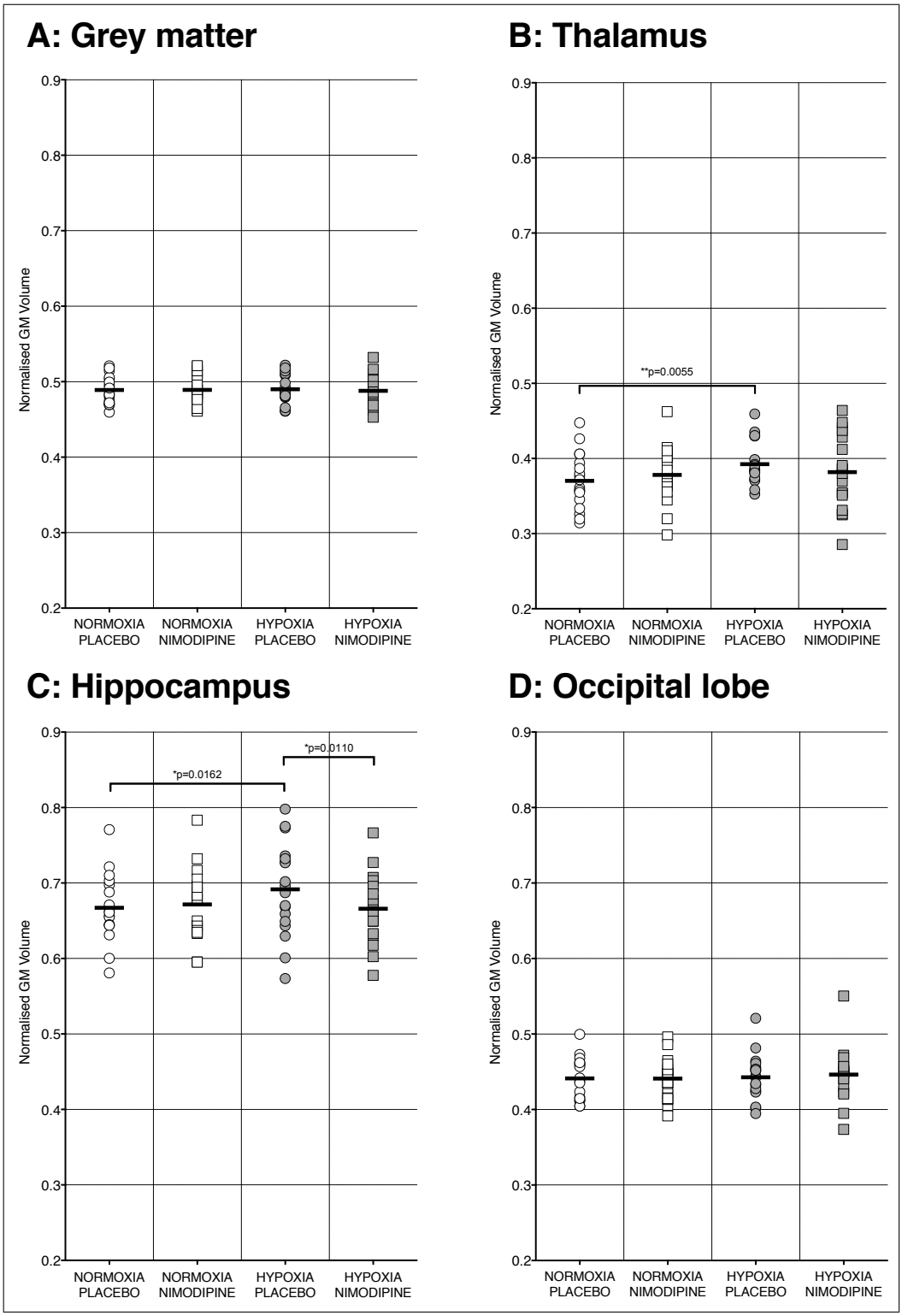


Fig. 7.6: Grey matter volume values for whole brain grey matter and thalamus, hippocampus and occipital lobe regions of interest for each of the four experimental conditions.

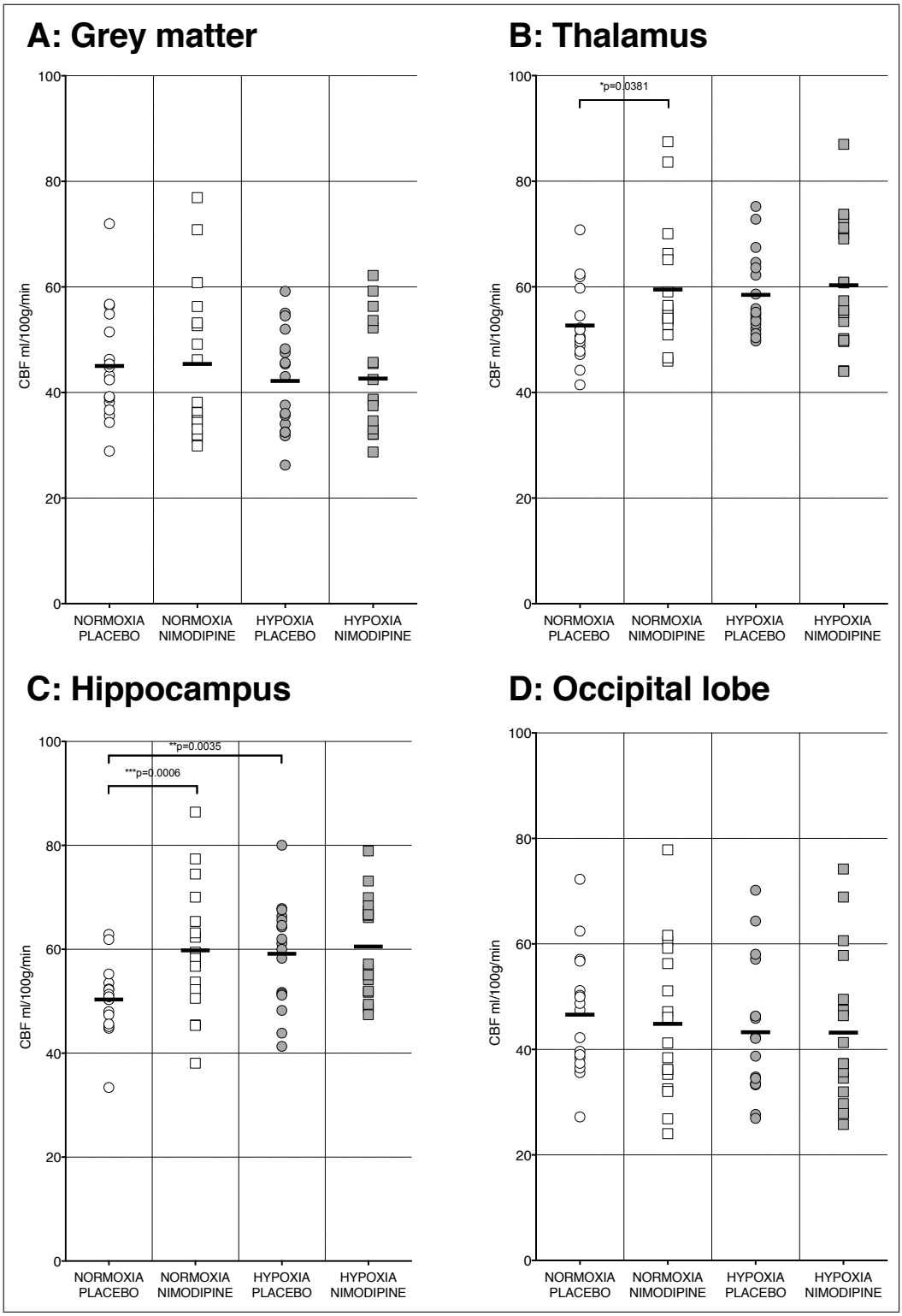


Fig. 7.7: Grey matter cerebral blood flow values for whole brain grey matter and thalamus, hippocampus and occipital lobe regions of interest for each of the four experimental conditions.

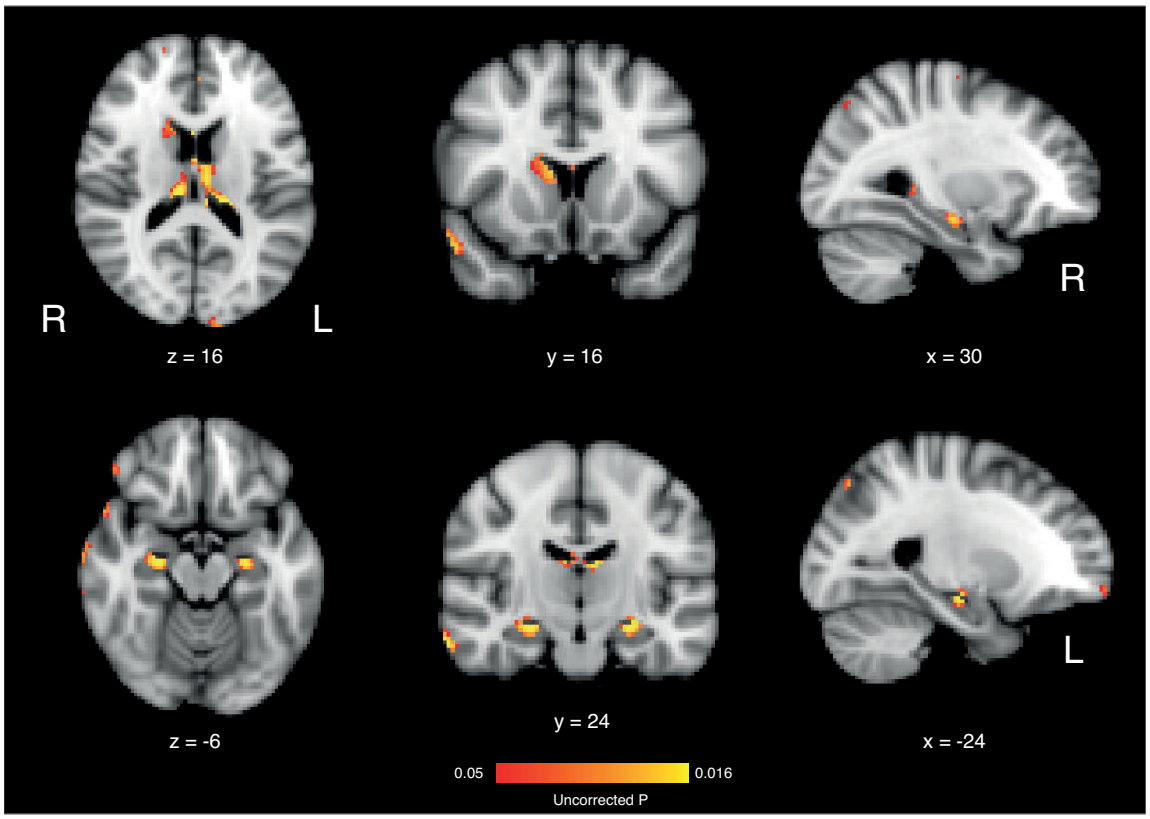


Fig. 7.8: Regional voxelwise increased cerebral blood flow (CBF) in the hypoxia/placebo condition compared to normoxia/placebo. (In red/yellow, p<0.0126 uncorrected, overlaid onto an MNI152 standard template).

Table 7.2: Phase contrast flow values for each carotid and vertebral artery. Results are presented as mean ± standard deviation. (**p=0.00183, *p=0.0328 Friedman test)

	Normoxia Placebo	Normoxia Nimodipine	Hypoxia Placebo	Hypoxia Nimodipine
Left carotid (ml/min)	**30.93**** ± **5.32**	28.66 ± 5.92	**28.37**** ± **4.97**	27.07 ± 4.46
Right carotid (ml/min)	**31.22*** ± **4.19**	31.05 ± 5.67	**30.38*** ± **5.21**	28.24 ± 5.03
Left vertebral(ml/min)	14.50 ± 3.55	14.28 ± 2.39	13.87 ± 3.43	13.22 ± 3.10
Right vertebral (ml/min)	11.95 ± 3.59	11.92 ± 4.43	11.96 ± 4.75	11.51 ± 2.99

Amplitude of low frequency fluctuations

Figure 7.9 shows the results from the ALFF data analysis.

There was a large decrease in normalised ALFF over the whole brain grey matter with hypoxia compared to normoxia (39.69 $\pm$ 2.28 v 64.37 $\pm$ 2.92, p =<0.0001, RM ANOVA – Figure 7.9-A). This was also the case for the thalamus (35.24 $\pm$ 2.43 v 41.20$\pm$ 1.85, p=<0.0001 RM ANOVA), hippocampus (42.66 $\pm$ 2.31 v 43.85 $\pm$ 1.96, p=<0.0001 RM ANOVA) and occipital lobe (39.36 $\pm$ 3.11 v 41.27 $\pm$ 2.33, p=0.0253 RM ANOVA).

Figure 7.10 shows spectrograms for all four experimental conditions over whole brain grey matter. Looking at whole brain grey matter, hypoxia is associated with a decrease in spectral power over the total frequency spectrum when compared to normoxia. Figure 7.11 shows this difference is the same in the thalamus ROI.

7.3.3 Effect of nimodipine under conditions of normoxia

Diffusion-Weighted Imaging

Nimodipine had no significant effect on whole brain grey matter ADC values in both normoxia conditions compared to placebo (963 $\pm$ 33 v 965 $\pm$ 35 x 10^{-6}mm^2/s, p=0.9042 RM ANOVA - Figure 7.4-A). There was also no significant difference compared to placebo in the thalamus (1061 $\pm$ 40 v 1050 $\pm$ 55 x 10^{-6}mm^2/s, p=0.4365 RM ANOVA - Figure 7.4-B), hippocampus (1033 $\pm$ 22 v 1036 $\pm$ 39 x 10^{-6}mm^2/s, p=0.9721 RM ANOVA - Figure 7.4-C) or occipital lobe (948 $\pm$ 41 v 943 $\pm$ 42 x 10^{-6}mm^2/s, p=0.8858 RM ANOVA - Figure 7.4-D) regions of interest.

Structural imaging

Compared to placebo, there was no significant difference in mean grey matter volume in the nimodipine condition for whole brain grey matter (0.489 $\pm$ 0.018 v 0.489 $\pm$ 0.019, p=0.9996 RM ANOVA), thalamus (0.370 $\pm$ 0.037 v 0.3781 $\pm$ 0.035, p=0.2567 RM ANOVA), hippocampus (0.667 $\pm$ 0.044 v 0.672 $\pm$ 0.048, p=0.5544 RM ANOVA) or occipital lobe (0.441 $\pm$ 0.028 v 0.441 $\pm$ 0.027, p=>0.999 RM ANOVA).

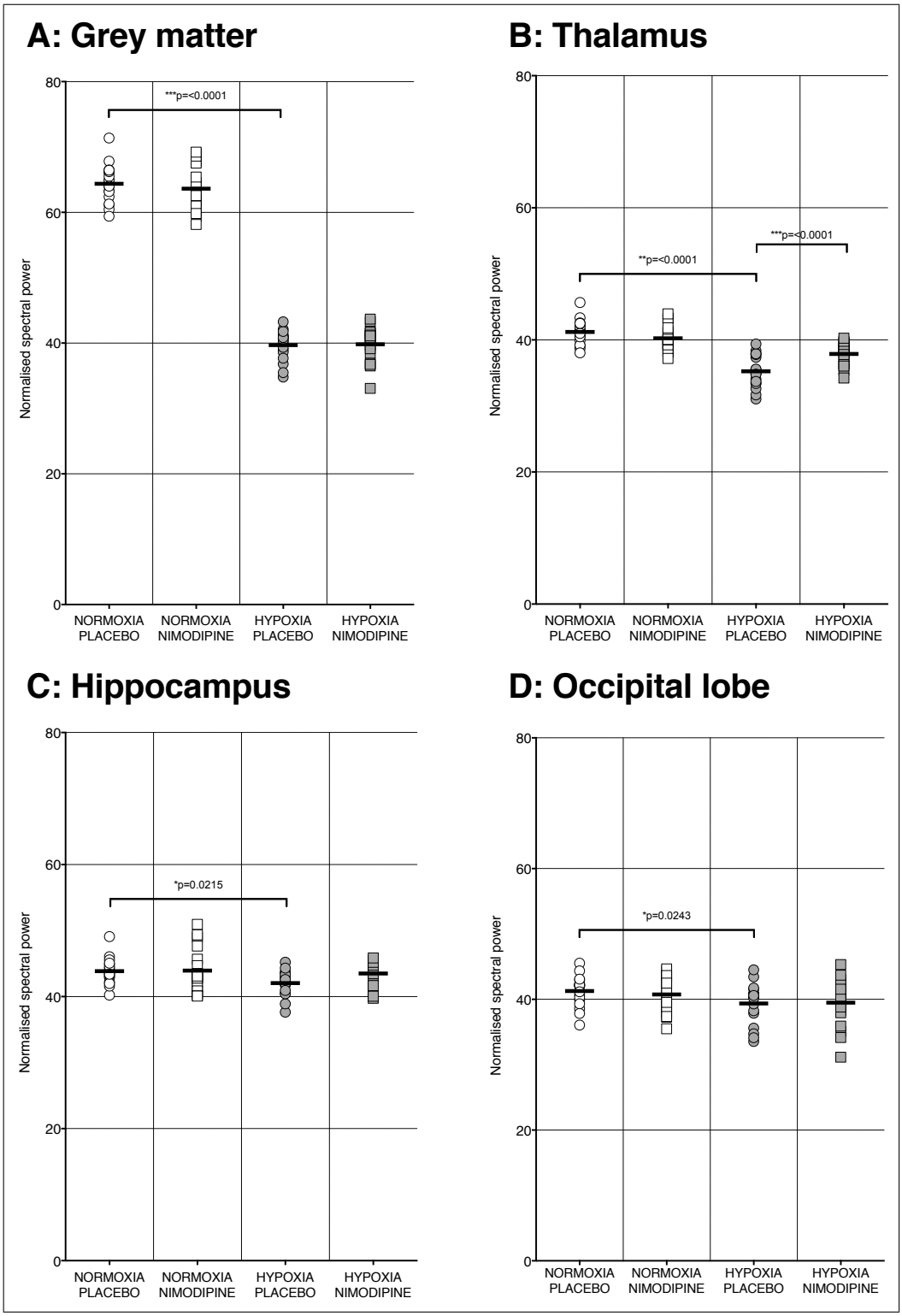


Fig. 7.9: Spectral power values for whole brain grey matter and thalamus, hippocampus and occipital lobe regions of interest for each of the four experimental conditions.

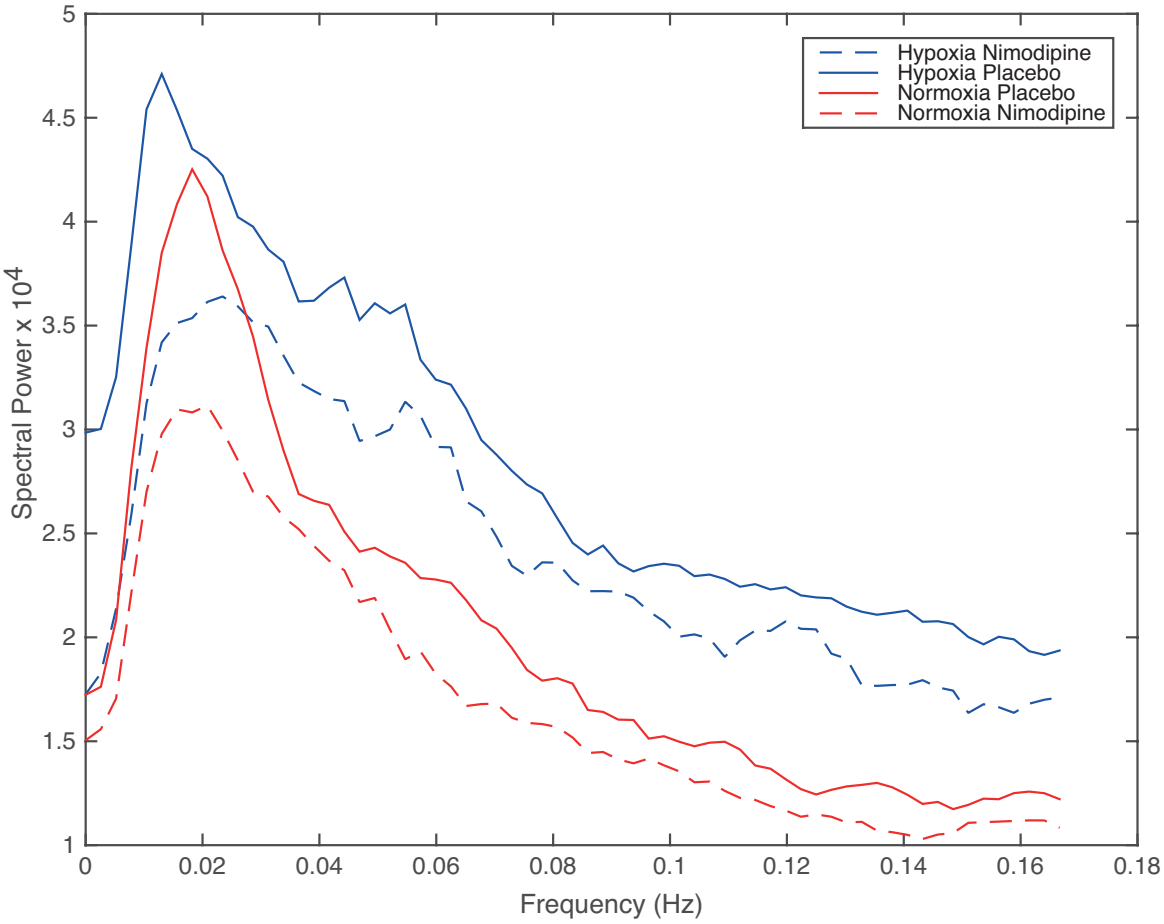


Fig. 7.10: Whole brain grey matter normalised frequency spectrograms for each of the experimental conditions

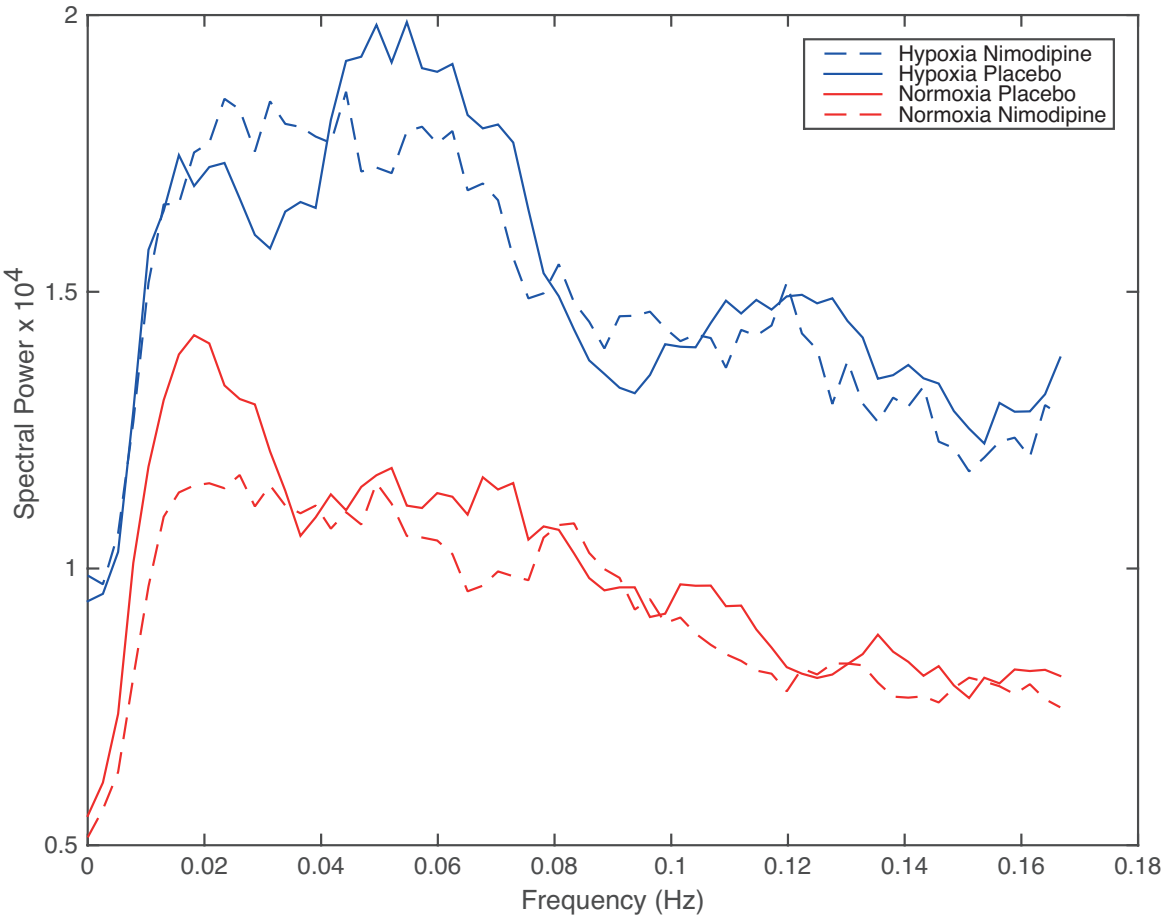


Fig. 7.11: Thalamus ROI normalised frequency spectrograms for each of the experimental conditions

Perfusion-weighed ASL imaging

There was no overall change in whole brain mean grey matter cerebral blood flow in the nimodipine condition compared to placebo (45.03 $\pm$ 10.58 v 45.42 $\pm$ 14.47, p=0.9995 RM ANOVA). There was also no difference for the hippocampus (50.34 $\pm$ 6.68 v 59.79 $\pm$ 8.43 ml/100g/min, p=0.0006 RM ANOVA) or occipital lobe (44.85 $\pm$ 14.51 v 46.59 $\pm$ 11.31 ml/100g/min, p=0.9674 RM ANOVA) ROIs. There was however a significant increase in CBF in the thalamus ROI (59.49 $\pm$ 2.84 v 52.69 $\pm$ 1.77 ml/100g/min, p=0.0381 RM ANOVA),

Looking at the phase contrast results, velocities through carotid and vertebral arteries were not significantly different between the nimodipine and placebo conditions (Table 7.2.

Amplitude of low frequency fluctuations

There was no significant difference in normalised ALFF over whole brain grey matter in the nimodipine condition compared to placebo (63.63 $\pm$ 3.55 v 64.37 $\pm$ 2.92, p=0.6672 RM ANOVA).

There was a non-significant decrease in normalised ALFF in the thalamus with nimodipine compared to placebo in the normoxia condition (41.20 $\pm$ 1.85 v 40.24 ± 1.88, p=0.6733, RM ANOVA, Figure 5D). However, this change was reversed in the hypoxia condition with a significant increase in thalamic ALFF with nimodipine versus placebo back towards baseline levels (37.87 $\pm$ 1.66 v 35.24 $\pm$ 2.43, p = 0.001, RM ANOVA).

Figure 7.10 shows the spectrograms for whole brain grey matter in the nimodipine and placebo normoxia conditions. Calcium channel blockade with nimodipine results in a lower spectral power over the whole frequency spectrum when compared to placebo.

7.3.4 Effect of nimodipine under conditions of hypoxia

Diffusion-Weighted Imaging

There was no significant difference in ADC values with nimodipine compared to placebo in hypoxia over the whole brain grey matter (957 $\pm$ 40 v 951 $\pm$ 36 x 10^{-6}mm^2/s, p=0.5936 RM ANOVA) nor regionally in the occipital lobe (940 $\pm$ 46 v 954 $\pm$ 40 x 10^{-6}mm^2/s, p=0.9777 RM ANOVA). However, there was a significant increase in ADC values back to baseline in

both the thalamus (1059 ± 49 v 1011 ± 34, p=0.0245 RM ANOVA) and hippocampus (1038 ± 37 v 999 ± 49, p=0.0127 RM ANOVA).

Figure 7.12 on 177 shows the voxelwise changes between the hypoxia placebo and hypoxia nimodipine conditions. There was a significant increase in ADC across multiple regions including the thalamus, basal ganglia (putamen and caudate), hippocampus and cerebellum with nimodipine when compared to placebo.

Structural imaging

Nimodipine had no significant effect on whole brain grey matter volume (0.488 ± 0.021 v 0.490 ± 0.019, p=0.7588 RM ANOVA). This was the same for the occipital lobe (0.4463 ± 0.036 v 0.4427 ± 0.030, p=0.7993) and the thalamus (0.382 ± 0.050 v 0.392 $/pm$ 0.028, p=0.5619 RM ANOVA). However, there was a significant reduction in grey matter volume in the hippocampus with nimodipine (0.666 ± 0.046 v 0.6916 ± 0.061, p=0.0110 RM ANOVA).

Perfusion-weighted ASL imaging

Again, there was no significant difference in whole brain mean grey matter CBF with nimodipine compared to placebo (42.65± 10.64 v 42.18 ± 9.71 ml/100g/min, p = 0.9977 RM ANOVA). There was also no change in the thalamus ROI (60.29 ± 12.00 v 58.48 ± 7.86 ml/100g/min, p=0.8575 RM ANOVA) nor the hippocampus and occipital lobe.

Under conditions of hypoxia, although mean grey matter CBF in the thalamus was higher for the nimodipine group, this difference was non-significant (53.46 ± 8.66 ml/100g/min v 59.49 ± 11.70 ml/100g/min). The same was the case for the hypoxia condition. Looking at the phase contrast results, velocities through both carotid and vertebral arteries were not significantly different between the nimodipine and placebo conditions (Table 7.2).

Amplitude of low frequency fluctuations

Under conditions of hypoxia, there was no significant change in normalised ALFF over whole brain grey matter with nimodipine compared to placebo (39.81 ± 2.66 v 39.69 ± 2.78, p=0.9970 RM ANOVA). However, in the thalamus ROI, there was a highly significant increase in ALFF with nimodipine back towards baseline (37.87 ± 1.66 v 35.24 ± 2.43, p=0.0001 RM ANOVA). Although there was also an increase with nimodipine in the hippocampus ROI, this was sub-statistical threshold (43.51 ± 2.00 v 42.04 ± 1.87, p=0.0621

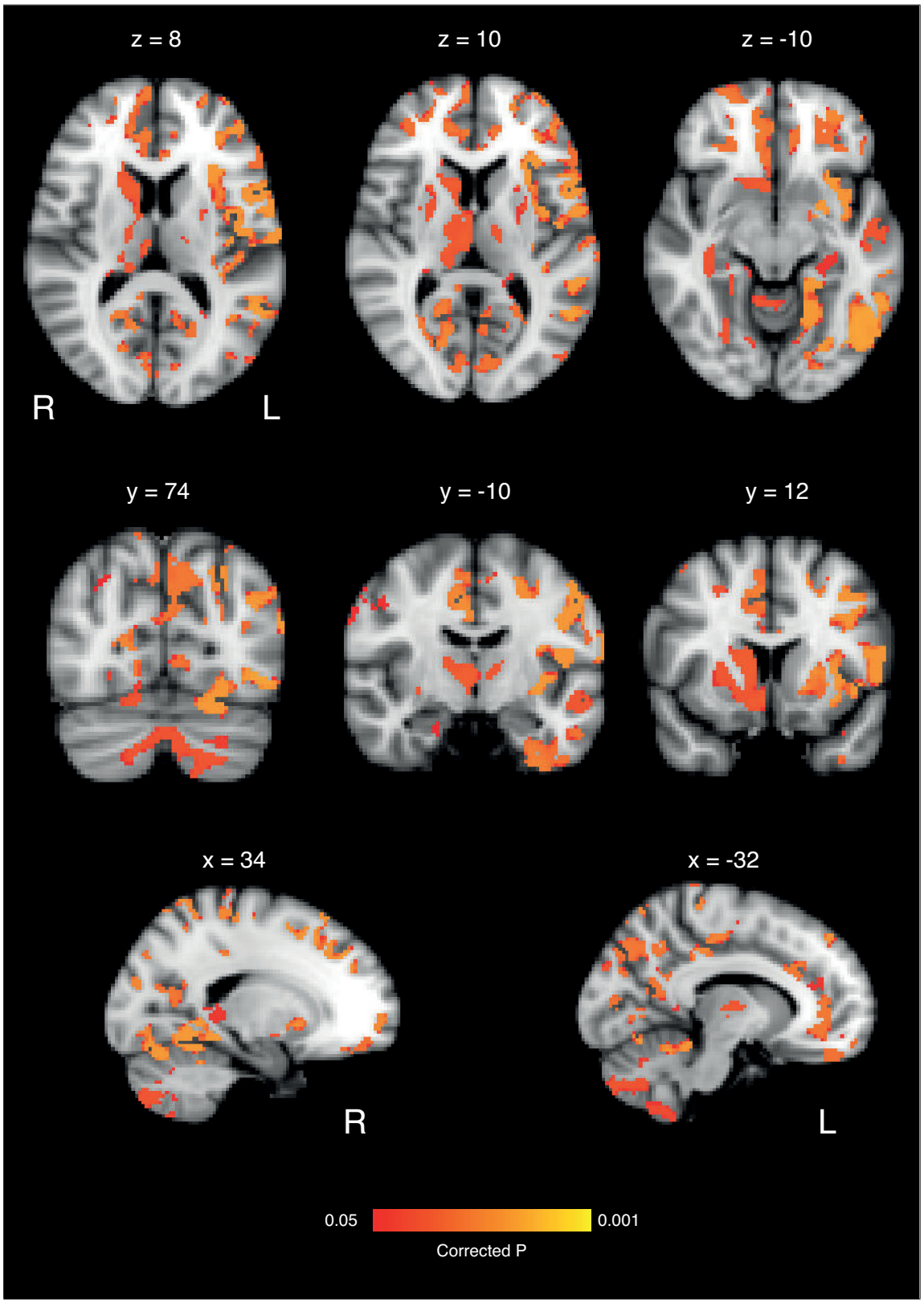


Fig. 7.12: Regional voxelwise areas of increased apparent diffusion coefficient (ADC) in the hypoxia/nimodipine condition compared to hypoxia/placebo. (In red/yellow, p<0.001 FWE-corrected, overlaid onto an MNI152 standard template

RM ANOVA). There was no difference with nimodipine in the occipital lobe compared to placebo (39.49 $\pm$ 3.61 v 39.36 $\pm$ 3.11, p=0.9979 RM ANOVA).

7.4 Discussion

Several notable findings have arisen from this study. Firstly, in healthy volunteers, acute normobaric poikilocapnic hypoxia causes a significant reduction in ADC values differentially throughout the brain - with the most significant effects in subcortical structures such as the thalamus and hippocampus as opposed to cortical areas such as the occipital lobe. These changes in ADC in subcortical regions are accompanied by a selective apparent increase in grey matter volume that seems independent of any significant change in regional cerebral blood flow. Finally, these regional changes in ADC and ALFF seen in the subcortical structures under conditions of hypoxia appear to be reversed with selective calcium channel blockade using the drug nimodipine.

7.4.1 Cerebral effects of acute hypoxia

Previous studies using DWI to investigate the effect of acute hypoxia have reported contradictory results of either increased [150, 274] or reduced [258, 262, 178] ADC values. We have shown decreased ADC values differentially throughout the brain to acute hypoxia using both a whole brain and ROI approach. Of most interest is the selectively decreased ADC in subcortical structures such as the thalamus, basal ganglia, hippocampus as well as the cerebellum. Reduced ADC values are generally interpreted as a consequence of cytotoxic oedema associated with intracellular swelling, and may be associated with changes in cellular energy status responsible for reduced Na^+/K^+ ATPase pump and altered ionic homeostasis. Studies investigating acute mountain sickness have also reported reductions in ADC in subjects with the highest symptom scores [150, 274] supporting the theory that cytotoxic cerebral oedema and intracellular swelling may be major pathophysiological factors contributing to altitude sickness.

Further data to support this theory is seen in the VBM analysis. Although there was no overall change in GM volume, selective increases in volume were seen in both thalamic and hippocampal grey matter ROIs. Other studies have reported similar changes following hypoxic exposure with reduced whole brain ADC and increased total brain and grey matter volumes [262, 259]. MRI evidence of cerebral oedema has also been noted as early as the

first hour of hypoxic exposure, associated with significant shifts in intracranial CSF volumes [88].

There was no significant effect of acute hypoxia on CBF - both over the whole brain grey matter and at each ROI. This is not however unsurprising given that we did not control for the effect of hypoxia on ventilatory rate and $ETCO_2$ and is in concordance with other studies which have reported no difference in grey matter CBF in acute poikilopcapnic hypoxia [262]. The unchanged CBF values suggest that cerebral blood volume (CBV) has not changed and lends further substance to the changes in ADC and volume relating to cerebral oedema rather than altered blood flow. Although caution needs to be exercised as the relationship between CBF and CBV is not straightforward and may be influenced by changes in venous volumes.

7.4.2 Effects of nimodipine on normal cerebral physiology

In normoxia, there was no significant effect of nimodipine on ADC or grey matter volume. Furthermore, nimodipine had no significant effect on grey matter cerebral blood flow when compared to placebo and there were no significant differences in CBF in either the hippocampus or occipital ROIs. However, there was a significant increase in grey matter CBF in the thalamus. As described in Chapter 2, nimodipine is characterised by a highly selective action on cerebral blood vessels and a high affinity to receptors in the cerebral cortex - hence the interest in its use in acute brain injury. However, the effect of nimodipine on cerebral blood flow, both in animal models, healthy volunteers and in patients is far from clear. Early ischaemic studies in animals demonstrated no effect on cerebral metabolism but increases in CBF due to a direct vasodilatory effect across all brain regions, particularly following disruption of the blood-brain barrier [125, 154, 126, 209]. However, nimodipine had no significant effect on normal CBF or metabolism in animals[101]. CBF measurements in both healthy volunteers and patients with ischaemic stroke have suggested a small overall increase in CBF after nimodipine treatment, with a redistribution of blood to hypoperfused regions in patients [272, 109]. However, subsequent studies have shown no effect of nimodipine in healthy volunteers in concordance with the results of our study [273]. This may be as a result of differences in drug dose and timing as well as CBF measurement techniques.

Although treatment with nimodipine is associated with increased mean CBF overall, there is also evidence from other studies that the flow enhancement is regionally heterogenous [288]. Our results are in agreement with this, showing significantly increased CBF in the thalamus

compared to other regions. The variation in the distribution of calcium channels in the brain may underlie this difference.

7.4.3 The effect of nimodipine under conditions of cerebral hypoxia

Results from this study suggest that calcium channel blockade with nimodipine reverses the regional and global decrease in ADC seen with cerebral hypoxia, returning values back towards the baseline seen in normoxia. There was also a significant decrease in hippocampal grey matter volume back to normoxic levels. There has been a great deal of interest in the potential therapeutic role of calcium channel blockade in patients. As described in Chapter 2, nimodipine has consistently been shown to reduce the incidence of delayed cerebral ischaemia (DCI) and improve clinical outcomes after aneurysmal subarachnoid haemorrhage. However, although the rationale for the use of nimodipine is sound, similar outcome benefits have not been seen in multiple large clinical studies of other conditions that cause acute neurological injury such as ischaemic stroke [135], cardiac arrest [252] and traumatic brain injury [173]. What is needed is a better understanding of the mechanisms behind this differential effect and the selectivity of outcome benefit in SAH.

There has been little investigation of the effect of nimodipine on cerebral oedema after acute brain injury. Damage to the brain in the first 72 hours following SAH caused by early brain injury is now being recognised as a key determinant of clinical outcomes. Global cerebral oedema is a well documented component of this injury and is an independent risk factor for mortality and cognitive dysfunction [57, 164]. Although there are similarities between early brain injury in SAH and other acute diseases such as TBI and cardiac arrest, the transient global ischaemia seen after SAH is pathophysiologically different. This is likely due to the association of SAH with more inflammation, oedema, oxidative stress and other inflammatory processes [193]. Animal models of SAH have suggested that nimodipine attenuates ischaemia-related cerebral oedema [123] and increases cerebral blood flow without affecting cerebral metabolism [125]. Other work has also suggested that nimodipine can alter cortical spreading ischaemia (a known component of early brain injury after SAH) back to a more physiological hyperaemic response [83]. Our study suggests that calcium channel blockade with nimodipine acts to reduce parenchymal swelling and cytotoxic cerebral oedema following acute cerebral hypoxia. This may help explain the beneficial effect exerted by nimodipine in SAH compared to other conditions such as TBI and cardiac arrest.

Finally, nimodipine does not seem to exert a significant impact on the effect of hyperventilation in reducing regional cerebral blood flow [349]. This may partially explain why there was no significant increase in CBF with nimodipine under conditions of hypoxia.

7.5 Effect of hypoxia and nimodipine on ALFF

Looking at the ALFF results, few studies have considered the exact role of the ALFF at rest and its implications in terms of cognitive dysfunction. ALFF in the frontal regions is increased in patients recovering from traumatic brain injury [228]. There is also evidence that low frequency oscillations (LFO) in calcium (marker of cellular oscillations) show frequencies similar to those of deoxyhemoglobin (the main contributor to the BOLD signal) and precede them by 5–6 seconds [87]. We have shown that there is no significant change in ALFF following calcium channel blockade with nimodipine in normoxia in either subcortical or cortical grey matter. Although there was a significant decrease in ALFF across all regions of interest in hypoxia compared to normoxia, this result remains difficult to interpret due to the likely effect of hypoxia on BOLD signal which has been shown to decrease by up to 50% [259]. However, in the presence of hypoxia, nimodipine appears to increase ALFF back towards baseline normoxic values. Previous research has demonstrated a differential effect of nimodipine on normal and hypoxic tissue [245]. Furthermore regional heterogeneity in the BOLD response to hypoxia has previously been reported in both animal studies [89, 148] and studies in humans [258]. The underlying mechanisms that could lead to differential sensitivity to BOLD and therefore ALFF are complex and include different changes in total deoxyhemoglobin for a fixed change in arterial oxygen saturation (due to different blood volumes and/or different oxygen extraction fractions) as well as flow-induced variation in saturation and signal intensity [89]. It may be that subcortical structures such as the thalamus and hippocampus have a different oxygen extraction fraction at rest than other areas of the brain and are therefore more sensitive to these changes in arterial oxygen content.

7.6 Methodological considerations

The study was designed to investigate the effects of nimodipine on the normal cerebral physiological response to acute normobaric hypoxia. We were therefore unable to disentangle the effects of calcium channel blockade on hypoxia and hypocapnia. We were also unable to distinguish between changes in ADC, ALFF and cerebral blood flow in white matter due to the low signal to noise of the DWI and VEPCASL sequences used. In addition,

hypoxia has been shown to have an effect on the BOLD response making interpretation of the reduced ALFF with hypoxia compared to placebo difficult. Furthermore, the actual frequency range for the BOLD signal (0.01 to 0.1Hz) may contain information from neural activity in multiple different ranges, and not confined to the frequency range we observed. Due to the sampling rate of 0.33Hz (TR 3 seconds), we were unable to identify cardiac and respiratory noise bands and future studies will address this by using multiband accelerated EPI sequences. A combined EEG-MRI study would also be required to investigate how neural signals from different frequency bands contributes to changes in ALFF associated with hypoxia and nimodipine. We were also unable to address the question of whether a different dose or dosing regime might have given us different results. We chose to give 30mg every 2 hours, starting after the onset of hypoxia to replicate clinical practice as accurately as possible. Due to differences in oral bioavailability, serum levels may have therefore differed between participants. We were unable to administer the nimodipine intravenously due to the requirement of a central venous catheter which would have been difficult ethically in healthy volunteers. Further investigation into the effect of route of administration (oral versus intravenous) and dose (standard versus modified release) on both bioavailability and hypoxic cerebral changes is required.

7.7 Conclusions

In summary, we have provided evidence for a preferential effect of calcium channel blockade with nimodipine under conditions of acute poikilocapnic normobaric hypoxia in reversing regional changes in ADC and ALFF. These changes to ADC and ALFF may underlie the benefit seen in aneurysmal subarachnoid haemorrhage in reducing the impact of global cytotoxic cerebral oedema seen with early brain injury. Further research is needed into the importance of changes in ALFF with hypoxia and whether this represents a biomarker of cerebral tissue hypoxia in acute neurological conditions such as SAH.

Chapter 8

Conclusions

Chapter Overview

The primary aim of this thesis was to use MRI to objectively quantify damage occuring due to early brain injury following SAH and to assess the impact of these changes on neurocognitive outcomes. In this Chapter, the main findings of the thesis are outlined and put into context with regards to future directions for research into SAH.

8.1 Main findings of the thesis

8.1.1 Structural and perfusion changes associated with early brain injury and neurocognitive outcomes after SAH

Early brain injury is now recognised as a significant pathological pathway after SAH that is likely to influence both short term outcomes from DCI as well as longer term neurocognitive impairment. In Chapter 4, we used structural and perfusion MRI sequences in a longitudinal fashion from the first 72 hours post-rupture to 3 months post-SAH, to quantify changes in cerebral physiology and correlate these with detailed neurocognitive outcomes. Despite being "good grade" SAH patients and when compared to healthy controls, there were significant global and regional increases in grey matter tissue volume in the first 72 hours post-SAH. These changes were associated with restricted diffusion, suggesting widespread cytotoxic cerebral oedema that remains undiagnosed using current diagnostic imaging. Furthermore, patients with DCI/DCI-related cerebral infarction had a significantly lower global grey matter CBF versus without in the first 72 hours but not between days 5-10 post-SAH - the peak incidence of DCI. Finally, based on the remaining structural VBM abnormalities seen at MRI scan 3 across all patients vs controls, in the first 72 hours post-rupture it is possible to predict with 84% accuracy and 86% specificity which patients will go on to develop poor neurocognitive outcomes from T1 structural images.

This study demonstrates the value of acute MRI scanning to objectively quantify early brain injury in the first 72 hours post-SAH. Scans were well tolerated by patients with no complications and results demonstrate the potential for objective and automated assessment of cerebral structure and perfusion to predict neurocognitive recovery from the start of the disease and risk stratify the need for critical care intervention.

8.1.2 Resting state functional connectivity after SAH

Following on from this, Chapter 5 investigated the impact of the structural and perfusion changes seen in the first 72 hours and longitudinally following SAH on functional connectivity. The study of brain activity and connectivity at rest provides a unique opportunity for the investigation of the brain substrates of neurocognitive impairment after SAH. This knowledge may contribute to improve clinical management during the acute phase post-rupture and help target novel therapeutic interventions to prevent loss of network integrity. There are

several notable findings from this chapter. At 3 months post-SAH, patients showed increased functional connectivity compared to healthy controls in a number of functional networks associated with complex cognitive or emotional functions including the DMN (medial and posterior divisions), cerebellum, basal ganglia/thalamus and executive function networks. These changes persisted despite correction for changes in grey matter density - important to note in the context of the widespread structural changes seen in Chapter 4. Secondly, these differences were already present in MRI scan 1 in a number of these networks, suggesting that the pathophysiological effects of early brain injury have a significant effect on functional connectivity from as early as the first 72 hours post-SAH. Finally, increased functional connectivity in the posterior default mode network at three months post-SAH correlates with neurocognitive outcomes with those patients with the highest functional connectivity having the least cognitive impairment. Patients without neurocognitive impairment also demonstrated higher functional connectivity in the first 72 hours - notably to the basal ganglia and cerebellum, suggesting that this increased connectivity may represent a compensatory or "adaptive" mechanism in response to structural disconnection due to early brain injury. Furthermore, the increased functional connectivity within the posterior default mode network is positively correlated with overall neurocognitive performance as measured using the ACE-R - a relationship observed across both patients and controls. These results suggest that dynamic changes in default mode network function may be made more efficient by greater functional connectivity at 'rest' [156], in which case an increase in default mode network functional connectivity could promote the appropriate and sustained deactivation necessary for focused goal-directed and cognitively demanding behaviour. Further work should employ diffusion tensor imaging to investigate the role played by white matter tract integrity in changes in functional connectivity.

8.1.3 The potential for the bedside clinical assessment of SAH patients using saccadometry

Chapter 6 investigated the efficacy of using a portable bedside saccadometer to measure eye movements and correlate these with MRI data on structural and perfusion changes following SAH. Improving the prediction of which patients are most at risk of developing significant neurocognitive impairment following SAH remains a key area for research focus. Whilst results in this thesis suggest there are many benefits to the routine MRI scanning of patients post-SAH, the practical difficulties and exclusion criteria mean this may not always be possible. Previous studies have shown that that measurements of saccadic latency can be

used reliably as an objective biomarker of neurocognitive function in chronic conditions such as Huntington's and Parkinson's diseases as well as in assessing recovery from acquired brain injury such as trauma. We hypothesised that saccadic latency would be increased acutely following aneurysm rupture and would correlate with the incidence of delayed cerebral ischaemia/cerebral infarction and neurocognitive impairment. Results from the study demonstrate that saccadic eye movement is adversely affected in patients in the first 72 hours post-rupture when compared to healthy control subjects with median saccadic latency significantly lower in patients. Furthermore, saccadic latency in the first 72 hours was negatively correlated with mean grey matter cerebral blood flow - the higher the CBF, the faster the saccadic latency. Those patients that progressed to developing DCI and/or DCI-related cerebral infarction had significantly slower saccades in the first 72 hours and between days 5-10 (the peak incidence for DCI) than those patients with no DCI/infarction. There was no significant difference in saccadic latency at either 72 hours or 3 months post-SAH between those patients diagnosed with neurocognitive impairment and those with no neurocognitive impairment. This emphasises the potential of incorporating objective measurements of saccadic latency into other potentially more subjective clinical assessments of neurological status after SAH. This might allow more rapid assessment of those patients most in need of neurocritical care intervention to mitigate worsening of early brain injury.

8.1.4 The role of calcium in early brain injury after SAH

Mortality due to subarachnoid hemorrhage has fallen consistently over the last 2 decades, due mainly to improved outcomes in cases surviving to reach hospital. However, despite huge improvement in the endovascular management of ruptured aneurysms, the calcium channel blocker nimodipine remains the only therapeutic intervention that has consistently been shown to improve outcomes in large randomised controlled trials. Nimodipine was originally trialled in SAH due to the cerebral vasodilation demonstrated in animal models. However, as described in Chapter 2, more recent research has demonstrated that nimodipine exerts it beneficial effects on outcomes without angiographic evidence of cerebral vasodilation [97, 237]. In Chapter 7, we investigated the effect of acute poikilopcapnic normobaric hypoxia on MRI biomarkers such as apparent diffusion coefficient (ADC), low frequency blood oxygen level dependent (BOLD) oscillations, cerebral blood flow and tissue volume in the thalamus and hippocampus compared to whole brain grey matter and the occipital lobe. Then we investigated the impact of nimodipine at standard clinical doses on any changes seen due to cerebral hypoxia. Several notable findings have arisen from this study. Firstly, in

healthy volunteers, acute normobaric hypoxia causes a significant reduction in ADC values differentially throughout the brain - with the most significant effects in subcortical structures such as the thalamus and hippocampus as opposed to cortical areas such as the occipital lobe. These changes in ADC in subcortical regions are accompanied by a selective increase in normalised grey matter volume and decrease in normalised ALFF that seems independent of any significant change in regional cerebral blood flow. Finally, these regional changes in ADC and ALFF seen in the subcortical structures under conditions of hypoxia appear to be reversed with selective calcium channel blockade using the drug nimodipine. Given the limited effect of nimodipine on cerebral blood flow, this potentially represents one pathway by which nimodipine might exert outcome benefit clinically in patients with SAH.

8.2 Directions for future research

8.2.1 Imaging early brain injury after SAH

As described in Chapter 2, although outcomes from SAH have improved, there is still significant risk of neurocognitive impairment. Although often subtle, neurocognitive deficits can exerts a disproportionate impact on functional outcomes in survivors often of working age and with dependents. Traditionally, CT is preferred to MRI for diagnostic purposes in the acute phase post-SAH due to the relative speed and ease of image acquisition when compared to MRI. However, the results in this thesis demonstrate the potential utility of using MRI acutely post-SAH to identify biomarkers of early brain injury and how routine clinical scanning might help advance our understanding of the pathophysiology that underlies poor neurocognitive outcomes.

Aside from PET imaging, the development of clinical metabolic imaging markers in SAH has been limited when compared to the focus on methods to assess perfusion. This is despite evidence that patients with SAH show significant metabolic changes, even in the absence of impaired perfusion or infarction [328]. Amide proton transfer MRI is a chemical exchange saturation transfer (CEST) technique that been used to derive cerebral intracellular pH in preclinical stroke models and has been proposed as a potential metabolic marker of ischaemic penumbra or tissue "at risk". Cerebral intracellular pH is maintained until CBF drops to levels associated with irreversible infarction [136]. CEST imaging can be used to generate a pH-weighted imaging signal through the assessment of the base-catalyzed and therefore pH-dependent intracellular transfer of protons between amide groups and water [354]. It

has been proposed that pH-weighted imaging may improve the delineation of tissue at risk by separating benign oligaemia from an acidotic ischaemic penumbra [355]. A number of studies have demonstrated potential clinical use of pH-weighted MRI in acute ischaemic stroke and it would be of great interest to track longitudinal changes in tissue pH associated with early brain injury.

Finally, incorporating these novel MRI sequences into routine clinical practice along with machine learning algorithms and predictive modelling such as linear discriminant analysis (LDA) has the potential to offer reliable and objective prediction of which patients are most at risk of morbidity and mortality after SAH. This may have huge implications for the resource allocation of neurocritical care beds which remain constantly in short supply to those patients most in need.

8.2.2 Therapeutic interventions

The failure of novel pharmacological interventions such as clazosentan to demonstrate outcome benefit after SAH has been disappointing and may have significant effects on the enthusiasm of pharmaceutical companies to invest money in future drug development. This is also reflected throughout a great deal of research into other neurological diseases where the enthusiam for neuroprotectant drugs has been substantially decreased by recurrent failure to translate positive results in animal models into clinical outcome benefits.

With regards to SAH, as described in Chapter 2, this may partly be due to the difficulty in accurately recreating SAH and the associated inflammatory and immunological cascade that occurs following endothelial rupture experimentally in animal models. Interestingly though, of late, there has been little research interest in exploring why the calcium channel blockade with nimodipine remains the only therapeutic intervention to show consistent outcome benefit after SAH. The study in Chapter 7 explores some of the potential mechanism behind this using MRI and a healthy volunteer model of hypoxia. Further research is needed into the precise mechanism of action of nimodipine and potential novel formulations e.g. modified release (as per [131]) that could be used clinically and offset some of the side effects such as reduced sleep due to regular dosing during the night and, most importantly, the deleterious effect of hypotension on cerebral physiology.

Finally, as discussed in Chapter 2, the more severe SAH patients often require surgical, endovascular or neurocritical care interventions where significant quantities of anaesthetic sedative agents are required - either to facilitate mechanical ventilation or control ICP.

Although current evidence indicates that volatile agents, barbiturates and propofol may have some potential neuroprotective actions, the interaction between these sedative agents and DCI remains unclear. If CSD plays some role in the pathogenesis of early brain injury and DCI (as is likely), then choice of sedative agent may be important and future research using MRI might help disentangle the pathophysiological effects of aneurysm rupture from potential positive and negative effects of sedation.

References

[1] Al-Khindi, T., Macdonald, R. L., and Schweizer, T. A. (2010). Cognitive and functional outcome after aneurysmal subarachnoid hemorrhage. *Stroke*, 41(8):e519–e536.

[2] Alberts, M. J., Graffagnino, C., Khurana, V. G., Meissner, I., Meyer, F. B., Nicoll, J. A., and Pepe, M. G. (1995). ApoE genotype and survival from intracerebral haemorrhage. 346(8974):575.

[3] Alexander, M. P. and Freedman, M. (1984). Amnesia after anterior communicating artery aneurysm rupture. *Neurology*, 34(6):752–757.

[4] Amin-Hanjani, S., Ogilvy, C. S., and Barker II, F. G. (2004). Does Intracisternal Thrombolysis Prevent Vasospasm after Aneurysmal Subarachnoid Hemorrhage? A Meta-analysis. *Neurosurgery*, 54(2):326–335.

[5] Antoniades, C. A., Altham, P. M. E., Mason, S. L., Barker, R. A., and Carpenter, R. (2007). Saccadometry: a new tool for evaluating presymptomatic Huntington patients. *Neuroreport*, 18(11):1133–1136.

[6] Antoniades, C. A., Buttery, P., FitzGerald, J. J., Barker, R. A., Carpenter, R. H. S., and Watts, C. (2012a). Deep brain stimulation: eye movements reveal anomalous effects of electrode placement and stimulation. *PLoS ONE*, 7(3):e32830.

[7] Antoniades, C. A., Carpenter, R. H. S., and Temel, Y. (2012b). Deep brain stimulation of the subthalamic nucleus in Parkinson's disease: similar improvements in saccadic and manual responses. *Neuroreport*, 23(3):179–183.

[8] Antoniades, C. A. and Kennard, C. (2015). Ocular motor abnormalities in neurodegenerative disorders. *Eye (London, England)*, 29(2):200–207.

[9] Antoniades, C. A., Xu, Z., Carpenter, R. H. S., and Barker, R. A. (2013). The relationship between abnormalities of saccadic and manual response times in Parkinson's disease. *Journal of Parkinson's disease*, 3(4):557–563.

[10] Antoniades, C. A., Xu, Z., Mason, S. L., Carpenter, R. H. S., and Barker, R. A. (2010). Huntington's disease: changes in saccades and hand-tapping over 3 years. *Journal of Neurology*, 257(11):1890–1898.

[11] Aoki, T. and Nishimura, M. (2011). The development and the use of experimental animal models to study the underlying mechanisms of CA formation. *Journal of Biomedicine and Biotechnology*, 2011:1–10.

[12] Aoyama, K., Fushimi, Y., Okada, T., Miyasaki, A., Taki, H., Shibamoto, K., and Togashi, K. (2012). Detection of symptomatic vasospasm after subarachnoid haemorrhage: initial findings from single time-point and serial measurements with arterial spin labelling. *European radiology*, 22(11):2382–2391.

[13] Arenivas, A., Diaz-Arrastia, R., Spence, J., Cullum, C. M., Krishnan, K., Bosworth, C., Culver, C., Kennard, B., and Marquez de la Plata, C. (2014). Three approaches to investigating functional compromise to the default mode network after traumatic axonal injury. *Brain imaging and behavior*, 8(3):407–419.

[14] Aries, M. J. H., Elting, J. W., De Keyser, J., Kremer, B. P. H., and Vroomen, P. C. A. J. (2010). Cerebral autoregulation in stroke: a review of transcranial Doppler studies. *Stroke*, 41(11):2697–2704.

[15] Arthur Ecker and Paul A Riemenschneider (1951). Arteriographic Demonstration of Spasm of the Intracranial Arteries with Special Reference to Saccular Arterial Aneurisms*. *Journal of neurosurgery*, 8(6):660–667.

[16] Asano, T. and Sano, K. (1977). Pathogenetic role of no-reflow phenomenon in experimental subarachnoid hemorrhage in dogs. *Journal of neurosurgery*, 46(4):454–466.

[17] Ashburner, J. and Friston, K. J. (2000). Voxel-Based Morphometry—The Methods. *NeuroImage*, 11(6):805–821.

[18] Aslan, S., Xu, F., Wang, P. L., Uh, J., Yezhuvath, U. S., van Osch, M., and Lu, H. (2010). Estimation of labeling efficiency in pseudocontinuous arterial spin labeling. *Magnetic resonance in medicine : official journal of the Society of Magnetic Resonance in Medicine / Society of Magnetic Resonance in Medicine*, 63(3):765–771.

[19] Ayer, R. and Zhang, J. (2010). Connecting the early brain injury of aneurysmal subarachnoid hemorrhage to clinical practice. *Turkish neurosurgery*, 20(2):159–166.

[20] Bakker, C. J., Hoogeveen, R. M., and Viergever, M. A. (1999). Construction of a protocol for measuring blood flow by two-dimensional phase-contrast MRA. *Journal of magnetic resonance imaging : JMRI*, 9(1):119–127.

[21] Bang, O. Y., Saver, J. L., Alger, J. R., Starkman, S., Ovbiagele, B., Liebeskind, D. S., and Investigators, U. C. (2008). Determinants of the distribution and severity of hypoperfusion in patients with ischemic stroke. *Neurology*, 71(22):1804–1811.

[22] Bang, O. Y., Saver, J. L., Kim, S. J., Kim, G.-M., Chung, C.-S., Ovbiagele, B., Lee, K. H., and Liebeskind, D. S. (2011). Collateral flow predicts response to endovascular therapy for acute ischemic stroke. *Stroke*, 42(3):693–699.

[23] Bareyre, F., Wahl, F., McIntosh, T. K., and Stutzmann, J. M. (1997). Time course of cerebral edema after traumatic brain injury in rats: effects of riluzole and mannitol. *Journal of neurotrauma*, 14(11):839–849.

[24] Barth, M., Capelle, H.-H., Münch, E., Thomé, C., Fiedler, F., Schmiedek, P., and Vajkoczy, P. (2007). Effects of the selective endothelin A (ET(A)) receptor antagonist Clazosentan on cerebral perfusion and cerebral oxygenation following severe subarachnoid

hemorrhage - preliminary results from a randomized clinical series. *Acta Neurochirurgica*, 149(9):911–8; discussion 918.

[25] Beadles, C. (1907). Aneurisms of the larger cerebral arteries. *Brain : a journal of neurology*, 30:285–336.

[26] Beckmann, C. F., DeLuca, M., Devlin, J. T., and Smith, S. M. (2005). Investigations into resting-state connectivity using independent component analysis. *Philosophical Transactions of the Royal Society of London B: Biological Sciences*, 360(1457):1001–1013.

[27] Beckmann, C. F. and Smith, S. M. (2004). Probabilistic independent component analysis for functional magnetic resonance imaging. *IEEE transactions on medical imaging*, 23(2):137–152.

[28] Bederson, J. B., Germano, I. M., and Guarino, L. (1995). Cortical blood flow and cerebral perfusion pressure in a new noncraniotomy model of subarachnoid hemorrhage in the rat. *Stroke*, 26(6):1086–91; discussion 1091–2.

[29] Bederson, J. B., Levy, A. L., Ding, W. H., Kahn, R., DiPerna, C. A., Jenkins, A. L., and Vallabhajosyula, P. (1998). Acute vasoconstriction after subarachnoid hemorrhage. *Neurosurgery*, 42(2):352–60; discussion 360–2.

[30] Bendel, P., Koivisto, T., Hänninen, T., Kolehmainen, A., Könönen, M., Hurskainen, H., Pennanen, C., and Vanninen, R. (2006). Subarachnoid hemorrhage is followed by temporomesial volume loss: MRI volumetric study. *Neurology*, 67(4):575–582.

[31] Berridge, M. J., Bootman, M. D., and Roderick, H. L. (2003). Calcium: Calcium signalling: dynamics, homeostasis and remodelling. *Nature Reviews Molecular Cell Biology*, 4(7):517–529.

[32] Biswal, B. B. (2013). The influence of the amplitude of low-frequency fluctuations on resting-state functional connectivity. pages 1–11.

[33] Biswal, B. B., Kannurpatti, S. S., and Rypma, B. (2007). Hemodynamic scaling of fMRI-BOLD signal: validation of low-frequency spectral amplitude as a scalability factor. *Magnetic Resonance Imaging*, 25(10):1358–1369.

[34] Biswal, B. B., Van Kylen, J., and Hyde, J. S. (1997). Simultaneous assessment of flow and BOLD signals in resting-state functional connectivity maps. *NMR in biomedicine*, 10(4-5):165–170.

[35] Bokkers, R. P. H., van Laar, P. J., van de Ven, K. C. C., Kapelle, L. J., Klijn, C. J. M., and Hendrikse, J. (2008). Arterial spin-labeling MR imaging measurements of timing parameters in patients with a carotid artery occlusion. *AJNR American journal of neuroradiology*, 29(9):1698–1703.

[36] Bonnelle, V., Leech, R., Kinnunen, K. M., Ham, T. E., Beckmann, C. F., De Boissezon, X., Greenwood, R. J., and Sharp, D. J. (2011). Default mode network connectivity predicts sustained attention deficits after traumatic brain injury. *Journal of Neuroscience*, 31(38):13442–13451.

[37] Bosche, B., Graf, R., Ernestus, R.-I., Dohmen, C., Reithmeier, T., Brinker, G., Strong, A. J., Dreier, J. P., and Woitzik, J. (2010). Recurrent spreading depolarizations after subarachnoid hemorrhage decreases oxygen availability in human cerebral cortex. *Annals of Neurology*, 67(5):607–617.

[38] Böttger, S., Prosiegel, M., Steiger, H.-J., and Yassouridis, A. (1998). Neurobehavioural disturbances, rehabilitation outcome, and lesion site in patients after rupture and repair of anterior communicating artery aneurysm. *Journal of Neurology, Neurosurgery & Psychiatry*, 65(1):93–102.

[39] Böttiger, B. W., Schmitz, B., Wiessner, C., Vogel, P., and Hossmann, K. A. (1998). Neuronal stress response and neuronal cell damage after cardiocirculatory arrest in rats. *Journal of cerebral blood flow and metabolism : official journal of the International Society of Cerebral Blood Flow and Metabolism*, 18(10):1077–1087.

[40] Branston, N. M., Ladds, A., Symon, L., and Wang, A. D. (1984). Comparison of the effects of ischaemia on early components of the somatosensory evoked potential in brainstem, thalamus, and cerebral cortex. *Journal of cerebral blood flow and metabolism : official journal of the International Society of Cerebral Blood Flow and Metabolism*, 4(1):68–81.

[41] Broderick, J. P., Brott, T. G., Duldner, J. E., Tomsick, T., and Leach, A. (1994). Initial and recurrent bleeding are the major causes of death following subarachnoid hemorrhage. *Stroke*, 25(7):1342–1347.

[42] Brück, W. (1997). The role of macrophages in Wallerian degeneration. *Brain pathology (Zurich, Switzerland)*, 7(2):741–752.

[43] Buchanan, K. M., Elias, L. J., and Goplen, G. B. (2000). Differing perspectives on outcome after subarachnoid hemorrhage: the patient, the relative, the neurosurgeon. *Neurosurgery*, 46(4):831–8– discussion 838–40.

[44] Busch, E., Beaulieu, C., de Crespigny, A., and Moseley, M. E. (1998). Diffusion MR imaging during acute subarachnoid hemorrhage in rats. *Stroke*, 29(10):2155–2161.

[45] Buxton, R. B. and Frank, L. R. (1997). A model for the coupling between cerebral blood flow and oxygen metabolism during neural stimulation. *Journal of cerebral blood flow and metabolism : official journal of the International Society of Cerebral Blood Flow and Metabolism*, 17(1):64–72.

[46] Cahill, J., Cahill, W. J., Calvert, J. W., Calvert, J. H., and Zhang, J. H. (2006). Mechanisms of early brain injury after subarachnoid hemorrhage. *Journal of cerebral blood flow and metabolism : official journal of the International Society of Cerebral Blood Flow and Metabolism*, 26(11):1341–1353.

[47] Camargo, E. C. S., Furie, K. L., Singhal, A. B., Roccatagliata, L., Cunnane, M. E., Halpern, E. F., Harris, G. J., Smith, W. S., Gonzalez, R. G., Koroshetz, W. J., and Lev, M. H. (2007). Acute brain infarct: detection and delineation with CT angiographic source images versus nonenhanced CT scans. *Radiology*, 244(2):541–548.

[48] Canese, R., Podo, F., Fortuna, S., Lorenzini, P., and Michalek, H. (1997). Transient global brain ischemia in the rat: spatial distribution, extension, and evolution of lesions evaluated by magnetic resonance imaging. *Magma (New York, N.Y.)*, 5(2):139–149.

[49] Caspers, S. (2013). Adult age-dependent differences in resting-state connectivity within and between visual-attention and sensorimotor networks. pages 1–10.

[50] Chang, C.-Z., Wu, S.-C., Lin, C.-L., Hwang, S.-L., Howng, S.-L., and Kwan, A.-L. (2010). Atorvastatin preconditioning attenuates the production of endothelin-1 and prevents experimental vasospasm in rats. *Acta Neurochirurgica*, 152(8):1399–1406.

[51] Chappell, M. A., Groves, A. R., Whitcher, B., and Woolrich, M. W. (2009). Variational Bayesian Inference for a Nonlinear Forward Model. *Signal Processing, IEEE Transactions on*, 57(1):223–236.

[52] Chappell, M. A., Macintosh, B. J., Donahue, M. J., Günther, M., Jezzard, P., and Woolrich, M. W. (2010). Separation of macrovascular signal in multi-inversion time arterial spin labelling MRI. *Magnetic resonance in medicine : official journal of the Society of Magnetic Resonance in Medicine / Society of Magnetic Resonance in Medicine*, 63(5):1357–1365.

[53] Chen, G., Tariq, A., Ai, J., Sabri, M., Jeon, H.-J., Tang, E. J. Y., Lakovic, K., Wan, H., and Macdonald, R. L. (2011). Different effects of clazosentan on consequences of subarachnoid hemorrhage in rats. *Brain Research*, 1392:132–139.

[54] Cheng, G., Wei, L., Zhi-Dan, S., Shi-Guang, Z., and Xiang-Zhen, L. (2009). Atorvastatin ameliorates cerebral vasospasm and early brain injury after subarachnoid hemorrhage and inhibits caspase-dependent apoptosis pathway. *BMC neuroscience*, 10:7.

[55] Cheung, J. Y., Bonventre, J. V., Malis, C. D., and Leaf, A. (1986). Calcium and ischemic injury. *The New England journal of medicine*, 314(26):1670–1676.

[56] Chou, S. H.-Y., Smith, E. E., Badjatia, N., Nogueira, R. G., Sims, J. R., Ogilvy, C. S., Rordorf, G. A., and Ayata, C. (2008). A randomized, double-blind, placebo-controlled pilot study of simvastatin in aneurysmal subarachnoid hemorrhage. *Stroke*, 39(10):2891–2893.

[57] Claassen, J., Carhuapoma, J., Kreiter, K., Du, E., Connolly, E., and Mayer, S. (2002). Global cerebral edema after subarachnoid hemorrhage: frequency, predictors, and impact on outcome. *Stroke*, 33(5):1225.

[58] Cohen, J. (1988). *Statistical Power Analysis for the Behavioural Sciences*. 2nd edition.

[59] Collette, F., Van der Linden, M., Laureys, S., Arigoni, F., Delfiore, G., Degueldre, C., Luxen, A., and Salmon, E. (2007). Mapping the updating process: common and specific brain activations across different versions of the running span task. *Cortex*, 43(1):146–158.

[60] Condette-Auliac, S., Bracard, S., Anxionnat, R., Schmitt, E., Lacour, J. C., Braun, M., Meloneto, J., Cordebar, A., Yin, L., and Picard, L. (2001). Vasospasm after subarachnoid hemorrhage: interest in diffusion-weighted MR imaging. *Stroke*, 32(8):1818–1824.

[61] Corder, E. H., Nicoll, J. A., Murray, G., Fiddes, M., Miyata, M., Smith, J. D., Pepe, M. G., Curtiss, L. K., and Kim, G. H. (1993). Gene dose of apolipoprotein E type 4 allele and the risk of Alzheimer's disease in late onset families. *Science*, 261(5123):921–923.

[62] Cremers, C. H. P., van der Schaaf, I. C., Wensink, E., Greving, J. P., Rinkel, G. J. E., Velthuis, B. K., and Vergouwen, M. D. I. (2014). CT perfusion and delayed cerebral ischemia in aneurysmal subarachnoid hemorrhage: a systematic review and meta-analysis. *Journal of cerebral blood flow and metabolism : official journal of the International Society of Cerebral Blood Flow and Metabolism*, 34(2):200–207.

[63] Dai, W., Garcia, D., de Bazelaire, C., and Alsop, D. C. (2008). Continuous flow-driven inversion for arterial spin labeling using pulsed radio frequency and gradient fields. *Magnetic resonance in medicine : official journal of the Society of Magnetic Resonance in Medicine / Society of Magnetic Resonance in Medicine*, 60(6):1488–1497.

[64] Damasio, A. R., Graff-Radford, N. R., Eslinger, P. J., Damasio, H., and Kassell, N. (1985). Amnesia following basal forebrain lesions. *Archives of neurology*, 42(3):263–271.

[65] Damoiseaux, J. S., Beckmann, C. F., Arigita, E. J. S., Barkhof, F., Scheltens, P., Stam, C. J., Smith, S. M., and Rombouts, S. A. R. B. (2008). Reduced resting-state brain activity in the "default network" in normal aging. 18(8):1856–1864.

[66] Damoiseaux, J. S., Rombouts, S. A. R. B., Barkhof, F., Scheltens, P., Stam, C. J., Smith, S. M., and Beckmann, C. F. (2006). Consistent resting-state networks across healthy subjects. *Proceedings of the National Academy of Sciences of the United States of America*, 103(37):13848–13853.

[67] Dankbaar, J. W., Slooter, A. J., Rinkel, G. J., and Schaaf, I. C. v. d. (2010). Effect of different components of triple-H therapy on cerebral perfusion in patients with aneurysmal subarachnoid haemorrhage: a systematic review. *Critical care (London, England)*, 14(1):R23.

[68] de Bresser, J., Vincken, K. L., Kaspers, A. J., Rinkel, G. J. E., Viergever, M. A., and Biessels, G. J. (2012). Quantification of cerebral volumes on MRI 6 months after aneurysmal subarachnoid hemorrhage. *Stroke*, 43(10):2782–2784.

[69] De Stefano, N., Iannucci, G., Sormani, M. P., Guidi, L., Bartolozzi, M. L., Comi, G., Federico, A., and Filippi, M. (2002). MR correlates of cerebral atrophy in patients with multiple sclerosis. *Journal of Neurology*, 249(8):1072–1077.

[70] Denny-Brown, D. (1951). The treatment of recurrent cerebrovascular symptoms and the question of "vasospasm". *The Medical clinics of North America*, 35(5):1457–1474.

[71] Desmond, J. E., Chen, S. H. A., and Shieh, P. B. (2005). Cerebellar transcranial magnetic stimulation impairs verbal working memory. *Annals of Neurology*, 58(4):553–560.

[72] Desmond, J. E., Gabrieli, J. D., Wagner, A. D., Ginier, B. L., and Glover, G. H. (1997). Lobular patterns of cerebellar activation in verbal working-memory and finger-tapping tasks as revealed by functional MRI. *Journal of Neuroscience*, 17(24):9675–9685.

[73] Detre, J. A., Leigh, J. S., Williams, D. S., and Koretsky, A. P. (1992). Perfusion imaging. *Magnetic resonance in medicine : official journal of the Society of Magnetic Resonance in Medicine / Society of Magnetic Resonance in Medicine*, 23(1):37–45.

[74] Di, X., Kannurpatti, S. S., Rypma, B., and Biswal, B. B. (2013). Calibrating BOLD fMRI activations with neurovascular and anatomical constraints. *Cerebral Cortex*, 23(2):255–263.

[75] Diringer, M. N., Bleck, T. P., Claude Hemphill, J., Menon, D., Shutter, L., Vespa, P., Bruder, N., Connolly, E. S., Citerio, G., Gress, D., Hänggi, D., Hoh, B. L., Lanzino, G., Roux, P., Rabinstein, A., Schmutzhard, E., Stocchetti, N., Suarez, J. I., Treggiari, M., Tseng, M.-Y., Vergouwen, M. D. I., Wolf, S., and Zipfel, G. (2011). Critical Care Management of Patients Following Aneurysmal Subarachnoid Hemorrhage: Recommendations from the Neurocritical Care Society's Multidisciplinary Consensus Conference. *Neurocritical Care*, 15(2):211–240.

[76] Dóczi, T. (1985). The pathogenetic and prognostic significance of blood-brain barrier damage at the acute stage of aneurysmal subarachnoid haemorrhage. Clinical and experimental studies. *Acta Neurochirurgica*, 77(3-4):110–132.

[77] Dohmen, C., Sakowitz, O. W., Fabricius, M., Bosche, B., Reithmeier, T., Ernestus, R.-I., Brinker, G., Dreier, J. P., Woitzik, J., Strong, A. J., Graf, R., and of Brain Injury Depolarisations COSBID, C.-O. S. (2008). Spreading depolarizations occur in human ischemic stroke with high incidence. *Annals of Neurology*, 63(6):720–728.

[78] Dorhout Mees, S. M., Rinkel, G. J. E., Feigin, V. L., Algra, A., van den Bergh, W. M., Vermeulen, M., and van Gijn, J. (2007a). Calcium antagonists for aneurysmal subarachnoid haemorrhage. *Cochrane database of systematic reviews (Online)*, (3):CD000277.

[79] Dorhout Mees, S. M., van den Bergh, W. M., Algra, A., and Rinkel, G. J. E. (2007b). Antiplatelet therapy for aneurysmal subarachnoid haemorrhage. *Cochrane database of systematic reviews (Online)*, (4):CD006184.

[80] Dorsch, N. (2011). A clinical review of cerebral vasospasm and delayed ischaemia following aneurysm rupture. *Acta neurochirurgica. Supplement*, 110(Pt 1):5–6.

[81] Dorsch, N. W. and King, M. T. (1994). A review of cerebral vasospasm in aneurysmal subarachnoid haemorrhage Part I: Incidence and effects. *Journal of Clinical Neuroscience*, 1(1):19–26.

[82] Douaud, G., Smith, S., Jenkinson, M., Behrens, T., Johansen-Berg, H., Vickers, J., James, S., Voets, N., Watkins, K., Matthews, P. M., and James, A. (2007). Anatomically related grey and white matter abnormalities in adolescent-onset schizophrenia. *Brain : a journal of neurology*, 130(Pt 9):2375–2386.

[83] Dreier, J. P., Körner, K., Ebert, N., Görner, A., Rubin, I., Back, T., Lindauer, U., Wolf, T., Villringer, A., Einhäupl, K. M., Lauritzen, M., and Dirnagl, U. (1998). Nitric oxide scavenging by hemoglobin or nitric oxide synthase inhibition by N-nitro-L-arginine induces cortical spreading ischemia when K+ is increased in the subarachnoid space. *Journal of cerebral blood flow and metabolism : official journal of the International Society of Cerebral Blood Flow and Metabolism*, 18(9):978–990.

[84] Dreier, J. P., Major, S., Manning, A., Woitzik, J., Drenckhahn, C., Steinbrink, J., Tolias, C., Oliveira-Ferreira, A. I., Fabricius, M., Hartings, J. A., Vajkoczy, P., Lauritzen, M., Dirnagl, U., Bohner, G., Strong, A. J., and study group, C. (2009). Cortical spreading ischaemia is a novel process involved in ischaemic damage in patients with aneurysmal subarachnoid haemorrhage. *Brain : a journal of neurology*, 132(Pt 7):1866–1881.

[85] Dreier, J. P., Windmüller, O., Petzold, G., Lindauer, U., Einhäupl, K. M., and Dirnagl, U. (2002). Ischemia triggered by red blood cell products in the subarachnoid space is inhibited by nimodipine administration or moderate volume expansion/hemodilution in rats. *Neurosurgery*, 51(6):1457–65; discussion 1465–7.

[86] Dreier, J. P., Woitzik, J., Fabricius, M., Bhatia, R., Major, S., Drenckhahn, C., Lehmann, T.-N., Sarrafzadeh, A., Willumsen, L., Hartings, J. A., Sakowitz, O. W., Seemann, J. H., Thieme, A., Lauritzen, M., and Strong, A. J. (2006). Delayed ischaemic neurological deficits after subarachnoid haemorrhage are associated with clusters of spreading depolarizations. *Brain : a journal of neurology*, 129(Pt 12):3224–3237.

[87] Du, C., Volkow, N. D., Koretsky, A. P., and Pan, Y. (2014). Low-frequency calcium oscillations accompany deoxyhemoglobin oscillations in rat somatosensory cortex. *Proceedings of the National Academy of Sciences of the United States of America*, 111(43):E4677–E4686.

[88] Dubowitz, D. J., Dyer, E. A. W., Theilmann, R. J., Buxton, R. B., and Hopkins, S. R. (2009). Early brain swelling in acute hypoxia. *Journal of applied physiology (Bethesda, Md : 1985)*, 107(1):244–252.

[89] Dunn, J. F., Wadghiri, Y. Z., and Meyerand, M. E. (1999). Regional heterogeneity in the brain's response to hypoxia measured using BOLD MR imaging. *Magnetic resonance in medicine : official journal of the Society of Magnetic Resonance in Medicine / Society of Magnetic Resonance in Medicine*, 41(4):850–854.

[90] Edelman, R. R., Siewert, B., Darby, D. G., Thangaraj, V., Nobre, A. C., Mesulam, M. M., and Warach, S. (1994). Qualitative mapping of cerebral blood flow and functional localization with echo-planar MR imaging and signal targeting with alternating radio frequency. *Radiology*, 192(2):513–520.

[91] Eickhoff, S. B., Paus, T., Caspers, S., Grosbras, M.-H., Evans, A. C., Zilles, K., and Amunts, K. (2007). Assignment of functional activations to probabilistic cytoarchitectonic areas revisited. *NeuroImage*, 36(3):511–521.

[92] Elliott, E. M., Malouf, A. T., and Catterall, W. A. (1995). Role of calcium channel subtypes in calcium transients in hippocampal CA3 neurons. *Journal of Neuroscience*, 15(10):6433–6444.

[93] Ettinger, U., Kumari, V., Crawford, T. J., Davis, R. E., Sharma, T., and Corr, P. J. (2003). Reliability of smooth pursuit, fixation, and saccadic eye movements. *Psychophysiology*, 40(4):620–628.

[94] Evers, E. A. T., Klaassen, E. B., Rombouts, S. A., Backes, W. H., and Jolles, J. (2012). The Effects of Sustained Cognitive Task Performance on Subsequent Resting State Functional Connectivity in Healthy Young and Middle-Aged Male Schoolteachers. *Brain Connectivity*, 2(2):102–112.

[95] Fair, D. A., Nigg, J. T., Iyer, S., Bathula, D., Mills, K. L., Dosenbach, N. U. F., Schlaggar, B. L., Mennes, M., Gutman, D., Bangaru, S., Buitelaar, J. K., Dickstein, D. P., Di Martino, A., Kennedy, D. N., Kelly, C., Luna, B., Schweitzer, J. B., Velanova, K., Wang, Y.-F., Mostofsky, S., Castellanos, F. X., and Milham, M. P. (2012). Distinct neural signatures detected for ADHD subtypes after controlling for micro-movements in resting state functional connectivity MRI data. *Frontiers in systems neuroscience*, 6:80.

[96] Farrell, B., Godwin, J., Richards, S., and Warlow, C. (1991). The United Kingdom transient ischaemic attack (UK-TIA) aspirin trial: final results. *Journal of Neurology, Neurosurgery & Psychiatry*, 54(12):1044–1054.

[97] Feigin, V. L., Rinkel, G. J., Algra, A., Vermeulen, M., and van Gijn, J. (1998). Calcium antagonists in patients with aneurysmal subarachnoid hemorrhage: a systematic review. *Neurology*, 50(4):876–883.

[98] Fergusen, S. and Macdonald, R. L. (2007). Predictors of cerebral infarction in patients with aneurysmal subarachnoid hemorrhage. *Neurosurgery*, 60(4):658–67; discussion 667.

[99] Filippini, N., Macintosh, B. J., Hough, M. G., Goodwin, G. M., Frisoni, G. B., Smith, S. M., Matthews, P. M., Beckmann, C. F., and Mackay, C. E. (2009). Distinct patterns of brain activity in young carriers of the APOE-epsilon4 allele. *Proceedings of the National Academy of Sciences of the United States of America*, 106(17):7209–7214.

[100] Fisher, C. M., Kistler, J. P., and Davis, J. M. (1980). Relation of cerebral vasospasm to subarachnoid hemorrhage visualized by computerized tomographic scanning. *Neurosurgery*, 6(1):1–9.

[101] Forsman, M., Fleischer, J. E., Milde, J. H., Steen, P. A., and Michenfelder, J. D. (1986). The effects of nimodipine on cerebral blood flow and metabolism. *Journal of cerebral blood flow and metabolism : official journal of the International Society of Cerebral Blood Flow and Metabolism*, 6(6):763–767.

[102] Fountas, K. N., Tasiou, A., Kapsalaki, E. Z., Paterakis, K. N., Grigorian, A. A., Lee, G. P., and Robinson, J. S. (2009). Serum and cerebrospinal fluid C-reactive protein levels as predictors of vasospasm in aneurysmal subarachnoid hemorrhage. Clinical article. *Neurosurgical FOCUS*, 26(5):E22.

[103] Fox, M. D. and Greicius, M. (2010). Clinical applications of resting state functional connectivity. *Frontiers in systems neuroscience*, 4:19.

[104] Fox, M. D. and Raichle, M. E. (2007). Spontaneous fluctuations in brain activity observed with functional magnetic resonance imaging. *Nature reviews Neuroscience*, 8(9):700–711.

[105] Fox, N. C. and Schott, J. M. (2004). Imaging cerebral atrophy: normal ageing to Alzheimer's disease. *Lancet (London, England)*, 363(9406):392–394.

[106] Frijns, C. J. M., Fijnheer, R., Algra, A., van Mourik, J. A., van Gijn, J., and Rinkel, G. J. E. (2006). Early circulating levels of endothelial cell activation markers in aneurysmal subarachnoid haemorrhage: associations with cerebral ischaemic events and outcome. *Journal of Neurology, Neurosurgery & Psychiatry*, 77(1):77–83.

[107] Frontera, J. A., Ahmed, W., Zach, V., Jovine, M., Tanenbaum, L., Sehba, F., Patel, A., Bederson, J. B., and Gordon, E. (2014). Acute ischaemia after subarachnoid haemorrhage, relationship with early brain injury and impact on outcome: a prospective quantitative MRI study. *Journal of Neurology, Neurosurgery & Psychiatry*.

[108] Frontera, J. A., Fernandez, A., Schmidt, J. M., Claassen, J., Wartenberg, K. E., Badjatia, N., Connolly, E. S., and Mayer, S. A. (2009). Defining Vasospasm After Subarachnoid Hemorrhage What Is the Most Clinically Relevant Definition? *Stroke*, 40(6):1963–1968.

[109] Gaab, M. R., Haubitz, I., Brawanski, A., Korn, A., and Czech, T. (1985). Acute effects of nimodipine on the cerebral blood flow and intracranial pressure. *Neurochirurgia*, 28 Suppl 1:93–99.

[110] Gao, J., Wang, H., Sheng, H., Lynch, J. R., Warner, D. S., Durham, L., Vitek, M. P., and Laskowitz, D. T. (2006). A novel apoE-derived therapeutic reduces vasospasm and improves outcome in a murine model of subarachnoid hemorrhage. *Neurocritical Care*, 4(1):25–31.

[111] Germanò, A., d'Avella, D., Imperatore, C., Caruso, G., and Tomasello, F. (2000). Time-course of blood-brain barrier permeability changes after experimental subarachnoid haemorrhage. *Acta Neurochirurgica*, 142(5):575–80– discussion 580–1.

[112] Gikakis, N., Khan, M. M., Hiramatsu, Y., Gorman, J. H., Hack, C. E., Sun, L., Rao, A. K., Niewiarowski, S., Colman, R. W., and Edmunds, L. H. (1996). Effect of factor Xa inhibitors on thrombin formation and complement and neutrophil activation during in vitro extracorporeal circulation. *Circulation*, 94(9 Suppl):II341–6.

[113] Glover, G. H., Li, T. Q., and Ress, D. (2000). Image-based method for retrospective correction of physiological motion effects in fMRI: RETROICOR. *Magnetic resonance in medicine : official journal of the Society of Magnetic Resonance in Medicine / Society of Magnetic Resonance in Medicine*, 44(1):162–167.

[114] Good, C. D., Johnsrude, I. S., Ashburner, J., Henson, R. N., Friston, K. J., and Frackowiak, R. S. (2001). A voxel-based morphometric study of ageing in 465 normal adult human brains. *NeuroImage*, 14(1 Pt 1):21–36.

[115] Greiner, C., Schmidinger, A., Hülsmann, S., Moskopp, D., Wölfer, J., Köhling, R., Speckmann, E. J., and Wassmann, H. (2000). Acute protective effect of nimodipine and dimethyl sulfoxide against hypoxic and ischemic damage in brain slices. *Brain Research*, 887(2):316–322.

[116] Greve, D. N. and Fischl, B. (2009). Accurate and robust brain image alignment using boundary-based registration. *NeuroImage*, 48(1):63–72.

[117] Griffanti, L., Salimi-Khorshidi, G., Beckmann, C. F., Auerbach, E. J., Douaud, G., Sexton, C. E., Zsoldos, E., Ebmeier, K. P., Filippini, N., Mackay, C. E., Moeller, S., Xu, J., Yacoub, E., Baselli, G., Ugurbil, K., Miller, K. L., and Smith, S. M. (2014). ICA-based artefact removal and accelerated fMRI acquisition for improved resting state network imaging. *NeuroImage*, 95:232–247.

[118] Grote, E. and Hassler, W. (1988). The critical first minutes after subarachnoid hemorrhage. *Neurosurgery*, 22(4):654–661.

[119] Habas, C., Kamdar, N., Nguyen, D., Prater, K., Beckmann, C. F., Menon, V., and Greicius, M. D. (2009). Distinct cerebellar contributions to intrinsic connectivity networks. *The Journal of neuroscience : the official journal of the Society for Neuroscience*, 29(26):8586–8594.

[120] Hackett, M. L. and Anderson, C. S. (2000). Health outcomes 1 year after subarachnoid hemorrhage: An international population-based study. The Australian Cooperative Research on Subarachnoid Hemorrhage Study Group. *Neurology*, 55(5):658–662.

[121] Haile, M., Limson, F., Gingrich, K., Li, Y.-S., Quartermain, D., Blanck, T., and Bekker, A. (2009). Nimodipine Prevents Transient Cognitive Dysfunction After Moderate Hypoxia in Adult Mice. *Journal of neurosurgical anesthesiology*, 21(2):140–144.

[122] Hajnal, J. V., Myers, R., Oatridge, A., Schwieso, J. E., Young, I. R., and Bydder, G. M. (1994). Artifacts due to stimulus correlated motion in functional imaging of the brain. *Magnetic resonance in medicine : official journal of the Society of Magnetic Resonance in Medicine / Society of Magnetic Resonance in Medicine*, 31(3):283–291.

[123] Hara, H., Nagasawa, H., and Kogure, K. (1990). Nimodipine attenuates both ischaemia-induced brain oedema and mortality in a rat novel transient middle cerebral artery occlusion model. *Acta neurochirurgica. Supplementum*, 51:251–253.

[124] Harman, A. W. and Maxwell, M. J. (1995). An evaluation of the role of calcium in cell injury. *Annual review of pharmacology and toxicology*, 35(1):129–144.

[125] Harper, A. M., Craigen, L., and Kazda, S. (1981). Effect of the calcium antagonist, nimodipine, on cerebral blood flow and metabolism in the primate. *Journal of cerebral blood flow and metabolism : official journal of the International Society of Cerebral Blood Flow and Metabolism*, 1(3):349–356.

[126] Haws, C. W., Gourley, J. K., and Heistad, D. D. (1983). Effects of nimodipine on cerebral blood flow. *The Journal of pharmacology and experimental therapeutics*, 225(1):24–28.

[127] Heitger, M. H., Anderson, T. J., and Jones, R. D. (2002). Saccade sequences as markers for cerebral dysfunction following mild closed head injury. *Progress in brain research*, 140:433–448.

[128] Heitger, M. H., Jones, R. D., Macleod, A. D., Snell, D. L., Frampton, C. M., and Anderson, T. J. (2009). Impaired eye movements in post-concussion syndrome indicate suboptimal brain function beyond the influence of depression, malingering or intellectual ability. *Brain : a journal of neurology*, 132(Pt 10):2850–2870.

[129] Helbok, R., Ko, S.-B., Schmidt, J. M., Kurtz, P., Fernandez, L., Choi, H. A., Connolly, E. S., Lee, K., Badjatia, N., Mayer, S. A., and Claassen, J. (2011). Global cerebral edema and brain metabolism after subarachnoid hemorrhage. *Stroke*, 42(6):1534–1539.

[130] Hernández-Cáceres, J., Macias-González, R., Brozek, G., and Bures, J. (1987). Systemic ketamine blocks cortical spreading depression but does not delay the onset of terminal anoxic depolarization in rats. *Brain Research*, 437(2):360–364.

[131] Hernández-Hernández, R., Coll, T., Rachitzky, P., Armas-Hernández, M. J., Armas-Padilla, M. C., Velasco, M., and Rizzo, A. (2002). Comparison of two nimodipine formulations in healthy volunteers. *Journal of human hypertension*, 16 Suppl 1:S142–4.

[132] Hikosaka, O., Takikawa, Y., and Kawagoe, R. (2000). Role of the basal ganglia in the control of purposive saccadic eye movements. *Physiological reviews*, 80(3):953–978.

[133] Hirashima, Y., Nakamura, S., Endo, S., Kuwayama, N., Naruse, Y., and Takaku, A. (1997a). Elevation of platelet activating factor, inflammatory cytokines, and coagulation factors in the internal jugular vein of patients with subarachnoid hemorrhage. *Neurochemical research*, 22(10):1249–1255.

[134] Hirashima, Y., Nakamura, S., Suzuki, M., Kurimoto, M., Endo, S., Ogawa, A., and Takaku, A. (1997b). Cerebrospinal fluid tissue factor and thrombin-antithrombin III complex as indicators of tissue injury after subarachnoid hemorrhage. *Stroke*, 28(9):1666–1670.

[135] Horn, J. and Limburg, M. (2001). Calcium antagonists for ischemic stroke: a systematic review. *Stroke*, 32(2):570–576.

[136] Hossmann, K. A. (1994). Viability thresholds and the penumbra of focal ischemia. *Annals of neurology*, 36(4):557–565.

[137] Huang, B. Y. and Castillo, M. (2008). Hypoxic-Ischemic Brain Injury: Imaging Findings from Birth to Adulthood1. *RadioGraphics*, 28(2):417–439.

[138] Huenges Wajer, I. M. C., Cremers, C. H. P., van Zandvoort, M. J. E., Vergouwen, M. D. I., van der Schaaf, I. C., Velthuis, B. K., Dankbaar, J. W., Vos, P. C., Visser-Meily, J. M. A., and Rinkel, G. J. E. (2014). CT perfusion on admission and cognitive functioning 3 months after aneurysmal subarachnoid haemorrhage. *Journal of Neurology*, pages 1–6.

[139] Hulme, S. R. and Connelly, W. M. (2014). L-type calcium channel-dependent inhibitory plasticity in the thalamus. *Journal of Neurophysiology*, 112(9):2037–2039.

[140] Hütter, B. O. and Gilsbach, J. M. (1993). Which neuropsychological deficits are hidden behind a good outcome (Glasgow = I) after aneurysmal subarachnoid hemorrhage? *Neurosurgery*, 33(6):999–1005; discussion 1005–6.

[141] Hütter, B. O., Gilsbach, J. M., and Kreitschmann, I. (1995). Quality of life and cognitive deficits after subarachnoid haemorrhage. *British journal of neurosurgery*, 9(4):465–475.

[142] Ikeda, K., Asakura, H., Futami, K., and Yamashita, J. (1997). Coagulative and fibrinolytic activation in cerebrospinal fluid and plasma after subarachnoid hemorrhage. *Neurosurgery*, 41(2):344–9; discussion 349–50.

[143] Jenkinson, M., Bannister, P., Brady, M., and Smith, S. (2002). Improved optimization for the robust and accurate linear registration and motion correction of brain images. *NeuroImage*, 17(2):825–841.

[144] Jenkinson, M., Beckmann, C. F., Behrens, T. E. J., Woolrich, M. W., and Smith, S. M. (2012). FSL. *NeuroImage*, 62(2):782–790.

[145] Jenkinson, M. and Smith, S. (2001). A global optimisation method for robust affine registration of brain images. *Medical image analysis*, 5(2):143–156.

[146] Jennett, B. and Bond, M. (1975). Assessment of outcome after severe brain damage. *The Lancet*, 1(7905):480–484.

[147] Jonas, S., Sugimori, M., and Llinás, R. (1997). Is low molecular weight heparin a neuroprotectant? *Annals of the New York Academy of Sciences*, 825:389–393.

[148] Jones, R. A., Müller, T. B., Haraldseth, O., Baptista, A. M., and Oksendal, A. N. (1996). Cerebrovascular changes in rats during ischemia and reperfusion: a comparison of BOLD and first pass bolus tracking techniques. *Magnetic resonance in medicine : official journal of the Society of Magnetic Resonance in Medicine / Society of Magnetic Resonance in Medicine*, 35(4):489–496.

[149] Juvela, S., Siironen, J., and Lappalainen, J. (2009). Apolipoprotein E genotype and outcome after aneurysmal subarachnoid hemorrhage. *Journal of neurosurgery*, 110(5):989–995.

[150] Kallenberg, K., Bailey, D. M., Christ, S., Mohr, A., Roukens, R., Menold, E., Steiner, T., Bärtsch, P., and Knauth, M. (2007). Magnetic resonance imaging evidence of cytotoxic cerebral edema in acute mountain sickness. *Journal of cerebral blood flow and metabolism : official journal of the International Society of Cerebral Blood Flow and Metabolism*, 27(5):1064–1071.

[151] Kassell, N., Torner, J., Clarke Haley Jr, E., Jane, J., Adams, H., Kongable, G., and Participants (1990). The International Cooperative Study on the Timing of Aneurysm Surgery. *Journal of neurosurgery*, 73(1):18–36.

[152] Kassell, N. F., Peerless, S. J., Durward, Q. J., Beck, D. W., Drake, C. G., and Adams, H. P. (1982). Treatment of ischemic deficits from vasospasm with intravascular volume expansion and induced arterial hypertension. *Neurosurgery*, 11(3):337–343.

[153] Kawai, K., Nitecka, L., Ruetzler, C. A., Nagashima, G., Joó, F., Mies, G., Nowak, T. S., Saito, N., Lohr, J. M., and Klatzo, I. (1992). Global cerebral ischemia associated with cardiac arrest in the rat: I. Dynamics of early neuronal changes. *Journal of cerebral blood flow and metabolism : official journal of the International Society of Cerebral Blood Flow and Metabolism*, 12(2):238–249.

[154] Kazda, S. and Towart, R. (1982). Nimodipine: a new calcium antagonistic drug with a preferential cerebrovascular action. *Acta Neurochirurgica*, 63(1-4):259–265.

[155] Keep, R. F., Andjelkovic, A. V., Stamatovic, S. M., Shakui, P., and Ennis, S. R. (2005). Ischemia-induced endothelial cell dysfunction. *Acta neurochirurgica. Supplement*, 95:399–402.

[156] Kelly, A. M. C., Uddin, L. Q., Biswal, B. B., Castellanos, F. X., and Milham, M. P. (2008). Competition between functional brain networks mediates behavioral variability. *NeuroImage*, 39(1):527–537.

[157] Kelly, M. E., Rowland, M. J., Okell, T. W., Chappell, M. A., Corkill, R., Kerr, R. S., Westbrook, J., Jezzard, P., and Pattinson, K. T. S. (2013). Pseudo-continuous arterial spin labelling MRI for non-invasive, whole-brain, serial quantification of cerebral blood flow following aneurysmal subarachnoid haemorrhage. *Translational Stroke Research*, 4(6):710–718.

[158] Khurana, V. G., Meissner, I., and Meyer, F. B. (2004). Update on genetic evidence for rupture-prone compared with rupture-resistant intracranial saccular aneurysms. *Neurosurgical FOCUS*, 17(5):E7.

[159] Kirkpatrick, P. J., Turner, C. L., Smith, C., Hutchinson, P. J., Murray, G. D., and STASH Collaborators (2014). Simvastatin in aneurysmal subarachnoid haemorrhage (STASH): a multicentre randomised phase 3 trial. *Lancet neurology*, 13(7):666–675.

[160] Kitahara, Y., Taga, K., Abe, H., and Shimoji, K. (2001). The effects of anesthetics on cortical spreading depression elicitation and c-fos expression in rats. *Journal of neurosurgical anesthesiology*, 13(1):26–32.

[161] Kiviniemi, V., Starck, T., Remes, J., Long, X., Nikkinen, J., Haapea, M., Veijola, J., Moilanen, I., Isohanni, M., Zang, Y.-F., and Tervonen, O. (2009). Functional segmentation of the brain cortex using high model order group PICA. *Human Brain Mapping*, 30(12):3865–3886.

[162] Ko, N. U., Rajendran, P., Kim, H., Rutkowski, M., Pawlikowska, L., Kwok, P.-Y., Higashida, R. T., Lawton, M. T., Smith, W. S., Zaroff, J. G., and Young, W. L. (2008). Endothelial nitric oxide synthase polymorphism (-786T->C) and increased risk of angiographic vasospasm after aneurysmal subarachnoid hemorrhage. *Stroke*, 39(4):1103–1108.

[163] Kosnik, E. J. and Hunt, W. E. (1976). Postoperative hypertension in the management of patients with intracranial arterial aneurysms. *Journal of neurosurgery*, 45(2):148–154.

[164] Kreiter, K. T., Copeland, D., Bernardini, G. L., Bates, J. E., Peery, S., Claassen, J., Du, Y. E., Stern, Y., Connolly, E. S., and Mayer, S. A. (2002). Predictors of cognitive dysfunction after subarachnoid hemorrhage. *Stroke*, 33(1):200–208.

[165] Kudo, C., Nozari, A., Moskowitz, M. A., and Ayata, C. (2008). The impact of anesthetics and hyperoxia on cortical spreading depression. *Experimental neurology*, 212(1):201–206.

[166] Kusaka, G., Ishikawa, M., Nanda, A., Granger, D. N., and Zhang, J. H. (2004). Signaling pathways for early brain injury after subarachnoid hemorrhage. *Journal of cerebral blood flow and metabolism : official journal of the International Society of Cerebral Blood Flow and Metabolism*, 24(8):916–925.

[167] Kwak, Y., Peltier, S. J., Bohnen, N. I., Müller, M. L. T. M., Dayalu, P., and Seidler, R. D. (2012). L-DOPA changes spontaneous low-frequency BOLD signal oscillations in Parkinson's disease: a resting state fMRI study. *Frontiers in systems neuroscience*, 6:52.

[168] Kwong, K. K., Chesler, D. A., Weisskoff, R. M., Donahue, K. M., Davis, T. L., Ostergaard, L., Campbell, T. A., and Rosen, B. R. (1995). MR perfusion studies with T1-weighted echo planar imaging. *Magnetic resonance in medicine : official journal of the Society of Magnetic Resonance in Medicine / Society of Magnetic Resonance in Medicine*, 34(6):878–887.

[169] Ladds, A., Branston, N. M., Vajda, J., McGillicuddy, J. E., and Symon, L. (1988). Changes in somatosensory evoked potentials following an experimental focal ischaemic lesion in thalamus. *Electroencephalography and clinical neurophysiology*, 71(3):233–240.

[170] Lagares, A., Cicuendez, M., Ramos, A., Salvador, E., Alén, J. F., Kaen, A., Jiménez-Roldán, L., and Millán, J. M. (2012). Acute perfusion changes after spontaneous SAH: a perfusion CT study. *Acta Neurochirurgica*, 154(3):405–11– discussion 411–2.

[171] Lagares, A., Gómez, P. A., Lobato, R. D., Alén, J. F., Alday, R., and Campollo, J. (2001). Prognostic factors on hospital admission after spontaneous subarachnoid haemorrhage. *Acta Neurochirurgica*, 143(7):665–672.

[172] Lang, E. W., Diehl, R. R., and Mehdorn, H. M. (2001). Cerebral autoregulation testing after aneurysmal subarachnoid hemorrhage: the phase relationship between arterial blood pressure and cerebral blood flow velocity. *Critical Care Medicine*, 29(1):158–163.

[173] Langham, J., Goldfrad, C., Teasdale, G., Shaw, D., and Rowan, K. (2003). Calcium channel blockers for acute traumatic brain injury. *Cochrane database of systematic reviews (Online)*, (4):CD000565.

[174] Lanterna, L. A., Ruigrok, Y., Alexander, S., Tang, J., Biroli, F., Dunn, L. T., and Poon, W. S. (2007). Meta-analysis of APOE genotype and subarachnoid hemorrhage: clinical outcome and delayed ischemia. *Neurology*, 69(8):766–775.

[175] Lauritzen, M. (1984). Long-lasting reduction of cortical blood flow of the brain after spreading depression with preserved autoregulation and impaired CO2 response. *Journal of cerebral blood flow and metabolism : official journal of the International Society of Cerebral Blood Flow and Metabolism*, 4(4):546–554.

[176] Lauritzen, M. (1994). Pathophysiology of the migraine aura. The spreading depression theory. *Brain : a journal of neurology*, 117 (Pt 1):199–210.

[177] Lauritzen, M., Dreier, J. P., Fabricius, M., Hartings, J. A., Graf, R., and Strong, A. J. (2011). Clinical relevance of cortical spreading depression in neurological disorders: migraine, malignant stroke, subarachnoid and intracranial hemorrhage, and traumatic brain injury. *Journal of cerebral blood flow and metabolism : official journal of the International Society of Cerebral Blood Flow and Metabolism*, 31(1):17–35.

[178] Lawley, J. S., Alperin, N., Bagci, A. M., Lee, S. H., Mullins, P. G., Oliver, S. J., and Macdonald, J. H. (2014). Normobaric hypoxia and symptoms of acute mountain sickness: Elevated brain volume and intracranial hypertension. *Annals of Neurology*, 75(6):890–898.

[179] Leao, A. (1944a). Pial circulation and spreading depression of activity in the cerebral cortex. *Journal of Neurophysiology*, 7(6):391–396.

[180] Leao, A. (1944b). Spreading depression of activity in the cerebral cortex. *Journal of Neurophysiology*, 7(6):359.

[181] Leech, R., Kamourieh, S., Beckmann, C. F., and Sharp, D. J. (2011). Fractionating the Default Mode Network: Distinct Contributions of the Ventral and Dorsal Posterior Cingulate Cortex to Cognitive Control. *Journal of Neuroscience*, 31(9):3217–3224.

[182] Leigh, R. J. and Kennard, C. (2003). Using saccades as a research tool in the clinical neurosciences. *Brain : a journal of neurology*, 127(3):460–477.

[183] Libersan, D., Khalil, A., Dagenais, P., Quan, E., Delorme, F., Uzan, A., and Latour, J. G. (1998). The low molecular weight heparin, enoxaparin, limits infarct size at reperfusion in the dog. *Cardiovascular research*, 37(3):656–666.

[184] Liebeskind, D. S. (2003). Collateral circulation. *Stroke*, 34(9):2279–2284.

[185] Lindvall, P., Runnerstam, M., Birgander, R., and Koskinen, L.-O. D. (2009). The Fisher grading correlated to outcome in patients with subarachnoid haemorrhage. *British journal of neurosurgery*, 23(2):188–192.

[186] Littow, H., Huossa, V., Karjalainen, S., Jääskeläinen, E., Haapea, M., Miettunen, J., Tervonen, O., Isohanni, M., Nikkinen, J., Veijola, J., Murray, G., and Kiviniemi, V. J. (2015). Aberrant Functional Connectivity in the Default Mode and Central Executive Networks in Subjects with Schizophrenia - A Whole-Brain Resting-State ICA Study. *Frontiers in psychiatry*, 6:26.

[187] Liu, Y., Soppi, V., Mustonen, T., Könönen, M., Koivisto, T., Koskela, A., Rinne, J., and Vanninen, R. L. (2007). Subarachnoid hemorrhage in the subacute stage: elevated apparent diffusion coefficient in normal-appearing brain tissue after treatment. *Radiology*, 242(2):518–525.

[188] Llinás, R. R. and Steriade, M. (2006). Bursting of thalamic neurons and states of vigilance. *Journal of Neurophysiology*, 95(6):3297–3308.

[189] Logothetis, N. K. and Wandell, B. A. (2004). Interpreting the BOLD signal. *Annual review of physiology*, 66:735–769.

[190] Lovelock, C. E., Rinkel, G. J. E., and Rothwell, P. M. (2010). Time trends in outcome of subarachnoid hemorrhage: Population-based study and systematic review. *Neurology*, 74(19):1494–1501.

[191] Lynch, J. R., Wang, H., Mcgirt, M. J., Floyd, J., Friedman, A. H., Coon, A. L., Blessing, R., Alexander, M. J., Graffagnino, C., Warner, D. S., and Laskowitz, D. T. (2005). Simvastatin reduces vasospasm after aneurysmal subarachnoid hemorrhage: results of a pilot randomized clinical trial. *Stroke*, 36(9):2024–2026.

[192] Macdonald, R. L., Kassell, N. F., Mayer, S., Ruefenacht, D., Schmiedek, P., Weidauer, S., Frey, A., Roux, S., Pasqualin, A., and Investigators, C.-. (2008). Clazosentan to overcome neurological ischemia and infarction occurring after subarachnoid hemorrhage (CONSCIOUS-1): randomized, double-blind, placebo-controlled phase 2 dose-finding trial. *Stroke*, 39(11):3015–3021.

[193] Macdonald, R. L., Pluta, R. M., and Zhang, J. H. (2007). Cerebral vasospasm after subarachnoid hemorrhage: the emerging revolution. *Nature clinical practice. Neurology*, 3(5):256–263.

[194] Maher, M., Churchill, N. W., de Oliveira Manoel, A. L., Graham, S. J., Macdonald, R. L., and Schweizer, T. A. (2015). Altered Resting-State Connectivity within Executive Networks after Aneurysmal Subarachnoid Hemorrhage. *PLoS ONE*, 10(7):e0130483.

[195] Marquez de la Plata, C. D., Garces, J., Shokri Kojori, E., Grinnan, J., Krishnan, K., Pidikiti, R., Spence, J., Devous, M. D., Moore, C., McColl, R., Madden, C., and Diaz-Arrastia, R. (2011). Deficits in functional connectivity of hippocampal and frontal lobe circuits after traumatic axonal injury. *Archives of neurology*, 68(1):74–84.

[196] Mathiesen, T., Edner, G., Ulfarsson, E., and Andersson, B. (1997). Cerebrospinal fluid interleukin-1 receptor antagonist and tumor necrosis factor-alpha following subarachnoid hemorrhage. *Journal of neurosurgery*, 87(2):215–220.

[197] Mayer, A. R., Mannell, M. V., Ling, J., Gasparovic, C., and Yeo, R. A. (2011). Functional connectivity in mild traumatic brain injury. *Human Brain Mapping*, 32(11):1825–1835.

[198] McCarron, M. O., Muir, K. W., Nicoll, J. A., Stewart, J., Currie, Y., Brown, K., and Bone, I. (2000). Prospective study of apolipoprotein E genotype and functional outcome following ischemic stroke. *Archives of neurology*, 57(10):1480–1484.

[199] Mcgirt, M. J., Blessing, R., Alexander, M. J., Nimjee, S. M., Woodworth, G. F., Friedman, A. H., Graffagnino, C., Laskowitz, D. T., and Lynch, J. R. (2006). Risk of cerebral vasopasm after subarachnoid hemorrhage reduced by statin therapy: A multivariate analysis of an institutional experience. *Journal of neurosurgery*, 105(5):671–674.

[200] Merlo, L., Cimino, F., Scibilia, A., Ricciardi, E., Chirafisi, J., Speciale, A., Angileri, F. F., Raffa, G., Priola, S., Saija, A., and Germanò, A. (2011). Simvastatin administration ameliorates neurobehavioral consequences of subarachnoid hemorrhage in the rat. *Journal of neurotrauma*, 28(12):2493–2501.

[201] Mesulam, M. M. (1998). From sensation to cognition. *Brain : a journal of neurology*, 121 (Pt 6):1013–1052.

[202] Meyer, C. H., Lowe, D., Meyer, M., Richardson, P. L., and Neil-Dwyer, G. (1982). Subarachnoid haemorrhage: older patients have low cerebral blood flow. *British medical journal (Clinical research ed)*, 285(6349):1149–1153.

[203] Mezue, M., Segerdahl, A. R., Okell, T. W., Chappell, M. A., Kelly, M. E., and Tracey, I. (2014). Optimization and reliability of multiple postlabeling delaypseudo-continuous arterial spin labeling during rest andstimulus-induced functional task activation. *Journal of cerebral blood flow and metabolism : official journal of the International Society of Cerebral Blood Flow and Metabolism*, pages 1–9.

[204] Miller, D. H., Barkhof, F., Frank, J. A., Parker, G. J. M., and Thompson, A. J. (2002). Measurement of atrophy in multiple sclerosis: pathological basis, methodological aspects and clinical relevance. *Brain : a journal of neurology*, 125(Pt 8):1676–1695.

[205] Minhas, P. S., Menon, D. K., Smielewski, P., Czosnyka, M., Kirkpatrick, P. J., Clark, J. C., and Pickard, J. D. (2003). Positron Emission Tomographic Cerebral Perfusion Disturbances and Transcranial Doppler Findings among Patients with Neurological Deterioration after Subarachnoid Hemorrhage. *Neurosurgery*, 52(5):1017–1024.

[206] Mioshi, E., Dawson, K., Mitchell, J., Arnold, R., and Hodges, J. R. (2006). The Addenbrooke's Cognitive Examination Revised (ACE-R): a brief cognitive test battery for dementia screening. *International Journal of Geriatric Psychiatry*, 21(11):1078–1085.

[207] Missiaen, L., Robberecht, W., van den Bosch, L., Callewaert, G., Parys, J. B., Wuytack, F., Raeymaekers, L., Nilius, B., Eggermont, J., and De Smedt, H. (2000). Abnormal intracellular ca(2+)homeostasis and disease. *Cell Calcium*, 28(1):1–21.

[208] Miyata, M. and Smith, J. D. (1996). Apolipoprotein E allele-specific antioxidant activity and effects on cytotoxicity by oxidative insults and beta-amyloid peptides. *Nature genetics*, 14(1):55–61.

[209] Mohamed, A. A., Mendelow, A. D., Teasdale, G. M., Harper, A. M., and McCulloch, J. (1985). Effect of the calcium antagonist nimodipine on local cerebral blood flow and metabolic coupling. *Journal of cerebral blood flow and metabolism : official journal of the International Society of Cerebral Blood Flow and Metabolism*, 5(1):26–33.

[210] Monti, M. M., Osherson, D. N., Martinez, M. J., and Parsons, L. M. (2007). Functional neuroanatomy of deductive inference: a language-independent distributed network. *NeuroImage*, 37(3):1005–1016.

[211] Moskowitz, S. I., Ahrens, C., Provencio, J. J., Chow, M., and Rasmussen, P. A. (2009). Prehemorrhage statin use and the risk of vasospasm after aneurysmal subarachnoid hemorrhage. *Surgical Neurology*, 71(3):311–7, discussion 317–8.

[212] Müri, R. M. and Nyffeler, T. (2008). Neurophysiology and neuroanatomy of reflexive and volitional saccades as revealed by lesion studies with neurological patients and transcranial magnetic stimulation (TMS). *Brain and cognition*, 68(3):284–292.

[213] Naidech, A. M., Drescher, J., Tamul, P., Shaibani, A., Batjer, H. H., and Alberts, M. J. (2006). Acute physiological derangement is associated with early radiographic cerebral infarction after subarachnoid haemorrhage. *Journal of Neurology, Neurosurgery & Psychiatry*, 77(12):1340–1344.

[214] Nelson, H. E. and Willison, J. R. (1991). *National Adult Reading Test–Test Manual (Second edition)*. Windsor: NFER-Nelson.

[215] Nezamzadeh, M., Matson, G. B., Young, K., Weiner, M. W., and Schuff, N. (2010). Improved pseudo-continuous arterial spin labeling for mapping brain perfusion. *Journal of magnetic resonance imaging : JMRI*, 31(6):1419–1427.

[216] Nieuwkamp, D. J., Algra, A., Blomqvist, P., Adami, J., Buskens, E., Koffijberg, H., and Rinkel, G. J. E. (2011). Excess Mortality and Cardiovascular Events in Patients Surviving Subarachnoid Hemorrhage: A Nationwide Study in Sweden. *Stroke*, 42(4):902–907.

[217] Niskakangas, T., Ohman, J., Niemela, M., Ilveskoski, E., Kunnas, T. A., and Karhunen, P. J. (2001). Association of apolipoprotein E polymorphism with outcome after aneurysmal subarachnoid hemorrhage: a preliminary study. *Stroke*, 32(5):1181–1184.

[218] Nornes, H. (1973). The role of intracranial pressure in the arrest of hemorrhage in patients with ruptured intracranial aneurysm. *Journal of neurosurgery*, 39(2):226–234.

[219] Nornes, H. and Magnaes, B. (1972). Intracranial pressure in patients with ruptured saccular aneurysm. *Journal of neurosurgery*, 36(5):537–547.

[220] Oakes, T. R., Fox, A. S., Johnstone, T., Chung, M. K., Kalin, N., and Davidson, R. J. (2007). Integrating VBM into the General Linear Model with voxelwise anatomical covariates. *NeuroImage*, 34(2):500–508.

[221] Ober, J. K., Przedpelska-Ober, E., Gryncewicz, W., Dylak, J., Carpenter, R., and Ober, J. J. (2003). Hand-held system for ambulatory measurement of saccadic durations of neurological patients. In Gajda, J., editor, *Modelling and Measurement in Medicine*, pages 187–198.

[222] Ogawa, S., Lee, T. M., Kay, A. R., and Tank, D. W. (1990). Brain magnetic resonance imaging with contrast dependent on blood oxygenation. *Proceedings of the National Academy of Sciences of the United States of America*, 87(24):9868–9872.

[223] Ogden, J. A., Mee, E. W., and Henning, M. (1993). A prospective study of impairment of cognition and memory and recovery after subarachnoid hemorrhage. *Neurosurgery*, 33(4):572–86; discussion 586–7.

[224] Okell, T. W., Chappell, M. A., Kelly, M. E., and Jezzard, P. (2013). Cerebral blood flow quantification using vessel-encoded arterial spin labeling. *Journal of cerebral blood flow and metabolism : official journal of the International Society of Cerebral Blood Flow and Metabolism*, 33(11):1716–1724.

[225] Oktar, S. O., Yücel, C., Karaosmanoglu, D., Akkan, K., Ozdemir, H., Tokgoz, N., and Tali, T. (2006). Blood-flow volume quantification in internal carotid and vertebral arteries: comparison of 3 different ultrasound techniques with phase-contrast MR imaging. *AJNR American journal of neuroradiology*, 27(2):363–369.

[226] O'Reilly, J. X., Beckmann, C. F., Tomassini, V., Ramnani, N., and Johansen-Berg, H. (2010). Distinct and overlapping functional zones in the cerebellum defined by resting state functional connectivity. *Cerebral Cortex*, 20(4):953–965.

[227] Ota, H., Eto, M., Kano, M. R., Kahyo, T., Setou, M., Ogawa, S., Iijima, K., Akishita, M., and Ouchi, Y. (2010). Induction of Endothelial Nitric Oxide Synthase, SIRT1, and Catalase by Statins Inhibits Endothelial Senescence Through the Akt Pathway. *Arteriosclerosis, Thrombosis, and Vascular Biology*, 30(11):2205–2211.

[228] Palacios, E. M., Sala-Llonch, R., Junque, C., Roig, T., Tormos, J. M., Bargallo, N., and Vendrell, P. (2013). Resting-State Functional Magnetic Resonance Imaging Activity and Connectivity and Cognitive Outcome in Traumatic Brain Injury. *JAMA Neurology*, 70(7):845–7.

[229] Park, S., Yamaguchi, M., Zhou, C., Calvert, J. W., Tang, J., and Zhang, J. H. (2004). Neurovascular protection reduces early brain injury after subarachnoid hemorrhage. *Stroke*, 35(10):2412–2417.

[230] Parra, A., Kreiter, K. T., Williams, S., Sciacca, R., Mack, W. J., Naidech, A. M., Commichau, C. S., Fitzsimmons, B.-F. M., Janjua, N., Mayer, S. A., and Connolly, E. S. (2005). Effect of prior statin use on functional outcome and delayed vasospasm after acute aneurysmal subarachnoid hemorrhage: a matched controlled cohort study. *Neurosurgery*, 56(3):476–84; discussion 476–84.

[231] Paulson, O. B., Strandgaard, S., and Edvinsson, L. (1990). Cerebral autoregulation. *Cerebrovascular and brain metabolism reviews*, 2(2):161–192.

[232] Pearson, B. C., Armitage, K. R., Horner, C. W. M., and Carpenter, R. H. S. (2007). Saccadometry: the possible application of latency distribution measurement for monitoring concussion. *British journal of sports medicine*, 41(9):610–612.

[233] Peltonen, S., Juvela, S., Kaste, M., and Lassila, R. (1997). Hemostasis and fibrinolysis activation after subarachnoid hemorrhage. *Journal of neurosurgery*, 87(2):207–214.

[234] Pepe, M. G. and Curtiss, L. K. (1986). Apolipoprotein E is a biologically active constituent of the normal immunoregulatory lipoprotein, LDL-In. *Journal of immunology (Baltimore, Md. : 1950)*, 136(10):3716–3723.

[235] Peroutka, S. J. and Allen, G. S. (1983). Calcium channel antagonist binding sites labeled by 3H-nimodipine in human brain. *Journal of neurosurgery*, 59(6):933–937.

[236] Peters, S. A. E., Palmer, M. K., Grobbee, D. E., Crouse, J. R., O'Leary, D. H., Raichlen, J. S., and Bots, M. L. (2010). C-reactive protein lowering with rosuvastatin in the METEOR study. *Journal of internal medicine*, 268(2):155–161.

[237] Petruk, K. C., West, M., Mohr, G., Weir, B. K., Benoit, B. G., Gentili, F., Disney, L. B., Khan, M. I., Grace, M., and Holness, R. O. (1988). Nimodipine treatment in poor-grade aneurysm patients. Results of a multicenter double-blind placebo-controlled trial. *Journal of neurosurgery*, 68(4):505–517.

[238] Petzold, A., Keir, G., Kay, A., Kerr, M., and Thompson, E. J. (2006). Axonal damage and outcome in subarachnoid haemorrhage. *Journal of Neurology, Neurosurgery & Psychiatry*, 77(6):753–759.

[239] Pickard, J. D., Murray, G. D., Illingworth, R., Shaw, M. D., Teasdale, G. M., Foy, P. M., Humphrey, P. R., Lang, D. A., Nelson, R., and Richards, P. (1989). Effect of oral nimodipine on cerebral infarction and outcome after subarachnoid haemorrhage: British aneurysm nimodipine trial. *BMJ (Clinical research ed)*, 298(6674):636–642.

[240] Piper, R. D. and Lambert, G. A. (1996). Inhalational anesthetics inhibit spreading depression: relevance to migraine. *Cephalalgia : an international journal of headache*, 16(2):87–92.

[241] Pisani, A., Calabresi, P., Tozzi, A., D'Angelo, V., and Bernardi, G. (1998a). L-type Ca2+ channel blockers attenuate electrical changes and Ca2+ rise induced by oxygen/glucose deprivation in cortical neurons. *Stroke*, 29(1):196–201; discussion 202.

[242] Pisani, A., Calabresi, P., Tozzi, A., D'Angelo, V., Bernardi, G., and Iadecola, C. (1998b). L-Type Ca2+ Channel Blockers Attenuate Electrical Changes and Ca2+ Rise Induced by Oxygen/Glucose Deprivation in Cortical Neurons. *Stroke*, 29(1):196–202.

[243] Polin, R. S., Coenen, V. A., Hansen, C. A., Shin, P., Baskaya, M. K., Nanda, A., and Kassell, N. F. (2000). Efficacy of transluminal angioplasty for the management of symptomatic cerebral vasospasm following aneurysmal subarachnoid hemorrhage. *Journal of neurosurgery*, 92(2):284–290.

[244] Power, J. D., Schlaggar, B. L., and Petersen, S. E. (2015). Recent progress and outstanding issues in motion correction in resting state fMRI. *NeuroImage*, 105(C):536–551.

[245] Raju, T. N., John, E., Shankararao, R., Fornell, L., Vasa, R., and Abu-Harb, M. (1996). Effect of nimodipine on systemic, renal, and cerebral haemodynamics after a mild hypoxic-ischaemic insult in newborn piglets. *Pharmacological research : the official journal of the Italian Pharmacological Society*, 33(1):5–12.

[246] Rätsep, T. and Asser, T. (2001). Cerebral hemodynamic impairment after aneurysmal subarachnoid hemorrhage as evaluated using transcranial doppler ultrasonography: relationship to delayed cerebral ischemia and clinical outcome. *Journal of neurosurgery*, 95(3):393–401.

[247] Richter, S., Gerwig, M., Aslan, B., Wilhelm, H., Schoch, B., Dimitrova, A., Gizewski, E. R., Ziegler, W., Karnath, H.-O., and Timmann, D. (2007). Cognitive functions in patients with MR-defined chronic focal cerebellar lesions. *Journal of Neurology*, 254(9):1193–1203.

[248] Rijsdijk, M., van der Schaaf, I. C., Velthuis, B. K., Wermer, M. J., and Rinkel, G. J. E. (2008). Global and focal cerebral perfusion after aneurysmal subarachnoid hemorrhage in relation with delayed cerebral ischemia. *Neuroradiology*, 50(9):813–820.

[249] Rinkel, G. J. E., Feigin, V. L., Algra, A., and van Gijn, J. (2004). Circulatory volume expansion therapy for aneurysmal subarachnoid haemorrhage. *Cochrane database of systematic reviews (Online)*, (4):CD000483.

[250] Robertson, E. G. (1949). Cerebral lesions due to intracranial aneurysms. *Brain : a journal of neurology*, 72(Pt. 2):150–185.

[251] Robinson, S., Basso, G., Soldati, N., Sailer, U., Jovicich, J., Bruzzone, L., Kryspin-Exner, I., Bauer, H., and Moser, E. (2009). A resting state network in the motor control circuit of the basal ganglia. *BMC neuroscience*, 10(1):137–14.

[252] Roine, R. O., Kaste, M., Kinnunen, A., Nikki, P., Sarna, S., and Kajaste, S. (1990). Nimodipine after resuscitation from out-of-hospital ventricular fibrillation. A placebo-controlled, double-blind, randomized trial. *JAMA: The Journal of the American Medical Association*, 264(24):3171–3177.

[253] Romano, J. G., Forteza, A. M., Concha, M., Koch, S., Heros, R. C., Morcos, J. J., and Babikian, V. L. (2002). Detection of microemboli by transcranial Doppler ultrasonography in aneurysmal subarachnoid hemorrhage. *Neurosurgery*, 50(5):1026–30; discussion 1030–1.

[254] Romero, J. R., Pikula, A., Nguyen, T. N., Nien, Y. L., Norbash, A., and Babikian, V. L. (2009). Cerebral collateral circulation in carotid artery disease. *Current cardiology reviews*, 5(4):279–288.

[255] Roos, Y. B., Rinkel, G. J., Vermeulen, M., Algra, A., and van Gijn, J. (2000). Antifibrinolytic therapy for aneurysmal subarachnoid haemorrhage. *Cochrane database of systematic reviews (Online)*, (2):CD001245.

[256] Ross, D. T. and Graham, D. I. (1993). Selective loss and selective sparing of neurons in the thalamic reticular nucleus following human cardiac arrest. *Journal of cerebral blood flow and metabolism : official journal of the International Society of Cerebral Blood Flow and Metabolism*, 13(4):558–567.

[257] Ross, D. T., Graham, D. I., and Adams, J. H. (1993). Selective loss of neurons from the thalamic reticular nucleus following severe human head injury. *Journal of neurotrauma*, 10(2):151–165.

[258] Rostrup, E., Larsson, H. B., Toft, P. B., Garde, K., and Henriksen, O. (1995). Signal changes in gradient echo images of human brain induced by hypo- and hyperoxia. *NMR in biomedicine*, 8(1):41–47.

[259] Rostrup, E., Larsson, H. B. W., Born, A. P., Knudsen, G. M., and Paulson, O. B. (2005). Changes in BOLD and ADC weighted imaging in acute hypoxia during sea-level and altitude adapted states. *NeuroImage*, 28(4):947–955.

[260] Rottach, K. G., Wohlgemuth, W. A., Dzaja, A. E., Eggert, T., and Straube, A. (2002). Effects of intravenous opioids on eye movements in humans: possible mechanisms. *Journal of Neurology*, 249(9):1200–1205.

[261] Rowland, M. J., Hadjipavlou, G., Kelly, M., Westbrook, J., and Pattinson, K. T. S. (2012). Delayed cerebral ischaemia after subarachnoid haemorrhage: looking beyond vasospasm. *British journal of anaesthesia*, 109(3):315–329.

[262] Rupp, T., Jubeau, M., Lamalle, L., Warnking, J. M., Millet, G. Y., Wuyam, B., Esteve, F. c. o., Levy, P., Krainik, A., and Verges, S. (2014). Cerebral volumetric changes induced by prolonged hypoxic exposure and whole-body exercise. 34(11):1802–1809.

[263] Sakowitz, O. W., Kiening, K. L., Krajewski, K. L., Sarrafzadeh, A. S., Fabricius, M., Strong, A. J., Unterberg, A. W., and Dreier, J. P. (2009). Preliminary evidence that ketamine inhibits spreading depolarizations in acute human brain injury. *Stroke*, 40(8):e519–22.

[264] Salimi-Khorshidi, G., Douaud, G., Beckmann, C. F., Glasser, M. F., Griffanti, L., and Smith, S. M. (2014). Automatic denoising of functional MRI data: Combining independent component analysis and hierarchical fusion of classifiers. *NeuroImage*, 90(C):449–468.

[265] Sandsmark, D. K., Sandsmark, D. K., Kumar, M. A., Kumar, M. A., Park, S., Park, S., Levine, J. M., and Levine, J. M. (2012). Multimodal monitoring in subarachnoid hemorrhage. *Stroke*, 43(5):1440–1445.

[266] Sasaki, R., Hirota, K., Asahi, T., and Yamazaki, M. (2002). The Effects of Thiopental on Spreading Depression Induced by Anoxia in the Rat Hippocampal Slice in Vitro. *Hiroshima Journal of Anaesthesia*, 38:211–214.

[267] Sato, K., Shimizu, H., Fujimura, M., Inoue, T., Matsumoto, Y., and Tominaga, T. (2010a). Acute-stage diffusion-weighted magnetic resonance imaging for predicting outcome of poor-grade aneurysmal subarachnoid hemorrhage. *Journal of cerebral blood flow and metabolism : official journal of the International Society of Cerebral Blood Flow and Metabolism*, pages 1–11.

[268] Sato, K., Shimizu, H., Fujimura, M., Inoue, T., Matsumoto, Y., and Tominaga, T. (2010b). Acute-stage diffusion-weighted magnetic resonance imaging for predicting outcome of poor-grade aneurysmal subarachnoid hemorrhage. *Journal of cerebral blood flow and metabolism : official journal of the International Society of Cerebral Blood Flow and Metabolism*, 30(6):1110–1120.

[269] Satterthwaite, T. D., Wolf, D. H., Loughead, J., Ruparel, K., Elliott, M. A., Hakonarson, H., Gur, R. C., and Gur, R. E. (2012). Impact of in-scanner head motion on multiple measures of functional connectivity: Relevance for studies of neurodevelopment in youth. *NeuroImage*, 60(1):623–632.

[270] Schmahmann, J. D. (1991). An Emerging Concept: The Cerebellar Contribution to Higher Function. *Archives of neurology*, 48(11):1178–1187.

[271] Schmahmann, J. D. (1996). From movement to thought: anatomic substrates of the cerebellar contribution to cognitive processing. *Human brain mapping*, 4(3):174–198.

[272] Schmidt, J. F. and Waldemar, G. (1990). Effect of nimodipine on cerebral blood flow in human volunteers. *Journal of cardiovascular pharmacology*, 16(4):568–571.

[273] Schmidt, J. F., Waldemar, G., and Paulson, O. B. (1991). The acute effect of nimodipine on cerebral blood flow, its CO2 reactivity, and cerebral oxygen metabolism in human volunteers. *Acta Neurochirurgica*, 111(1-2):49–53.

[274] Schoonman, G. G., Sándor, P. S., Nirkko, A. C., Lange, T., Jaermann, T., Dydak, U., Kremer, C., Ferrari, M. D., Boesiger, P., and Baumgartner, R. W. (2008). Hypoxia-induced acute mountain sickness is associated with intracellular cerebral edema: a 3 T magnetic resonance imaging study. *Journal of cerebral blood flow and metabolism : official journal of the International Society of Cerebral Blood Flow and Metabolism*, 28(1):198–206.

[275] Schraa-Tam, C. K. L., van Broekhoven, P., van der Geest, J. N., Frens, M. A., Smits, M., and van der Lugt, A. (2008). Cortical and cerebellar activation induced by reflexive and voluntary saccades. *Experimental brain research. Experimentelle Hirnforschung. Expérimentation cérébrale*, 192(2):175–187.

[276] Schwartz, A. Y., Masago, A., Sehba, F. A., and Bederson, J. B. (2000). Experimental models of subarachnoid hemorrhage in the rat: a refinement of the endovascular filament model. *Journal of neuroscience methods*, 96(2):161–167.

[277] Scott, R. B., Eccles, F., Lloyd, A., and Carpenter, K. (2008). From multidimensional neuropsychological outcomes to a cognitive complication rate: The International Subarachnoid Aneurysm Trial. *Trials*, 9(1):13.

[278] Scott, R. B., Eccles, F., Molyneux, A. J., Kerr, R. S. C., Rothwell, P. M., and Carpenter, K. (2010). Improved Cognitive Outcomes With Endovascular Coiling of Ruptured Intracranial Aneurysms: Neuropsychological Outcomes From the International Subarachnoid Aneurysm Trial (ISAT). *Stroke*, 41(8):1743–1747.

[279] Scott, R. B., Farmer, E., Smiton, A., Tovey, C., Clarke, M., and Carpenter, K. (2004). Methodology of neuropsychological research in multicentre randomized clinical trials: a model derived from the International Subarachnoid Aneurysm Trial. *Clinical Trials*, 1(1):31–39.

[280] Sehba, F. A. and Bederson, J. B. (2006). Mechanisms of acute brain injury after subarachnoid hemorrhage. *Neurological research*, 28(4):381–398.

[281] Sharp, D. J., Beckmann, C. F., Greenwood, R., Kinnunen, K. M., Bonnelle, V., De Boissezon, X., Powell, J. H., Counsell, S. J., Patel, M. C., and Leech, R. (2011). Default mode network functional and structural connectivity after traumatic brain injury. *Brain : a journal of neurology*, 134(Pt 8):2233–2247.

[282] Shaw, M. D., Vermeulen, M., Murray, G. D., Pickard, J. D., Bell, B. A., and Teasdale, G. M. (2000). Efficacy and safety of the endothelin, receptor antagonist TAK-044 in treating subarachnoid hemorrhage: a report by the Steering Committee on behalf of the UK/Netherlands/Eire TAK-044 Subarachnoid Haemorrhage Study Group. *Journal of neurosurgery*, 93(6):992–997.

[283] Sheldon, S., Macdonald, R. L., Cusimano, M., Spears, J., and Schweizer, T. A. (2013). Long-term consequences of subarachnoid hemorrhage: examining working memory. *Journal of the Neurological Sciences*, 332(1-2):145–147.

[284] Shin, H. K., Dunn, A. K., Jones, P. B., Boas, D. A., Moskowitz, M. A., and Ayata, C. (2006). Vasoconstrictive neurovascular coupling during focal ischemic depolarizations. *Journal of cerebral blood flow and metabolism : official journal of the International Society of Cerebral Blood Flow and Metabolism*, 26(8):1018–1030.

[285] Siironen, J., Juvela, S., Varis, J., Porras, M., Poussa, K., Ilveskero, S., Hernesniemi, J., and Lassila, R. (2003). No effect of enoxaparin on outcome of aneurysmal subarachnoid hemorrhage: a randomized, double-blind, placebo-controlled clinical trial. *Journal of Neurosurgery: Pediatrics*, 99(6).

[286] Singhal, A. B., Topcuoglu, M. A., Dorer, D. J., Ogilvy, C. S., Carter, B. S., and Koroshetz, W. J. (2005). SSRI and statin use increases the risk for vasospasm after subarachnoid hemorrhage. *Neurology*, 64(6):1008–1013.

[287] Smith, M. L., Auer, R. N., and Siesjö, B. K. (1984). The density and distribution of ischemic brain injury in the rat following 2-10 min of forebrain ischemia. *Acta neuropathologica*, 64(4):319–332.

[288] Smith, M. L., Kågström, E., Rosén, I., and Siesjö, B. K. (1983). Effect of the calcium antagonist nimodipine on the delayed hypoperfusion following incomplete ischemia in the rat. *Journal of cerebral blood flow and metabolism : official journal of the International Society of Cerebral Blood Flow and Metabolism*, 3(4):543–546.

[289] Smith, S. M. (2002). Fast robust automated brain extraction. *Human Brain Mapping*, 17(3):143–155.

[290] Smith, S. M., Fox, P. T., Miller, K. L., Glahn, D. C., Fox, P. M., Mackay, C. E., Filippini, N., Watkins, K. E., Toro, R., Laird, A. R., and Beckmann, C. F. (2009). Correspondence of the brain's functional architecture during activation and rest. *Proceedings of the National Academy of Sciences of the United States of America*, 106(31):13040–13045.

[291] Smith, S. M. and Nichols, T. E. (2009). Threshold-free cluster enhancement: Addressing problems of smoothing, threshold dependence and localisation in cluster inference. *NeuroImage*, 44(1):83–98.

[292] Smith, S. M., Zhang, Y., Jenkinson, M., Chen, J., Matthews, P. M., Federico, A., and De Stefano, N. (2002). Accurate, robust, and automated longitudinal and cross-sectional brain change analysis. *NeuroImage*, 17(1):479–489.

[293] Sobey, C. G. (2001). Cerebrovascular dysfunction after subarachnoid haemorrhage: novel mechanisms and directions for therapy. *Clinical and experimental pharmacology & physiology*, 28(11):926–929.

[294] Stein, S. C., Browne, K. D., Chen, X.-H., Smith, D. H., and Graham, D. I. (2006). Thromboembolism and delayed cerebral ischemia after subarachnoid hemorrhage: an autopsy study. *Neurosurgery*, 59(4):781–7; discussion 787–8.

[295] Stenhouse, L. M., Knight, R. G., Longmore, B. E., and Bishara, S. N. (1991). Long-term cognitive deficits in patients after surgery on aneurysms of the anterior communicating artery. *Journal of Neurology, Neurosurgery & Psychiatry*, 54(10):909–914.

[296] Stoodley, C. J. and Schmahmann, J. D. (2009). Functional topography in the human cerebellum: a meta-analysis of neuroimaging studies. *NeuroImage*, 44(2):489–501.

[297] Stoodley, C. J., Valera, E. M., and Schmahmann, J. D. (2012). Functional topography of the cerebellum for motor and cognitive tasks: An fMRI study. *NeuroImage*, 59(2):1560–1570.

[298] Straube, A., Deubel, H., Ditterich, J., and Eggert, T. (2001). Cerebellar lesions impair rapid saccade amplitude adaptation. *Neurology*, 57(11):2105–2108.

[299] Strong, A. J., Fabricius, M., Boutelle, M. G., Hibbins, S. J., Hopwood, S. E., Jones, R., Parkin, M. C., and Lauritzen, M. (2002). Spreading and synchronous depressions of cortical activity in acutely injured human brain. *Stroke*, 33(12):2738–2743.

[300] Sudlow, C. L. and Warlow, C. P. (1997). Comparable studies of the incidence of stroke and its pathological types: results from an international collaboration. International Stroke Incidence Collaboration. *Stroke*, 28(3):491–499.

[301] Suzuki, S., Kimura, M., Souma, M., Ohkima, H., Shimizu, T., and Iwabuchi, T. (1990). Cerebral microthrombosis in symptomatic cerebral vasospasm–a quantitative histological study in autopsy cases. 30(5):309–316.

[302] Swift, D. M. and Solomon, R. A. (1988). Subarachnoid hemorrhage fails to produce vasculopathy or chronic blood flow changes in rats. *Stroke*, 19(7):878–882.

[303] Szapary, L., Horvath, B., Marton, Z., Alexy, T., Kesmarky, G., Habon, T., Szots, M., Koltai, K., Juricskay, I., Czopf, J., and Toth, K. (2004). Short-term effect of low-dose atorvastatin on haemorrheological parameters, platelet aggregation and endothelial function in patients with cerebrovascular disease and hyperlipidaemia. *CNS drugs*, 18(3):165–172.

[304] Teasdale, G. M., Nicoll, J. A., Murray, G., and Fiddes, M. (1997). Association of apolipoprotein E polymorphism with outcome after head injury. 350(9084):1069–1071.

[305] Thomalla, G., Glauche, V., Weiller, C., and Röther, J. (2005). Time course of wallerian degeneration after ischaemic stroke revealed by diffusion tensor imaging. *Journal of Neurology, Neurosurgery & Psychiatry*, 76(2):266–268.

[306] Thomson, H., Harper, N. J., and Parkes, A. (2007). Use of the AnaConDa anaesthetic delivery system to treat life-threatening asthma. *Anaesthesia*, 62(3):295–296.

[307] Tidswell, P., Dias, P. S., Sagar, H. J., Mayes, A. R., and Battersby, R. D. (1995). Cognitive outcome after aneurysm rupture: relationship to aneurysm site and perioperative complications. *Neurology*, 45(5):875–882.

[308] Tollard, E., Galanaud, D., Perlbarg, V., Sanchez-Peña, P., Le Fur, Y., Abdennour, L., Cozzone, P., Lehericy, S., Chiras, J., and Puybasset, L. (2009). Experience of diffusion tensor imaging and 1H spectroscopy for outcome prediction in severe traumatic brain injury: Preliminary results. *Critical Care Medicine*, 37(4):1448–1455.

[309] Toni, D., Fiorelli, M., Bastianello, S., Falcou, A., Sette, G., Ceschin, V., Sacchetti, M., and Argentino, C. (1997). Acute ischemic strokes improving during the first 48 hours of onset: predictability, outcome, and possible mechanisms. A comparison with early deteriorating strokes. *Stroke*, 28(1):10–14.

[310] Tseng, M.-Y., Czosnyka, M., Richards, H., Pickard, J. D., and Kirkpatrick, P. J. (2005). Effects of acute treatment with pravastatin on cerebral vasospasm, autoregulation, and delayed ischemic deficits after aneurysmal subarachnoid hemorrhage: a phase II randomized placebo-controlled trial. *Stroke*, 36(8):1627–1632.

[311] Vajkoczy, P., Meyer, B., Weidauer, S., Raabe, A., Thome, C., Ringel, F., Breu, V., and Schmiedek, P. (2005). Clazosentan (AXV-034343), a selective endothelin A receptor antagonist, in the prevention of cerebral vasospasm following severe aneurysmal subarachnoid hemorrhage: results of a randomized, double-blind, placebo-controlled, multicenter phase IIa study. *Journal of neurosurgery*, 103(1):9–17.

[312] van den Bergh, W. M., Algra, A., van der Sprenkel, J. W. B., Tulleken, C. A. F., and Rinkel, G. J. E. (2003). Hypomagnesemia after aneurysmal subarachnoid hemorrhage. *Neurosurgery*, 52(2):276–81; discussion 281–2.

[313] van den Bergh, W. M., Group, M. S., Algra, A., Dorhout Mees, S. M., van Kooten, F., Dirven, C. M. F., van Gijn, J., Vermeulen, M., and Rinkel, G. J. E. (2006). Randomized controlled trial of acetylsalicylic acid in aneurysmal subarachnoid hemorrhage: the MASH Study. *Stroke*, 37(9):2326–2330.

[314] van den Bergh, W. M., Zuur, J. K., Kamerling, N. A., van Asseldonk, J. T. H., Rinkel, G. J. E., Tulleken, C. A. F., and Nicolay, K. (2002). Role of magnesium in the reduction of ischemic depolarization and lesion volume after experimental subarachnoid hemorrhage. *Journal of neurosurgery*, 97(2):416–422.

[315] Van Den Kerckhoff, W. and Drewes, L. R. (1985). Transfer of the Ca-antagonists nifedipine and nimodipine across the blood-brain barrier and their regional distribution in vivo. *Journal of Cerebral Blood Flow & Metabolism*, 5:459–460.

[316] van der Hel, W. S., van den Bergh, W. M., Nicolay, K., Tulleken, K. A., and Dijkhuizen, R. M. (1998). Suppression of cortical spreading depressions after magnesium treatment in the rat. *Neuroreport*, 9(10):2179–2182.

[317] van der Schaaf, I., Wermer, M. J., van der Graaf, Y., Hoff, R. G., Rinkel, G. J. E., and Velthuis, B. K. (2006). CT after subarachnoid hemorrhage: relation of cerebral perfusion to delayed cerebral ischemia. *Neurology*, 66(10):1533–1538.

[318] Vergouwen, M., Meijers, J., Geskus, R., Coert, B., Horn, J., Stroes, E., van der Poll, T., Vermeulen, M., and Roos, Y. (2009). Biologic effects of simvastatin in patients with aneurysmal subarachnoid hemorrhage: a double-blind, placebo-controlled randomized trial. *Journal of Cerebral Blood Flow & Metabolism*, 29(8):1444–1453.

[319] Vergouwen, M. D. I., de Haan, R. J., Vermeulen, M., and Roos, Y. B. W. E. M. (2010a). Effect of statin treatment on vasospasm, delayed cerebral ischemia, and functional outcome in patients with aneurysmal subarachnoid hemorrhage: a systematic review and meta-analysis update. *Stroke*, 41(1):e47–52.

[320] Vergouwen, M. D. I., Etminan, N., Ilodigwe, D., and Macdonald, R. L. (2011a). Lower incidence of cerebral infarction correlates with improved functional outcome after aneurysmal subarachnoid hemorrhage. *Journal of cerebral blood flow and metabolism : official journal of the International Society of Cerebral Blood Flow and Metabolism*, 31(7):1545–1553.

[321] Vergouwen, M. D. I., Ilodigwe, D., and Macdonald, R. L. (2011b). Cerebral infarction after subarachnoid hemorrhage contributes to poor outcome by vasospasm-dependent and -independent effects. *Stroke*, 42(4):924–929.

[322] Vergouwen, M. D. I., Vermeulen, M., de Haan, R. J., Levi, M., and Roos, Y. B. W. E. M. (2006). Dihydropyridine calcium antagonists increase fibrinolytic activity: a systematic review. *Journal of cerebral blood flow and metabolism : official journal of the International Society of Cerebral Blood Flow and Metabolism*, 27(7):1293–1308.

[323] Vergouwen, M. D. I., Vermeulen, M., van Gijn, J., Rinkel, G. J. E., Wijdicks, E. F., Muizelaar, J. P., Mendelow, A. D., Juvela, S., Yonas, H., Terbrugge, K. G., Macdonald, R. L., Diringer, M. N., Broderick, J. P., Dreier, J. P., and Roos, Y. B. W. E. M. (2010b). Definition of Delayed Cerebral Ischemia After Aneurysmal Subarachnoid Hemorrhage as an Outcome Event in Clinical Trials and Observational Studies: Proposal of a Multidisciplinary Research Group. *Stroke*, 41(10):2391–2395.

[324] Vernieri, F., Pasqualetti, P., Matteis, M., Passarelli, F., Troisi, E., Rossini, P. M., Caltagirone, C., and Silvestrini, M. (2001). Effect of collateral blood flow and cerebral vasomotor reactivity on the outcome of carotid artery occlusion. *Stroke*, 32(7):1552–1558.

[325] Voets, N. L., Beckmann, C. F., Cole, D. M., Hong, S., Bernasconi, A., and Bernasconi, N. (2012). Structural substrates for resting network disruption in temporal lobe epilepsy. *Brain : a journal of neurology*, 135(Pt 8):2350–2357.

[326] Volpe, B. T. and Hirst, W. (1983). Amnesia following the rupture and repair of an anterior communicating artery aneurysm. *Journal of Neurology, Neurosurgery & Psychiatry*, 46(8):704–709.

[327] Waespe, W. and Baumgartner, R. (1992). Enduring dysmetria and impaired gain adaptivity of saccadic eye movements in Wallenberg's lateral medullary syndrome. *Brain : a journal of neurology*, 115 (Pt 4):1123–1146.

[328] Wagner, M., Jurcoane, A., Hildebrand, C., Guresir, E., Vatter, H., Zanella, F. E., Berkefeld, J., Pilatus, U., and Hattingen, E. (2013). Metabolic Changes in Patients with Aneurysmal Subarachnoid Hemorrhage Apart from Perfusion Deficits: Neuronal Mitochondrial Injury? *American Journal of Neuroradiology*, 34(8):1535–1541.

[329] Wang, C., Qin, W., Zhang, J., Tian, T., Li, Y., Meng, L., Zhang, X., and Yu, C. (2014). Altered functional organization within and between resting-state networks in chronic subcortical infarction. *Journal of cerebral blood flow and metabolism : official journal of the International Society of Cerebral Blood Flow and Metabolism*, 34(4):597–605.

[330] Wang, Z., Yan, C., Zhao, C., Qi, Z., Zhou, W., Lu, J., He, Y., and Li, K. (2011). Spatial patterns of intrinsic brain activity in mild cognitive impairment and Alzheimer's disease: a resting-state functional MRI study. *Human Brain Mapping*, 32(10):1720–1740.

[331] Weir, B., Grace, M., Hansen, J., and Rothberg, C. (1978). Time course of vasospasm in man. *Journal of neurosurgery*, 48(2):173–178.

[332] Wentlandt, K., Samoilova, M., Carlen, P. L., and El Beheiry, H. (2006). General anesthetics inhibit gap junction communication in cultured organotypic hippocampal slices. *Anesthesia and analgesia*, 102(6):1692–1698.

[333] Whitfield-Gabrieli, S., Thermenos, H. W., Milanovic, S., Tsuang, M. T., Faraone, S. V., McCarley, R. W., Shenton, M. E., Green, A. I., Nieto-Castanon, A., LaViolette, P., Wojcik, J., Gabrieli, J. D. E., and Seidman, L. J. (2009). Hyperactivity and hyperconnectivity of the default network in schizophrenia and in first-degree relatives of persons with schizophrenia. *Proceedings of the National Academy of Sciences of the United States of America*, 106(4):1279–1284.

[334] Williams, D. S., Detre, J. A., Leigh, J. S., and Koretsky, A. P. (1992). Magnetic resonance imaging of perfusion using spin inversion of arterial water. *Proceedings of the National Academy of Sciences of the United States of America*, 89(1):212–216.

[335] Winkler, A. M., Ridgway, G. R., Webster, M. A., Smith, S. M., and Nichols, T. E. (2014). Permutation inference for the general linear model. *NeuroImage*, 92:381–397.

[336] Woitzik, J., Dreier, J. P., Hecht, N., Fiss, I., Sandow, N., Major, S., Winkler, M., Dahlem, Y. A., Manville, J., Diepers, M., Muench, E., Kasuya, H., Schmiedek, P., and Vajkoczy, P. (2012). Delayed cerebral ischemia and spreading depolarization in absence of angiographic vasospasm after subarachnoid hemorrhage. *Journal of cerebral blood*

flow and metabolism : official journal of the International Society of Cerebral Blood Flow and Metabolism, 32(2):203–212.

[337] Wong, G. K., Boet, R., Poon, W. S., Chan, M. T., Gin, T., Ng, S. C., and Zee, B. C. (2011). Intravenous magnesium sulphate for aneurysmal subarachnoid hemorrhage: an updated systemic review and meta-analysis. *Critical Care*, 15(1):R52.

[338] Wong, G. K. C., Chan, D. Y. C., Siu, D. Y. W., Zee, B. C. Y., Poon, W. S., Chan, M. T. V., Gin, T., Leung, M., and HDS-SAH Investigators (2015a). High-dose simvastatin for aneurysmal subarachnoid hemorrhage: multicenter randomized controlled double-blinded clinical trial. *Stroke*, 46(2):382–388.

[339] Wong, G. K. C., Lam, S. W., Ngai, K., Wong, A., Siu, D., Poon, W. S., Mok, V., and Cognitive Dysfunction after Aneurysmal Subarachnoid Hemorrhage Investigators (2013). Cognitive domain deficits in patients with aneurysmal subarachnoid haemorrhage at 1 year. *Journal of Neurology, Neurosurgery & Psychiatry*.

[340] Wong, G. K. C. and Poon, W. S. (2011). Clazosentan for patients with subarachnoid haemorrhage: lessons learned. *The Lancet Neurology*, 10(10):871.

[341] Wong, G. K. C., Poon, W. S., Chan, M. T. V., Boet, R., Gin, T., Ng, S. C. P., and Zee, B. C. Y. (2010a). Plasma magnesium concentrations and clinical outcomes in aneurysmal subarachnoid hemorrhage patients: post hoc analysis of intravenous magnesium sulphate for aneurysmal subarachnoid hemorrhage trial. *Stroke*, 41(8):1841–1844.

[342] Wong, G. K. C., Poon, W. S., Chan, M. T. V., Boet, R., Gin, T., Ng, S. C. P., Zee, B. C. Y., and IMASH Investigators (2010b). Intravenous magnesium sulphate for aneurysmal subarachnoid hemorrhage (IMASH): a randomized, double-blinded, placebo-controlled, multicenter phase III trial. *Stroke*, 41(5):921–926.

[343] Wong, G. K. C., Wong, A., Zee, B. C. Y., Poon, W. S., Chan, M. T. V., Gin, T., Siu, D. Y. W., and Mok, V. C. T. (2015b). Cognitive outcome in acute simvastatin treatment for aneurysmal subarachnoid hemorrhage: A propensity matched analysis. *Journal of the Neurological Sciences*, pages 1–4.

[344] Worsley, K. J. and Friston, K. J. (1995). Analysis of fMRI time-series revisited–again. *NeuroImage*, 2(3):173–181.

[345] Wright, I. C., McGuire, P. K., Poline, J. B., Travere, J. M., Murray, R. M., Frith, C. D., Frackowiak, R. S., and Friston, K. J. (1995). A voxel-based method for the statistical analysis of gray and white matter density applied to schizophrenia. *NeuroImage*, 2(4):244–252.

[346] Wu, T., Zang, Y., Wang, L., Long, X., Hallett, M., Chen, Y., Li, K., and Chan, P. (2007). Aging influence on functional connectivity of the motor network in the resting state. *Neuroscience letters*, 422(3):164–168.

[347] Wurm, G., Tomancok, B., Nussbaumer, K., Adelwöhrer, C., and Holl, K. (2004). Reduction of ischemic sequelae following spontaneous subarachnoid hemorrhage: a double-blind, randomized comparison of enoxaparin versus placebo. *Clinical neurology and neurosurgery*, 106(2):97–103.

[348] Xi, G., Wagner, K. R., Keep, R. F., Hua, Y., de Courten-Myers, G. M., Broderick, J. P., Brott, T. G., and Hoff, J. T. (1998). Role of blood clot formation on early edema development after experimental intracerebral hemorrhage. *Stroke*, 29(12):2580–2586.

[349] Young, W. L. and Chien, S. (1989). Effect of nimodipine on cerebral blood flow and metabolism in rats during hyperventilation. *Stroke*, 20(2):275–280.

[350] Zetterling, M., Hallberg, L., Hillered, L., Karlsson, T., Enblad, P., and Ronne Engström, E. (2010). Brain energy metabolism in patients with spontaneous subarachnoid hemorrhage and global cerebral edema. *Neurosurgery*, 66(6):1102–1110.

[351] Zhang, D. and Raichle, M. E. (2010). Disease and the brain's dark energy. *Nature reviews. Neurology*, 6(1):15–28.

[352] Zhang, J., Wei, L., Hu, X., Zhang, Y., Zhou, D., Li, C., Wang, X., Feng, H., Yin, X., Xie, B., and Wang, J. (2013). Specific frequency band of amplitude low-frequency fluctuation predicts Parkinson's disease. *Behavioural Brain Research*, 252:18–23.

[353] Zhang, Y., Brady, M., and Smith, S. (2001). Segmentation of brain MR images through a hidden Markov random field model and the expectation-maximization algorithm. *IEEE transactions on medical imaging*, 20(1):45–57.

[354] Zhou, J., Payen, J.-F., Wilson, D. A., Traystman, R. J., and van Zijl, P. C. M. (2003). Using the amide proton signals of intracellular proteins and peptides to detect pH effects in MRI. *Nature medicine*, 9(8):1085–1090.

[355] Zhou, J. and van Zijl, P. C. M. (2011). Defining an Acidosis-Based Ischemic Penumbra from pH-Weighted MRI. *Translational stroke research*, 3(1):76–83.

[356] Zils, E., Sprenger, A., Heide, W., Born, J., and Gais, S. (2005). Differential effects of sleep deprivation on saccadic eye movements. *Sleep*, 28(9):1109–1115.

Appendix A: Delayed Cerebral Ischaemia: Looking Beyond Vasospasm

British Journal of Anaesthesia **109** (3): 315–29 (2012)
doi:10.1093/bja/aes264

BJA

Delayed cerebral ischaemia after subarachnoid haemorrhage: looking beyond vasospasm

M. J. Rowland*, G. Hadjipavlou, M. Kelly, J. Westbrook and K. T. S. Pattinson

Nuffield Division of Anaesthetics and FMRIB Centre, University of Oxford, John Radcliffe Hospital, Oxford OX3 9DU, UK

* Corresponding author. E-mail: mrowland@fmrib.ox.ac.uk

Editor's key points

- Delayed cerebral ischaemia (DCI) is the major cause of morbidity and mortality after aneurysmal subarachnoid haemorrhage.
- Nimodipine remains the only proven therapeutic intervention.
- Some early advances have been made in understanding the pathophysiology of DCI.
- Better understanding is required to drive therapeutic advances.

Summary. Despite improvements in the clinical management of aneurysmal subarachnoid haemorrhage over the last decade, delayed cerebral ischaemia (DCI) remains the single most important cause of morbidity and mortality in those patients who survive the initial bleed. The pathological mechanisms underlying DCI are still unclear and the calcium channel blocker nimodipine remains the only therapeutic intervention proven to improve functional outcomes after SAH. The recent failure of the drug clazosentan to improve functional outcomes despite reducing vasoconstriction has moved the focus of research into DCI away from cerebral artery constriction towards a more multifactorial aetiology. Novel pathological mechanisms have been suggested, including damage to cerebral tissue in the first 72 h after aneurysm rupture ('early brain injury'), cortical spreading depression, and microthrombosis. A greater understanding of the significance of these pathophysiological mechanisms and potential genetic risk factors is required, if new approaches to the prophylaxis, diagnosis, and treatment of DCI are to be developed. Furthermore, objective and reliable biomarkers are needed for the diagnosis of DCI in poor grade SAH patients requiring sedation and to assess the efficacy of new therapeutic interventions. The purpose of this article is to appraise these recent advances in research into DCI, relate them to current clinical practice, and suggest potential novel avenues for future research.

Keywords: cerebral vasospasm; cortical spreading depression; delayed cerebral ischaemia; early brain injury; microthrombosis; subarachnoid haemorrhage

Aneurysmal subarachnoid haemorrhage (SAH) is a devastating disease frequently leading to death or poor functional outcome. Although it only accounts for 3–5% of all strokes,[1] the economic cost of SAH is disproportionately high as it affects younger patients, who often require long-term care and cannot return to work. Only one-third of those patients who survive to discharge resume the same employment as before the event[2] and even those patients with 'good' functional outcomes are frequently left with significant residual neurocognitive deficits in areas such as memory, executive functioning, and language.[3 4]

Delayed cerebral ischaemia (DCI) is a clinical syndrome of focal neurological, cognitive deficits, or both that occurs unpredictably in ~30% of patients unpredictably 3–14 days after the initial haemorrhage.[5] While aneurysmal re-bleeding is still a significant complication in the hours following the initial bleed, DCI remains the single most important cause of mortality and morbidity in those patients who survive to definitive aneurysm treatment.[6]

Historically, it was widely considered that the primary mechanism underlying delayed neurological deterioration after SAH was narrowing of cerebral blood vessels (due to endothelial hypertrophy and vasoconstriction), leading to tissue ischaemia. This process was thought to be mediated by the presence of extravasated blood in the subarachnoid space. Arterial constriction visualized angiographically, in association with neurological deterioration seen clinically soon led to the use of the term 'vasospasm' to describe both the clinical and radiological changes. However, an emerging body of evidence now suggests that DCI is likely to have a multifactorial aetiology beyond pure cerebral arterial constriction. This has significant implications on the identification of patients at risk, diagnosis, and therapeutic interventions currently available for prophylaxis and treatment of DCI.

In the past, research into DCI has been complicated by the wide range of terms used to define the condition resulting in confusion regarding the underlying pathophysiology. The differing approaches to treating the ruptured cerebral aneurysm (either surgical clipping or endovascular coil embolization) have made comparison of trials investigating DCI difficult. In 2010, a consensus statement by a multidisciplinary group proposed new definitions for clinical deterioration caused by DCI and cerebral infarction after SAH (Table 1),[7] which will hopefully simplify study comparisons, standardize clinical endpoints, and allow accurate meta-analyses to be conducted. In 2011, the Neurocritical Care Society published consensus guidelines on the critical care management of patients after SAH.[8]

© The Author [2012]. Published by Oxford University Press on behalf of the British Journal of Anaesthesia. All rights reserved.
For Permissions, please email: journals.permissions@oup.com

Downloaded from http://bja.oxfordjournals.org/ at Bodleian Library on October 7, 2012

Table 1 Proposed definitions of DCI and cerebral infarction after SAH for use as an outcome event in clinical trials and observational studies[13]

Clinical deterioration caused by DCI
The occurrence of focal neurological impairment (such as hemiparesis, aphasia, apraxia, or neglect), or a decrease of at least 2 points on the Glasgow coma scale (either on the total score or on one of the components)
This should
(1) Last for at least 1 h (2) Not be apparent immediately after aneurysm occlusion (3) Not be attributed to other causes by means of clinical assessment, CT or MRI scanning of the brain, and appropriate laboratory studies
Cerebral infarction
The presence of cerebral infarction on either:
(1) CT or MRI scan of the brain within 6 weeks after SAH (2) The latest CT or MRI scan made before death within 6 weeks after SAH (3) Proven at autopsy
This evidence must not be present on the CT or MRI scan between 24 and 48 h after early aneurysm occlusion and must not be attributable to other causes such as surgical clipping or endovascular treatment
Hypodensities on CT imaging resulting from ventricular catheter or intraparenchymal haematoma should not be regarded as cerebral infarctions from DCI

This review concentrates on clarifying the role of vasoconstriction in DCI, highlights novel theories regarding the pathogenesis behind DCI, and summarizes the evidence for current and new therapeutic strategies. Through this, we hope to explore unanswered questions and propose directions for future research into DCI.

Vasoconstriction and DCI

Acute clinical deterioration during the period after SAH has long been known to occur after aneurysmal rupture. Early case reports showed that some patients with early improvement in neurological state after SAH rapidly and unexpectedly deteriorated and died in the days after the initial SAH.[9] Although the cause of the initial bleed was identified as cerebral aneurysm rupture, the mechanism behind this subsequent deterioration was unclear. In 1949, post-mortem examination of 27 fatal cases of SAH demonstrated infarction remote from the site of the ruptured aneurysm, despite apparently patent cerebral vessels.[10] This was attributed to 'temporary spasm of the supplying vessels . . . even of those vessels remote to the aneurysm' and was the first suggestion that cerebral arterial vasoconstriction was linked to delayed clinical deterioration after SAH.

Radiological evidence of cerebral vasoconstriction in association with SAH in patients was first described in 1951 using serial carotid arteriograms.[11] Vessel narrowing was greatest near the site of the ruptured aneurysm and correlated with extravasated blood products. It was noted that vasoconstriction was rarely seen in angiograms performed 26 days post-SAH. The hypothesis was that after the initial bleed, 'vasospasm' of cerebral arteries might lead to impaired circulation in the territory of the brain supplied by the affected vessel. In 1978, a classification for SAH based on the pattern of blood distribution seen on computed tomography (CT) in a case series of 47 patients with SAH reported an almost exact correlation between the site of the major subarachnoid blood clots and the location of severe angiographic vasoconstriction.[12] Conversely, angiographic vasoconstriction was invariably absent in those patients with minimal subarachnoid blood load. Further angiographic evidence in almost 300 SAH patients showed that this vasoconstriction began day 3 post-SAH, was maximal at days 6–8, and had disappeared by day 12.[13] As a result of this work, the concept of extravasated blood from aneurysm rupture leading to a chain reaction of cerebral artery vasoconstriction, tissue infarction, and clinical deterioration has been widely held. However, although SAH is associated with cerebral vasoconstriction[13 14] and cerebral infarction after SAH is strongly associated with poor clinical outcomes,[15 16] the exact contribution of cerebral vasoconstriction in DCI remains unclear for the following reasons:

(1) Although the incidence of angiographic vasoconstriction during the second week post-SAH (the peak incidence) is around 70%,[5] the clinically detected incidence of DCI is only around 30%.[17]
(2) After SAH, patients can develop cerebral infarction in a vascular distribution unaffected by angiographic vasoconstriction[18] and cerebral infarction seems to exert a direct effect on poor outcome independent of angiographic vasospasm.[19]
(3) The temporal relationship between angiographic evidence of vessel constriction and DCI is poor.[20]
(4) The calcium channel antagonist nimodipine remains the only pharmacological treatment to improve outcomes from DCI, yet this benefit is achieved without angiographic evidence of cerebral vasodilation.[21 22]
(5) Treating angiographic vasospasm does not always lead to improvements in clinical and functional outcomes.[23 24]

Recently, a number of new theories have been proposed that may contribute towards understanding the pathophysiology behind DCI.

Novel theories regarding DCI pathogenesis

Early brain injury

Although the initial acute cerebral ischaemia caused by aneurysmal rupture accounts for the majority of the mortality and morbidity from SAH,[25] the pathophysiological changes that occur at this time remain poorly understood and few therapeutic or diagnostic interventions are available. 'Early brain injury' is a term that refers to the damage that occurs to the brain in the first 72 h after the initial bleed

Downloaded from http://bja.oxfordjournals.org/ at Bodleian Library on October 7, 2012

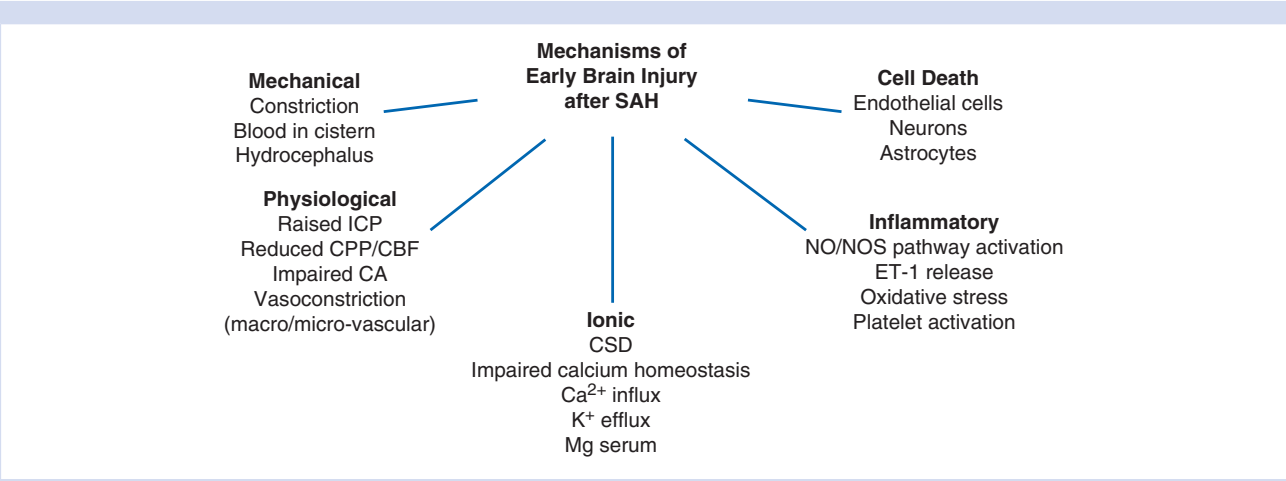


Fig 1 Mechanisms of early brain injury after SAH. ICP, intracranial pressure; CPP, cerebral perfusion pressure; CBF, cerebral blood flow; CA, cerebral autoregulation; CSD, cortical spreading depression; NO/NOS, nitric oxide/nitric oxide synthetase; ET-1, endothelin-1. Adapted, with permission, from Sehba and colleagues.[148]

(Fig. 1).[26] Although this is before the onset of DCI, it seems probable that the physiological changes occurring at this time may directly influence the likelihood and severity of later ischaemic complications in patients after SAH.

The majority of data on the pathophysiological changes that occur at the time of aneurysm rupture derives primarily from animal studies of SAH, mainly in rats. Although experimental results seem to mirror measurements in patients with aneurysmal re-bleeding and intracranial pressure (ICP) monitoring *in situ*, the majority of animal models rely on iatrogenic damage to cerebral vessels to simulate aneurysm rupture and induce subarachnoid bleeding. As a result, some authors have questioned the applicability of rat models to the study of SAH in humans,[27] and there is a need for new animal models of SAH with a high incidence of spontaneous cerebral aneurysm rupture.[28]

Initial physiological changes

At the time of the SAH, blood extravasates from a rupture in the aneurysm and leaks under high pressure into the subarachnoid space. The size of the rupture defect correlates with the volume of blood clot present.[29] Within minutes of aneurysm rupture, there is an associated rapid increase in ICP, with the rate of increase reflecting the severity of the initial bleed. This accounts for the 'thunderclap' headache seen clinically in patients and is often accompanied by syncope caused by a sudden reduction in cerebral blood flow (CBF) and cerebral perfusion pressure (CPP).[30] This sharp increase in ICP is thought to be a mechanism for arresting the initial aneurysmal bleed and preventing subsequent re-bleeding—so called 'brain tamponade'.[30] Putative causative mechanisms include increased intracranial volume secondary to the bleed, vasoparalysis (leading to increased cerebral blood volume), and cerebrospinal fluid (CSF) drainage obstruction due to blood clot.[31] There are two distinct patterns to this increase in ICP. In most patients, ICP increases to a value approximating diastolic arterial pressure, then decreases to slightly above baseline.[32] This is usually accompanied by small volume haemorrhage and the presence of cerebral oedema. The second pattern of ICP increase is less common and is characterized by a sustained increase in ICP due to enlarging haematoma or the development of acute hydrocephalus.[33 34] The peak ICP values at the time of aneurysmal rupture correspond to both the amount of blood released into the subarachnoid space and the rate of haemorrhage.[14 32 35] Marked acute cerebral vasoconstriction at this time has also been described that seems to occur independently of changes in CPP and ICP and is likely to contribute to the cerebral ischaemia from aneurysmal rupture.[14]

Cerebral oedema

Cerebral oedema is a common feature of both experimental and clinical subarachnoid haemorrhage. It is evident on admission CT scans in 6–8% of patients[6 36] and develops over the first 6 days in an additional 12%.[36] After SAH, there is substantial damage to blood–brain barrier integrity due to apoptosis of endothelial cells and perivascular astrocyte cell death.[37]

Cerebral autoregulation

Acute impairment of cerebral autoregulation is seen as a consequence of the initial aneurysmal rupture.[38 39] Cerebral autoregulation is the inherent ability of blood vessels to maintain CBF constant over a wide range of arterial pressure levels by means of complex myogenic, neurogenic, and metabolic mechanisms.[40] In humans, CBF autoregulation typically operates between mean arterial pressures of ~60 and 150 mm Hg.[41] If these autoregulatory mechanisms are disrupted, CBF becomes dependent on CPP and blood viscosity and changes in systemic arterial pressure

Downloaded from http://bja.oxfordjournals.org/ at Bodleian Library on October 7, 2012

and ICP can worsen cerebral oedema and brain tissue ischaemia.

Inflammation and oxidative stress

There is evidence to suggest early activation of inflammatory pathways after aneurysmal rupture and that the extravasated blood is responsible for a cascade of reactions involving the release of pro-inflammatory and vasoactive factors.[42] An early increase in pro-inflammatory cytokines including tumour necrosis factor-α, interleukin-6, and interleukin-1 receptor antagonist has been documented in both serum and CSF of patients after SAH, and correlates with acute and DCI and poor outcome.[43 44]

Cortical spreading depression and DCI

Over the last few years, cortical spreading depression (CSD) has been identified as a potential pathophysiological mechanism contributing to DCI. The term describes a depolarization wave in cerebral grey matter that propagates across the brain at 2–5 mm min^{-1} and results in depression of evoked and spontaneous EEG activity.[45] First demonstrated experimentally in the 1940s in rabbit cortex, the process was originally regarded as experimental artifact with little relevance to neurological disease in humans. Recently, however, there has been a resurgence of interest in CSD. Electrocorticographic recordings from invasive subdural recording strips, combined with laser Doppler measurements of regional CBF have allowed accurate quantification of the vascular changes associated with CSD. As a result, it has been implicated in the pathophysiology of a number of neurological diseases, including migraine,[46] malignant hemispheric stroke,[47] traumatic brain injury,[48] and DCI after SAH.[49]

To demonstrate CSD experimentally in healthy brain tissue, either mechanical or electrical stimulation of the cortex is required.[50] Propagation of the CSD wave silences spontaneous and evoked synaptic activity in the brain for 5–15 min, and is followed by spontaneous return to normal function.[51] Characteristic cerebrovascular changes include a brief period of vasoconstriction before the CSD, vasodilation accompanying the spreading wave front followed by delayed tissue hypoperfusion after the wave.[52]

In contrast to this, in the injured brain, CSDs can occur spontaneously and recovery of normal function can be prolonged, contributing to tissue ischaemia. The classic pattern of transient, hyperperfusion accompanying the CSD wave front seems to be different. In SAH, there is good evidence from animal models and patient studies that CSDs occur after the initial bleed.[49 53] CSDs can occur as isolated events or as clusters and there appear to be three distinct vascular responses to CSD in SAH: physiological (spreading hyperperfusion), absent (no change from baseline), and inverse haemodynamic (spreading ischaemia) (Fig. 2).[49] Spreading ischaemia was first described in a rat model of DCI and results from local microvascular dysfunction. It is thought that with each depolarization, there is an associated profound hypoperfusion of the cortex due to vasoconstriction.[54] With each wave of spreading depression, the hypoperfused segments of the cortex do not get the chance to recover and are therefore exposed to recurrent episodes of tissue ischaemia.

The incidence of CSDs measured in patients after SAH also seems to correlate with the time frame for the development of DCI, with data from one study demonstrating that 75% of all CSDs recorded occurred between the fifth and seventh day after SAH.[55] CSDs also seem to occur in the absence of angiographic vasoconstriction. Despite placement of nicardipine pellets around the middle cerebral artery (at the time of surgery) to minimize proximal vasoconstriction, spontaneous depolarizations still occurred in 10 out of 13 patients,[56] casting further doubt on the exact nature of the contribution of proximal vessel constriction to DCI.

Microthrombosis

A number of studies have shown that the coagulation cascade is activated early after the initial SAH and importantly, preceding the onset of DCI. This is most likely as a result of endothelial damage from aneurysm rupture and subsequent acute cerebral ischaemia and there is serological, clinical, and post-mortem evidence that this early activation is an early predictor of both DCI and cerebral infarction (Fig. 3).

Serological studies of patients after SAH have demonstrated activation of the coagulation cascade and impairment of the fibrinolytic cascade. Levels of platelet-activating factor start to increase within 4 days after SAH, suggesting increased platelet activation and adhesion.[57] Elevated concentrations of von Willebrand factor and CSF tissue factor (the primary initiator of coagulation) in the first few days after SAH have been shown to predict the occurrence of DCI, cerebral infarction, and poor outcome.[58 59] Other studies have shown that overactive inhibition of fibrinolysis is associated with DCI[60] and that elevated levels of fibrin degradation products and D-dimer in the CSF of patients after SAH are associated with DCI, cerebral infarction, and poor outcome.[61]

Further evidence to support the role of microthrombosis in DCI is provided by trans-cranial Doppler (TCD) detection of micro-emboli. A prospective study using TCD showed that micro-embolic signals were present in up to 70% of SAH patients, with a non-significant trend towards an increased incidence of micro-emboli in those patients who went on to develop DCI.[62]

Post-mortem studies of SAH patients have also demonstrated evidence of microthrombi. Patients with DCI have significantly more microthrombi in areas showing cerebral infarction than those patients that die from aneurysmal re-bleed or hydrocephalus.[63] Microthrombosis also correlated with the amount of overlying free subarachnoid blood and clinical and pathological signs of ischaemia.[64] Interestingly, a post-mortem study into microthrombosis after SAH showed that while cortical ischaemic lesions were present

Downloaded from http://bja.oxfordjournals.org/ at Bodleian Library on October 7, 2012

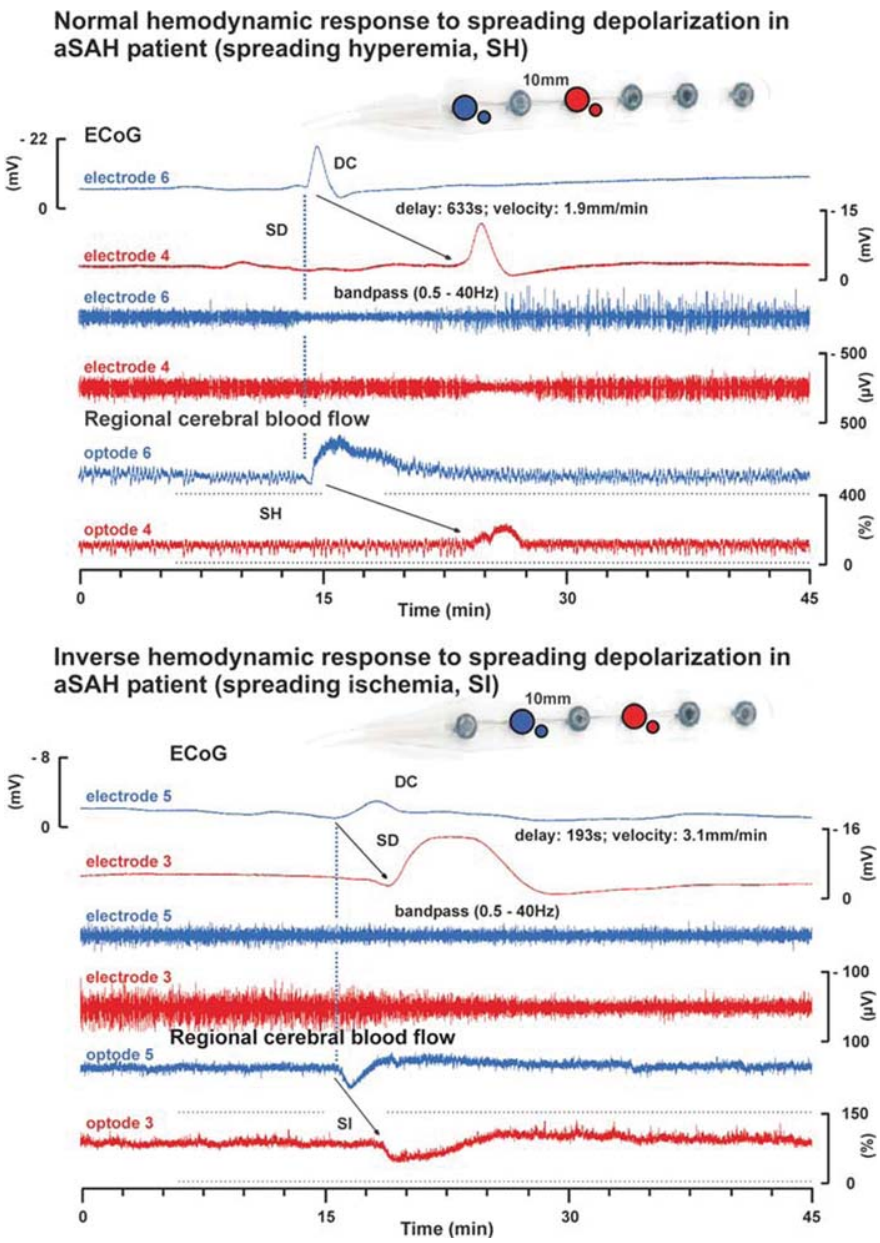


Fig 2 Normal and pathological response to cortical spreading depression (CSD) in patients with aneurysmal subarachnoid hemorrhage (aSAH). The upper half of the figure shows the normal hemodynamic response to spreading depolarization (CSD) in the human brain in a patient with aSAH. The subdural opto-electrode strip is shown in the upper right corner. The six traces represent simultaneous recordings of a single spreading depolarization that propagates from opto-electrode 6 (blue) to 4 (red). The calibration bar of trace 4 also applies to trace 3 and that of trace 6 also applies to trace 5. The four upper traces identify the spreading depolarization electrophysiologically. Traces 1 and 2: direct current (DC) electrocorticogram (ECoG) with negative shift of spreading depolarization. Traces 3 and 4: band-pass filtered ECoG (0.5 to 45 Hz) with spreading depression of activity. The spreading depolarization propagates at a rate of about 1.9 mm min^{-1} assuming an ideal linear spread along the recording strip. Traces 5 and 6: Normal spreading hyperaemia in response to spreading depolarization recorded by laser-Doppler flowmetry as reported previously (Dreier *et al.*, 2009[49]). The lower half of the figure demonstrates the inverse hemodynamic response to spreading depolarization in another patient with aSAH. In this case, the spreading depolarization propagates from opto-electrode 5 (blue) to 3 (red) (propagation rate: 3.1 mm min^{-1}). The high-frequency activity is already suppressed by a preceding CSD at electrode 4 (trace 9), when depression of activity is induced by spreading depolarization at electrode 5 (trace 10). Traces 11 and 12: typical inverse haemodynamic response to spreading depolarization as characterized by a severe decrease of regional cerebral blood flow (CBF) in response to the depolarization. Such severe decrease of regional CBF in response to CSD is termed spreading ischaemia. The prolonged negative cortical DC shift (compare trace 8) is the defining electrophysiological feature for the inverse haemodynamic response. It indicates that the hypoperfusion is significant enough to produce a mismatch between neuronal energy demand and supply (Dreier *et al.*, 1998,[149] 2009[49]). Figure and text adapted from Lauritzen *et al.*, 2011[51] JCBFM. Reprinted by permission from Macmillan Publishers Ltd, © 2011.

Downloaded from http://bja.oxfordjournals.org/ at Bodleian Library on October 7, 2012

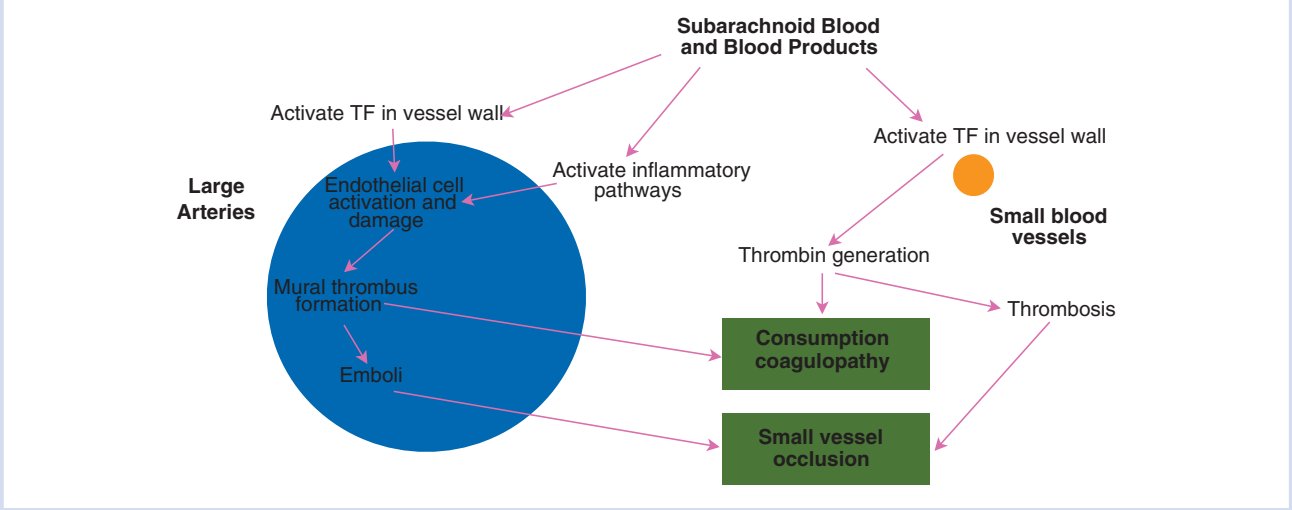


Fig 3 Potential mechanisms of microthrombosis formation after SAH. TF, tissue factor. Adapted, with permission, from Stein and colleagues.[64]

in 77% of patients, there was no significant association between the presence of these lesions and angiographic vasospasm or aneurysm location.[65]

Collateral cerebral circulation

Although the importance of the pathophysiological recruitment of collaterals in the setting of chronic haemodynamic insufficiency (such as carotid artery stenosis) has been well documented,[66 67] the impact of collateral flow in acute cerebral ischaemia is less clear. The cerebral collateral circulation consists of a subsidiary network of vascular channels that stabilize CBF when principal conduits fail.[68] Primary collaterals include the anterior and posterior communicating arteries of the circle of Willis, which immediately divert cerebral blood flow to ischaemic regions through existing anastomoses. Secondary collaterals include leptomeningeal vessels and reversal of blood flow in the ophthalmic artery, and are normally only recruited when the primary collateral circulation is inadequate.

Early clinical improvement in ischaemic stroke patients is linked to the presence of cerebral collateral blood supply.[69] Magnetic resonance imaging (MRI) studies of patients with ischaemic stroke have also shown that collateral flow in the circle of Willis is associated with a reduction in the prevalence of ischaemic lesions and minimizes the degree of residual tissue hypoperfusion after arterial occlusion.[70] Little attention is generally paid to pre-treatment collateral status in clinical practice in SAH patients. This is despite considerable heterogeneity in the presence of collateral vessels demonstrated in patients with ischaemic stroke.[70 71]

Following SAH, we speculate that patients with greater capacity for collateral flow may suffer less initial ischaemic damage from early brain injury. Furthermore, recruitment of collateral vessels may be the mechanism behind the reversal of neurological deficits seen with induced hypertension as part of triple-H therapy. Clinical assessment of collateral flow is usually limited to CT or MR angiography with the former requiring ionizing radiation and both requiring i.v. contrast. Improvements in MRI sequences now allow the non-invasive assessment of flow in the circle of Willis and other cerebral collateral pathways such as the ophthalmic artery. Identifying those patients with poor collateral flow may enable earlier treatment strategies, such as induced hypertension, to improve cerebral perfusion.

How have clinical therapeutic interventions aided the understanding of DCI?

At present, the majority of therapeutic strategies targeting DCI are focused on reducing secondary ischaemic brain injury and treating cerebral vasoconstriction. However, the exact role of cerebral vasoconstriction remains unclear and as a result, the rationale behind some treatment strategies requires further examination.

Clazosentan

Clazosentan is an endothelin (ET)-A antagonist that was heralded as a potential pharmacological treatment for DCI after SAH. As ET is known to play a key role in maintaining vascular tone in blood vessels, it was hypothesized that pharmacological antagonism of ET receptors might be of therapeutic benefit in reducing cerebral vasospasm and DCI. The ET receptor antagonist TAK-044 was studied but showed no beneficial effects on DCI, cerebral infarction, or functional outcome at 3 months (as measured by the Glasgow outcome score). This was attributed to non-selective antagonism of both ET-A and ET-B receptors.[72] Further studies using clazosentan, a selective ET-A receptor antagonist, showed promise with a reduction in the frequency and severity of vasospasm after SAH[73] and a reduction in vasospasm-associated impaired cerebral perfusion.[74]

Downloaded from http://bja.oxfordjournals.org/ at Bodleian Library on October 7, 2012

Unfortunately, the subsequent multicentre CONSCIOUS-1 randomized control trial (RCT) showed that despite significant reductions in angiographic cerebral vasoconstriction, clazosentan failed to show a significant effect on morbidity and mortality and no obvious effect on functional outcome.[23] Furthermore, clazosentan showed no significant benefit in a subgroup of SAH patients treated with surgical clipping, leading to the early termination of the CONSCIOUS-2 trial[75] and the cancellation of the planned CONSCIOUS-3 trial in SAH patients treated with endovascular coiling.[76] From the CONSCIOUS trials, it would appear that, despite questions raised regarding study design, duration of treatment, and scoring scales,[77] the pathophysiological mechanism behind DCI is likely to extend beyond pure large vessel vasoconstriction. The effect of clazosentan on the cerebral microcirculation is unclear and the drug seems to have little effect on the coagulation disturbances seen after SAH such as microthrombosis.[78]

Nimodipine

Despite extensive research into pharmacological treatment of DCI, the L-type dihydropyridine calcium channel antagonist nimodipine remains the only intervention to consistently reduce the incidence of DCI and improve outcomes after SAH. Calcium plays a critical role in cellular communication and regulation and is important for the maintenance of normal cerebral vascular tone.[79] Uncontrolled intracellular shifts in calcium concentration associated with cerebral ischaemia cause irreversible cell destruction and death, especially in the central nervous system[80] and as a result, calcium is likely to play an important role in initiating, mediating, and propagating damage to cells after SAH.

Nimodipine was first tested as a treatment for DCI due to its preferential vasodilation of the cerebral circulation and experimental work showing reduced impairment of post-ischaemic reperfusion.[81] The largest clinical trial of nimodipine on DCI (the British Aneurysm Nimodipine Trial) randomized patients to either oral nimodipine 60 mg at 4 h intervals or placebo for 21 days after SAH[82] and showed significant reductions in both the incidence of cerebral infarction and poor neurological outcomes at 3 months post-SAH. Further meta-analyses including a Cochrane review in 2007[83] have echoed these findings and led to oral nimodipine becoming a standard of care for patients from the time of the initial haemorrhage.[22 83]

The precise mechanism behind the beneficial effects of nimodipine remains unclear and seems independent of any action on large vessel angiographic vasoconstriction.[21] It may be that nimodipine has a neuroprotective effect in SAH by blocking calcium influx after tissue ischaemia at a neuronal level.[84] However, as nimodipine does not exert a beneficial effect on other diseases that lead to cerebral ischaemia such as ischaemic stroke[85] or traumatic brain injury,[86] it seems likely that it acts on a mechanism specific to SAH. A systematic review of calcium antagonists showed that nimodipine significantly increases endogenous fibrinolytic activity and that this effect is not found with other calcium antagonists such as phenylalkylamines.[87] This may act to reduce the incidence of microthrombosis after SAH. Finally, there is evidence that nimodipine antagonizes cortical spreading ischaemia in rats,[88] and this may be of importance, given the potential role of CSD in the pathogenesis of DCI.

Induced hypertension, hypervolaemia, and haemodilution ('triple-H therapy')

Haemodynamic strategies to induce hypertension, hypervolaemia, and haemodilution remain the mainstay of the neurocritical care management of DCI. However, despite its widespread use, much of the literature supporting triple-H therapy is only of moderate quality with RCTs only addressing prophylactic use.

The physiological rationale behind triple-H therapy is based on the haemodynamic consequences of cerebral arterial vasoconstriction. As vessel diameter decreases, cerebrovascular resistance shifts from smaller penetrating arterioles to the major branches of the circle of Willis. As a result, brain tissue supplied by these narrowed proximal branches loses its capacity for autoregulation and CBF varies directly with systemic arterial pressure according to the Hagen–Poiseuille law. Therefore, given that the vessel diameter is fixed, the only variables that can potentially be manipulated to improve CBF in patients after SAH are the pressure gradient (i.e. systemic arterial pressure) and blood viscosity (i.e. haematocrit).

Early anecdotal evidence suggested that hypotension could lead to neurological deficits in patients after 'cerebrovascular accidents'.[89] This seemed especially significant in those patients where hypotension was associated with evidence of structural narrowing of major cerebral blood vessels. As a result, induced hypertension was tried in patients after SAH with an early case series showing reversal of neurological deficits in six out of seven patients through the use of norepinephrine to increase arterial pressure and volume expansion with colloid.[90] A larger retrospective review of induced hypertension and volume expansion in 58 patients supported these findings.[91] However, there were significant complications including aneurysmal re-bleeding (19%), pulmonary oedema (17%), dilutional hyponatraemia (3%), and coagulopathy (3%).

Recent studies of triple-H therapy in DCI have attempted to use physiological outcome measures such as brain tissue oxygenation and CBF to assess the individual contribution of each of the components of haemodynamic augmentation, that is, induced systemic hypertension (either through vasopressors or inotropes), volume expansion, and haemodilution. A Cochrane review of three studies analysing the evidence supporting volume expansion therapy concluded a lack of benefit, and that hypervolaemia could potentially increase complications after SAH.[92] A recent meta-analysis found no good evidence for a positive effect of triple-H therapy or any of its components on CBF after SAH.[93]

Downloaded from http://bja.oxfordjournals.org/ at Bodleian Library on October 7, 2012

Haemodilution did not increase CBF and hypervolaemia was only beneficial in one of seven trials.

The consensus guidelines recently published by the Neurocritical Care Society[8] make a number of recommendations regarding each of the individual components of triple-H therapy. It seems that any benefit that might occur from haemodynamic manipulation of SAH patients is likely to primarily derive from increasing or stabilizing systemic arterial pressure and avoidance of hypovolaemia. Owing to its widespread use, randomized outcome studies of induced hypertension and untreated control groups are now unlikely. Further research is needed into the timing and effects of different pharmacological and mechanical strategies for inducing hypertension on outcomes from DCI.

Magnesium

Magnesium is a non-competitive calcium channel antagonist and potent vasodilator with known neuroprotective properties. Hypomagnesaemia occurs in more than 50% of patients with SAH, is related to severity of bleed, and is predictive of DCI.[94] As a result, a number of studies have investigated the role of i.v. magnesium therapy in preventing and treating DCI.

In animal models of SAH, magnesium reverses delayed cerebral arterial vasoconstriction and reduces the size of ischaemic lesions.[95] There is evidence to suggest that magnesium reduces the rate and frequency of CSD.[96] However, the only phase III RCT conducted to date [Intravenous Magnesium Sulphate for Aneurysmal Subarachnoid Haemorrhage (IMASH) trial] showed no difference in the proportion of patients with a favourable outcome at 6 months or in the incidence of DCI or cerebral infarction. A *post hoc* analysis showed an association between high plasma magnesium concentrations and worse clinical outcomes.[97]

The results of this trial have considerably dampened enthusiasm for the routine use of magnesium and an updated systematic review and meta-analysis further demonstrated no beneficial effect of magnesium in DCI.[98] As a result, it has been recommended in the Neurocritical Care Society guidelines that magnesium should not routinely be given to patients after SAH (although hypomagnesaemia should be avoided).[8]

Statins

There has been interest in using statins in SAH, for both the prevention and treatment of DCI. The pleiotropic vascular effects of statins include beneficial actions on endothelial inflammation,[99] oxidative stress,[100] and the inhibition of platelet adhesion and aggregation[101] and these underlie the benefits they exert on atherosclerotic cardiovascular disease. Given that statins are relatively safe, cheap, and easy to administer, they seem a logical intervention to trial in the prevention of DCI.

Animal studies have demonstrated that statins may ameliorate early brain injury after experimental SAH[102] and improve neurocognitive outcomes.[103] To date, four prospective, randomized, placebo-controlled trials have been published evaluating the efficacy of statins in the prevention of DCI. These investigated a combined total of 190 patients with three of the studies trialling simvastatin 80 mg for 14–21 days[104–106] and one study trialling pravastatin 40 mg for a maximum of 14 days.[107] Although the first two published studies reported beneficial effects in reducing episodes of DCI, TCD vasospasm, and mortality, these findings were not found in the more recent studies. There was also significant variation in the proportion of clipped and coiled patients and high-grade patients between the studies making comparison difficult. Additionally, although up to 50% of patients in the pravastatin trial did not complete the course of treatment, results were still analysed on an intention-to-treat basis.[107] A recent meta-analysis of RCTs included these four studies and reported that statins had no significant effect on any of the relevant outcomes, including clinical episodes of DCI, mortality, poor neurological recovery, and TCD vasospasm.[108]

Given the efficacy of statin pre-treatment in animal models,[109] the impact of prior statin use in patients presenting with SAH has also been investigated in observational studies. Two studies demonstrated reductions in DCI and improved clinical outcomes in SAH patients with previous statin use.[110 111] However, continuity of statin therapy on admission was not clearly discussed in either study and further studies have shown either no benefit or increased risk of DCI in patients pre-treated with statins, although this latter finding was reported as being caused by statin withdrawal on admission.[112 113]

Although statin therapy seems safe post-SAH in statin-naïve patients, it remains unclear whether statins exert a beneficial effect in preventing DCI and improving clinical outcomes. The Neurocritical Care Society Guidelines recommend that patients on statins before presentation with SAH should have their medication continued in the acute phase but only suggest that acute statin therapy 'may be considered' in statin-naïve patients.[8] Hopefully, the results of a larger, prospective randomized controlled study—the Simvastatin in Aneurysmal Subarachnoid Haemorrhage ('STASH') Trial—that has recently restarted patient recruitment should help clarify whether statins should be routinely given to all patients after SAH.[114]

Anti-coagulant/anti-fibrinolytic therapy

As activation of the coagulation cascade and microthrombi may play a role in the pathogenesis of DCI, attention has focused on drugs targeting these processes. Aspirin was used in an attempt to reduce DCI by reducing platelet adhesion and aggregation. A systematic review of five trials with a total of 700 patients suggested a reduction in the risk of DCI in SAH patients. However, an RCT investigating the effect of 100 mg aspirin was stopped early as an interim analysis suggested that the probability of a beneficial effect was negligible.[115] Although a Cochrane review in 2007 suggested a trend towards better outcome in patients treated with anti-

Downloaded from http://bja.oxfordjournals.org/ at Bodleian Library on October 7, 2012

platelet agents, this was non-significant and accompanied by the possibility of an increase in the risk of haemorrhagic complications.[116]

The role of low molecular weight heparins (LMWHs) in DCI has also been investigated. The anti-coagulant activity (antagonism of antithrombin III) of LMWH may prevent the formation and spread of microthrombi and there is evidence of neuroprotective effects. They act on complement and neutrophils to reduce cerebral inflammation in response to ischaemic lesions,[117 118] have anti-oedema properties,[119] and may reduce intra-neuronal calcium release after ischaemic injury.[120] However, two large placebo-controlled RCTs studying enoxaparin and DCI demonstrated contradictory results,[121 122] and further, large, multicentre trials are required to clarify whether these drugs have a beneficial effect on reducing DCI.

A Cochrane review of anti-fibrinolytic therapy for the prevention of aneurysmal re-bleeding showed that reductions in mortality from re-bleeding were offset by an increase in poor outcome from DCI.[123] The potential of intrathecal fibrinolysis has been investigated and although a systematic review showed a significant risk reduction in DCI and poor outcome, only one of the nine studies was an RCT and its role remains unclear.[124]

Future directions for DCI research

Determining the genetic determinants of DCI

It seems logical that genotypic variability may define the susceptibility of individual patients to both the initial ischaemic injury caused by aneurysmal rupture and subsequent secondary damage caused by DCI. Genetic predisposition to the individual pathophysiological mechanisms that may underlie DCI such as cerebral vasoconstriction, CSD, and microthrombosis may vary between individual patients.

Endothelial nitric oxide synthase

Much of the research into genetic influences underlying DCI has focused on reducing cerebral vasoconstriction—in particular through targeting the gene encoding the endothelial isoform of nitric oxide synthase (eNOS). Nitric oxide (NO) inhibits smooth muscle proliferation and inflammation—both pathophysiological features of the cerebral vasoconstriction seen after SAH. There is evidence that certain eNOS polymorphisms are significantly associated with angiographic cerebral arterial narrowing after SAH, and also cerebral aneurysm rupture.[125 126] However, others have shown no association between eNOS polymorphisms and cerebral infarction or the incidence of clinical deterioration in patients.[127] This suggests that the influence of eNOS polymorphisms is primarily limited to vascular constriction and further questions the significance of the contribution of vessel narrowing to DCI.

Apolipoprotein E

The association between apolipoprotein E (ApoE) and neurocognitive outcomes after SAH has been investigated. ApoE is a carrier protein that combines with lipids to form lipoprotein particles which is involved in the metabolism and transport of lipids in the central nervous system. Three common alleles of the ApoE gene are found in humans—ε2, ε3, and ε4. The presence of the ε4 allele is known to be associated with increased risk of developing Alzheimer's disease[128] and poor outcomes after traumatic brain injury,[129] and intracerebral haemorrhage,[130] although this association does not seem to extend to ischaemic stroke.[131]

The association between ApoE and DCI is conflicting, with an animal model of SAH showing that mice expressing the ε4 protein have greater cerebral vasoconstriction, functional deficit, and mortality after SAH than those with the ε3 protein.[132] However, in SAH patients, an association between ApoE4 and poor functional outcomes[133] and a meta-analysis of eight observational studies concluded that the expression of the ε4 allele is associated with an increased risk of poor outcome and delayed ischaemia.[134]

The most recent prospective study found that neither the ε2 nor the ε4 allele was associated with infarction or poor outcome and concluded that ApoE polymorphisms have no prognostic value for outcome after SAH.[135] The largest association study of ApoE and SAH showed no significant difference between the presence of the ApoE4 genotype and functional outcomes at 3 and 6 months when controlling for age, size of haemorrhage, and clinical severity of SAH.[136] However, when severity of cerebral arterial vasospasm was controlled between the groups, individuals with the ε4 allele had worse functional outcomes at both time points. This suggests that the ε4 allele may not directly influence cerebral vasoconstriction and may instead act to modulate the response of brain tissue to ischaemia.

Although a number of theories have been proposed including protection from oxidative injury[136] and suppression of lymphocyte proliferation and glial cytokine secretion,[137] further work is required to clarify the specific mechanism by which ApoE is associated with DCI and whether certain alleles can be used to reliably identify patients at risk. Further investigation of the impact of genetic influences in response to therapeutic interventions such as induced hypertension, statins, and nimodipine is required, in addition to further research into those genes that regulate inflammation and fibrinolysis.

The interaction between anaesthetic agents and CSD

Many SAH patients require surgical, endovascular, or neurocritical care interventions where significant quantities of anaesthetic sedative agents are required either to facilitate mechanical ventilation or control ICP. Although current evidence indicates that volatile agents, barbiturates, and propofol may have neuroprotective actions, the interaction between these sedative agents and DCI remains unclear. If CSD plays some role in the pathogenesis of DCI, the choice of sedative agent may be important. Most of the research on anaesthetic agents and CSD has focused on the effect of volatile inhalation agents on animal models of brain

Downloaded from http://bja.oxfordjournals.org/ at Bodleian Library on October 7, 2012

injury, looking for changes in CSD frequency and intensity. Studies in rats have shown that halothane, and to a lesser extent isoflurane and nitrous oxide, protect against the initiation of CSDs in the cortex[138] and that nitrous oxide decreases CSD propagation speed and duration.[139] Increasing the concentration of volatile anaesthetic agents results in a dose-dependent reduction in CSD frequency,[140] possibly linked to the increase in CBF seen with most volatile anaesthetic agents. Although the use of volatile anaesthetic agents in the intensive care or emergency room setting is rare, the AnaConDa device (anaesthetic conserving device) has enabled their use in the treatment of refractory status asthmaticus[141] and may offer a potential solution in SAH.

There is currently no data published comparing the effects of inhalation and i.v. agents on CSD. This is especially important as i.v. agents such as propofol, fentanyl, and remifentanil are extensively used in both neuroanaesthesia and neurocritical care. The effect of propofol on CSD has yet to be formally investigated, although evidence that propofol, and thiopental, attenuate gap–junction coupling[142] and that thiopental may reduce the incidence of CSD *in vitro* may be relevant.[143] Ketamine, known to increase ICP and therefore rarely used in the management of patients with SAH, may also behave like volatile agents and block CSD.[144] This evidence has been reinforced by case reports showing the inhibition of CSD and restoration of normal electrocorticographic activity with ketamine in intracranial haemorrhage.[145] As a result, more research into the choice of sedative agent and CSD is needed.

Biomarkers for DCI

The delay between aneurysmal rupture and the onset of DCI offers a unique opportunity to apply a therapeutic intervention to patients after SAH. The recent consensus definitions quoted earlier in this article should be commended for providing a clear 'threshold' for the clinical diagnosis of DCI in patients. However, given that the majority of patients with poor grade SAH require sedation and mechanical ventilation, diagnosis of DCI by clinical assessment is often impossible. It also seems logical to suggest that DCI is in fact a spectrum of disease with patients exhibiting varying degrees of severity. If this is the case, then the reliance of this clinical definition on a change in Glasgow coma scale, which is relatively insensitive to subtle changes in neurocognitive function, may leave some patients with sub-threshold DCI undiagnosed and untreated.

Identifying objective biomarkers for DCI therefore remains a key research priority. Unfortunately, the uncertain pathophysiology of DCI has made this process difficult with no specific or sensitive serum or CSF biomarker currently available. Measures of axonal degeneration such as CSF neurofilament heavy chains (NfH) have shown some early promise in identifying secondary ischaemic damage caused by DCI and may be useful in those patients who require CSF diversion on the neurocritical care unit.[146] Other serum markers such as high-sensitivity C-reactive protein may identify the inflammatory activation that is specifically related to DCI.[147]

Currently, the invasive nature of the monitoring required negates investigation of the incidence of CSD in those patients who do not require neurosurgical intervention. Quantifying the vascular changes associated with CSD—such as the suppression of low-frequency vascular oscillations[49]—non-invasively using MRI or near-infrared spectroscopy may offer a surrogate measure of CSDs in those patients with less severe grade SAH who undergo endovascular aneurysm treatment.

Evidence suggests that CSDs are associated with cerebral ischaemia after poor grade SAH and are likely to contribute towards DCI. However, the absence of non-invasive biomarkers of CSD means the overall frequency of CSDs in patients after SAH remains unknown and the role of inhalation and i.v. anaesthetic agents and also treatments such as nimodipine and magnesium on CSD requires further investigation. Future studies into DCI will benefit from clear consensus definitions and clinical endpoints and should focus on the following questions that currently remain unanswered:

(1) Why is nimodipine the only pharmacological treatment to reduce the incidence of DCI and improve ischaemic outcomes and what is the mechanism behind this effect?
(2) Can we develop more accurate experimental models of spontaneous aneurysm rupture that might replicate the physiological changes more accurately?
(3) Does the initial period post-aneurysmal rupture offer a diagnostic and therapeutic target for interventions aimed at reducing the incidence of DCI and improving outcomes?
(4) How important is CSD in the aetiology of DCI and what effect do current therapeutic interventions used in SAH have on its incidence and progression?
(5) Is it possible to identify objective biochemical, electrocortical, or neuroimaging biomarkers of DCI that will allow earlier identification of those at risk (especially in sedated patients) and act as a target for future research into novel treatments?
(6) Can we influence DCI at a genetic level both to identify patients at risk and to guide application of therapeutic interventions?

In conclusion, DCI remains the major cause of mortality and morbidity in those patients who survive the initial bleed to hospital treatment. It now seems clear that DCI has a multifactorial aetiology beyond pure cerebral vasoconstriction and that future management strategies are likely to be based on combination therapies targeting vasoconstriction, disturbed neuronal function, and disturbed neurovascular coupling.[49] The interval between aneurysmal rupture and the onset of DCI provides a window for the application of preventative pharmacological therapies. Currently, however, the majority of therapeutic strategies in clinical use remain focused on improving cerebral perfusion in patients *after* the onset of DCI symptoms. More research is therefore required into the acute changes in cerebral physiology

Downloaded from http://bja.oxfordjournals.org/ at Bodleian Library on October 7, 2012

occurring in the first 72 h after SAH that may offer potential diagnostic and therapeutic targets for DCI in the future.

Declaration of interest

None declared.

Funding

The authors' research into subarachnoid haemorrhage is supported by a *BJA*/RCOA grant from the National Institute of Academic Anaesthesia. M.J.R. is supported by the NIHR Oxford Biomedical Research Centre and the Oxford University Clinical Academic Graduate School. K.T.S.P. and M.J.R. are supported by the Medical Research Council, UK.

References

1 Sudlow CL, Warlow CP. Comparable studies of the incidence of stroke and its pathological types: results from an international collaboration. International Stroke Incidence Collaboration. *Stroke* 1997; **28**: 491–9

2 Passier PECA, Visser-Meily JMA, Rinkel GJE, Lindeman E, Post MWM. Life satisfaction and return to work after aneurysmal subarachnoid hemorrhage. *J Stroke Cerebrovasc Dis* 2011; **20**: 324–9

3 Al-Khindi T, Macdonald RL, Schweizer TA. Cognitive and functional outcome after aneurysmal subarachnoid hemorrhage. *Stroke* 2010; **41**: e519–36

4 Scott RB, Eccles F, Molyneux AJ, Kerr RSC, Rothwell PM, Carpenter K. Improved cognitive outcomes with endovascular coiling of ruptured intracranial aneurysms: neuropsychological outcomes from the International Subarachnoid Aneurysm Trial (ISAT). *Stroke* 2010; **41**: 1743–7

5 Dorsch NW, King MT. A review of cerebral vasospasm in aneurysmal subarachnoid haemorrhage Part I: incidence and effects. *J Clin Neurosci* 1994; **1**: 19–26

6 Kassell N, Torner J, Clarke Haley E Jr, *et al.* The international cooperative study on the timing of aneurysm surgery. *J Neurosurg* 1990; **73**: 18–36

7 Vergouwen MDI, Vermeulen M, van Gijn J, *et al.* Definition of delayed cerebral ischemia after aneurysmal subarachnoid hemorrhage as an outcome event in clinical trials and observational studies: proposal of a multidisciplinary research group. *Stroke* 2010; **41**: 2391–5

8 Diringer MN, Bleck TP, Claude Hemphill J, *et al.* Critical care management of patients following aneurysmal subarachnoid hemorrhage: recommendations from the Neurocritical Care Society's Multidisciplinary Consensus Conference. *Neurocrit Care* 2011; **15**: 211–40

9 Beadles C. Aneurisms of the larger cerebral arteries. *Brain* 1907; **30**: 285–336

10 Robertson EG. Cerebral lesions due to intracranial aneurysms. *Brain* 1949; **72** (Pt 2): 150–85

11 Ecker A, Riemenschneider P. Arteriographic demonstration of spasm of the intracranial arteries, with special reference to saccular arterial aneurysms. *J Neurosurg* 1951; **8**: 660–7

12 Fisher CM, Kistler JP, Davis JM. Relation of cerebral vasospasm to subarachnoid hemorrhage visualized by computerized tomographic scanning. *Neurosurgery* 1980; **6**: 1–9

13 Weir B, Grace M, Hansen J, Rothberg C. Time course of vasospasm in man. *J Neurosurg* 1978; **48**: 173–8

14 Bederson JB, Levy AL, Ding WH, *et al.* Acute vasoconstriction after subarachnoid hemorrhage. *Neurosurgery* 1998; **42**: 352–60

15 Fergusen S, Macdonald RL. Predictors of cerebral infarction in patients with aneurysmal subarachnoid hemorrhage. *Neurosurgery* 2007; **60**: 658–67

16 Vergouwen MDI, Etminan N, Ilodigwe D, Macdonald RL. Lower incidence of cerebral infarction correlates with improved functional outcome after aneurysmal subarachnoid hemorrhage. *J Cereb Blood Flow Metab* 2011; **31**: 1545–53

17 Dorsch N. A clinical review of cerebral vasospasm and delayed ischaemia following aneurysm rupture. *Acta Neurochir Suppl* 2011; **110** (Pt 1): 5–6

18 Naidech AM, Drescher J, Tamul P, Shaibani A, Batjer HH, Alberts MJ. Acute physiological derangement is associated with early radiographic cerebral infarction after subarachnoid haemorrhage. *J Neurol Neurosurg Psychiatr* 2006; **77**: 1340–4

19 Vergouwen MDI, Ilodigwe D, Macdonald RL. Cerebral infarction after subarachnoid hemorrhage contributes to poor outcome by vasospasm-dependent and -independent effects. *Stroke* 2011; **42**: 924–9

20 Minhas PS, Menon DK, Smielewski P, *et al.* Positron emission tomographic cerebral perfusion disturbances and transcranial Doppler findings among patients with neurological deterioration after subarachnoid hemorrhage. *Neurosurgery* 2003; **52**: 1017–24

21 Petruk KC, West M, Mohr G, *et al.* Nimodipine treatment in poor-grade aneurysm patients. Results of a multicenter double-blind placebo-controlled trial. *J Neurosurg* 1988; **68**: 505–17

22 Feigin VL, Rinkel GJ, Algra A, Vermeulen M, van Gijn J. Calcium antagonists in patients with aneurysmal subarachnoid hemorrhage: a systematic review. *Neurology* 1998; **50**: 876–83

23 Macdonald RL, Kassell NF, Mayer S, *et al.* Clazosentan to overcome neurological ischemia and infarction occurring after subarachnoid hemorrhage (CONSCIOUS-1): randomized, double-blind, placebo-controlled phase 2 dose-finding trial. *Stroke* 2008; **39**: 3015–21

24 Polin RS, Coenen VA, Hansen CA, *et al.* Efficacy of transluminal angioplasty for the management of symptomatic cerebral vasospasm following aneurysmal subarachnoid hemorrhage. *J Neurosurg* 2000; **92**: 284–90

25 Broderick JP, Brott TG, Duldner JE, Tomsick T, Leach A. Initial and recurrent bleeding are the major causes of death following subarachnoid hemorrhage. *Stroke* 1994; **25**: 1342–7

26 Kusaka G, Ishikawa M, Nanda A, Granger DN, Zhang JH. Signaling pathways for early brain injury after subarachnoid hemorrhage. *J Cereb Blood Flow Metab* 2004; **24**: 916–25

27 Swift DM, Solomon RA. Subarachnoid hemorrhage fails to produce vasculopathy or chronic blood flow changes in rats. *Stroke* 1988; **19**: 878–82

28 Aoki T, Nishimura M. The development and the use of experimental animal models to study the underlying mechanisms of CA formation. *J Biomed Biotechnol* 2011; **2011**: 1–10

29 Sobey CG. Cerebrovascular dysfunction after subarachnoid haemorrhage: novel mechanisms and directions for therapy. *Clin Exp Pharmacol Physiol* 2001; **28**: 926–9

30 Nornes H. The role of intracranial pressure in the arrest of hemorrhage in patients with ruptured intracranial aneurysm. *J Neurosurg* 1973; **39**: 226–34

31 Grote E, Hassler W. The critical first minutes after subarachnoid hemorrhage. *Neurosurgery* 1988; **22**: 654

32 Bederson JB, Germano IM, Guarino L. Cortical blood flow and cerebral perfusion pressure in a new non-craniotomy model

Downloaded from http://bja.oxfordjournals.org/ at Bodleian Library on October 7, 2012

of subarachnoid hemorrhage in the rat. *Stroke* 1995; **26**: 1086–91
33 Nornes H, Magnaes B. Intracranial pressure in patients with ruptured saccular aneurysm. *J Neurosurg* 1972; **36**: 537–47
34 Asano T, Sano K. Pathogenetic role of no-reflow phenomenon in experimental subarachnoid hemorrhage in dogs. *J Neurosurg* 1977; **46**: 454–66
35 Schwartz AY, Masago A, Sehba FA, Bederson JB. Experimental models of subarachnoid hemorrhage in the rat: a refinement of the endovascular filament model. *J Neurosci Methods* 2000; **96**: 161–7
36 Claassen J, Carhuapoma J, Kreiter K, Du E, Connolly E, Mayer S. Global cerebral edema after subarachnoid hemorrhage: frequency, predictors, and impact on outcome. *Stroke* 2002; **33**: 1225
37 Keep RF, Andjelkovic AV, Stamatovic SM, Shakui P, Ennis SR. Ischemia-induced endothelial cell dysfunction. *Acta Neurochir Suppl* 2005; **95**: 399–402
38 Rätsep T, Asser T. Cerebral hemodynamic impairment after aneurysmal subarachnoid hemorrhage as evaluated using transcranial Doppler ultrasonography: relationship to delayed cerebral ischemia and clinical outcome. *J Neurosurg* 2001; **95**: 393–401
39 Lang EW, Diehl RR, Mehdorn HM. Cerebral autoregulation testing after aneurysmal subarachnoid hemorrhage: the phase relationship between arterial blood pressure and cerebral blood flow velocity. *Crit Care Med* 2001; **29**: 158–63
40 Aries MJH, Elting JW, De Keyser J, Kremer BPH, Vroomen PCAJ. Cerebral autoregulation in stroke: a review of transcranial Doppler studies. *Stroke* 2010; **41**: 2697–704
41 Paulson OB, Strandgaard S, Edvinsson L. Cerebral autoregulation. *Cerebrovasc Brain Metab Rev* 1990; **2**: 161–92
42 Ayer R, Zhang J. Connecting the early brain injury of aneurysmal subarachnoid hemorrhage to clinical practice. *Turk Neurosurg* 2010; **20**: 159–66
43 Osuka K, Suzuki Y, Tanazawa T, *et al.* Interleukin-6 and development of vasospasm after subarachnoid haemorrhage. *Acta Neurochir* 1998; **140**: 943–51
44 Mathiesen T, Edner G, Ulfarsson E, Andersson B. Cerebrospinal fluid interleukin-1 receptor antagonist and tumor necrosis factor-alpha following subarachnoid hemorrhage. *J Neurosurg* 1997; **87**: 215–20
45 Leao A. Spreading depression of activity in the cerebral cortex. *J Neurophysiol* 1944; **7**: 359
46 Lauritzen M. Pathophysiology of the migraine aura. The spreading depression theory. *Brain* 1994; **117** (Pt 1): 199–210
47 Dohmen C, Sakowitz OW, Fabricius M, *et al.* Spreading depolarizations occur in human ischemic stroke with high incidence. *Ann Neurol* 2008; **63**: 720–8
48 Strong AJ, Fabricius M, Boutelle MG, *et al.* Spreading and synchronous depressions of cortical activity in acutely injured human brain. *Stroke* 2002; **33**: 2738–43
49 Dreier JP, Major S, Manning A, *et al.* Cortical spreading ischaemia is a novel process involved in ischaemic damage in patients with aneurysmal subarachnoid haemorrhage. *Brain* 2009; **132** (Pt 7): 1866–81
50 Leao A. Pial circulation and spreading depression of activity in the cerebral cortex. *J Neurophysiol* 1944; **7**: 391–6
51 Lauritzen M, Dreier JP, Fabricius M, Hartings JA, Graf R, Strong AJ. Clinical relevance of cortical spreading depression in neurological disorders: migraine, malignant stroke, subarachnoid and intracranial hemorrhage, and traumatic brain injury. *J Cereb Blood Flow Metab* 2011; **31**: 17–35
52 Lauritzen M. Long-lasting reduction of cortical blood flow of the brain after spreading depression with preserved autoregulation and impaired CO_2 response. *J Cereb Blood Flow Metab* 1984; **4**: 546–54
53 Dreier JP, Woitzik J, Fabricius M, *et al.* Delayed ischaemic neurological deficits after subarachnoid haemorrhage are associated with clusters of spreading depolarizations. *Brain* 2006; **129** (Pt 12): 3224–37
54 Shin HK, Dunn AK, Jones PB, Boas DA, Moskowitz MA, Ayata C. Vasoconstrictive neurovascular coupling during focal ischemic depolarizations. *J Cereb Blood Flow Metab* 2006; **26**: 1018–30
55 Bosche B, Graf R, Ernestus R-I, *et al.* Recurrent spreading depolarizations after subarachnoid hemorrhage decreases oxygen availability in human cerebral cortex. *Ann Neurol* 2010; **67**: 607–17
56 Woitzik J, Dreier JP, Hecht N, *et al.* Delayed cerebral ischemia and spreading depolarization in absence of angiographic vasospasm after subarachnoid hemorrhage. *J Cereb Blood Flow Metab* 2012; **32**: 203–12
57 Hirashima Y, Nakamura S, Endo S, Kuwayama N, Naruse Y, Takaku A. Elevation of platelet activating factor, inflammatory cytokines, and coagulation factors in the internal jugular vein of patients with subarachnoid hemorrhage. *Neurochem Res* 1997; **22**: 1249–55
58 Frijns CJM, Fijnheer R, Algra A, van Mourik JA, van Gijn J, Rinkel GJE. Early circulating levels of endothelial cell activation markers in aneurysmal subarachnoid haemorrhage: associations with cerebral ischaemic events and outcome. *J Neurol Neurosurg Psychiatr* 2006; **77**: 77–83
59 Hirashima Y, Nakamura S, Suzuki M, *et al.* Cerebrospinal fluid tissue factor and thrombin–antithrombin III complex as indicators of tissue injury after subarachnoid hemorrhage. *Stroke* 1997; **28**: 1666–70
60 Ikeda K, Asakura H, Futami K, Yamashita J. Coagulative and fibrinolytic activation in cerebrospinal fluid and plasma after subarachnoid hemorrhage. *Neurosurgery* 1997; **41**: 344–9
61 Peltonen S, Juvela S, Kaste M, Lassila R. Hemostasis and fibrinolysis activation after subarachnoid hemorrhage. *J Neurosurg* 1997; **87**: 207–14
62 Romano JG, Forteza AM, Concha M, *et al.* Detection of microemboli by transcranial Doppler ultrasonography in aneurysmal subarachnoid hemorrhage. *Neurosurgery* 2002; **50**: 1026–30; discussion 1030–1
63 Suzuki S, Kimura M, Souma M, Ohkima H, Shimizu T, Iwabuchi T. Cerebral microthrombosis in symptomatic cerebral vasospasm—a quantitative histological study in autopsy cases. *Neurol Med Chir (Tokyo)* 1990; **30**: 309–16
64 Stein SC, Browne KD, Chen X-H, Smith DH, Graham DI. Thromboembolism and delayed cerebral ischemia after subarachnoid hemorrhage: an autopsy study. *Neurosurgery* 2006; **59**: 781–7
65 Neil-Dwyer G, Lang DA, Doshi B, Gerber CJ, Smith PW. Delayed cerebral ischaemia: the pathological substrate. *Acta Neurochir* 1994; **131**: 137–45
66 Vernieri F, Pasqualetti P, Matteis M, *et al.* Effect of collateral blood flow and cerebral vasomotor reactivity on the outcome of carotid artery occlusion. *Stroke* 2001; **32**: 1552–8
67 Romero JR, Pikula A, Nguyen TN, Nien YL, Norbash A, Babikian VL. Cerebral collateral circulation in carotid artery disease. *Curr Cardiol Rev* 2009; **5**: 279–88
68 Liebeskind D. Collateral circulation. *Stroke* 2003; **34**: 2279–84
69 Toni D, Fiorelli M, Bastianello S, *et al.* Acute ischemic strokes improving during the first 48 hours of onset: predictability,

Downloaded from http://bja.oxfordjournals.org/ at Bodleian Library on October 7, 2012

outcome, and possible mechanisms. A comparison with early deteriorating strokes. *Stroke* 1997; **28**: 10–4

70 Bang OY, Saver JL, Buck BH, *et al.* Impact of collateral flow on tissue fate in acute ischaemic stroke. *J Neurol Neurosurg Psychiatr* 2008; **79**: 625–9

71 Bang OY, Saver JL, Alger JR, *et al.* Determinants of the distribution and severity of hypoperfusion in patients with ischemic stroke. *Neurology* 2008; **71**: 1804–11

72 Shaw MD, Vermeulen M, Murray GD, Pickard JD, Bell BA, Teasdale GM. Efficacy and safety of the endothelin, receptor antagonist TAK-044 in treating subarachnoid hemorrhage: a report by the Steering Committee on behalf of the UK/Netherlands/Eire TAK-044 Subarachnoid Haemorrhage Study Group. *J Neurosurg* 2000; **93**: 992–7

73 Vajkoczy P, Meyer B, Weidauer S, *et al.* Clazosentan (AXV-034343), a selective endothelin A receptor antagonist, in the prevention of cerebral vasospasm following severe aneurysmal subarachnoid hemorrhage: results of a randomized, double-blind, placebo-controlled, multicenter phase IIa study. *J Neurosurg* 2005; **103**: 9–17

74 Barth M, Capelle H-H, Münch E, *et al.* Effects of the selective endothelin A (ET(A)) receptor antagonist clazosentan on cerebral perfusion and cerebral oxygenation following severe subarachnoid hemorrhage—preliminary results from a randomized clinical series. *Acta Neurochir* 2007; **149**: 911–8

75 Actelion website. Available from http://www.actelion.com/en/our-company/news-and-events/index.page?newsId=1446888. Last accessed 18 May 2011

76 Clinicaltrials.gov website. Available from http://clinicaltrials.gov/ct2/show/study/NCT00940095?term=Vasospasm&rank=14#locn. Last accessed 18 May 2011

77 Wong GKC, Poon WS. Clazosentan for patients with subarachnoid haemorrhage: lessons learned. *Lancet Neurol* 2011; **10**: 871

78 Chen G, Tariq A, Ai J, *et al.* Different effects of clazosentan on consequences of subarachnoid hemorrhage in rats. *Brain Res* 2011; **1392**: 132–9

79 Peroutka SJ, Allen GS. Calcium channel antagonist binding sites labeled by 3H-nimodipine in human brain. *J Neurosurg* 1983; **59**: 933–7

80 Cheung JY, Bonventre JV, Malis CD, Leaf A. Calcium and ischemic injury. *N Engl J Med* 1986; **314**: 1670–6

81 Kazda S, Towart R. Nimodipine: a new calcium antagonistic drug with a preferential cerebrovascular action. *Acta Neurochir* 1982; **63**: 259–65

82 Pickard JD, Murray GD, Illingworth R, *et al.* Effect of oral nimodipine on cerebral infarction and outcome after subarachnoid haemorrhage: British aneurysm nimodipine trial. *Br Med J* 1989; **298**: 636–42

83 Dorhout Mees SM, Rinkel GJE, Feigin VL, *et al.* Calcium antagonists for aneurysmal subarachnoid haemorrhage. *Cochrane Database Syst Rev* 2007; CD000277

84 Pisani A, Calabresi P, Tozzi A, D'Angelo V, Bernardi G. L-type Ca^{2+} channel blockers attenuate electrical changes and Ca^{2+} rise induced by oxygen/glucose deprivation in cortical neurons. *Stroke* 1998; **29**: 196–201; discussion 202

85 Horn J, Limburg M. Calcium antagonists for ischemic stroke: a systematic review. *Stroke* 2001; **32**: 570–6

86 Langham J, Goldfrad C, Teasdale G, Shaw D, Rowan K. Calcium channel blockers for acute traumatic brain injury. *Cochrane Database Syst Rev* 2003; CD000565

87 Vergouwen MDI, Vermeulen M, de Haan RJ, Levi M, Roos YBWEM. Dihydropyridine calcium antagonists increase fibrinolytic activity: a systematic review. *J Cereb Blood Flow Metab* 2006; **27**: 1293–308

88 Dreier JP, Windmüller O, Petzold G, Lindauer U, Einhäupl KM, Dirnagl U. Ischemia triggered by red blood cell products in the subarachnoid space is inhibited by nimodipine administration or moderate volume expansion/hemodilution in rats. *Neurosurgery* 2002; **51**: 1457–65

89 Denny-Brown D. The treatment of recurrent cerebrovascular symptoms and the question of 'vasospasm'. *Med Clin North Am* 1951; **35**: 1457–74

90 Kosnik EJ, Hunt WE. Postoperative hypertension in the management of patients with intracranial arterial aneurysms. *J Neurosurg* 1976; **45**: 148–54

91 Kassell NF, Peerless SJ, Durward QJ, Beck DW, Drake CG, Adams HP. Treatment of ischemic deficits from vasospasm with intravascular volume expansion and induced arterial hypertension. *Neurosurgery* 1982; **11**: 337–43

92 Rinkel GJE, Feigin VL, Algra A, van Gijn J. Circulatory volume expansion therapy for aneurysmal subarachnoid haemorrhage. *Cochrane Database Syst Rev* 2004; CD000483

93 Dankbaar JW, Slooter AJ, Rinkel GJ, Schaaf ICVD. Effect of different components of triple-H therapy on cerebral perfusion in patients with aneurysmal subarachnoid haemorrhage: a systematic review. *Crit Care* 2010; **14**: R23

94 van den Bergh WM, Algra A, van der Sprenkel JWB, Tulleken CAF, Rinkel GJE. Hypomagnesemia after aneurysmal subarachnoid hemorrhage. *Neurosurgery* 2003; **52**: 276–81

95 van den Bergh WM, Zuur JK, Kamerling NA, *et al.* Role of magnesium in the reduction of ischemic depolarization and lesion volume after experimental subarachnoid hemorrhage. *J Neurosurg* 2002; **97**: 416–22

96 van der Hel WS, van den Bergh WM, Nicolay K, Tulleken KA, Dijkhuizen RM. Suppression of cortical spreading depressions after magnesium treatment in the rat. *Neuroreport* 1998; **9**: 2179–82

97 Wong GKC, Poon WS, Chan MTV, *et al.* Plasma magnesium concentrations and clinical outcomes in aneurysmal subarachnoid hemorrhage patients: post hoc analysis of intravenous magnesium sulphate for aneurysmal subarachnoid hemorrhage trial. *Stroke* 2010; **41**: 1841–4

98 Wong GK, Boet R, Poon WS, *et al.* Intravenous magnesium sulphate for aneurysmal subarachnoid hemorrhage: an updated systemic review and meta-analysis. *Crit Care* 2011; **15**: R52

99 Peters SAE, Palmer MK, Grobbee DE, *et al.* C-reactive protein lowering with rosuvastatin in the METEOR study. *J Intern Med* 2010; **268**: 155–61

100 Ota H, Eto M, Kano MR, *et al.* Induction of endothelial nitric oxide synthase, sirt1, and catalase by statins inhibits endothelial senescence through the Akt pathway. *Arterioscler Thromb Vasc Biol* 2010; **30**: 2205–11

101 Szapary L, Horvath B, Marton Z, *et al.* Short-term effect of low-dose atorvastatin on haemorrheological parameters, platelet aggregation and endothelial function in patients with cerebrovascular disease and hyperlipidaemia. *CNS Drugs* 2004; **18**: 165–72

102 Cheng G, Wei L, Zhi-Dan S, Shi-Guang Z, Xiang-Zhen L. Atorvastatin ameliorates cerebral vasospasm and early brain injury after subarachnoid hemorrhage and inhibits caspase-dependent apoptosis pathway. *BMC Neurosci* 2009; **10**: 7

103 Merlo L, Cimino F, Scibilia A, *et al.* Simvastatin administration ameliorates neurobehavioral consequences of subarachnoid hemorrhage in the rat. *J Neurotrauma* 2011; **28**: 2493–501

Downloaded from http://bja.oxfordjournals.org/ at Bodleian Library on October 7, 2012

104 Lynch JR, Wang H, Mcgirt MJ, *et al.* Simvastatin reduces vasospasm after aneurysmal subarachnoid hemorrhage: results of a pilot randomized clinical trial. *Stroke* 2005; **36**: 2024–6

105 Chou SH-Y, Smith EE, Badjatia N, *et al.* A randomized, double-blind, placebo-controlled pilot study of simvastatin in aneurysmal subarachnoid hemorrhage. *Stroke* 2008; **39**: 2891–3

106 Vergouwen M, Meijers J, Geskus R, *et al.* Biologic effects of simvastatin in patients with aneurysmal subarachnoid hemorrhage: a double-blind, placebo-controlled randomized trial. *J Cereb Blood Flow Metab* 2009; **29**: 1444–53

107 Tseng M-Y, Czosnyka M, Richards H, Pickard JD, Kirkpatrick PJ. Effects of acute treatment with pravastatin on cerebral vasospasm, autoregulation, and delayed ischemic deficits after aneurysmal subarachnoid hemorrhage: a phase II randomized placebo-controlled trial. *Stroke* 2005; **36**: 1627–32

108 Vergouwen MDI, de Haan RJ, Vermeulen M, Roos YBWEM. Effect of statin treatment on vasospasm, delayed cerebral ischemia, and functional outcome in patients with aneurysmal subarachnoid hemorrhage: a systematic review and meta-analysis update. *Stroke* 2010; **41**: e47–52

109 Chang C-Z, Wu S-C, Lin C-L, Hwang S-L, Howng S-L, Kwan A-L. Atorvastatin preconditioning attenuates the production of endothelin-1 and prevents experimental vasospasm in rats. *Acta Neurochir* 2010; **152**: 1399–406

110 Parra A, Kreiter KT, Williams S, *et al.* Effect of prior statin use on functional outcome and delayed vasospasm after acute aneurysmal subarachnoid hemorrhage: a matched controlled cohort study. *Neurosurgery* 2005; **56**: 476–84

111 Mcgirt MJ, Blessing R, Alexander MJ, *et al.* Risk of cerebral vasopasm after subarachnoid hemorrhage reduced by statin therapy: A multivariate analysis of an institutional experience. *J Neurosurg* 2006; **105**: 671–4

112 Moskowitz SI, Ahrens C, Provencio JJ, Chow M, Rasmussen PA. Prehemorrhage statin use and the risk of vasospasm after aneurysmal subarachnoid hemorrhage. *Surg Neurol* 2009; **71**: 311–7

113 Singhal AB, Topcuoglu MA, Dorer DJ, Ogilvy CS, Carter BS, Koroshetz WJ. SSRI and statin use increases the risk for vasospasm after subarachnoid hemorrhage. *Neurology* 2005; **64**: 1008–13

114 STASH Trial Website. Available from http://www.stashtrial.com/home.html. Last accessed 4 June 2011.

115 van den Bergh WM, MASH Study Group, Algra A, *et al.* Randomized controlled trial of acetylsalicylic acid in aneurysmal subarachnoid hemorrhage: the MASH Study. *Stroke* 2006; **37**: 2326–30

116 Dorhout Mees SM, van den Bergh WM, Algra A, Rinkel GJE. Antiplatelet therapy for aneurysmal subarachnoid haemorrhage. *Cochrane Database Syst Rev* 2007; CD006184

117 Libersan D, Khalil A, Dagenais P, *et al.* The low molecular weight heparin, enoxaparin, limits infarct size at reperfusion in the dog. *Cardiovasc Res* 1998; **37**: 656–66

118 Gikakis N, Khan MM, Hiramatsu Y, *et al.* Effect of factor Xa inhibitors on thrombin formation and complement and neutrophil activation during in vitro extracorporeal circulation. *Circulation* 1996; **94** (9 Suppl.): II341–6

119 Xi G, Wagner KR, Keep RF, *et al.* Role of blood clot formation on early edema development after experimental intracerebral hemorrhage. *Stroke* 1998; **29**: 2580–6

120 Jonas S, Sugimori M, Llinás R. Is low molecular weight heparin a neuroprotectant? *Ann N Y Acad Sci* 1997; **825**: 389–93

121 Siironen J, Juvela S, Varis J, *et al.* No effect of enoxaparin on outcome of aneurysmal subarachnoid hemorrhage: a randomized, double-blind, placebo-controlled clinical trial. *J Neurosurg* 2003; **99**: 953–9

122 Wurm G, Tomancok B, Nussbaumer K, Adelwöhrer C, Holl K. Reduction of ischemic sequelae following spontaneous subarachnoid hemorrhage: a double-blind, randomized comparison of enoxaparin versus placebo. *Clin Neurol Neurosurg* 2004; **106**: 97–103

123 Roos YB, Rinkel GJ, Vermeulen M, Algra A, van Gijn J. Antifibrinolytic therapy for aneurysmal subarachnoid haemorrhage. *Cochrane Database Syst Rev* 2000; CD001245

124 Amin-Hanjani S, Ogilvy CS, Barker FG II. Does intracisternal thrombolysis prevent vasospasm after aneurysmal subarachnoid hemorrhage? A meta-analysis. *Neurosurgery* 2004; **54**: 326–35

125 Starke RM, Kim GH, Komotar RJ, *et al.* Endothelial nitric oxide synthase gene single-nucleotide polymorphism predicts cerebral vasospasm after aneurysmal subarachnoid hemorrhage. *J Cereb Blood Flow Metab* 2008; **28**: 1204–11

126 Khurana VG, Meissner I, Meyer FB. Update on genetic evidence for rupture-prone compared with rupture-resistant intracranial saccular aneurysms. *Neurosurg Focus* 2004; **17**: E7

127 Ko NU, Rajendran P, Kim H, *et al.* Endothelial nitric oxide synthase polymorphism (-786T->C) and increased risk of angiographic vasospasm after aneurysmal subarachnoid hemorrhage. *Stroke* 2008; **39**: 1103–8

128 Corder EH, Nicoll JA, Murray G, *et al.* Gene dose of apolipoprotein E type 4 allele and the risk of Alzheimer's disease in late onset families. *Science* 1993; **261**: 921–3

129 Teasdale GM, Nicoll JA, Murray G, Fiddes M. Association of apolipoprotein E polymorphism with outcome after head injury. *Lancet* 1997; **350**: 1069–71

130 Alberts MJ, Graffagnino C, Khurana VG, *et al.* ApoE genotype and survival from intracerebral haemorrhage. *Lancet* 1995; **346**: 575

131 McCarron MO, Muir KW, Nicoll JA, *et al.* Prospective study of apolipoprotein E genotype and functional outcome following ischemic stroke. *Arch Neurol* 2000; **57**: 1480–4

132 Gao J, Wang H, Sheng H, *et al.* A novel apoE-derived therapeutic reduces vasospasm and improves outcome in a murine model of subarachnoid hemorrhage. *Neurocrit Care* 2006; **4**: 25–31

133 Niskakangas T, Ohman J, Niemela M, Ilveskoski E, Kunnas TA, Karhunen PJ. Association of apolipoprotein E polymorphism with outcome after aneurysmal subarachnoid hemorrhage: a preliminary study. *Stroke* 2001; **32**: 1181–4

134 Lanterna LA, Ruigrok Y, Alexander S, *et al.* Meta-analysis of APOE genotype and subarachnoid hemorrhage: clinical outcome and delayed ischemia. *Neurology* 2007; **69**: 766–75

135 Juvela S, Siironen J, Lappalainen J. Apolipoprotein E genotype and outcome after aneurysmal subarachnoid hemorrhage. *J Neurosurg* 2009; **110**: 989–95

136 Miyata M, Smith JD. Apolipoprotein E allele-specific antioxidant activity and effects on cytotoxicity by oxidative insults and beta-amyloid peptides. *Nat Genet* 1996; **14**: 55–61

137 Pepe MG, Curtiss LK. Apolipoprotein E is a biologically active constituent of the normal immunoregulatory lipoprotein, LDL-In. *J Immunol* 1986; **136**: 3716–23

138 Piper RD, Lambert GA. Inhalational anesthetics inhibit spreading depression: relevance to migraine. *Cephalalgia* 1996; **16**: 87–92

Downloaded from http://bja.oxfordjournals.org/ at Bodleian Library on October 7, 2012

139 Kudo C, Nozari A, Moskowitz MA, Ayata C. The impact of anesthetics and hyperoxia on cortical spreading depression. *Exp Neurol* 2008; **212**: 201–6

140 Kitahara Y, Taga K, Abe H, Shimoji K. The effects of anesthetics on cortical spreading depression elicitation and c-fos expression in rats. *J Neurosurg Anesthesiol* 2001; **13**: 26–32

141 Thomson H, Harper NJ, Parkes A. Use of the AnaConDa anaesthetic delivery system to treat life-threatening asthma. *Anaesthesia* 2007; **62**: 295–6

142 Wentlandt K, Samoilova M, Carlen PL, Beheiry El H. General anesthetics inhibit gap junction communication in cultured organotypic hippocampal slices. *Anesth Analg* 2006; **102**: 1692–8

143 Sasaki R, Hirota K, Asahi T, Yamazaki M. The effects of thiopental on spreading depression induced by anoxia in the rat hippocampal slice in vitro. *Hiroshima J Anaesth* 2002; **38**: 211–4

144 Hernández-Cáceres J, Macias-González R, Brozek G, Bures J. Systemic ketamine blocks cortical spreading depression but does not delay the onset of terminal anoxic depolarization in rats. *Brain Res* 1987; **437**: 360–4

145 Sakowitz OW, Unterberg AW. Detecting and treating microvascular ischemia after subarachnoid hemorrhage. *Curr Opin Crit Care* 2006; **12**: 103–11

146 Petzold A, Keir G, Kay A, Kerr M, Thompson EJ. Axonal damage and outcome in subarachnoid haemorrhage. *J Neurol Neurosurg Psychiatr* 2006; **77**: 753–9

147 Fountas KN, Tasiou A, Kapsalaki EZ, *et al.* Serum and cerebrospinal fluid C-reactive protein levels as predictors of vasospasm in aneurysmal subarachnoid hemorrhage. Clinical article. *Neurosurg Focus* 2009; **26**: E22

148 Sehba FA, Pluta RM, Zhang JH. Metamorphosis of subarachnoid hemorrhage research: from delayed vasospasm to early brain injury. *Mol Neurobiol* 2011; **43**: 27–40

149 Dreier JP, Körner K, Ebert, *et al.* Nitric oxide scavenging by hemoglobin or nitric oxide synthase inhibition by N-nitro-L-arginine induces cortical spreading ischemia when K+ is increased in the subarachnoid space. *J Cereb Blood Flow Metab* 1998; **18**: 978–90

Downloaded from http://bja.oxfordjournals.org/ at Bodleian Library on October 7, 2012

Appendix B: Pseudo-Continuous Arterial Spin Labelling MRI for Non-Invasive, Whole-Brain, Serial Quantification of Cerebral Blood Flow Following Aneurysmal Subarachnoid Haemorrhage

Transl. Stroke Res.
DOI 10.1007/s12975-013-0269-y

ORIGINAL ARTICLE

Pseudo-Continuous Arterial Spin Labelling MRI for Non-Invasive, Whole-Brain, Serial Quantification of Cerebral Blood Flow Following Aneurysmal Subarachnoid Haemorrhage

Michael E. Kelly · Matthew J. Rowland · Thomas W. Okell · Michael A. Chappell · Rufus Corkill · Richard S. Kerr · Jon Westbrook · Peter Jezzard · Kyle T. S. Pattinson

Received: 3 May 2013 / Revised: 27 June 2013 / Accepted: 28 June 2013
© Springer Science+Business Media New York 2013

Abstract Delayed cerebral ischaemia (DCI) is the major cause of mortality and morbidity following aneurysmal subarachnoid haemorrhage (SAH). Recent experimental evidence from animal models has highlighted the need for non-invasive and robust measurements of brain tissue perfusion in patients in order to help understand the pathophysiology underlying DCI. Quantitative, serial, whole-brain cerebral perfusion measurements were obtained with pseudo-continuous arterial spin labelling (PCASL) magnetic resonance imaging (MRI) in six SAH patients acutely following endovascular coiling. This technique requires no injected contrast or radioactive isotopes. MRI scanning was well tolerated. Artefact from endovascular coils was minimal. PCASL MRI was able to detect time-dependent and patient-specific changes in voxel-wise and regional cerebral blood flow. These changes reflected changes in clinical condition. Data obtained in healthy controls using the same experimental protocol confirm the reliability and reproducibility of these results. This is the first study to use whole-brain, quantitative PCASL to identify time-dependent changes in cerebral blood flow at the tissue level in the acute period following SAH. This technique has the potential to better understand changes in cerebral pathophysiology as a consequence of aneurysm rupture.

Keywords Aneurysmal subarachnoid haemorrhage · Delayed cerebral ischaemia · Arterial spin labelling · Magnetic resonance imaging

Introduction

Aneurysmal subarachnoid haemorrhage (SAH) remains a disease of young adults characterised by high mortality and poor neurocognitive and functional outcomes. Delayed cerebral ischaemia (DCI) is a syndrome of neurological and neurocognitive deficits [1] that is the leading cause of morbidity and mortality in those patients that survive the initial haemorrhage [2]. Although cerebral arterial vasoconstriction occurs following SAH and is associated with poor clinical outcomes [2, 3], the established theory that SAH leads to arterial vasospasm, tissue ischaemia and DCI has recently been questioned [4]. Changes in cerebral perfusion following aneurysm rupture that occur as part of early brain injury [5] may act as a diagnostic and therapeutic biomarker for DCI and subsequent clinical and functional outcomes.

Current clinical techniques for measuring localised changes in brain tissue perfusion require either ionising radiation or bolus

Michael E. Kelly and Matthew J. Rowland are joint first authors.

Electronic supplementary material The online version of this article (doi:10.1007/s12975-013-0269-y) contains supplementary material, which is available to authorized users.

M. E. Kelly · M. J. Rowland · T. W. Okell · J. Westbrook · P. Jezzard · K. T. S. Pattinson (✉)
Nuffield Department of Clinical Neurosciences and Oxford Acute Vascular Imaging Centre, University of Oxford, John Radcliffe Hospital, Oxford OX3 9DU, UK
e-mail: kyle.pattinson@nda.ox.ac.uk

M. J. Rowland · R. Corkill · R. S. Kerr · J. Westbrook · K. T. S. Pattinson
Neurointensive Care, Oxford University Hospitals, NHS Trust, Oxford OX3 9DU, UK

M. A. Chappell
Institute of Biomedical Engineering, University of Oxford, Oxford OX3 7DQ, UK

Published online: 18 July 2013

injection of intravenous contrast, limiting their use in longitudinal studies in patients. Arterial spin labelling (ASL) MRI is a relatively new technique that can be used to quantify regional cerebral perfusion without the use of ionising radiation or contrast agents. The technique uses magnetically labelled arterial blood water as a non-invasive, endogenous tracer for the assessment of cerebral perfusion and can provide whole-brain, quantitative maps of cerebral blood flow (CBF) (in units of ml/100 g/min). Clinical applications of ASL MRI have begun to increase in recent years. The first study to use ASL to investigate CBF changes following SAH was performed by Aoyama et al. [6]. A single inversion time, pulsed ASL (PASL) technique identified a link between DCI and hemispherical CBF decline, while serial time point ASL showed time-dependent relative changes in CBF after SAH. The more recently developed pseudo-continuous ASL (PCASL) technique [7] has a number of advantages compared to PASL, primarily the ability to provide whole-brain quantitative CBF maps. The ability to reliably measure absolute cerebral perfusion instead of relying on relative measures is clearly advantageous, not only because it is possible to directly measure tissue at risk, but also because relative measures are no longer reliable when vascular disease is bilateral or when cardiac output decreases [8].

In this preliminary study, we used PCASL and vessel-encoded PCASL (VEPCASL) [9, 10] to assess CBF changes in SAH patients. PCASL was used to generate quantitative CBF maps in all subjects, whilst VEPCASL was trialled in one subject only to investigate the additional information that this technique can provide on the relative contribution of the main cerebral arteries to downstream perfusion in the brain. The study aimed to test the feasibility of performing PCASL in this patient group, specifically in terms of patient tolerability and potential artefacts arising from the platinum coils used in endovascular treatment of SAH. Furthermore, we aimed to investigate the sensitivity of the PCASL technique to subtle changes in cerebral perfusion in SAH patients and in doing so establish whether or not PCASL can become a useful clinical tool for larger research studies and routine clinical assessment of SAH patients.

Methods

Six SAH patients were recruited following endovascular coiling (Table 1). Four healthy control volunteers of comparable age were also included to confirm the reproducibility/reliability of the ASL methods used. Patients were included if they had a World Federation of Neurosurgeons (WFNS) Grade 1 or 2 SAH (less severe), had uncomplicated endovascular aneurysm treatment, no contraindications to MRI scanning and had the capacity to consent to participation. All study interventions were performed following endovascular aneurysm treatment.

Patients were scheduled to be scanned on three occasions in a 3-T Siemens Trio MRI scanner (Siemens Healthcare, Erlangen, Germany) during the acute period following endovascular coiling. To maximise patient tolerability, MRI scanning was limited to 25 min. The following sequences were included in each session: time-of-flight angiography in the neck (to allow optimal placement of the labelling plane for ASL), multi-inversion time PCASL and a T1-weighted structural scan. VEPCASL was trialled in patient 4 only. (*Further details on MRI methods are outlined in the Supplementary material*). Whole-brain CBF was quantified by fitting PCASL data to the ASL general kinetic model [11]. The reproducibility of the PCASL technique was assessed by calculating the within-subject coefficient of variation (wsCV) of the CBF values obtained from the healthy control data. Control subjects were scanned on three occasions allowing the wsCV (in percent) to be calculated from the ratio of the standard deviation of the difference between repeated measurements to the mean of repeated measurements [12]. (*Note: the healthy control validation of the PCASL technique is described in full in the accompanying Supplementary Information*).

Daily clinical assessment of patients included Glasgow Coma Scale (GCS), National Institutes of Health Stroke Scale (NIHSS) scoring and neurological examination of tone, power, reflexes and sensation.

Results

Six SAH patients were recruited following endovascular coiling to secure the ruptured aneurysm (Table 1). The 25-min duration in the MRI scanner was generally well tolerated by patients. The variability in the number of scanning sessions and day on which scanning was performed for each patient (Table 2) can be attributed to the following factors: claustrophobia in the MRI scanner (patient 2), withdrawal of consent (patient 5) and fluctuating clinical symptoms (patient 1, 3, 4 and 6).

Clinical Results

For all patients, mean arterial pressure and end-tidal CO_2 remained consistent both within and across scanning sessions (Table 3). This is important as impaired cerebral autoregulation is common following SAH [13]. None of the six patients suffered significant post-SAH complications such as aneurysm re-bleeding, hydrocephalus (requiring drainage) or DCI (as defined by Vergouwen et al. [2]) Review of all treatment angiograms showed that none

Table 1 SAH patient data: gender, SAH grade, age, location of aneurysm, no. of days between SAH and endovascular coiling to secure the aneurysm

Patient	Gender	Age	WFNS grade	Fisher grade	Location of ruptured aneurysm	Coiling—no. of days post-SAH
1	F	58	1	4	Solitary PcommA	1
2	M	44	1	4	Solitary AcommA	2
3	F	52	1	3	A1/A2 junction AcommA	1
4	F	66	1	3	Right PcommA	1
5	F	61	2	3	Solitary distal-lateral ICA	1
6	M	40	1	3	A1/A2 junction AcommA	2

F female, *M* male, *PcommA* posterior communicating artery, *AcommA* anterior communicating artery, *ICA* internal carotid artery

of the subjects had evidence of angiographic vasospasm at the time of coil embolisation and no patients received repeat angiography during the course of the study. All patients were discharged from hospital following treatment. During the course of the admission, there was no change in daily GCS or NIHSS noted in any of the six patients and no focal neurological deficit was reported or identified at any point during clinical examination. However, although all patients reported fluctuations in clinical symptoms (e.g. headache, photophobia and nausea), patient 4 demonstrated a noticeably significant observed and self-reported clinical deterioration—to such an extent that the final MRI scan was delayed by a number of days. This change was not reflected in the routine clinical scoring systems used in the study.

MRI Results

Figure 1 shows the image artefacts resulting from the endovascular coils used to secure the initial haemorrhage. The coils result in a prominent metal streak artefact (Fig. 1a) in computed tomography (CT) images (all SAH patients undergo routine pre- and post-coiling CT imaging as part of routing clinical assessment). In the MRI images, only the region immediately surrounding the endovascular coil suffers from signal dropout (Fig. 1b, c). Therefore, the signal dropout artefact has a minimal effect when investigating global changes following SAH.

The healthy control data demonstrated high within-subject reproducibility of the PCASL technique. The wsCV of mean grey matter CBF was 4.5 %±1.8 % (mean±standard deviation wsCV across all control subjects). This is considerably smaller

Table 2 Regional CBF (ml/100 g/min) for all patients and all scan sessions. Within-subject coefficient of variation was calculated for all patients that were scanned on three occasions

Patient	Scan session (no. days post-SAH)	Cerebellum		Frontal lobe		Occipital lobe	
		Left	Right	Left	Right	Left	Right
1	3	60.3	62.3	52.0	52.1	44.1	49.8
	5	59.5	63.0	52.5	50.5	40.0	50.5
2	3	43.7	42.6	44.5	46.8	47.8	46.1
3	2	60.9	68.3	58.8	61.5	59.2	60.2
	6	62.4	60.4	57.6	53.3	63.5	54.2
	8	56.9	57.3	57.8	53.2	58.0	52.2
	wsCV(%)	6.1	6.4	1.3	8.4	8.2	5.5
4	2	55.3	61.1	44.2	47.6	62.2	51.0
	4	35.4	39.4	35.5	39.4	44.7	40.9
	11	53.5	56.7	42.6	45.5	55.9	52.7
	wsCV(%)	39.5	37.3	19.4	16.2	16.7	22.7
5	2	57.8	52.7	55.3	54.9	60.1	57.3
6	2	58.1	64.0	38.7	40.2	39.3	42.3
	6	58.9	65.8	40.6	42.0	41.5	44.2
	8	62.3	70.6	42.6	44.3	45.3	51.3
	wsCV(%)	3.0	3.6	2.7	2.9	4.5	8.0

Table 3 Mean arterial pressure, end-tidal CO_2 and O_2 saturation for all patients and all scanning sessions (end-tidal CO_2 data for patient 3; scan 3 was missing due to gas analyser fault)

Patient	Scan number	Mean arterial pressure (mmHg)	Mean end-tidal CO_2 (KPa)	O_2 saturation (%)
1	1	94.1	5.4	98.3
	2	94.1	5.0	98.7
2	1	108.6	4.7	99.1
3	1	81.5	4.7	97.7
	2	83.1	5.2	97.9
	3	78.4	–	97.2
4	1	84.4	4.2	98.5
	2	87.4	4.8	98.1
	3	85.7	4.7	99.1
5	1	87.3	3.9	99.2
6	1	113.4	4.3	99.3
	2	113.9	4.2	99.1
	3	112.4	4.7	99.1

than the wsCV seen in the patient data (Table 2). (*Note: the results of the healthy control validation study are presented in full in the accompanying Supplementary Information.*)

Figure 2 shows the variation in regional CBF over time in the three patients that were scanned on three occasions, patients 3, 4 and 6 (regional grey matter CBF values are given for all patients and all scanning occasions in Table 2). CBF values are presented for the left and right cerebellum and frontal and occipital lobe regions. The location of the aneurysm in these three patients is also identified in Fig. 2. Patient 3 demonstrated consistent CBF values on all scanning occasions (Fig. 2a). Patient 4 demonstrated a global reduction in grey matter CBF on day 4 post-SAH, with the decline in CBF being most prominent in the cerebellum and occipital lobe regions (Fig. 2b). These CBF changes occured simultaneously with observed and patient-reported worsening clinical symptoms (headache, photophobia, nausea). A return towards baseline CBF was measured on day 11 post-SAH. Patient 6 demonstrated elevated CBF in the cerebellum region on all scanning occasions (Fig. 2c). Data from one healthy control subject are included in Fig. 2d for comparison with patient data.

Due to the simultaneous decline in CBF and the clinical symptoms of patient 4, we carried out a further statistical analysis of the CBF maps in order to identify which brain regions demonstrated the most significant decline in CBF on day 4 post-SAH. Figure 3 shows the results of a voxel-wise test for statistically significant CBF differences in patient 4 on days 2, 4 and 11 post-SAH. The *t* statistic maps were generated by dividing the voxel-wise difference in CBF by the pooled standard deviation in CBF for each pair of CBF maps. The level of statistical significance was set at $p=0.05$ (uncorrected). Figure 3a shows clusters of statistically significant decrease in CBF in the cerebellum region obtained by comparing CBF on day 4 with CBF on day 2. Figure 3b shows clusters of statistically significant increases in CBF in the cerebellum region obtained by comparing CBF on day 4 with CBF on day 11. This indicates a return towards day 2 CBF levels on day 11.

Figure 4 shows VEPCASL perfusion territory maps from 4 sample slices from patient 4 on days 2, 4 and 11 post-SAH. The right internal carotid artery (RICA), left internal carotid artery (LICA), right vertebral artery (RVA) and left vertebral artery LVA are represented in the colour maps by the colours

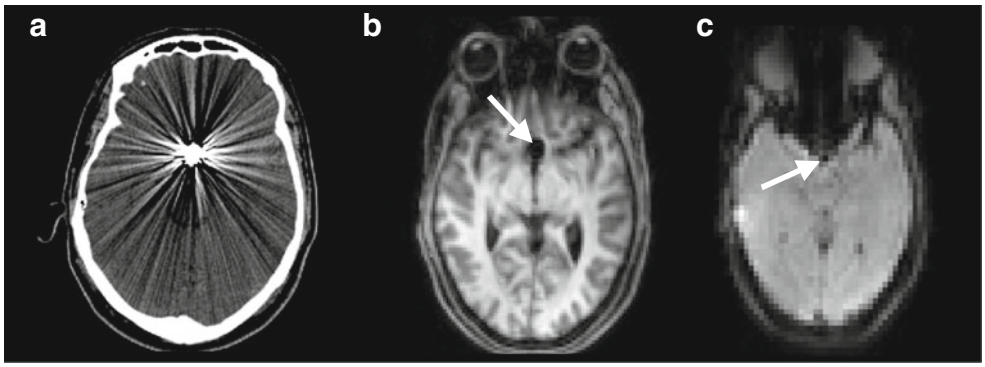


Fig. 1 Comparison of endovascular coil artefact. **a** Computed tomography (CT) image—prominent metal streak artefact. **b** T1-weighted structural image—signal dropout indicated by *white arrowhead*. **c** Gradient echo EPI image (used for acquisition of PCASL and VEPCASL data)—signal dropout indicated by *white arrowhead*

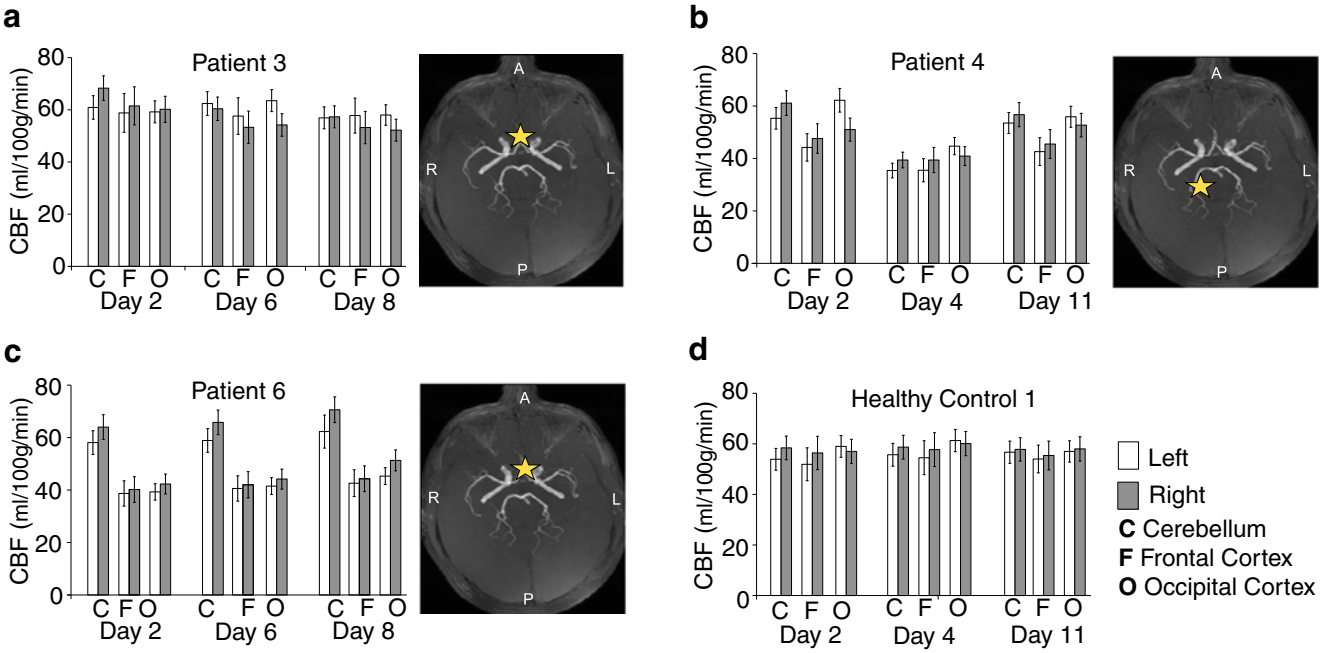


Fig. 2 PCASL regional grey matter CBF for patients that were scanned on three occasions (data from all six patients are provided in Table 2). **a**–**c** Data from patients 3, 4 and 6, respectively. Patient 4 demonstrated a decline in CBF in all regions on day 4 post-SAH and a simultaneous decline in clinical condition (photophobia, headache, nausea). Patient 6 demonstrated elevated CBF in the cerebellum region on all scanning occasions. Patient 3 demonstrated consistent CBF on all scanning occasions. **d** Regional grey matter CBF for one healthy control, scanned on three occasions (data from all healthy controls are provided in the Supplementary Information, Fig. S1)

red, green, blue and pink, respectively. In Fig. 5, the results from analysis of the VEPCASL data are shown. A similar trend to that was shown for patient 4 in Fig. 2c (PCASL data) was identified for the territories supplied by the RICA, LICA

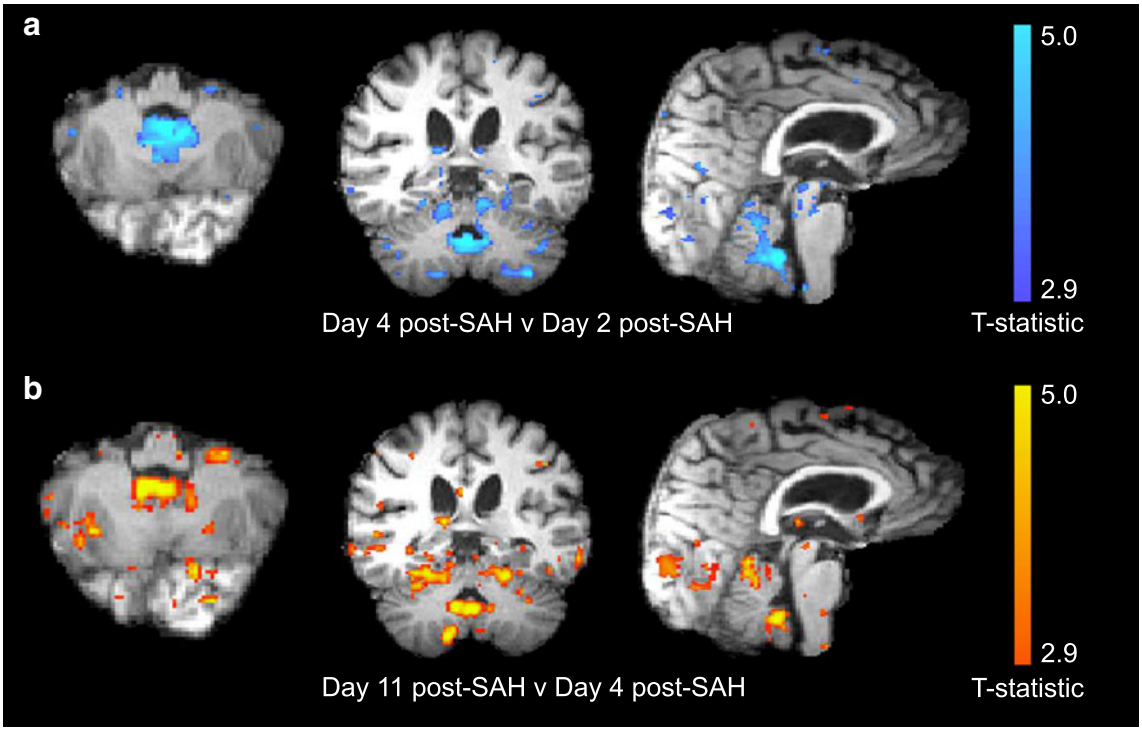


Fig. 3 Maps of statistically significant variation in CBF in patient 4 (t statistic thresholded at t=2.92 for significance at p=0.05, corrected). **a** Decreased CBF in cerebellum region on day 4 post-SAH compared to day 2 post-SAH. **b** Increased CBF in cerebellum region on day 11 post-SAH compared to day 4 post-SAH

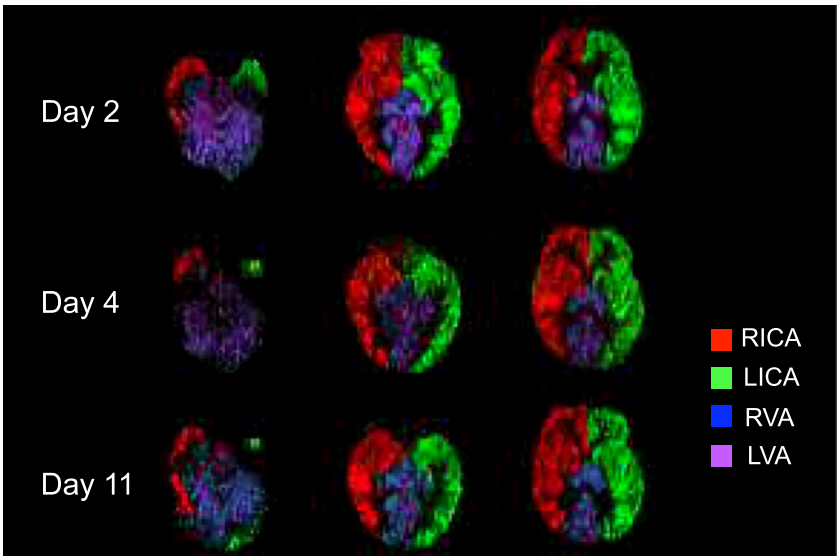


Fig. 4 VEPCASL perfusion territory maps from four representative slices of patient 4, acquired on days 2, 4 and 11 post-SAH. The maps allow an assessment of the perfusion territories of each of the four main feeding arteries: right and left internal carotid artery (*RICA* and *LICA*) and right and left vertebral artery (*RVA* and *RVA*)

and RVA (i.e. significant decrease in CBF on day 4, with a return toward day 2 CBF levels on day 11). The CBF contribution of the LVA remains suppressed on day 11.

Discussion

This is the first study to demonstrate that multi-inversion time PCASL can be used to obtain whole-brain, quantitative and serial measurements of brain tissue perfusion following SAH. The endovascular coils used to secure the haemorrhage did not result in significant artefacts in any of the MRI sequences used in the study and in general patients tolerated 25 min in the MRI scanner—even those with clinical symptoms such as moderate to severe headache and nausea.

Statistical analysis of the CBF maps obtained from patient 4 on days 2, 4 and 11 post-SAH revealed that the most significant deficit in CBF occurred on day 4 in the cerebellum region (Fig. 3a, b). This finding is supported by analysis of the VEPCASL data obtained in the same patient which demonstrates that the left vertebral artery, supplying approximately 50 % of blood to the cerebellum, remained suppressed on day 11 post-SAH (Fig. 5). Statistically significant decreases are not widespread in the CBF maps due to low SNR and high variance of CBF quantification by ASL techniques, particularly when comparing on a voxel-wise basis. The fact that this patient scored a maximum of 15 on the GCS and showed no deficit on the NIHSS on the same day suggests that subtle underlying changes in brain perfusion are not captured by current bedside clinical assessments. It also potentially supports the hypothesis that delayed cerebral ischaemia is in fact a spectrum of disease [4, 5] and that measurements of underlying brain tissue perfusion may be more important than qualitative assessment of cerebral vessel vasoconstriction.

Although some groups have reported quantitative white matter CBF values obtained from 3 T PCASL data, in this work, we have not reported white matter CBF. The reasons for this are twofold: (1) We believe that white matter perfusion levels (approx. 10–15 ml/100 g/min) are at the limit of the sensitivity of the PCASL technique at 3 T, when taking low SNR into account, and (2) perfusion in the white matter is generally not considered to be of interest in studies of perfusion deficits following ischaemic and/or haemorrhagic stroke. As a result, the white matter was segmented out of the PCASL data in this study, leaving pure grey matter tissue to be analysed and compared across sessions.

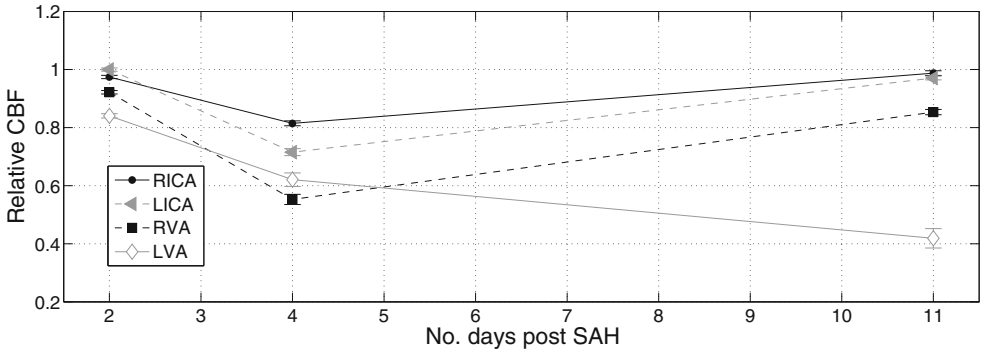


Fig. 5 VEPCASL measurement of variation in relative CBF of perfusion territories of RICA, LICA, RVA and LCA in patient 4 on days 2, 4 and 11 post-SAH. A significant decrease in relative CBF was measured in all perfusion territories on day 4. Blood supply from the LVA remains suppressed on day 11

The values obtained in patients are broadly in agreement with other MRI perfusion and positron emission tomography (PET) CBF values obtained after SAH [14–16]. Looking at the results from the validation study in 4 age-matched healthy controls, we conclude that the CBF results from patients 3 and 6 do not vary more than the intrinsic variability of the PCASL technique, i.e. no significant CBF change was detected. These patients also did not demonstrate any deterioration in clinical condition as measured using the GCS and NIHSS. Patient 6 did however show a persistently high CBF in the cerebellum region throughout all three scan sessions. Subsequent review of the angiogram taken at the time of embolization showed an aneurysm at the A1/A2 junction and bilateral foetal posterior cerebral arteries. Although there was no angiographic evidence of vessel constriction at this point, this normal variant of the cerebral circulation means that the posterior fossa may have been isolated from any subsequent changes in CBF in the anterior circulation. Although VEPCASL imaging was not performed on this patient, we feel that this highlights the potential of both ASL to complement and inform commonly used clinical imaging techniques such as angiography and CT that are often used in the period post-SAH.

PCASL offers a number of advantages over other imaging techniques currently used clinically in patients with subarachnoid haemorrhage. Firstly, it has the ability to acquire CBF data at multiple time points acutely in patients without concerns regarding accumulation of ionising radiation dose and contrast-induced nephropathy—especially a problem with serial scanning. Secondly, ASL can provide quantitative measurements of whole-brain CBF. The majority of MRI perfusion techniques used in clinical assessments are qualitative and show relative changes in cerebral blood volume, CBF and mean transit time. The quantification method in ASL quantifies true CBF in units of ml/100 g/min and therefore allows for regional and global assessments of CBF. Relative perfusion measurements are inherently incapable of revealing global hypo- or hyperperfusion. Quantification on an absolute scale allows easy recognition of states such as hypercapnia or diffuse hypoxic brain injury. Finally, bolus techniques such as DCS-MRI require accurate knowledge of the arterial input function into the voxel in which the CBF is to be calculated [17]. It is generally impossible to do this, as there is never an artery that can be resolved close enough at standard resolutions. Measurements of arterial input function are generally made in a large vessel (typically in the MCA) that is remote from the cortex. It is then assumed that there is no delay or dispersion from the point where arterial input function is measured to the point where CBF is quantified. This incorrect assumption leads to poor estimates of CBF. Alternatively, simpler metrics such as time-to-peak of the DSC-MRI bolus are used as a CBF surrogate; however, this is not true CBF. The quantification of ASL data does not depend on the local arterial input function. Instead, the ASL response is measured on a voxel-wise basis and the resultant voxel-wise signal time course is fitted to a general kinetic model to provide CBF estimates in absolute units of ml/100-g/min. This true estimate of CBF can be compared to gold standard PET estimates of CBF.

Although ASL has been widely used in research studies for over 20 years, a number of factors including sequence availability and hardware limitations of typical clinical scanners have prevented the technique from being used routinely to inform the clinical management of patients. Recent advances in scanner technology and ASL methods, in particular the development of the PCASL technique [7], have brought ASL closer to becoming a viable and useful clinical tool. The CBF values obtained from the multi-TI PCASL data in this study are in agreement with both gold standard PET values [16] and other MRI perfusion techniques [17]. The validation study of CBF quantification using PCASL demonstrated high reproducibility of the technique (*see Supplementary Information*). This provides confidence that the PCASL technique can be used in patient studies to detect physiological variations in CBF that are greater than the intrinsic variance of the technique.

The use of PCASL in clinical imaging studies is relatively new, and as a result, the technique has some limitations. PCASL (and all other ASL techniques) are based on the subtraction of tag and control images. The measurement is typically averaged over 100 repetitions, resulting in a total imaging time for one resting CBF map of 5–10 min. Motion artefacts may therefore be problematic, particularly in patient studies. Retrospective motion correction prior to CBF quantification has been shown to improve temporal signal-to-noise ratio and test–retest reproducibility of CBF measurements [18].

Another potential issue when using PCASL to assess CBF in patients with abnormal blood flow characteristics is the effect that variations in blood velocity at the labelling plane (i.e. the carotid and vertebral arteries in the neck) may have on the labelling efficiency of the PCASL labelling pulse [7]. If blood velocity at the labelling plane is outside the optimal range, failure to account for this effect may lead to inaccurate estimates of CBF. Subsequent to starting this study, a new approach has been introduced by Aslan et al. [19], in which labelling efficiency is estimated using a separate phase-contrast velocity MRI scan on a patient-specific basis. We intend to use this approach in future studies of SAH patients. Such variations in labelling plane blood velocity may also affect the arterial arrival time sensitivity of the PCASL technique, which may in turn necessitate the use of patient-specific PCASL inversion times [20]. There is the potential to correct for these sources of error on a patient-specific basis in future studies, which when combined with the considerable advantages of PCASL over alternative perfusion techniques would make it an attractive option for future perfusion imaging studies of SAH patients.

The main purpose of this feasibility study was to test this novel PCASL technique in patients post-SAH to inform the design of future larger studies. The preliminary data presented here therefore suffer from some limitations for the understanding of disease mechanisms in SAH, but this was not the primary intention of the study. None of the patients included in the study developed DCI as defined by the empirical criteria suggested by Vergouwen et al. [1], although as described above, there was a worsening of clinical symptoms in one patient suggestive of underlying cerebral ischaemia. We also intended to scan patients on set of days post-SAH, but there was a degree of variability in the number of days post-SAH on which patients were actually scanned due to changes in clinical symptoms and limitations in scanner availability at the time of the study. Given that this was a preliminary proof of concept study rather than a full clinical study, we erred on the side of caution when deciding to scan a patient and actively avoided scanning those with deterioration of clinical symptoms. As a result, the present study investigated less severe SAH patients (WFNS I and II), and a larger study that includes higher grade SAH patients is planned to investigate the potential of PCASL to inform clinical management of patients post-SAH.

Conclusion

The findings of this preliminary study suggest that the PCASL technique is sensitive to changes in brain tissue perfusion that would go undetected by current routine clinical assessment. Future work on correlating changes in cerebral blood flow with patient outcome, particularly in higher grade SAH patients, holds much potential to provide an improved understanding of the pathophysiology that occurs at the tissue level in the days immediately following SAH.

Acknowledgments The research was supported by the National Institute for Health Research Oxford Biomedical Research Centre based at Oxford University Hospitals NHS Trust and University of Oxford, the Oxfordshire Health Services Research Committee, the UK Medical Research Council and the National Institute of Academic Anaesthesia.

Compliance with Ethics Requirements All procedures followed were in accordance with the ethical standards of the responsible committee on human experimentation (institutional and national) and with the Helsinki Declaration of 1975, as revised in 2008 (5). Informed consent was obtained from all patients for being included in the study. Ethical approval for the study was obtained from the Oxfordshire NHS Research Ethics Committee B (09/H0605/128).

Conflict of Interest Michael Kelly, Matthew Rowland, Thomas Okell, Michael Chappell, Rufus Corkill, Jon Westbrook, Peter Jezzard and Kyle Pattinson declare that they have no conflict of interest. Travel expenses of Richard Kerr were paid by Target Therapeutics to attend the 2003 Association of American Neurosurgeons Annual Scientific Meeting to deliver a lecture regarding the International Subarachnoid Aneurysm Trial.

References

1. Vergouwen MD, Vermeulen M, van Gijn J, Rinkel GJ, Wijdicks EF, Muizelaar JP, et al. Definition of delayed cerebral ischemia after aneurysmal subarachnoid hemorrhage as an outcome event in clinical trials and observational studies: proposal of a multidisciplinary research group. Stroke. 2010;41:2391–5.
2. Dorsch NW. Therapeutic approaches to vasospasm in subarachnoid hemorrhage. Curr Opin Crit Care. 2002;8:128–33.
3. Weir B, Rothberg C, Grace M, Davis F. Relative prognostic significance of vasospasm following subarachnoid hemorrhage. Can J Neurol Sci. 1975;2:109–14.
4. Rowland MJ, Hadjipavlou G, Kelly M, Westbrook J, Pattinson KT. Delayed cerebral ischaemia after subarachnoid haemorrhage: looking beyond vasospasm. Br J Anaesth. 2012;109:315–29.
5. Cahill J, Calvert JW, Zhang JH. Mechanisms of early brain injury after subarachnoid hemorrhage. J Cereb Blood Flow Metab. 2006;26:1341–53.
6. Aoyama K, Fushimi Y, Okada T, Miyasaki A, Taki H, Shibamoto K, et al. Detection of symptomatic vasospasm after subarachnoid haemorrhage: initial findings from single time-point and serial measurements with arterial spin labelling. Eur J Radiol. 2012;22:2382–91.
7. Dai W, Garcia D, de Bazelaire C, Alsop DC. Continuous flow-driven inversion for arterial spin labeling using pulsed radio frequency and gradient fields. Magn Reson Med. 2008;60:1488–97.
8. Wolf RL, Detre JA. Clinical neuroimaging using arterial spin-labeled perfusion magnetic resonance imaging. Neurotherapeutics. 2007;4:346–59.
9. Wong EC. Vessel-encoded arterial spin-labeling using pseudo-continuous tagging. Magn Reson Med. 2007;58:1086–91.
10. Okell TW, Chappell MA, Woolrich MW, Gunther M, Feinberg DA, Jezzard P. Vessel-encoded dynamic magnetic resonance angiography using arterial spin labeling. Magn Reson Med. 2010;64:698–706.
11. Buxton RB, Frank LR, Wong EC, Siewert B, Warach S, Edelman RR. A general kinetic model for quantitative perfusion imaging with arterial spin labeling. Magn Reson Med. 1998;40:383–96.
12. Chen Y, Wang DJ, Detre JA. Test-retest reliability of arterial spin labeling with common labeling strategies. J Magn Reson Imaging. 2011;33:940–9.
13. Budohoski KP, Czosnyka M, Smielewski P, Kasprowicz M, Helmy A, Bulters D, et al. Impairment of cerebral autoregulation predicts delayed cerebral ischemia after subarachnoid hemorrhage: a prospective observational study. Stroke. 2012;43:3230–7.
14. Hattingen E, Blasel S, Dettmann E, Vatter H, Pilatus U, Seifert V, et al. Perfusion-weighted MRI to evaluate cerebral autoregulation in aneurysmal subarachnoid haemorrhage. Neuroradiology. 2008;50:929–38.
15. Minhas PS, Menon DK, Smielewski P, Czosnyka M, Kirkpatrick PJ, Clark JC, et al. Positron emission tomographic cerebral perfusion disturbances and transcranial Doppler findings among patients with neurological deterioration after subarachnoid hemorrhage. Neurosurgery. 2003;52:1017–22.
16. Ito H, Kanno I, Kato C, Sasaki T, Ishii K, Ouchi Y, et al. Database of normal human cerebral blood flow, cerebral blood volume, cerebral oxygen extraction fraction and cerebral metabolic rate of oxygen measured by positron emission tomography with 15O-labelled carbon dioxide or water, carbon monoxide and oxygen: a multicentre study in Japan. Eur J Nucl Med Mol Imaging. 2004;31:635–43.

17. Knutsson L, Stahlberg F, Wirestam R. Absolute quantification of perfusion using dynamic susceptibility contrast MRI: pitfalls and possibilities. MAGMA. 2010;23:1–21.
18. Wang Z. Improving cerebral blood flow quantification for arterial spin labeled perfusion MRI by removing residual motion artifacts and global signal fluctuations. J Magn Reson Imaging. 2012;30:1409–15.
19. Aslan S, Xu F, Wang PL, Uh J, Yezhuvath US, Van Osch M, et al. Estimation of labeling efficiency in pseudocontinuous arterial spin labeling. Magn Reson Med. 2010;63:765–71.
20. Xie J, Gallichan D, Gunn RN, Jezzard P. Optimal design of pulsed arterial spin labeling MRI experiments. Magn Reson Med. 2008; 59:826–34.

Appendix C: The role of the nitric oxide pathway in brain injury and its treatment - From bench to bedside

Experimental Neurology 263 (2015) 235–243

Contents lists available at ScienceDirect

Experimental Neurology

journal homepage: www.elsevier.com/locate/yexnr

Review

The role of the nitric oxide pathway in brain injury and its treatment — From bench to bedside ☆

P.S. Garry [a,*], M. Ezra [a], M.J. Rowland [a], J. Westbrook [b], K.T.S. Pattinson [a]

[a] Nuffield Department of Clinical Neurosciences, University of Oxford, John Radcliffe Hospital, Oxford OX3 9DU, UK
[b] Neurosciences Intensive Care Unit, Oxford University Hospitals NHS Trust, John Radcliffe Hospital, Oxford OX3 9DU, UK

ARTICLE INFO

Article history:
Received 12 August 2014
Revised 9 October 2014
Accepted 22 October 2014
Available online 29 October 2014

Keywords:
Nitric oxide
Nitric oxide synthase
Autoregulation
Subarachnoid haemorrhage
Stroke
Traumatic brain injury
Neonatal hypoxic–ischaemic insult
Inhaled nitric oxide

ABSTRACT

Nitric oxide (NO) is a key signalling molecule in the regulation of cerebral blood flow. This review summarises current evidence regarding the role of NO in the regulation of cerebral blood flow at rest, under physiological conditions, and after brain injury, focusing on subarachnoid haemorrhage, traumatic brain injury, and ischaemic stroke and following cardiac arrest. We also review the role of NO in the response to hypoxic insult in the developing brain. NO depletion in ischaemic brain tissue plays a pivotal role in the development of subsequent morbidity and mortality through microcirculatory disturbance and disordered blood flow regulation. NO derived from endothelial nitric oxide synthase (eNOS) appears to have neuroprotective properties. However NO derived from inducible nitric oxide synthase (iNOS) may have neurotoxic effects. Cerebral NO donor agents, for example sodium nitrite, appear to replicate the effects of eNOS derived NO, and therefore have neuroprotective properties. This is true in both the adult and immature brain. We conclude that these agents should be further investigated as targeted pharmacotherapy to protect against secondary brain injury.

© 2014 The Authors. Published by Elsevier Inc. This is an open access article under the CC BY-NC-ND license (http://creativecommons.org/licenses/by-nc-nd/3.0/).

Contents

Introduction . . . 236
Nitric oxide synthase — expression and functions . . . 236
Role of NO in regulation of cerebral blood flow . . . 236
  Autoregulation . . . 236
  Neurovascular coupling . . . 236
NO and the cerebral blood flow response during hypoxia and hypercapnia . . . 237
  Hypoxia . . . 237
  Hypercapnia . . . 237
The role of NO in the CBF response to disease . . . 237
  NO depletion . . . 237
  eNOS function . . . 238
  eNOS uncoupling . . . 238
  Ischaemia/reperfusion injury . . . 238
  The role of iNOS . . . 239
The role of NO signalling in the developing brain . . . 239
Current therapies . . . 240
Future perspectives . . . 240
Conclusion . . . 241
List of abbreviations . . . 241
Details of authors' contributions . . . 241
Declaration of interests . . . 241
Funding . . . 241

☆ This study was performed at the John Radcliffe Hospital, Oxford.

* Corresponding author at: Nuffield Department of Clinical Neurosciences, Level 6, The West Wing, John Radcliffe Hospital, Oxford OX3 9DU, UK.
E-mail address: payashi.garry@ndcn.ox.ac.uk (P.S. Garry).

http://dx.doi.org/10.1016/j.expneurol.2014.10.017
0014-4886/© 2014 The Authors. Published by Elsevier Inc. This is an open access article under the CC BY-NC-ND license (http://creativecommons.org/licenses/by-nc-nd/3.0/).

Acknowledgments . . . 241
References . . . 241

Introduction

Nitric oxide (NO) is a gaseous molecule synthesised from L-arginine by the enzyme nitric oxide synthase (NOS) (Stuehr and Griffith, 1992). It acts as a neurotransmitter and is a component of the signalling pathways that operate between cerebral blood vessels, neurons and glial cells. Three isoforms of NOS exist: endothelial nitric oxide synthase (eNOS), neuronal nitric oxide synthase (nNOS), and inducible nitric oxide synthase (iNOS). Disruption to the NO pathway underlies many of the mechanisms behind brain injury and NO produced from each of the three isoforms influences the evolution of brain damage in different ways (Toda et al., 2009). This article will explore the current evidence surrounding the role of the NO signalling pathway and NOS isoforms in the regulation of resting cerebral blood flow and in the neuroprotective and pathophysiological processes that occur after injury. We will also examine the potential for manipulation of this pathway as potential treatment strategy.

Nitric oxide synthase — expression and functions

Nitric oxide is derived from three isoforms of the enzyme NOS. The different sites of expression and activity of these enzymes play a critical role in the differing functions of NO.

eNOS is expressed in the vascular endothelium and choroid plexus. NO derived from eNOS (eNOS-NO) plays a role in preserving and maintaining the brain's microcirculation (Toda et al., 2009), inhibiting platelet aggregation, leukocyte adhesion and migration (Broos et al., 2011), and reducing smooth muscle proliferation (Toda et al., 2009).

nNOS is expressed in neuronal cell bodies and NO derived from nNOS (nNOS-NO) acts as an important neurotransmitter associated with neuronal plasticity, memory formation, regulation of central nervous system blood flow, transmission of pain signals and neurotransmitter release (Schuman and Madison, 1994; Toda and Okamura, 2003).

iNOS is expressed in macrophages, glial cells and tumour cells in response to pro-inflammatory cytokines or endotoxin (Marletta, 1988) and unlike eNOS and nNOS it is not expressed unless induced by cytokines or other agents. It can produce a large amount (100–1000 times greater) of NO in relation to eNOS and nNOS (Pautz et al., 2010), due to its independence from calcium dependent mechanisms for activation. After induction, iNOS continuously produces NO until the enzyme is degraded (MacMicking et al., 1997).

Role of NO in regulation of cerebral blood flow

The brain accounts for 20% of the body's energy consumption despite only accounting for 2% of its mass. One of the major roles of the cerebral circulation is to supply oxygen to the brain tissues as neuronal activation requires large amounts of energy to regulate the ion fluxes that occur on depolarisation. Therefore, it is essential that cerebral blood flow (CBF) is tightly regulated.

The NO signalling pathway plays a major role in the regulation of CBF at rest and during physiological and pathological stresses. Understanding the mechanisms behind the regulation of these processes may therefore give useful insights into the CBF changes that occur during cerebral injury.

Two main mechanisms underlie the regulation of CBF at rest, autoregulation and neurovascular coupling. eNOS-NO plays a key role in autoregulation, whereas nNOS derived NO appears crucial for neurovascular coupling.

Autoregulation

Autoregulation is the mechanism by which a consistent supply of blood to the brain tissues in the face of changing cerebral perfusion pressure (CPP) is maintained. eNOS derived NO is essential for extending the lower limit of autoregulation. This is demonstrated by a right shift of the autoregulation curve in eNOS knockout mice at low perfusion pressures (Huang et al., 1996) (see Fig. 1). Elevation of CBF near the lower limit of autoregulation and an increase in the hypotensive portion of the autoregulatory curve are also NO dependent (Jones et al., 2003). During pathological processes where CBF is reduced, such as subarachnoid haemorrhage or ischaemic stroke, NO depletion could therefore further exacerbate decreased flow conditions and increase the likelihood of permanent neuronal damage.

Neurovascular coupling

Neurovascular coupling is the process by which increased neuronal activity is linked to the local regulation of CBF. This ensures that the supply of oxygen is always greater than the demand, and is also known as functional hyperaemia. It is achieved via an integrated action of neurons, glial cells and blood vessels that form a 'neurovascular unit' (Attwell et al., 2010). Several signalling pathways exist to mediate flow/metabolism coupling in this unit, and these interact on multiple levels to ensure a coordinated blood flow response.

Disruption to neurovascular coupling is a common process that underlies many brain disease states (Girouard and Iadecola, 2006). Studies where nNOS is knocked out or inhibited have shown a decrease in neuronal activity related blood flow by up to 90% in the cerebellum (Akgoren et al., 1994), that is reversible in the presence of an exogenously administered NO donor (Piknova et al., 2011). nNOS inhibition in rats causes significant attenuation of the cerebral blood flow response to forepaw stimulation, which is disproportionate to the degree of attenuation of somatosensory evoked potentials (Stefanovic et al., 2007), indicating disruption to neurovascular coupling.

Metabolic pathways activated by glutamate also play a key role via activation of neuronal NMDA receptors (Attwell et al., 2010). This causes an influx of calcium that activates NOS, resulting in increased blood flow. Glutamate also stimulates prostaglandin and epoxyeicosatrienoic acid

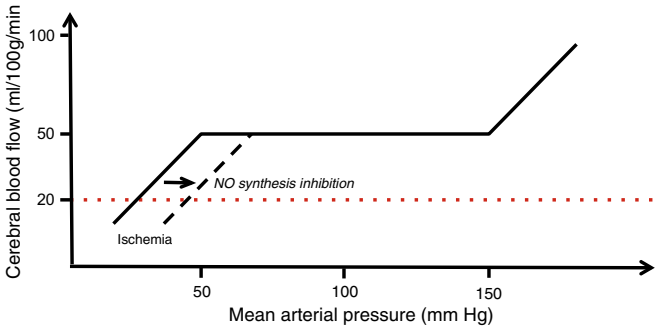


Fig. 1. Inhibition of NO synthesis results in right shift of hypotensive portion of cerebral autoregulatory curve. Cerebral autoregulation maintains an adequate and stable cerebral blood flow in the face of changes in mean arterial pressure (flat portion of the curve). The brain becomes vulnerable to ischaemia when cerebral blood flow falls below 20 ml/100 g/min (red dashed line). NOS inhibition results in right shift of the hypotensive portion of the autoregulatory curve, resulting in the brain becoming susceptible to ischaemia at higher perfusion pressures. Therefore NO signalling is essential in maintaining adequate cerebral blood flow under conditions of fluctuating mean arterial pressure.

(EET) synthesis in astrocytes via arachidonic acid (AA) pathways (Hamilton et al., 2010). This pathway can cause both vasoconstriction and vasodilatation (Golanov and Reis, 1994). Under conditions of NO depletion vasoconstriction is favoured via predominance of 20-hydroxyeicosatetraenoic acid (20-HETE) and decreased production of vasodilatory epoxyeicosatrienoic acids (EETs). These pathways are illustrated in Fig. 2.

NO and the cerebral blood flow response during hypoxia and hypercapnia

Hypoxia and hypercapnia are used as examples of physiological stresses as alterations in tissue partial pressures of oxygen and carbon dioxide are extremely common in critical illness following a brain insult (Peers et al., 2007). The NO signalling pathway plays a central role in the cerebral blood flow response to these alterations. NO pathway dysfunction occurs after brain tissue ischaemia, causing dysregulation of these normal physiological responses.

Hypoxia

Decreased arterial oxygen supply (hypoxia) increases the baseline level of CBF in humans (Mintun et al., 2001). NO plays a role in both signalling this event and the CBF response (Ho et al., 2012). Nonselective NOS inhibition abolishes the increased CBF response to hypoxia in rats (Takuwa et al., 2010). The evidence for this in humans is more indirect, but it has been demonstrated that exposure to hypoxia during adaptation to high altitudes increases NO levels and high-altitude dwellers such as Tibetans have increased circulating NO levels (Beall et al., 2012).

Hypercapnia

The modulation of cerebral vascular tone in response to changes in arterial partial pressure of carbon dioxide is known as chemoregulation, and this process may be viewed as one of the main regulators of cerebral vascular tone.

The cerebral vasodilatory response to hypercapnia is inhibited by L-arginine analogues, which act by blocking the NO synthesis pathway, and by NOS inhibitors (Wang et al., 1992; Kirkeby et al., 2000). Cerebral vasodilatation in response to hypercapnia is reduced after experimental traumatic brain injury in a rodent model and exogenous NO acts to reverse this (Zhang et al., 2002), helping to restore the normal physiological response.

A study on human cell cultures showed an increase in NO production in response to increased CO_2 levels (Fathi et al., 2011b). However, it is likely that the in vivo response differs from the in vitro response, due to multiple interactions of the NO pathway with other intracellular signalling pathways within the neurovascular unit.

Both hypoxia and hypercapnia are common after a cerebral insult due to decreased conscious levels that lead to hypoventilation. Therefore, in the face of a focal brain injury, NO depletion leads to disruption to the normal physiological response to alterations in oxygen and carbon dioxide, further exacerbating neuronal damage. Restoration of the normal adaptive response via replenishing cerebral NO levels may be efficacious at reducing secondary brain injury.

There is therefore a need for further investigation into the NO signalling pathway in a 'whole brain' model in humans, to precisely elucidate the specific mechanisms underlying the observed blood flow effects. Healthy volunteer studies examining the role for NO in the CBF responses to hypoxia and hypercapnia would enable clarification of the role of NO signalling during global disruptions to cerebral physiology, while studies in patients with cerebral injury would enable the effects of NO signalling during the evolution of focal brain pathology to be quantified.

The role of NO in the CBF response to disease

The NO signalling pathway influences the evolution of secondary brain injury in multiple ways, dependent on site, mechanism and timing of NO synthesis and concentration. NO has effects both on the vasculature and on a cellular level, and interacts with many other signalling pathways. This makes it difficult to translate results from animal models where conditions are tightly controlled to the patient population where the evolution of injury occurs unpredictably.

NO depletion

Relative NO depletion appears to occur in the early stages of cerebral injury regardless of the aetiology, e.g. after traumatic brain injury (TBI), subarachnoid haemorrhage (SAH), post-cardiac arrest and ischaemic stroke (Cherian et al., 2000; Tuzgen et al., 2003; Ahn et al., 2004). This occurs simultaneously with a reduction in blood flow (Hlatky et al.,

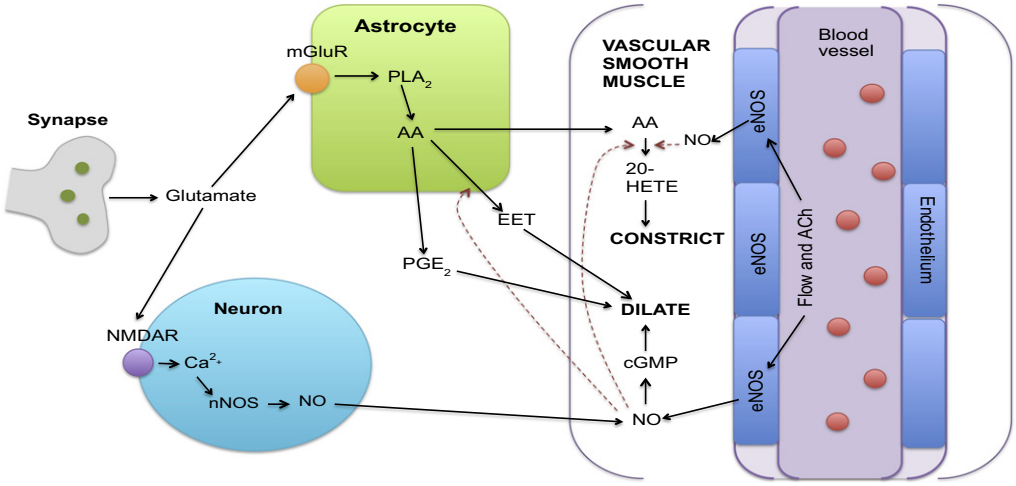


Fig. 2. Nitric oxide inhibits the production of key arachidonic acid-derived messengers. NO inhibits (dashed lines) the production of the vasoconstricting 20-HETE as well as the vasodilating EET. Endothelial nitric oxide synthase (eNOS) can be activated by flow-induced shear stress or by acetylcholine (ACh). This may be one mechanism whereby it may improve blood flow to the brain. NO = nitric oxide, NMDAR = NMDA receptor, PLA_2 = phospholipase A_2, nNOS = neuronal nitric oxide synthase, AA = arachidonic acid, mGLUr = metabotropic glutamate receptor, and PGE_2 = prostaglandin E_2.
Adapted with permission from Attwell et al. *Nature* 468(7321): 232–43.

2003). L-arginine, which enhances NO production, increases CBF (Cherian and Robertson, 2003; Lundblad and Bentzer, 2007). This indicates that disruption to NO signalling is part of a common pathophysiological pathway that leads to the development of secondary brain injury regardless of the mechanism of insult. NO depletion appears to be central in particular to many of the abnormal processes that occur after SAH.

SAH is usually caused by the rupture of a cerebral aneurysm located in the circle of Willis (van Gijn et al., 2007). The decrease in cerebrospinal fluid (CSF) NO metabolites is seen within 10 min of SAH and this is associated with vasoconstriction (Sehba et al., 2000). This is thought to be secondary to destruction of NOS function by haemoglobin (Tanishima, 1980; Reiter et al., 2002; Pluta, 2008). Decreased NO bioavailability is also caused by cerebral NO reacting with superoxide anions to produce peroxynitrite (ONOO) (Radi, 2013). Peroxynitrite formation may cause damage to mitochondria, the vascular endothelium and smooth muscle cells (Moro et al., 2005). In patients with SAH, increased CSF levels of the endogenous NOS synthase inhibitor asymmetric dimethylarginine (ADMA) were observed, and higher levels predicted poorer long term outcome (Li et al., 2014). However, another study showed a rise in CSF NO metabolites 24 h after SAH and the higher the level the worse the outcome (Ng et al., 2001). The discrepancies may be explained by the complexity surrounding the biochemical pathways relevant to the generation and elimination of NO and ADMA. An increase in NO metabolites is only an indirect measure of NO levels (the short half life of NO making it difficult to measure directly), and gives no information regarding the source or activity of the NO generated.

SAH is associated with microvascular constriction, resulting in microthrombus formation (Sabri et al., 2012) and microinfarctions (Stein et al., 2006). There is an associated global decrease in cerebral NO levels and a corresponding increase in cerebral P-selectin levels (Sabri et al., 2012). P-selectin is an endothelial cell adhesion molecule that promotes platelet aggregation and fibrin deposition (Zimmerman et al., 1992). The inhibition of NO synthesis results in increased P-selectin expression (Davenpeck et al., 1994), therefore NO depletion favours microthrombosis formation.

Cortical spreading depression (CSD) consists of a wave of electroencephalogram (EEG) silence moving across the cortical surface (Leao, 1944). CSDs play a role in both early brain injury (Nishizawa, 2013) and in delayed cerebral ischaemia after SAH (Dreier et al., 2006), as well as traumatic brain injury and stroke (Dreier, 2011). In healthy brain tissue, spreading depolarisation is associated with vasodilatation. However, in damaged brain tissue an inverse blood brain flow response occurs which results in vasoconstriction and tissue ischaemia (Dreier et al., 2013). Reduced levels of NO render the brain more susceptible to CSDs. Basal levels of NO determine the threshold of CSDs (Petzold et al., 2008) and NO also acts to restore impaired cerebrovascular reactivity after CSD (Scheckenbach et al., 2006).

Therefore it can be seen that NO signalling plays a crucial role in the blood flow changes that occur after subarachnoid haemorrhage. NO depletion plays a major role in early brain injury, microthrombus formation and cortical spreading depression. Targeting this pathway may enable partial restoration of physiological blood flow, helping to prevent secondary neuronal injury.

eNOS function

Impairment of eNOS activity is also implicated in many cellular mechanisms of neuronal injury (Srivastava et al., 2012) and is seen after SAH, TBI and ischaemic stroke. Innate eNOS activity determines susceptibility to injury, with possession of isoforms with greater activity conferring protection against secondary neuronal insult.

One of the major causes of morbidity and mortality following SAH is delayed cerebral ischaemia (DCI). This occurs in about 30% of patients (Weir and MacDonald, 1993; Khurana and Besser, 1997) typically between days 3 and 12 following SAH (Khurana and Besser, 1997). Originally this was thought to be caused by 'spasm' of cerebral arteries seen on CT angiography, but emerging evidence suggests that this is unlikely to be directly causal (Rowland et al., 2012). Recently it has been discovered that the NO signalling pathway plays a significant role in the pathogenesis of DCI (Vellimana et al., 2011). Genetic variation in the eNOS gene in humans influences the risk of DCI after SAH, as possession of an isoform that results in lower eNOS activity results in greater risk (Khurana et al., 2004; Starke et al., 2008).

eNOS activity is also important after TBI. The immunoreactivity of eNOS is increased in the area surrounding the contused area in the first 3 days after experimental trauma (Cobbs et al., 1997). eNOS knockout mice have greater reduction in CBF than wild type variants in the first 2 h after trauma (Lundblad et al., 2009). Genetic variants of eNOS influence the maintenance of CBF after severe TBI. As in SAH, patients with decreased endogenous eNOS levels had poorer outcomes than patients with alleles that did not affect eNOS levels (Robertson et al., 2011).

This is also the case in ischaemic stroke. Stroke is most often caused by a thrombotic or embolic blockage of a cerebral artery, causing interruption to blood flow, ischaemia and tissue death. eNOS deficient mice have bigger infarcts than wild type after middle cerebral artery occlusion in an animal model of ischaemic stroke (Huang et al., 1996).

eNOS uncoupling

Functional uncoupling of eNOS from its co-factor tetrahydrobiopterin (BH4) also occurs after cerebral insult. eNOS uncoupling occurs under ischaemic conditions, causing superoxide to be generated instead of NO (Vasquez-Vivar et al., 1998; Stuehr et al., 2001). Superoxide reacts with NO to form peroxynitrite, which is in itself a neurotoxin, decreasing levels of bioactive NO (Wink et al., 1993; Pluta et al., 2001). This reduction in NO bioavailability contributes further to secondary brain injury (Drexler and Hornig, 1999; Cai and Harrison, 2000).

eNOS uncoupling contributes to injury after SAH (Sabri et al., 2011a) and simvastatin acts to re-couple eNOS after SAH (Sabri et al., 2011b) in an experimental blood injection model of SAH in rodents. This implies that recoupling of eNOS may be a promising therapeutic target. However, a large multicentre randomised phase 3 trial failed to detect any benefit in the use of simvastatin for long- or short-term outcome in patients with aneurysmal SAH (Kirkpatrick et al., 2014). It is unclear why this was the case but it is likely that pathological aneurysm rupture triggers pathways that are not activated by a blood injection animal model, therefore statins may not be acting in the same fashion as in experimental models. Another possibility is that eNOS uncoupling has metabolic and cellular effects that affect other cellular signalling pathways, and the physiological differences between rodents and humans render results from animal studies difficult to interpret. For example, eNOS knockout appeared to confer neuroprotection in one study, indicating that the detrimental effects of eNOS uncoupling may outweigh the benefits of eNOS activity in this particular model (Sabri et al., 2013).

Ischaemia/reperfusion injury

This is a pathophysiological process responsible for organ injury in a variety of conditions such as myocardial infarction, organ transplantation and cardiac arrest. NO plays a pivotal role in the development of this condition, with NO donor agent administration reducing ischaemia/reperfusion (I/R) injury in animal models (Shiva et al., 2007). A systematic review of NO donor administration during animal stroke models demonstrated an overall improvement in cerebral blood flow and a decrease in infarction volume (Willmot et al., 2005). However, whether these results translate into the patient population with cerebral I/R injury (e.g. ischaemic stroke, cardiac arrest) has not yet been tested (Roberts et al., 2013) and represents an important area of future research. It is also likely that many of the neuroprotective effects of NO

donors are as a result of their metabolic and cellular effects and not simply the improvement of cerebral blood flow.

Cardiac arrest and subsequent recovery result in complete interruption followed by restoration of blood supply, and therefore may provide the best clinical model of ischaemia/reperfusion. Inhaled NO and intravenous sodium nitrite (a NO donor) have been shown to confer neuroprotection in mice and rats (Dezfulian et al., 2012; Ichinose, 2013), and this appears to be mediated by S-nitrosation of proteins rather than the canonical cyclic GMP signalling pathways (Dezfulian et al., 2012). eNOS mediated mechanisms are responsible for the neuroprotective effects of therapeutic hypothermia after cardiac arrest, and inhaled NO conferred neuroprotection in eNOS knockout mice, replicating the beneficial effects of hypothermia (Kida et al., 2014). Therefore, there is preliminary evidence for NO donors as a potential neurotherapeutic agent after cardiac arrest.

The role of iNOS

It has been thought that NO derived from iNOS is responsible for some of the neurotoxic actions of NO post-brain injury. One proposed mechanism by which this occurs is via the reaction of iNOS generated NO with superoxide generated from uncoupled eNOS to form peroxynitrite. The putative mechanism behind this is illustrated in Fig. 3.

However, this is an oversimplified view, and it is more likely that iNOS derived NO, like eNOS-NO, has several roles to play and that the balance between neurotoxicity and neuroprotection is dependent on many factors. As iNOS derived NO has multiple actions, results from animal studies may be focusing on its effects on cerebral blood flow (which is an easily measurable outcome) without accounting for the cellular and metabolic effects (which are more difficult to quantify).

NO derived from iNOS appears to contribute to neurotoxicity after ischaemic stroke, as animal knockout models have smaller infarcts than their wild type counterparts (Iadecola et al., 1997). An increase in NO above basal levels secondary to iNOS occurs 12–24 h after MCA occlusion and contributes to neurotoxicity, with iNOS inhibition leading to reduced infarct volume (Iadecola et al., 1995).

There is also evidence that NO produced by iNOS contributes to neurotoxicity following TBI. iNOS expression is significantly induced by brain injury, with peak concentrations occurring around 1–2 days after TBI (Clark et al., 1996; Wada et al., 1998). Patients with higher levels went on to have a worse outcome (Tisdall et al., 2013). A recent phase II clinical trial (NOSTRA) in TBI patients using the NOS inhibitor 4-amino-(6R,S)-5,6,7,8-tetrahydro-L-biopterin (VAS203), which preferentially inhibits iNOS (Terpolilli et al., 2009), showed significantly improved extended Glasgow Outcome Scores compared to placebo (Stover et al., 2014).

Data on the role of iNOS after TBI is conflicting. Attenuation of CBF at 72 h after TBI was demonstrated in iNOS knockout mice (Foley et al., 2008), which also correlated with long-term functional outcome (Sinz et al., 1999; Bayir et al., 2005). The inhibition of iNOS appeared to lead to exacerbation of deficits in cognitive performance and increased neuron loss (Sinz et al., 1999). However, these studies are confined to rodent models of controlled cortical impact injury, and the CBF results may be linked to pathological vasodilatation linked to inflammation. This may explain the apparent contradictory results shown, and emphasises that simply measuring cerebral blood flow does not give the entire picture with regard to the effects of NO in the brain after injury. Overall, the balance of evidence is in favour of iNOS activity being harmful in the patient population, and therefore inhibition of destructive cascades mediated via iNOS may have promise as a potential future therapy.

The role of NO signalling in the developing brain

Neonatal hypoxic–ischaemic insult is a major cause of acute mortality and is often associated with permanent neuropsychiatric problems, presenting a major public health concern. There is a lack of specific treatments besides hypothermia available for this condition; therefore identification and investigation of potential molecular therapeutic targets are of utmost importance.

NO is involved in several critical processes in the developing brain, including myelination (Olivier et al., 2010). It also plays a key role in the immature brain's response to hypoxic–ischaemic insult. Inhaled NO is neuroprotective in the developing brain, with reduction in the size of excitotoxic and ischaemic lesions in rats (Pansiot et al., 2010; Charriaut-Marlangue et al., 2012). Boosting NO-cGMP signalling using sildenafil, a phosphodiesterase type 5 inhibitor increases blood flow and has neuroprotective effects in the rat model of hypoxic–ischaemic brain injury (Charriaut-Marlangue et al., 2014).

However, as in the developed brain, it appears that dosage and timing of exposure to NO or molecules that influence the NO signalling pathway are extremely important. Inhaled NO given during the reperfusion period appears to have neurotoxic effects (Charriaut-Marlangue et al., 2012). This may be due to the activation of nNOS as inhibition leads to improved CBF and perfusion early after reoxygenation (Hsu et al., 2014). As in the developed brain, iNOS activation may be responsible for damage in the late (>24 h) phase (Higuchi et al., 1998). Therefore further work is needed to determine the optimal timing,

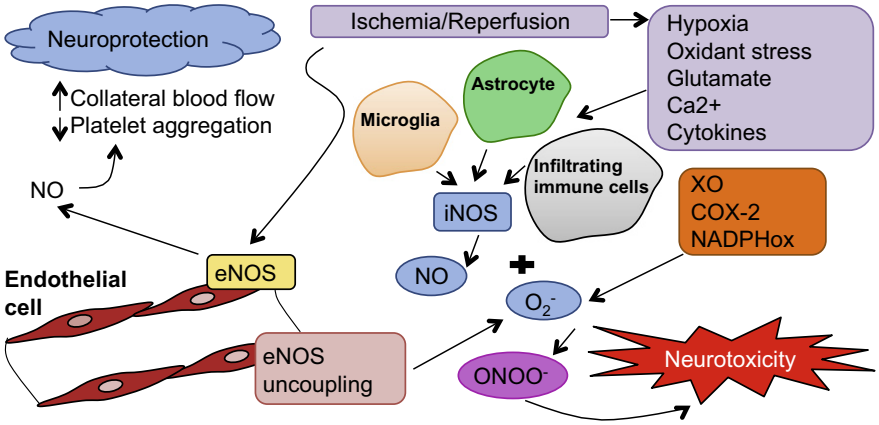


Fig. 3. Roles of NO and peroxynitrite in the pathophysiology of acute brain injury. Brain ischaemia and reperfusion leads to stimulation of endothelial NOS (eNOS), resulting in brief increases in endothelial NO generation, associated with neuroprotective actions. Ischaemic energy depletion and oxidant production trigger the release of glutamate, which results in stimulated activity inducible NOS (iNOS) in astrocytes, microglia and infiltrating inflammatory cells. iNOS activation also occurs in response to the release of inflammatory cytokines such as TNFα and IFNβ, and cellular signalling pathways responsible for the response to hypoxia. During the same period of time, superoxide production is enhanced due to uncoupling of eNOS, mitochondrial dysfunction, and the stimulated activity of NADPH oxidase, xanthine oxidase (XO), and cyclooxygenase-2 (COX-2). Formation of peroxynitrite is then favoured, damaging lipids, proteins and DNA that contributes significantly to neurotoxicity.
Adapted with permission from Pacher P et al. *Physiol Rev* 2007; 87:31.

Table 1
A selection of pharmacological studies detailing the effects of NO donors on animal models of brain injury.

Study	Model use	Type of agent	Dose	Outcomes
Terpolilli et al. (2013)	TBI; mice	Inhaled NO	50 ppm	Reduced lesion volume Improved neurological function
Terpolilli et al. (2012)	MCA occlusion; mice	Inhaled NO	5–50 ppm	Reduced infarct volume by 40%
Zhang et al. (1994)	MCA occlusion; rats	Intravenous SNP Intravenous SIN 1	3 mg/kg/h 1.5–6 mg/kg/h	Reduction in infarct size
Morikawa et al. (1994)	MCA occlusion; rats	Intravenous L-arginine	300 mg/kg	Reduced infarct volume by 35%
Jung et al. (2006)	MCA occlusion; rats	Intravenous sodium nitrite	48 and 480 nmol	33% and 77% reduction in infarct size Reduced neurological deficit
Li et al. (2013)	MCA occlusion; mice	Inhaled NO	10, 20, 40, 60 or 80 ppm	Dose and duration dependent reduction in infarct volume up to 50%
Fathi et al. (2011a)	Subarachnoid blood clot implantation; macaques	Intravenous sodium nitrite	300 μg/kg/h	26.9% reduction in vasospasm
Pluta et al. (2005)	Subarachnoid blood clot implantation; monkeys	Intravenous sodium nitrite	90 mg over 24 h	Prevention of vasospasm development

SNP = sodium nitroprusside.
SIN 1 = 3-morpholino-sydnonimine.

concentration and duration of NO therapy, and translation of these results to a human model is also needed.

Current therapies

Despite the controversies surrounding NO dysfunction after brain injury, there is animal evidence that increasing cerebral NO levels either directly using inhaled NO or indirectly using NO donors has neuroprotective effects. Table 1 summarises a selection of these pharmacological studies.

Future perspectives

Manipulation of the NO synthesis pathway shows great promise as a pharmacological therapeutic target. Exogenous NO appears to replicate the actions of eNOS derived NO, without contributing to neurotoxicity. NO donors may be neuroprotective by preventing NO depletion, helping to normalize capillary blood flow and improve oxygen delivery to the tissue (Shiva, 2013). Cellular mechanisms such as S-nitrosylation of proteins and effects on mitochondrial respiration also play an important role (Dezfulian et al., 2012).

However, the majority of this evidence has come from experimental animal models, largely focussing on ischaemic stroke whereas SAH, TBI and post-cardiac arrest are relatively under researched.

Cardiovascular instability when using classic NO donors such as glyceryl trinitrate (GTN) and sodium nitroprusside precludes their use in critically ill unstable patients, and makes results of drug trials difficult to interpret as local effects are negated by systemic blood pressure effects.

However, sodium nitrite is emerging as a feasible, safe NO donor with minimal effects on the systemic vasculature in patients after SAH (Pluta et al., 2011; Oldfield et al., 2013). It has also been used safely in cardiac arrest survivors (Dezfulian et al., 2012). This is because cerebral tissue is able to convert endogenous nitrite to NO without the need for oxygen as a substrate (van Faassen et al., 2009), meaning that when the tissues are hypoxic (such as after cerebral injury) nitrite is only converted to NO locally. The mechanisms underlying this are illustrated in Fig. 4.

The results from animal studies have been promising, with prevention and reversal of cerebral vasospasm after experimental SAH (Pluta et al., 2005; Fathi et al., 2011a). However, these are based on autologous blood clot injection models, and as discussed previously pathological aneurysm rupture is likely to activate multiple cellular signalling pathways that may not be replicated in these experimental models. Therefore large-scale clinical trials are needed to translate these results to patients.

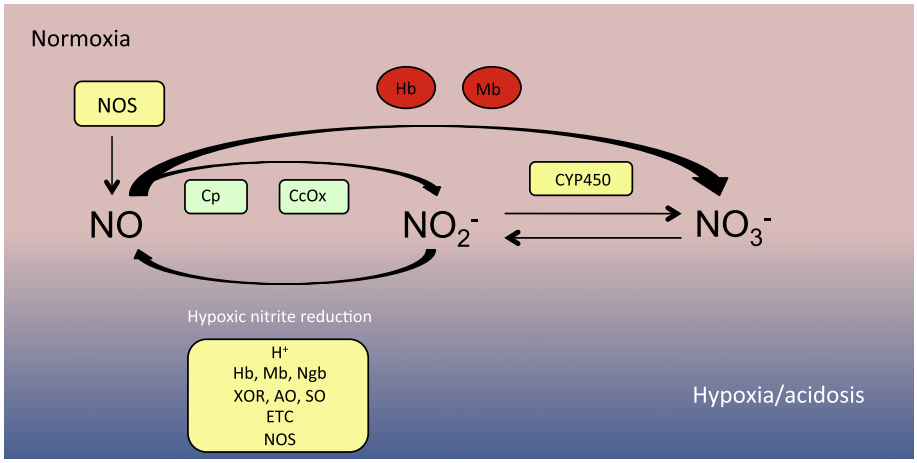


Fig. 4. The nitrate–NO cycle. In normoxia NOS is functional and generates NO, which is oxidised by haemoglobin (Hb) and myoglobin (Mb) to nitrate (NO_3^-) and by cytochrome c oxidase (ccox) and ceruloplasmin (Cp) to nitrite (NO_2^-). Nitrate is also derived from the diet as well as the normoxic oxidation of nitrite by cytochrome P450 enzymes (CYP450). In hypoxia, nitrite is reduced to bioactive NO by a number of mammalian nitrite reductase enzymes including Hb, Mb, neuroglobin (Ngb), xanthine oxidoreductase (XOR), aldehyde oxidase (AO), sulphite oxidase (SO), components of the mitochondrial electron transport chain (ETC.) and NOS.
Adapted with permission from Shiva S. *Redox Biol* 2013; 1(1): 40–44.

Conclusion

NO is an important mediator in the regulation of CBF in the resting state, acting as a key modulator on the pathways responsible for maintaining resting CBF and perfusion under physiological stresses such as fluctuations of blood pressure, hypoxia and hypercapnia. It also plays a key role in the development of the healthy brain. Disruption to NO synthesis and metabolism underlies many of the pathophysiological processes that occur after brain injury, and appears to occur regardless of the mode of injury. The available evidence suggests that NO derived from eNOS is neuroprotective after acquired brain injury whereas NO synthesised by iNOS contributes to further damage, and that this difference is due to differences in timing, spatial location and concentration of NO generated by each isoform. This has led to investigation of drugs that influence NO signalling as potential therapeutic agents. In particular, NO donors have been shown to be neuroprotective and efficacious in reducing secondary brain injury in animals, potentially by replicating some of the effects of endogenous NO derived from eNOS. iNOS inhibitors may also hold promise as a future neurotherapeutic target. Future studies should focus on investigating the therapeutic potential of the many other signalling molecules that interact with the NO synthesis pathway and determining long-term side effects of NO pathway manipulation in the injured brain. The hypotheses presented in this review must be tested in large-scale clinical trials to verify whether promising results from animal studies can translate into the patient population. Better understanding of the role of the NO pathway may lead to the development of exciting new pharmacotherapies designed to minimise secondary brain injury, with the aim of reducing the morbidity and mortality from devastating conditions such as subarachnoid haemorrhage, ischaemic stroke, traumatic brain injury and neonatal hypoxic–ischaemic insult.

List of abbreviations

ADMA	asymmetric dimethylarginine
CO_2	carbon dioxide
CBF	cerebral blood flow
CPP	cerebral perfusion pressure
CSF	cerebrospinal fluid
CT	computerised tomography
CSD	cortical spreading depression
cGMP	cyclic guanosine monophosphate
20-HETE	20-hydroxyeicosatetraenoic acid
EEG	electroencephalogram
DCI	delayed cerebral ischaemia
eNOS	endothelial nitric oxide synthase
EET	epoxyeicosatrienoic acid
GTN	glyceryl tri nitrate
iNOS	inducible nitric oxide synthase
I/R	ischaemia/reperfusion
MCA	middle cerebral artery
NMDA	N-methyl D-aspartic acid
nNOS	neuronal nitric oxide synthase
NO	nitric oxide
ONOO	peroxynitrite
SIN 1	3-morpholino-sydnonimine
SNP	sodium nitroprusside
SAH	subarachnoid haemorrhage
TBI	traumatic brain injury

Details of authors' contributions

All authors contributed to the conception, writing, critical review and revision of the manuscript.

Declaration of interests

We declare no competing interests.

Funding

The authors are supported by the National Institute for Health Research of Oxford Biomedical Research Centre based at Oxford University Hospitals NHS Trust and University of Oxford.

ME and MJR are supported by the Oxford University Clinical Academic Graduate School. MJR is supported by the Medical Research Council, UK.

Acknowledgments

We thank Professor Duncan Young for critically reviewing a previous version of this manuscript.

References

Ahn, M.J., Sherwood, E.R., Prough, D.S., Lin, C.Y., DeWitt, D.S., 2004. The effects of traumatic brain injury on cerebral blood flow and brain tissue nitric oxide levels and cytokine expression. J. Neurotrauma 21, 1431–1442.

Akgoren, N., Fabricius, M., Lauritzen, M., 1994. Importance of nitric oxide for local increases of blood flow in rat cerebellar cortex during electrical stimulation. Proc. Natl. Acad. Sci. U. S. A. 91, 5903–5907.

Attwell, D., Buchan, A.M., Charpak, S., Lauritzen, M., Macvicar, B.A., Newman, E.A., 2010. Glial and neuronal control of brain blood flow. Nature 468, 232–243.

Bayir, H., Kagan, V.E., Borisenko, G.G., Tyurina, Y.Y., Janesko, K.L., Vagni, V.A., Billiar, T.R., Williams, D.L., Kochanek, P.M., 2005. Enhanced oxidative stress in iNOS-deficient mice after traumatic brain injury: support for a neuroprotective role of iNOS. J. Cereb. Blood Flow Metab. 25, 673–684.

Beall, C.M., Laskowski, D., Erzurum, S.C., 2012. Nitric oxide in adaptation to altitude. Free Radic. Biol. Med. 52, 1123–1134.

Broos, K., Feys, H.B., De Meyer, S.F., Vanhoorelbeke, K., Deckmyn, H., 2011. Platelets at work in primary hemostasis. Blood Rev. 25, 155–167.

Cai, H., Harrison, D.G., 2000. Endothelial dysfunction in cardiovascular diseases: the role of oxidant stress. Circ. Res. 87, 840–844.

Charriaut-Marlangue, C., Bonnin, P., Gharib, A., Leger, P.L., Villapol, S., Pocard, M., Gressens, P., Renolleau, S., Baud, O., 2012. Inhaled nitric oxide reduces brain damage by collateral recruitment in a neonatal stroke model. Stroke 43, 3078–3084.

Charriaut-Marlangue, C., Nguyen, T., Bonnin, P., Duy, A.P., Leger, P.L., Csaba, Z., Pansiot, J., Bourgeois, T., Renolleau, S., Baud, O., 2014. Sildenafil mediates blood-flow redistribution and neuroprotection after neonatal hypoxia–ischemia. Stroke 45, 850–856.

Cherian, L., Robertson, C.S., 2003. L-Arginine and free radical scavengers increase cerebral blood flow and brain tissue nitric oxide concentrations after controlled cortical impact injury in rats. J. Neurotrauma 20, 77–85.

Cherian, L., Goodman, J.C., Robertson, C.S., 2000. Brain nitric oxide changes after controlled cortical impact injury in rats. J. Neurophysiol. 83, 2171–2178.

Clark, R.S., Kochanek, P.M., Obrist, W.D., Wong, H.R., Billiar, T.R., Wisniewski, S.R., Marion, D.W., 1996. Cerebrospinal fluid and plasma nitrite and nitrate concentrations after head injury in humans. Crit. Care Med. 24, 1243–1251.

Cobbs, C.S., Fenoy, A., Bredt, D.S., Noble, L.J., 1997. Expression of nitric oxide synthase in the cerebral microvasculature after traumatic brain injury in the rat. Brain Res. 751, 336–338.

Davenpeck, K.L., Gauthier, T.W., Lefer, A.M., 1994. Inhibition of endothelial-derived nitric oxide promotes P-selectin expression and actions in the rat microcirculation. Gastroenterology 107, 1050–1058.

Dezfulian, C., Alekseyenko, A., Dave, K.R., Raval, A.P., Do, R., Kim, F., Perez-Pinzon, M.A., 2012. Nitrite therapy is neuroprotective and safe in cardiac arrest survivors. Nitric Oxide 26, 241–250.

Dreier, J.P., 2011. The role of spreading depression, spreading depolarization and spreading ischemia in neurological disease. Nat. Med. 17, 439–447.

Dreier, J.P., Woitzik, J., Fabricius, M., Bhatia, R., Major, S., Drenckhahn, C., Lehmann, T.N., Sarrafzadeh, A., Willumsen, L., Hartings, J.A., Sakowitz, O.W., Seemann, J.H., Thieme, A., Lauritzen, M., Strong, A.J., 2006. Delayed ischaemic neurological deficits after subarachnoid haemorrhage are associated with clusters of spreading depolarizations. Brain 129, 3224–3237.

Dreier, J.P., Drenckhahn, C., Woitzik, J., Major, S., Offenhauser, N., Weber-Carstens, S., Wolf, S., Strong, A.J., Vajkoczy, P., Hartings, J.A., 2013. Spreading ischemia after aneurysmal subarachnoid hemorrhage. Acta Neurochir. Suppl. 115, 125–129.

Drexler, H., Hornig, B., 1999. Endothelial dysfunction in human disease. J. Mol. Cell. Cardiol. 31, 51–60.

Fathi, A.R., Pluta, R.M., Bakhtian, K.D., Qi, M., Lonser, R.R., 2011a. Reversal of cerebral vasospasm via intravenous sodium nitrite after subarachnoid hemorrhage in primates. J. Neurosurg. 115, 1213–1220.

Fathi, A.R., Yang, C., Bakhtian, K.D., Qi, M., Lonser, R.R., Pluta, R.M., 2011b. Carbon dioxide influence on nitric oxide production in endothelial cells and astrocytes: cellular mechanisms. Brain Res. 1386, 50–57.

Foley, L.M., Hitchens, T.K., Melick, J.A., Bayir, H., Ho, C., Kochanek, P.M., 2008. Effect of inducible nitric oxide synthase on cerebral blood flow after experimental traumatic brain injury in mice. J. Neurotrauma 25, 299–310.
Girouard, H., Iadecola, C., 2006. Neurovascular coupling in the normal brain and in hypertension, stroke, and Alzheimer disease. J. Appl. Physiol. 100, 328–335.
Golanov, E.V., Reis, D.J., 1994. Nitric oxide and prostanoids participate in cerebral vasodilation elicited by electrical stimulation of the rostral ventrolateral medulla. J. Cereb. Blood Flow Metab. 14, 492–502.
Hamilton, N.B., Attwell, D., Hall, C.N., 2010. Pericyte-mediated regulation of capillary diameter: a component of neurovascular coupling in health and disease. Front. Neuroenerg. 2.
Higuchi, Y., Hattori, H., Kume, T., Tsuji, M., Akaike, A., Furusho, K., 1998. Increase in nitric oxide in the hypoxic–ischemic neonatal rat brain and suppression by 7-nitroindazole and aminoguanidine. Eur. J. Pharmacol. 342, 47–49.
Hlatky, R., Goodman, J.C., Valadka, A.B., Robertson, C.S., 2003. Role of nitric oxide in cerebral blood flow abnormalities after traumatic brain injury. J. Cereb. Blood Flow Metab. 23, 582–588.
Ho, J.J., Man, H.S., Marsden, P.A., 2012. Nitric oxide signaling in hypoxia. J. Mol. Med. (Berl.) 90, 217–231.
Hsu, Y.C., Chang, Y.C., Lin, Y.C., Sze, C.I., Huang, C.C., Ho, C.J., 2014. Cerebral microvascular damage occurs early after hypoxia–ischemia via nNOS activation in the neonatal brain. J. Cereb. Blood Flow Metab. 34, 668–676.
Huang, Z., Huang, P.L., Ma, J., Meng, W., Ayata, C., Fishman, M.C., Moskowitz, M.A., 1996. Enlarged infarcts in endothelial nitric oxide synthase knockout mice are attenuated by nitro-L-arginine. J. Cereb. Blood Flow Metab. 16, 981–987.
Iadecola, C., Zhang, F., Xu, X., 1995. Inhibition of inducible nitric oxide synthase ameliorates cerebral ischemic damage. Am. J. Physiol. 268, R286–R292.
Iadecola, C., Zhang, F., Casey, R., Nagayama, M., Ross, M.E., 1997. Delayed reduction of ischemic brain injury and neurological deficits in mice lacking the inducible nitric oxide synthase gene. J. Neurosci. 17, 9157–9164.
Ichinose, F., 2013. Improving outcomes after cardiac arrest using NO inhalation. Trends Cardiovasc. Med. 23, 52–58.
Jones, S.C., Easley, K.A., Radinsky, C.R., Chyatte, D., Furlan, A.J., Perez-Trepichio, A.D., 2003. Nitric oxide synthase inhibition depresses the height of the cerebral blood flow-pressure autoregulation curve during moderate hypotension. J. Cereb. Blood Flow Metab. 23, 1085–1095.
Jung, K.H., Chu, K., Ko, S.Y., Lee, S.T., Sinn, D.I., Park, D.K., Kim, J.M., Song, E.C., Kim, M., Roh, J.K., 2006. Early intravenous infusion of sodium nitrite protects brain against in vivo ischemia–reperfusion injury. Stroke 37, 2744–2750.
Khurana, V.G., Besser, M., 1997. Pathophysiological basis of cerebral vasospasm following aneurysmal subarachnoid haemorrhage. J. Clin. Neurosci. 4, 122–131.
Khurana, V.G., Sohni, Y.R., Mangrum, W.I., McClelland, R.L., O'Kane, D.J., Meyer, F.B., Meissner, I., 2004. Endothelial nitric oxide synthase gene polymorphisms predict susceptibility to aneurysmal subarachnoid hemorrhage and cerebral vasospasm. J. Cereb. Blood Flow Metab. 24, 291–297.
Kida, K., Shirozu, K., Yu, B., Mandeville, J.B., Bloch, K.D., Ichinose, F., 2014. Beneficial effects of nitric oxide on outcomes after cardiac arrest and cardiopulmonary resuscitation in hypothermia-treated mice. Anesthesiology 120, 880–889.
Kirkeby, O.J., Kutzsche, S., Risoe, C., Rise, I.R., 2000. Cerebral nitric oxide concentration and microcirculation during hypercapnia, hypoxia, and high intracranial pressure in pigs. J. Clin. Neurosci. 7, 531–538.
Kirkpatrick, P.J., Turner, C.L., Smith, C., Hutchinson, P.J., Murray, G.D., 2014. Simvastatin in aneurysmal subarachnoid haemorrhage (STASH): a multicentre randomised phase 3 trial. Lancet Neurol. 13 (7), 666–675.
Leao, 1944. Spreading depression of activity in the cerebral cortex. Neurophysiology 7, 359–390.
Li, Y.S., Shemmer, B., Stone, E., AN, M., Jonas, S., Quartermain, D., 2013. Neuroprotection by inhaled nitric oxide in a murine stroke model is concentration and duration dependent. Brain Res. 1507, 134–145.
Li, H., Wu, W., Liu, M., Zhang, X., Zhang, Q.R., Ni, L., Hang, C.H., 2014. Increased cerebrospinal fluid concentrations of asymmetric dimethylarginine correlate with adverse clinical outcome in subarachnoid hemorrhage patients. J. Clin. Neurosci. 21 (8), 1404–1408.
Lundblad, C., Bentzer, P., 2007. Effects of L-arginine on cerebral blood flow, microvascular permeability, number of perfused capillaries, and brain water content in the traumatized mouse brain. Microvasc. Res. 74, 1–8.
Lundblad, C., Grande, P.O., Bentzer, P., 2009. Hemodynamic and histological effects of traumatic brain injury in eNOS-deficient mice. J. Neurotrauma 26, 1953–1962.
MacMicking, J., Xie, Q.W., Nathan, C., 1997. Nitric oxide and macrophage function. Annu. Rev. Immunol. 15, 323–350.
Marletta, M.A., 1988. Mammalian synthesis of nitrite, nitrate, nitric oxide, and N-nitrosating agents. Chem. Res. Toxicol. 1, 249–257.
Mintun, M.A., Lundstrom, B.N., Snyder, A.Z., Vlassenko, A.G., Shulman, G.L., Raichle, M.E., 2001. Blood flow and oxygen delivery to human brain during functional activity: theoretical modeling and experimental data. Proc. Natl. Acad. Sci. U. S. A. 98, 6859–6864.
Morikawa, E., Moskowitz, M.A., Huang, Z., Yoshida, T., Irikura, K., Dalkara, T., 1994. L-arginine infusion promotes nitric oxide-dependent vasodilation, increases regional cerebral blood flow, and reduces infarction volume in the rat. Stroke 25, 429–435.
Moro, M.A., Almeida, A., Bolanos, J.P., Lizasoain, I., 2005. Mitochondrial respiratory chain and free radical generation in stroke. Free Radic. Biol. Med. 39, 1291–1304.
Ng, W.H., Moochhala, S., Yeo, T.T., Ong, P.L., Ng, P.Y., 2001. Nitric oxide and subarachnoid hemorrhage: elevated level in cerebrospinal fluid and their implications. Neurosurgery 49, 622–626 (discussion 626–627).
Nishizawa, S., 2013. The roles of early brain injury in cerebral vasospasm following subarachnoid hemorrhage: from clinical and scientific aspects. Acta Neurochir. Suppl. 115, 207–211.
Oldfield, E.H., Loomba, J.J., Monteith, S.J., Crowley, R.W., Medel, R., Gress, D.R., Kassell, N.F., Dumont, A.S., Sherman, C., 2013. Safety and pharmacokinetics of sodium nitrite in patients with subarachnoid hemorrhage: a phase IIA study. J. Neurosurg. 119, 634–641.
Olivier, P., Loron, G., Fontaine, R.H., Pansiot, J., Dalous, J., Thi, H.P., Charriaut-Marlangue, C., Thomas, J.L., Mercier, J.C., Gressens, P., Baud, O., 2010. Nitric oxide plays a key role in myelination in the developing brain. J. Neuropathol. Exp. Neurol. 69, 828–837.
Pansiot, J., Loron, G., Olivier, P., Fontaine, R., Charriaut-Marlangue, C., Mercier, J.C., Gressens, P., Baud, O., 2010. Neuroprotective effect of inhaled nitric oxide on excitotoxic-induced brain damage in neonatal rat. PLoS ONE 5, e10916.
Pautz, A., Art, J., Hahn, S., Nowag, S., Voss, C., Kleinert, H., 2010. Regulation of the expression of inducible nitric oxide synthase. Nitric Oxide 23, 75–93.
Peers, C., Pearson, H.A., Boyle, J.P., 2007. Hypoxia and Alzheimer's disease. Essays Biochem. 43, 153–164.
Petzold, G.C., Haack, S., von Bohlen Und Halbach, O., Priller, J., Lehmann, T.N., Heinemann, U., Dirnagl, U., Dreier, J.P., 2008. Nitric oxide modulates spreading depolarization threshold in the human and rodent cortex. Stroke 39, 1292–1299.
Piknova, B., Kocharyan, A., Schechter, A.N., Silva, A.C., 2011. The role of nitrite in neurovascular coupling. Brain Res. 1407, 62–68.
Pluta, R.M., 2008. Dysfunction of nitric oxide synthases as a cause and therapeutic target in delayed cerebral vasospasm after SAH. Acta Neurochir. Suppl. 104, 139–147.
Pluta, R.M., Rak, R., Wink, D.A., Woodward, J.J., Khaldi, A., Oldfield, E.H., Watson, J.C., 2001. Effects of nitric oxide on reactive oxygen species production and infarction size after brain reperfusion injury. Neurosurgery 48, 884–892 (discussion 892–883).
Pluta, R.M., Dejam, A., Grimes, G., Gladwin, M.T., Oldfield, E.H., 2005. Nitrite infusions to prevent delayed cerebral vasospasm in a primate model of subarachnoid hemorrhage. JAMA 293, 1477–1484.
Pluta, R.M., Oldfield, E.H., Bakhtian, K.D., Fathi, A.R., Smith, R.K., Devroom, H.L., Nahavandi, M., Woo, S., Figg, W.D., Lonser, R.R., 2011. Safety and feasibility of long-term intravenous sodium nitrite infusion in healthy volunteers. PLoS ONE 6, e14504.
Radi, R., 2013. Peroxynitrite, a stealthy biological oxidant. J. Biol. Chem. 288, 26464–26472.
Reiter, C.D., Wang, X., Tanus-Santos, J.E., Hogg, N., Cannon 3rd, R.O., Schechter, A.N., Gladwin, M.T., 2002. Cell-free hemoglobin limits nitric oxide bioavailability in sickle-cell disease. Nat. Med. 8, 1383–1389.
Roberts, B.W., Mitchell, J., Kilgannon, J.H., Chansky, M.E., Trzeciak, S., 2013. Nitric oxide donor agents for the treatment of ischemia/reperfusion injury in human subjects: a systematic review. Shock 39, 229–239.
Robertson, C.S., Gopinath, S.P., Valadka, A.B., Van, M., Swank, P.R., Goodman, J.C., 2011. Variants of the endothelial nitric oxide gene and cerebral blood flow after severe traumatic brain injury. J. Neurotrauma 28, 727–737.
Rowland, M.J., Hadjipavlou, G., Kelly, M., Westbrook, J., Pattinson, K.T., 2012. Delayed cerebral ischaemia after subarachnoid haemorrhage: looking beyond vasospasm. Br. J. Anaesth. 109, 315–329.
Sabri, M., Ai, J., Knight, B., Tariq, A., Jeon, H., Shang, X., Marsden, P.A., Loch Macdonald, R., 2011a. Uncoupling of endothelial nitric oxide synthase after experimental subarachnoid hemorrhage. J. Cereb. Blood Flow Metab. 31, 190–199.
Sabri, M., Ai, J., Marsden, P.A., Macdonald, R.L., 2011b. Simvastatin re-couples dysfunctional endothelial nitric oxide synthase in experimental subarachnoid hemorrhage. PLoS ONE 6, e17062.
Sabri, M., Ai, J., Lakovic, K., D'Abbondanza, J., Ilodigwe, D., Macdonald, R.L., 2012. Mechanisms of microthrombi formation after experimental subarachnoid hemorrhage. Neuroscience 224, 26–37.
Sabri, M., Ai, J., Lass, E., D'Abbondanza, J., Macdonald, R.L., 2013. Genetic elimination of eNOS reduces secondary complications of experimental subarachnoid hemorrhage. J. Cereb. Blood Flow Metab. 33, 1008–1014.
Scheckenbach, K.E., Dreier, J.P., Dirnagl, U., Lindauer, U., 2006. Impaired cerebrovascular reactivity after cortical spreading depression in rats: restoration by nitric oxide or cGMP. Exp. Neurol. 202, 449–455.
Schuman, E.M., Madison, D.V., 1994. Nitric oxide and synaptic function. Annu. Rev. Neurosci. 17, 153–183.
Sehba, F.A., Schwartz, A.Y., Chereshnev, I., Bederson, J.B., 2000. Acute decrease in cerebral nitric oxide levels after subarachnoid hemorrhage. J. Cereb. Blood Flow Metab. 20, 604–611.
Shiva, S., 2013. Nitrite: a physiological store of nitric oxide and modulator of mitochondrial function. Redox Biol. 1, 40–44.
Shiva, S., Sack, M.N., Greer, J.J., Duranski, M., Ringwood, L.A., Burwell, L., Wang, X., MacArthur, P.H., Shoja, A., Raghavachari, N., Calvert, J.W., Brookes, P.S., Lefer, D.J., Gladwin, M.T., 2007. Nitrite augments tolerance to ischemia/reperfusion injury via the modulation of mitochondrial electron transfer. J. Exp. Med. 204, 2089–2102.
Sinz, E.H., Kochanek, P.M., Dixon, C.E., Clark, R.S., Carcillo, J.A., Schiding, J.K., Chen, M., Wisniewski, S.R., Carlos, T.M., Williams, D., DeKosky, S.T., Watkins, S.C., Marion, D.W., Billiar, T.R., 1999. Inducible nitric oxide synthase is an endogenous neuroprotectant after traumatic brain injury in rats and mice. J. Clin. Invest. 104, 647–656.
Srivastava, K., Bath, P.M., Bayraktutan, U., 2012. Current therapeutic strategies to mitigate the eNOS dysfunction in ischaemic stroke. Cell. Mol. Neurobiol. 32, 319–336.
Starke, R.M., Kim, G.H., Komotar, R.J., Hickman, Z.L., Black, E.M., Rosales, M.B., Kellner, C.P., Hahn, D.K., Otten, M.L., Edwards, J., Wang, T., Russo, J.J., Mayer, S.A., Connolly Jr., E.S., 2008. Endothelial nitric oxide synthase gene single-nucleotide polymorphism predicts cerebral vasospasm after aneurysmal subarachnoid hemorrhage. J. Cereb. Blood Flow Metab. 28, 1204–1211.
Stefanovic, B., Schwindt, W., Hoehn, M., Silva, A.C., 2007. Functional uncoupling of hemodynamic from neuronal response by inhibition of neuronal nitric oxide synthase. J. Cereb. Blood Flow Metab. 27, 741–754.
Stein, S.C., Browne, K.D., Chen, X.H., Smith, D.H., Graham, D.I., 2006. Thromboembolism and delayed cerebral ischemia after subarachnoid hemorrhage: an autopsy study. Neurosurgery 59, 781–787 (discussion 787–788).

Stover, J., Belli, A., Boret, H., Bulters, D., Sahuquillo, J., Schmutzhard, E., Zavala, E., Ungerstedt, U., Schinzel, R., Tegtmeier, F., 2014. NO-synthase inhibition with the antipterin VAS203 improves outcome in moderate and severe traumatic brain injury: a placebo-controlled randomised phase II trial (NOSTRA). J. Neurotrauma 31 (19), 1599–1606.
Stuehr, D.J., Griffith, O.W., 1992. Mammalian nitric oxide synthases. Adv. Enzymol. Relat. Areas Mol. Biol. 65, 287–346.
Stuehr, D., Pou, S., Rosen, G.M., 2001. Oxygen reduction by nitric-oxide synthases. J. Biol. Chem. 276, 14533–14536.
Takuwa, H., Matsuura, T., Bakalova, R., Obata, T., Kanno, I., 2010. Contribution of nitric oxide to cerebral blood flow regulation under hypoxia in rats. J. Physiol. Sci. 60, 399–406.
Tanishima, T., 1980. Cerebral vasospasm: contractile activity of hemoglobin in isolated canine basilar arteries. J. Neurosurg. 53, 787–793.
Terpolilli, N.A., Zweckberger, K., Trabold, R., Schilling, L., Schinzel, R., Tegtmeier, F., Plesnila, N., 2009. The novel nitric oxide synthase inhibitor 4-amino-tetrahydro-L-biopterine prevents brain edema formation and intracranial hypertension following traumatic brain injury in mice. J. Neurotrauma 26, 1963–1975.
Terpolilli, N.A., Kim, S.W., Thal, S.C., Kataoka, H., Zeisig, V., Nitzsche, B., Klaesner, B., Zhu, C., Schwarzmaier, S., Meissner, L., Mamrak, U., Engel, D.C., Drzezga, A., Patel, R.P., Blomgren, K., Barthel, H., Boltze, J., Kuebler, W.M., Plesnila, N., 2012. Inhalation of nitric oxide prevents ischemic brain damage in experimental stroke by selective dilatation of collateral arterioles. Circ. Res. 110, 727–738.
Terpolilli, N.A., Kim, S.W., Thal, S.C., Kuebler, W.M., Plesnila, N., 2013. Inhaled nitric oxide reduces secondary brain damage after traumatic brain injury in mice. J. Cereb. Blood Flow Metab. 33, 311–318.
Tisdall, M.M., Rejdak, K., Kitchen, N.D., Smith, M., Petzold, A., 2013. The prognostic value of brain extracellular fluid nitric oxide metabolites after traumatic brain injury. Neurocrit. Care. 19, 65–68.
Toda, N., Okamura, T., 2003. The pharmacology of nitric oxide in the peripheral nervous system of blood vessels. Pharmacol. Rev. 55, 271–324.
Toda, N., Ayajiki, K., Okamura, T., 2009. Cerebral blood flow regulation by nitric oxide: recent advances. Pharmacol. Rev. 61, 62–97.
Tuzgen, S., Tanriover, N., Uzan, M., Tureci, E., Tanriverdi, T., Gumustas, K., Kuday, C., 2003. Nitric oxide levels in rat cortex, hippocampus, cerebellum, and brainstem after impact acceleration head injury. Neurol. Res. 25, 31–34.
van Faassen, E.E., Bahrami, S., Feelisch, M., Hogg, N., Kelm, M., Kim-Shapiro, D.B., Kozlov, A.V., Li, H., Lundberg, J.O., Mason, R., Nohl, H., Rassaf, T., Samouilov, A., Slama-Schwok, A., Shiva, S., Vanin, A.F., Weitzberg, E., Zweier, J., Gladwin, M.T., 2009. Nitrite as regulator of hypoxic signaling in mammalian physiology. Med. Res. Rev. 29, 683–741.
van Gijn, J., Kerr, R.S., Rinkel, G.J., 2007. Subarachnoid haemorrhage. Lancet 369, 306–318.
Vasquez-Vivar, J., Kalyanaraman, B., Martasek, P., Hogg, N., Masters, B.S., Karoui, H., Tordo, P., Pritchard Jr., K.A., 1998. Superoxide generation by endothelial nitric oxide synthase: the influence of cofactors. Proc. Natl. Acad. Sci. U. S. A. 95, 9220–9225.
Vellimana, A.K., Milner, E., Azad, T.D., Harries, M.D., Zhou, M.L., Gidday, J.M., Han, B.H., Zipfel, G.J., 2011. Endothelial nitric oxide synthase mediates endogenous protection against subarachnoid hemorrhage-induced cerebral vasospasm. Stroke 42, 776–782.
Wada, K., Chatzipanteli, K., Kraydieh, S., Busto, R., Dietrich, W.D., 1998. Inducible nitric oxide synthase expression after traumatic brain injury and neuroprotection with aminoguanidine treatment in rats. Neurosurgery 43, 1427–1436.
Wang, Q., Paulson, O.B., Lassen, N.A., 1992. Effect of nitric oxide blockade by NG-nitro-L-arginine on cerebral blood flow response to changes in carbon dioxide tension. J. Cereb. Blood Flow Metab. 12, 947–953.
Weir, B., MacDonald, L., 1993. Cerebral vasospasm. Clin. Neurosurg. 40, 40–55.
Willmot, M., Gray, L., Gibson, C., Murphy, S., Bath, P.M., 2005. A systematic review of nitric oxide donors and L-arginine in experimental stroke; effects on infarct size and cerebral blood flow. Nitric Oxide 12, 141–149.
Wink, D.A., Hanbauer, I., Krishna, M.C., DeGraff, W., Gamson, J., Mitchell, J.B., 1993. Nitric oxide protects against cellular damage and cytotoxicity from reactive oxygen species. Proc. Natl. Acad. Sci. U. S. A. 90, 9813–9817.
Zhang, F., White, J.G., Iadecola, C., 1994. Nitric oxide donors increase blood flow and reduce brain damage in focal ischemia: evidence that nitric oxide is beneficial in the early stages of cerebral ischemia. J. Cereb. Blood Flow Metab. 14, 217–226.
Zhang, F., Sprague, S.M., Farrokhi, F., Henry, M.N., Son, M.G., Vollmer, D.G., 2002. Reversal of attenuation of cerebrovascular reactivity to hypercapnia by a nitric oxide donor after controlled cortical impact in a rat model of traumatic brain injury. J. Neurosurg. 97, 963–969.
Zimmerman, G.A., Prescott, S.M., McIntyre, T.M., 1992. Endothelial cell interactions with granulocytes: tethering and signaling molecules. Immunol. Today 13, 93–100.